HIGH PRECISION SPECTROPOLARIMETRY OF STARS AND PLANETS

by

Robert John Smith

A dissertation submitted for
the degree of PhD
in the University of Edinburgh

PhD

MAY 1981

"In an orchard there should be enough to eat,
enough to lay up, enough to be stolen and
enough to rot upon the ground."

Samuel Maddon

ABSTRACT

A pre-existing spectropolarimeter is described from the user's point of view, and the important factors affecting its operation as a high precision device are fully explained. The instrument is applied to studies of the atmospheres of Jupiter and Saturn, and of properties of grains in the interstellar medium.

Linear and circular polarisation measurements have been made of the integrated discs of both Jupiter and Saturn at moderate resolution (50 Å). Enhancements in the linear polarisation across the 7270 Å methane band are found in both planets. The effect is attributed to the increased importance of low order scattering in the centre of the band since here higher levels of the atmosphere are being probed than in the continuum. It is suggested that circular polarisation variations across this band seen in Jupiter are caused by total internal reflection in ammonia aerosols. Polarisation measurements have also been made across other bands in the spectra of each planet. Continuum circular polarisation measurements have been obtained of Saturn at phase angle $2^{\circ}.7$. A large enhancement in the circular polarisation is observed, increasing very rapidly towards longer wavelengths, reaching 0.15% by 7400 Å. A future program of research is detailed.

Linear polarisation measurements in the range 3100 Å to 7600 Å have been obtained on three stars whose light has been attenuated and polarised by the interstellar medium. The stars are ζ Ophiuchi, 55 Cygni and χ Aurigae. Structure in the polarisation of ζ Ophiuchi has been detected with scale lengths of 400 Å to 1400 Å at wavelengths around 6000 Å. No exact correspondence is found with published high quality extinction curves of various stars. The structure is tentatively suggested as being due to magnetite impurities in large grains. A

broad (100 Å to 200 Å) feature has also been found in the polarisation of this star centred on 4100 Å. This appears to arise in larger than average grains and may be associated with an extinction feature seen at slightly longer wavelengths in other stars. It may be due to an absorption in the grain mantles. Broad band variations in the position angle of polarisation observed in all three stars have been interpreted as implying multiple dust clouds in the lines of sight to each of these stars. A future program of research is mapped out.

I declare this Thesis to be entirely my own work except where explicit reference is made to the work of others. In particular:

(a) The spectropolarimeter described in Chapter A of this Thesis was a pre-existing instrument. Measurements, investigations and modifications described in the text and not explicitly attributed to others were carried out, or specified, by myself.

(b) The observations described in Chapters B and C of this Thesis were made either by myself or at my request. Other contributing observers are acknowledged.

No part of this Thesis has been submitted to any other University or College in respect of another degree or award. Some of the measurements of Jupiter presented here have been previously published (Wolstencroft and Smith, 1979 : see list of literature cited in Chapter B).

R.J. Smith

Acknowledgements

I owe a deep debt of gratitude to my supervisor R.D. Wolstencroft for initiating and sustaining my interest in the fields of research described in this Thesis, and in others yet to bear significant fruit. His kindness and enthusiasm have been unfailing. I must thank the R.O.E. engineers involved with the spectropolarimeter, and especially W.A. Cormack whose experience, skill, common sense and good humour were all invaluable. I am pleased to acknowledge the contributions of various members of the Department of Astronomy, including my University supervisor, Professor V.C. Reddish.

I am grateful to the following people for help with observing: R. Wolstencroft, W. Cormack, A. Hutton, C. Impey, A. Pickup, C. Lonsdale, M. Eccles. I am also grateful to R.D. Wolstencroft, C.D. Impey, G.V. Coyne and A.M. Magalhaes for further observations made with the ROE Spectropolarimeter at my request. I should like to thank G. Slater, P. Frame and M. Cannell who typed this Thesis and M. Fretwell and R. Wilson who prepared the diagrams.

Finally I must mention Professor D.W.N. Stibbs whose determination led to my undertaking this course, and my wife whose patience and understanding have never failed to amaze me.

R.J. Smith
May 1981

Table of Contents

General Introduction

Most of the information we gain from the outside world comes from interpreting the patterns of light detected by our eyes, either directly, by watching a phenomenon ourselves, or indirectly, by observing our instruments as they react to a phenomenon. These light beams have various properties, and most obvious to us are their colour and intensity. However, our eyes are only slightly sensitive to two other important properties of the beam: the orientation of the electric vector of the electromagnetic transverse waves; and their phase. It is these qualities of light we study when we examine its state of polarisation.

We may consider any beam of light to be a mixture of unpolarised or 'natural' light, of linearly polarised light and of circularly polarised light. The intensity of the beam is the sum of the intensities of the three components. Intensity has been studied in the astronomical context since ancient times - quantitatively since Hipparchus who first classified the stars by their apparent brightness. Early measurements of astronomical polarisation were made by Arago (1809: comets, moon), Liais (1858: solar corona), Lord Rosse (1872: Venus) and Hale (1908: circular polarisation of sunspots). It is now reasonably well understood that a full description of the state of polarisation of an incident beam of light is necessary to obtain the maximum information about its origin and history whilst travelling to the observer. This implies that measurement must be made of all four Stokes parameters (I, Q, U, V) and not just the first (I). The "Principle of Optical Equivalence", enunciated by Stokes in 1852, shows that these four parameters are sufficient to give a complete description of the

polarisation properties of a beam of light, and that two beams with the same four Stokes parameters will be indistinguishable when these properties are considered.

Studies of linear polarisation at the 0.5 to 1.0% level of precision are relatively easy when using a photoelectric device as a detector. A polarimeter consisting solely of a rotatable analyser - even polaroid - will suffice. Faint objects, where photon collection is a problem rarely allow a better precision than 1% to be obtained within reasonable integration times. Polarimetry at the 0.05% level can be done with a rotating waveplate polarimeter. In these instruments a retarder (usually half-wave) is continuously rotated before an analyser, which can be either a polarising prism or a piece of polaroid. Difficulties in rotating a waveplate uniformly to better than the 0.1% level limit such polarimeters to what we shall term the medium precision regime. For the highest accuracy (0.02% or better) photoelastic or piezo-optic crystal modulators replace the mechanically rotating waveplate. This Thesis is concerned with this high precision region.

In chapter A, a pre-existing high precision polarimeter based upon a photoelastic modulator is fully described. Each component in the optical train is examined and the properties that affect the performance of the instrument as a high precision instrument examined. It will be seen that there are a number of ways in which the presently existing instrument could be improved. The polarimeter is then used in studies of the atmospheres of Jupiter and Saturn (chapter B) and of the interstellar dust grains (chapter C). Both fields require high precision (0.01%) medium resolution (10-50 Å) measurements of linear polarisation. The former also makes use of circular polarisation measurements.

Chapter A

The R.O.E. Spectropolarimeter

1. The Spectropolarimeter to be described originated as a scanning spectrometer, and was built in 1974 by W.A. Cormack under the supervision of J.W. Campbell (both of the Royal Observatory, Edinburgh). The addition of a photoelastic modulator polarimeter was made in 1975 with the collaboration of R.D. Wolstencroft, then at the University of Hawaii.

The following subsections introduce the spectropolarimeter used to obtain the data described later in this thesis. After an outline description of the instrument (1.1) and its intended mode of operation (1.2), the Mueller calculus is used to show how the instrument measures polarisation in the ideal case. Section 2 is devoted to a more detailed examination of the components of the spectropolarimeter and their functioning.

1.1 Brief description

The ROE Spectropolarimeter divides by function and design into three components. A polarimeter is mounted before the entrance aperture of a grating spectrometer while a photomultiplier, with its Fabry optics, is mounted after the exit slit.

The polarimeter was originally designed for the high precision measurement of circular polarisation, and is built around a fused silica photoelastic modulator, followed by an analyser of HNP'B polaroid (see figure A1). The axis of the polaroid is orientated at 45 degrees to the stress axis of the

(the page numbered 21 should follow this page)

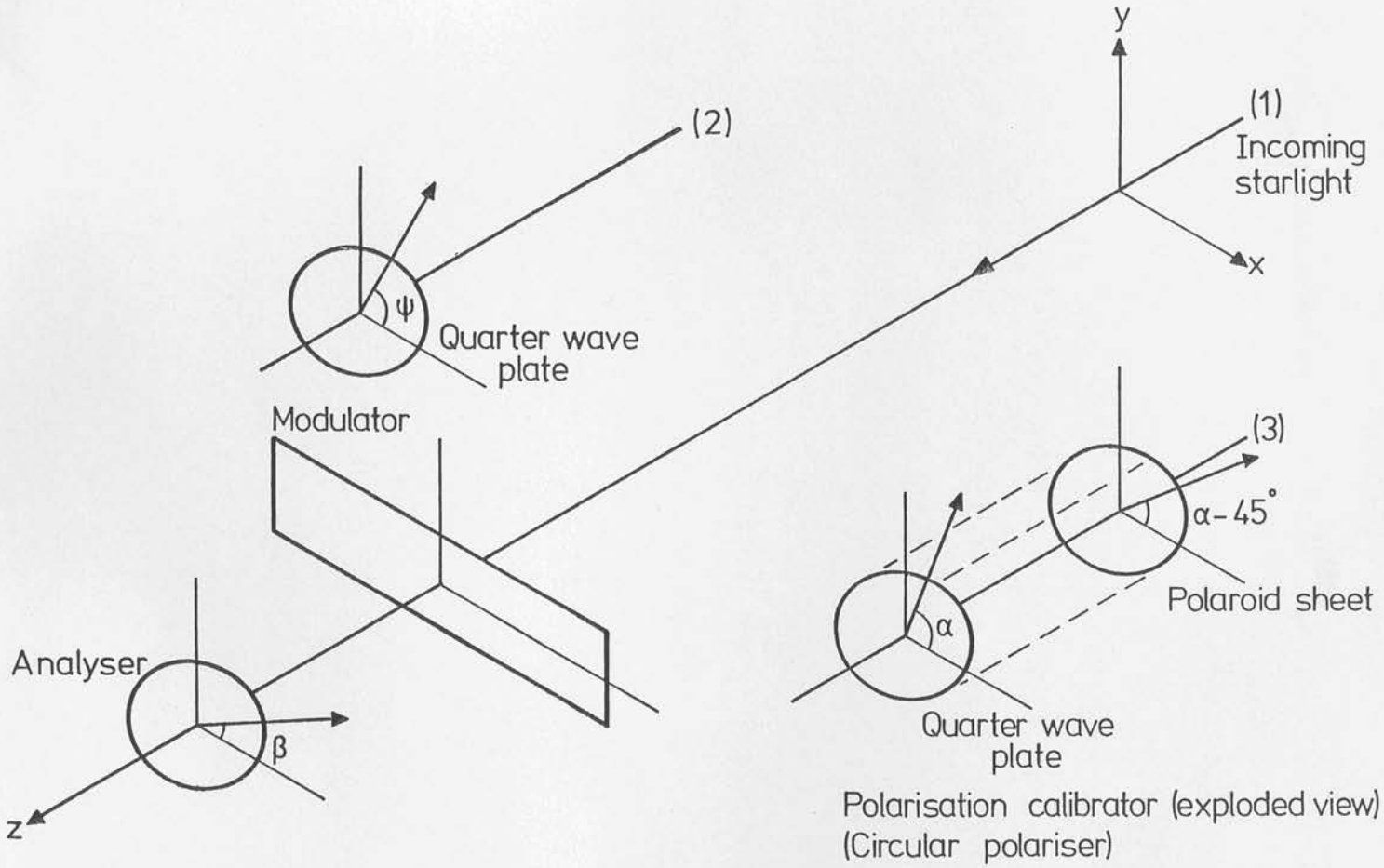

Figure A1: The optical train of the polarimeter section of the instrument. The three cases are (1) the measurement of circular polarisation, (2) the measurement of linear polarisation and (3) the measurement of calibration polarisation.

scanning and the analyser chopping under program control. The order sorter wheel and the wheel containing the wave-plates are under remote control through thumbswitches.

1.2 Method of operation

The spectropolarimeter measures polarisation in the following manner. The modulator is driven such that it acts as a variable retarder, oscillating harmonically with a frequency of around 50 kHz. A two channel photon counter is phase locked to the modulator drive signal, and counts are collected during windows centred in the positive and negative halves of the cycle. The peak retardance of the modulator is chosen such that the retardance averages $\pi/2$ in the positive half of the cycle, and $-\pi/2$ in the negative half. If completely circularly polarised light passes through the modulator, it is converted to linearly polarised light. The position angle of this linear polarisation is at $\pm$ 45 degrees to the stress axis of the modulator, the sign being positive in one half of the modulator cycle and negative in the other. Since the analyser is aligned with its axis also at 45° to the modulator stress axis, it will only pass light during one half of the modulator cycle. Our instrumental measure of circular polarisation is

$$q_{INST} = \frac{I_+ - I_-}{I_+ + I_-}$$

where I_+ = intensity in positive half of cycle

I_- = intensity in negative half of cycle.

and these intensities are in actual fact numbers of photo-electrons counted over many cycles.

If we put 100% circularly polarised light into the system we would have an optical switch, flashing at 50 kHz. Normally, however, there will be an unpolarised component and possibly a linearly polarised component as well. The unpolarised light will not be affected by the modulator and will contribute an exactly equivalent amount of flux in both halves of the cycle. It will hence cancel in the above expression. Any linearly polarised component will be more "active". Any such component can be regarded as the resultant of two independant components with axes of 45^{o} to each other - the Stokes parameters Q and U. Q, being parallel to the stress axis of the modulator, is not affected by it and will cancel in the same way as an unpolarised flux. U is converted into circularly polarised light of one sign in one half of the cycle, and of the other sign in the other half. Both should be able to pass with equal efficiency through the analyser and so this component too should cancel.

The measurement of linear polarisation is effected by simply converting it to circularly polarised light, and then measuring it in exactly the same way as above. The two components Q and U are detected separately by introducing in turn two $\lambda/4$ waveplates into the beam. The first has its fast axis perpendicular to U. This converts Q to circular, but does not affect U. The system then measures the circular component which corresponds to Q. Any circular polarisation originally present in the beam is converted to linear by the waveplate and hence will not affect the measurement. The second waveplate is parallel to

Q, i.e. at +45 degrees to the first, and this leaves Q unaffected while converting U to circular for measurement.

What relation does "q_{INST}" defined above have to 'q', the degree of circular polarisation? The detailed analysis (to follow) shows that it should be identical - if the modulator chops with a square waveform between $\pm \pi/2$. Since the waveform is sinusoidal, $q_{INST} < q$ and we must investigate the relation between them. This is done by inserting a calibration filter before the modulator. This filter consists of a $\lambda/4$ waveplate which is identical to the others used in the measurement of linear polarisation with a piece of HNP'B polaroid cemented to it, such that the waveplate lies between the polaroid and the modulator. The polarising axis of the polaroid is aligned at 45° to the fast axis of the waveplate. The calibration filter provides a source of 100% circularly polarised light at a particular (known) wavelength, and a known proportion of circularly polarised light at other wavelengths. The resulting measure, q_{CAL}, can be regarded as the instrumental efficiency for the detection of polarisation. It gives the required relation:

$$q = q_{INST}/K \; q_{CAL}$$

where K is the proportion of circular polarisation produced by the calibrator.

The linear polarisation is calibrated in the same way

$$p_Q = p_{INST}(Q) \; / \; q_{CAL} \quad \text{and} \quad p_U = p_{INST}(U) \; / \; q_{CAL}$$

where the factor K is now omitted because the waveplates used for the measurement of linear polarisation are

identical to the waveplate in the calibrator.

1.3 A Mueller Calculus analysis of the ideal polarimeter

Definitions of the Stokes parameters and a description of the matrices used in the Mueller Calculus are given in Appendix A1. Using these tools it is possible to develop expressions to describe how the Stokes parameters of the incident light are measured. The derivations of the system matrices are carried out in Appendix A2. These are used below to show how linear and circular polarisation are measured by the ideal polarimeter. It is presumed that all components are perfect and exactly aligned.

1.3.1 The measurement of circular polarisation

Eight measurements are taken, four with the incident light passing through the modulator and then through the analyser (circular measurements); and four with the polarisation calibrator inserted in front of the modulator (calibration measurements). At wavelength λ_0, the retardance of the calibrator waveplate $\gamma = 90^\circ$ and the calibrator will produce 100% circularly polarised light. In each case the four measurements are taken at the two positions of the analyser inclined at 45° to the stress axis of the modulator ($\beta = 45^\circ$ and 135°) (figure A1) and at each of the two orientations of the polarimeter, 90° apart (the spectrometer does not rotate). At time t, the intensity of light transmitted by the analyser in the

case of the circular measurement is

$$I_t = \tfrac{1}{2}(I + U\cos\delta_t + V\sin\delta_t) \qquad 1a$$

$$I_t = \tfrac{1}{2}(I - U\cos\delta_t - V\sin\delta_t) \qquad 1b$$

$$I_t = \tfrac{1}{2}(I - U\cos\delta_t - V\sin\delta_t) \qquad 1c$$

$$I_t = \tfrac{1}{2}(I + U\cos\delta_t + V\sin\delta_t) \qquad 1d$$

and in the case of the calibration measurement it is

$$I_t = \tfrac{1}{4}(I + Q\sin2\alpha - U\cos2\alpha)(1 + \sin\tau\sin\delta_t - \cos\tau\cos2\alpha\cos\delta_t) \qquad 2a$$

$$I_t = \tfrac{1}{4}(I + Q\sin2\alpha - U\cos2\alpha)(1 - \sin\tau\sin\delta_t + \cos\tau\cos2\alpha\cos\delta_t) \qquad 2b$$

$$I_t = \tfrac{1}{4}(I - Q\sin2\alpha + U\cos2\alpha)(1 + \sin\tau\sin\delta_t - \cos\tau\cos2\alpha\cos\delta_t) \qquad 2c$$

$$I_t = \tfrac{1}{4}(I - Q\sin2\alpha + U\cos2\alpha)(1 - \sin\tau\sin\delta_t + \cos\tau\cos2\alpha\cos\delta_t) \qquad 2d$$

where δ_t is the instantaneous retardance of the modulator, α is the orientation of the fast axis of the quarter waveplate and τ is its retardance. Equations (a) and (c) refer to $\beta = 45^\circ$; (b) and (d) to $\beta = 135^\circ$; (a) and (b) to the 0° orientation of the polarimeter, and (c) and (d) to the 90° orientation (see figure A1).

Assuming the modulator is driven sinusoidally such that its retardance is given by $\delta_t = A\sin\omega t$ and that counts I_+ and I_- are collected between $\omega t = \pi/2 \pm \Delta$ and $3\pi/2 \pm \Delta$ respectively, then in cases (1a) and (2a) we have

$$R_{1a} = \frac{I_+ - I_-}{I_+ + I_-}_{1a} = \frac{a}{\Delta} \cdot \frac{V}{I + (b/\Delta)U}$$

$$\text{and } R_{2a} = \frac{a}{\Delta} \cdot \frac{\sin\tau}{1 - (b/\Delta)c}$$

$$\text{where } a = 2J_1(A)\frac{\sin\Delta}{1} - 2J_3(A)\frac{\sin3\Delta}{3} + 2J_5(A)\frac{\sin5\Delta}{5} - \ldots\ldots$$

$$b = J_o(A) - 2J_2(A)\frac{\sin 2\Delta}{2} + 2J_4(A)\frac{\sin 4\Delta}{4} \quad \ldots\ldots$$

$$c = \cos 2\alpha \cos \tau$$

and the $J_i(A)$ are Bessel functions of the first kind, of order i. By driving the modulator to A $\simeq 107^\circ$ the coefficient b/Δ becomes zero and for this value

$$(R_{1a}/R_{2a}) = \frac{V}{I} \cdot \frac{1}{\sin \tau}$$

where τ is given with adequate precision by $\tau = 90^\circ \times \lambda_Q/\lambda$ for the whole visual range, and λ_Q is known. In practice the modulator will not be driven at exactly the optimum value of A, and (b/Δ) will be small but not zero. It is readily shown that

$$\frac{R_{1a}}{R_{2a}} = \frac{V}{(I + (b/\Delta)U)} \frac{(1 - (b/\Delta)c)}{\sin \tau}, \quad \frac{R_{1b}}{R_{2b}} = \frac{V}{(I - (b/\Delta)U)} \cdot \frac{(1 - (b/\Delta)c)}{\sin \tau}$$

$$\frac{R_{1c}}{R_{1c}} \quad \frac{V}{(I - (b/\Delta)U)} \frac{(1 + (b/\Delta)c)}{\sin \tau}, \quad \frac{R_{1d}}{R_{1d}} \quad \frac{V}{(I + (b/\Delta)U)} \frac{(1 + (b/\Delta)c)}{\sin \tau}$$

Hence provided (b/Δ) is small

$$\frac{1}{4}\left\{\frac{R_{1a}}{R_{2a}} + \frac{R_{1b}}{R_{2b}} + \frac{R_{1c}}{R_{2c}} + \frac{R_{1d}}{R_{2d}}\right\} = \frac{V}{I} \frac{1}{\sin \tau}$$

1.3.2 The measurement of linear polarisation

In this case, twelve measurements are taken, four with the incident light passing in order through a quarter wave-plate (with fast axis at angle Ψ), the modulator and the analyser; four through the same components but with the waveplate at angle ($\Psi + 45$); and four in the calibration position described in Section 3.1. The equations corresponding to 1a to 1d for the first four measurements are

$$I_t = \tfrac{1}{2}\,(I + f_0\cos\delta_t + g_0\sin\delta_t) \qquad 3a$$

$$I_t = \tfrac{1}{2}\,(I - f_0\cos\delta_t - g_0\sin\delta_t) \qquad 3b$$

$$I_t = \tfrac{1}{2}\,(I - f_{90}\cos\delta_t - g_{90}\sin\delta_t) \qquad 3c$$

$$I_t = \tfrac{1}{2}\,(I + f_{90}\cos\delta_t + g_{90}\sin\delta_t) \qquad 3d$$

where

$$f_0 = (Q\cos2\psi+U\sin2\psi)\sin2\psi+(-Q\sin2\psi+U\cos2\psi)\cos2\psi\cos\tau+V\cos2\psi\sin\tau$$

$$f_{90} = (Q\cos2\psi+U\sin2\psi)\sin2\psi+(-Q\sin2\psi+U\cos2\psi)\cos2\psi\cos\tau-V\cos2\psi\sin\tau$$

$$g_0 = (Q\sin2\psi-U\cos2\psi)\sin\tau+V\cos\tau$$

$$g_{90} = (Q\sin2\psi-U\cos2\psi)\sin\tau-V\cos\tau$$

The difference over the sum, as defined in section 3.1, is,

for case 3a,

$$R_{3a} = \frac{a}{\Delta}\,\frac{g_0}{I + (b/\Delta)f_0}$$

and it can be shown that

$$\frac{R_{3a}}{R_{2a}} = \frac{g_0}{(I + (b/\Delta)f_0)}\,\frac{(I - (b/\Delta)c)}{\sin\tau}\quad \frac{R_{3b}}{R_{2b}}\quad \frac{g_0}{(I - (b/\Delta)f_0)}\,\frac{(I + (b/\Delta)c)}{\sin\tau}$$

$$\frac{R_{3c}}{R_{2c}}\quad \frac{-g_{90}}{(I - (b/\Delta)f_{90})}\,\frac{(I - (b/\Delta)c)}{\sin\tau}\quad \frac{R_{3d}}{R_{2d}}\quad \frac{-g_{90}}{(I + (b/\Delta)f_{90})}\,\frac{(I + (b/\Delta)c)}{\sin\tau}$$

where a, b and c were defined above.

Hence, neglecting terms of order $(b/\Delta)^2$ and higher

$$p_1 = \frac{1}{I}\left\{\frac{R_{3a}}{R_{2a}} + \frac{R_{3b}}{R_{2b}} - \frac{R_{3c}}{R_{2c}} - \frac{R_{3d}}{R_{2d}}\right\}$$

$$= \frac{1}{2}\left\{\frac{g_0}{\sin\tau} + \frac{g_{90}}{\sin\tau}\right\}$$

$$= 1/2(Q/I)\sin2\psi - (U/I)\cos2\psi - (V/I)\cot\tau + (Q/I)\sin2\psi$$

$$- (U/I)\cos2\psi + (V/I)\cot\tau)$$

$$\underline{p_1 = (Q/I)\sin2\psi - (U/I)\cos2\psi}$$

The second set of four measurements are used in a similar way to yield

$$p_2 = (Q/I)\sin 2(\psi+45) - (U/I)\cos 2(\psi+45)$$

$$\underline{p_2 = (Q/I)\cos 2\psi + (U/I)\sin 2\psi}$$

The degree of linear polarisation, p, and the instrumental position angle, ϕ, may be derived from p_1 and p_2, viz

$$p^2 = p_1^2 + p_2^2 \quad \text{and} \quad \tan 2\phi = \frac{p_2}{p_1}$$

ϕ is measured in the same sense as the equatorial position angle, θ, (east of north) but with respect to an arbitrary zero which is determined by observation of standard objects.

2. Detailed description of the instrument

The practical implementation of the ideal instrument described above presents a number of problems. In the sub-sections to follow a detailed description is given of every part of the instrument, and of the methods of data collection and reduction.

2.1 Guiding

There are a number of reasons why accurate guiding is essential in a spectropolarimeter such as this, and these reasons are explained as they occur in different parts of this Thesis. The ROE spectropolarimeter uses a simple offset guiding system employing a large (26 cm x 19 cm) flat mirror placed at 45° to the beam and ahead of the polarimeter. This central part of the mirror can be flipped into place whenever it is desired to use the guiding eyepiece as a finder. Offset stars are found and observed visually in a widefield eyepiece mounted on an X-Y crosshead.

The maximum travel of the eyepiece on its crosshead is 10 cm in each of the X- and Y- directions. In accordance with the specification on the instrument to accept an f/7.5 beam, and so that the full travel of the crosshead may be used, the flat mirror must be made bigger than 21 cm x 17 cm. It can be seen that the specification has been met. The flat mirror is some 50 cm from the focus of the telescope. The circular aperture should, of course, have been elliptical, with a major axis of 9 cm and a minor of about $6\frac{1}{2}$ cm.

Let us now consider some of the optical properties of this system. If the instrument is fitted to a 60 inch telescope, working at f/16, we obtain a platescale of 8.5 arcseconds per mm. For a 90 inch, operating at f/9, the figure is 10.0 arcsec mm^{-1}. For the 60 inch, this gives a total field of some 0.055 square degrees. We lose a fair amount of this by cutting out the central circle. Consider the diagram, which shows a view of the 45^{o} flat from the eyepiece. EFGH represents the crosshead and ABCD the central hole. It is clear that any star that appears in the eyepiece to be on the ellipse ABCD will be roughly 50% vignetted. Hence we may define our effective field as:

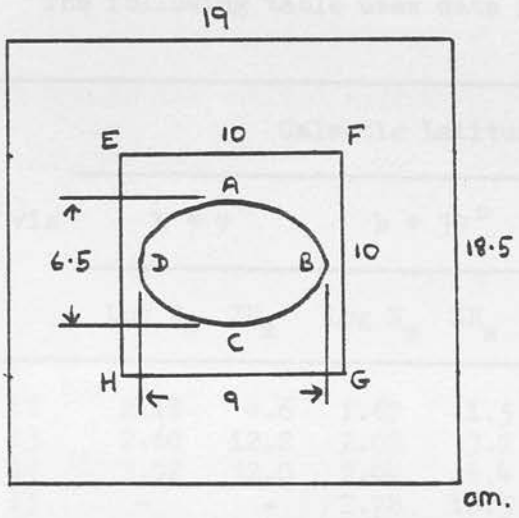

$$Z = 1 - \frac{\text{Area ABCD}}{\text{Area EFGH}} \times .055$$

$$= 1 - \frac{\pi \times 9 \times 9}{4 \times 2 \times 100} \times .055$$

$$= .030 \text{ deg.}^2$$

Note that at f/7.5, the entire field is vignetted to some extent whilst a fair proportion is even at f/16.

What magnitude of star could we see in the eyepiece? The eye has a pupil of around 0.3 inches. The telescope's pupil is 60 inches, but loses some light between its various mirrors and lenses. If we presume an efficiency for the telescope of 65%, the ratio in the intensity of the light reaching the unaided eye and that when the eye is placed behind the guiding eyepiece, is:

$$\text{Ratio} = \frac{60 \times 60 \times .65}{.3 \times .3} = 26000$$

This is equivalent to 11 magnitudes. Since the unaided eye can see stars of visual magnitude 6.5, we should be able to detect stars of magnitude $17\frac{1}{2}$ with a 60 inch telescope. With a 40 inch, the corresponding figure is $16\frac{1}{2}$. In practice, seeing conditions and the imperfect telescope optics will mean that guiding on a star fainter than 16^m would not be feasible (15^m for a 40").

Is there likely to be a star in the field of view to guide on?

The following table uses data from ALLEN (1973)

	Galactic Latitude					
m_{vis}	$b = 0^\circ$		$b = 30^\circ$		$b = 90^\circ$	
	Log N_m	ZN_m	Log N_m	ZN_m	Log N_m	ZN_m
12	2.18	4.6	1.67	1.5	1.33	0.6
13	2.60	12.2	2.08	3.7	1.69	1.5
14	3.02	32.0	2.44	8.4	2.01	3.2
15	-	-	2.78	18.5	2.27	5.7
16	-	-	3.09	37.7	2.54	10.6
17	-	-	-	-	2.78	18.5
18	-	-	-	-	3.02	32.0

N_m = number of stars per square degree brighter than visual magnitude m_{vis}.

ZN_m = average number of stars to be expected in the field of the offset guider.

To be sure of having a guide star in the field for 95% of all stars, we need to have:

$$(ZN_m) - 1.645\sqrt{(ZN_m)} > 1$$

i.e. $(ZN_m) > 4\frac{1}{2}$ (Assuming Poisson statistics)

It seems that at least in theory the guiding system will meet our needs. However we have not taken vignetting into account, and this may well account for half a magnitude. In fact, in practice things are not nearly so satisfactory. A mirror badly in need of aluminising, a poor eyepiece and difficulties with both the crosshead and the focussing have made guiding a great problem on the telescopes on which it has been required. On telescopes smaller than 60 inches aperture, the off-axis errors introduced at the edge of the field give images highly affected by coma. This again reduces the number of stars available for guiding.

In conclusion, it seems that while this method of offset guiding is the correct approach, the present implementation could be improved.

2.2 The waveplate wheel

In front of the modulator is located a filter wheel with nine positions, dubbed the 'polariser' wheel by the project engineer. It is rotated by a stepper motor between positions defined by an optical encoder. The gearing ratio of 10 : 1 implies a step size of $0^{\circ}.1$. The wheel is bored with code holes such that the photodiode of the optical encoder only sees the LED when a position is located. The diameter of the code holes is equivalent to about 2° in the rotation of the wheel. The wheel always rotates in the same direction and should position repeatably to $0^{\circ}.1$.

In the wheel are mounted two sets of three retarders. Both sets contain two quarter wave plates mounted with their fast axes nominally at 45° to each other, and a

calibration filter. The actual value of this angle was measured in the laboratory for both sets of optics. For the set to be used in the ultraviolet, it was $47^{\circ}.75 \pm 0^{\circ}.35$, and for the set to be used in the visual, it was $50^{\circ}.00 \pm 0^{\circ}.35$. Unfortunately, these values were measured only after the data presented later in this Thesis were obtained (and in fact in response to the effects this data showed). To adjust the angles of the waveplates' fast axes, the polarimeter must be dismantled. This makes fine tuning of these angles exceedingly difficult. The effect of these misalignments is discussed later. The calibration filter is a piece of HNP'B polaroid cemented to a further $\lambda/4$ waveplate, such that the axis of the polaroid is at 45° to the fast axis of the waveplate. The polaroid of the calibration filter is aligned with its axis nominally perpendicular to the stress axis of the modulator. If light is incident upon the polaroid side of the filter, light leaving it should be 100% circularly polarised at the design wavelength. The filter produces right handed polarisation which is measured as positive by the instrument. Each of the three waveplates are zero order retardation plates made of crystal quartz and are made of two components with their optic axes crossed such that the resultant retardance for paraxial rays is $\lambda/4$. For each of the two components, the three waveplates were cut from the same piece of material in order to produce plates as identical as possible. The two sets of plates are designed to give $\lambda/4$ retardance at 3800 Å and 5825 Å respectively. These are mechanical measures rather than optical ones, i.e. the

wavelength quoted is derived from the measured thickness of the plates and the published values of the birefringence of crystal quartz. Presumeably, therefore, no allowance is made for different batches of quartz, or in alignment errors in crossing the optic axes of the two components. Such alignment errors might also lead to differences between the waveplates. The manufacturer's (Continental Optics) quoted errors on the retarders are 3800 Å $\pm$ 50 Å and 5825 Å $\pm$ 80 Å (i.e. $\lambda/300$). The thickness of each of the two components of every waveplate was controlled to 0.2μ, and the fast axes were crossed to an accuracy of 1 arcmin.

The waveplates will not be quarterwave at other wavelengths. These components are in no way achromatic. For normal incidence retardance is given by the expression:

$$\tau_\lambda \simeq 2\pi (n_e - n_o) s/\lambda \qquad (2.2.1)$$

where: n_o, n_e = ordinary and extraordinary refractive indices

$n_e - n_o$ = birefringence of material

s = thickness of waveplate

λ = wavelength of light

There is an explicit dependence on wavelength in the term $1/\lambda$ and further, an implicit dependence in so far as $(n_e - n_o)$ is also dependant on wavelength. A graph of $(n_e - n_o)$ against λ for crystal quartz is given as figure A2. The variation of τ with λ in units of $\pi/2$ and normalised at 3800 Å and 5825 Å is given as table A1.

The angular aperture of the single order plates is limited to about 10°. This limitation arises because off-axis rays see a different birefringence depending on the

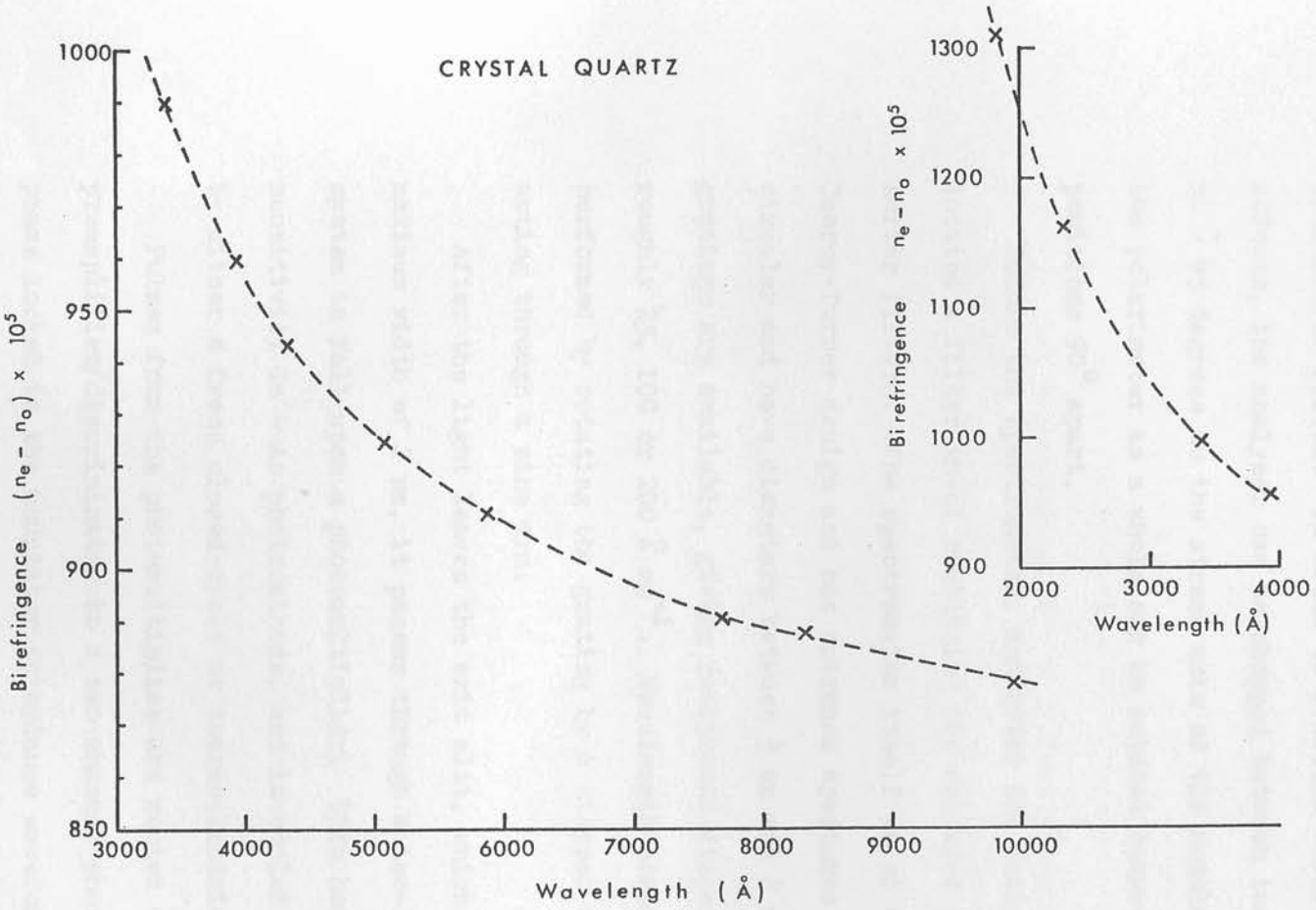

Figure A2: The birefringence of crystal quartz. Taken from the American Institute of Physics Handbook, 1972.

modulator. For the measurements of linear polarisation, two quarter wave retarders with fast axes 45 degrees apart are inserted sequentially before the modulator. The two waveplates are mounted in a wheel which also contains a calibration filter. In order to overcome various instrumental effects, the analyser can be chopped between two positions at $\pm$ 45 degrees to the stress axis of the modulator, while the polarimeter as a whole can be rotated between two positions 90° apart.

Before the spectrometer, and after the analyser is located a filter wheel containing the coloured glass order sorter filters. The spectrometer itself is of crossed Czerny-Turner design and has entrance apertures which are circular and have diameters between $\frac{1}{2}$ mm and 8 mm. Three gratings are available, giving reciprocal dispersions of roughly 25, 100 or 200 $\mathring{A}\ mm^{-1}$. Wavelength scanning is performed by rotating the grating by a stepper motor acting through a sine arm.

After the light leaves the exit slit, which has a maximum width of 2 mm, it passes through a two-lens Fabry system to fall upon a photomultiplier. This has a high sensitivity Ga - As photocathode, and is cooled to $-20^{\circ}C$ by either a freon closed-cycle or thermoelectric cooler.

Pulses from the photomultiplier are routed via a preamplifier/discriminator to a two channel photon counter phase locked to the modulator retardance waveform.

Data acquisition and reduction are handled by an HP 9810 calculator, interfaced to a fast cassette drive memory store and a plotter. The calculator also has the wavelength

angle of incidence. If the direction of incident light makes a small angle, i, with the normal to the surface of the retarder, and the plane of incidence makes an angle ψ with the optic axis of the crystal, the retardance at wavelength λ is given by (SERKOWSKI, 1974)

$$\tau \cong 2\pi (n_e - n_o)(s/\lambda)\left\{1 - \frac{i^2}{2n_o}\left(\frac{\cos^2\psi}{n_o} - \frac{\sin^2\psi}{n_e}\right)\right\} \quad (2.2.2)$$

where s, n_e and n_o have the same meaning as above. If the waveplate has two components of thicknesses s and s + δs with optical axes crossed, the resultant retardance is

$$\tau \cong 2\pi (n_e - n_o)\frac{\delta s}{\lambda}\left\{1 - \frac{i^2}{2n_o}\left(\frac{\cos^2\psi}{n_o} - \frac{\sin^2\psi}{n_e}\right)\right\}$$
$$- 2\pi (n_e - n_o)\frac{s}{\lambda}\cdot\frac{i^2}{2n_o}\cos 2\psi\left(\frac{1}{n_o} + \frac{1}{n_e}\right) \quad (2.2.3)$$

Consider the case of crystal quartz at 5080 Å. Then n_o = 1.54822, n_e = 1.55746 and δs = 13.7μ for a quarter waveplate (figures from the American Institute of Physics Handbook, 1972). Setting s = 1.5mm and ψ = 0, we find

$$\tau \simeq \frac{\pi}{2}(1 - 45.6\, i^2) \quad (2.2.4)$$

For a paraxial f/9 beam, i = 3°.2 at maximum, and for an f/16 beam, i = 1°.8, and therefore the retardance varies across the beam by 14.0% and 4.5% respectively for each focal ratio. The effect of this is to make the wavelength, λ_Q, at which the waveplate exhibits $\lambda/4$ retardance dependant on the focal ratio of the telescope, as an average is made over the whole beam. Such a property will not affect the measurement of linear polarisation but will make a slight difference to the circular measurement where λ_Q must be assumed.

2.3 The modulator

There are a number of materials that exhibit birefringence when stressed. Common examples are car windscreens and various plastics. Fused silica is such a material, and one which has the useful additional properties of being very hard and stiff, and being very transparent at visual, U.V. (to 90% at 180 nm) and I.R. (90% at 2.2μ) wavelengths.

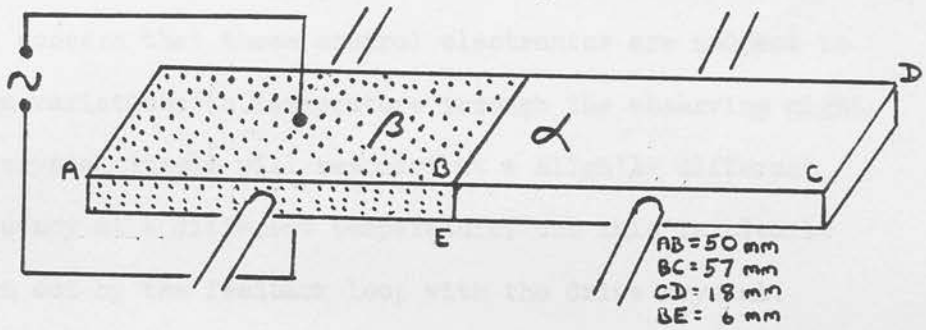

In the modulator, a fused silica bar (α) is cemented to a piezoelectric crystal (β), both crystals being supported at their centres. On the face of the piezoelectric crystal are attached foil electrodes. An initial pulse to the piezoelectric drive crystal starts the fused silica bar vibrating. Once oscillating the crystal will alternately compress and expand the piezoelectric crystal, so giving rise to an alternating voltage across the terminals of the driver. The drive electronics take this signal, amplify it, and feed it back to the drive crystal. The fused silica bar is hence maintained in oscillation at its resonant frequency. The waveform appearing across the terminals has at least one harmonic present and is not purely sinusoidal. It is shown below. The modulator control circuitry produces an accurately sinusoidal phase reference signal from this waveform and this is used to synchronise a two channel

counter. Some considerable shaping of the waveform is involved and careful regard to the phase of the resultant

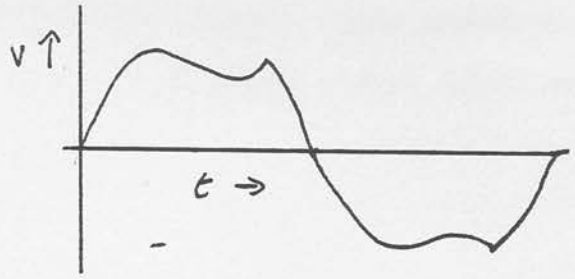

waveform is taken by the manufacturers. It is perhaps of some concern that these control electronics are subject to large variations in temperature through the observing night. The crystal itself will resonant at a slightly different frequency at a different temperature, but this is clearly taken out by the feedback loop with the drive crystal.

The resonant frequency of the fused silica bar is close to 50 kHz. Such a high chopping speed leads to some problems in the gating electronics in the counter, but a modulator which resonated at the more reasonable rate of 1 kHz would be unmanageably large. The fused silica crystal is supported at its centre in order to produce a node here. For modest exciting voltages, the crystal will oscillate sinusoidally to give a sinusoidally varying stress (and hence birefringence) as its node. Clearly the resultant birefringence is going to depend on distance from the node. In the ROE spectropolarimeter, the modulator lies some 134 mm from the focus of the telescope. At f/16, a point image at the focus would be formed by a cone which was 8.4 mm in diameter at the modulator. Since the largest aperture is 8 mm in diameter, this circle on the modulator may move up to 4 mm from the node. At this point the

birefringence will be reduced by a factor cos $(90 \times \frac{4}{28.5}) =$ 0.976 - about 2½%. We see that a field effect will arise, measured polarisation possibly being dependant on the position of the object in the aperture. If an object such as a planet was being observed and the planet filled a large proportion of the largest aperture, a slight centre-weighting in the measurement of the polarisation would result. The effect only arises along the one axis, and in the perpendicular axis all we need to confirm is that the entire beam passes through the modulator, and that no edge effects are present. In fact the limiting factor on the f/ratio of the beam that can be put into the instrument is the size of the modulator. Only the central 16 mm of the crystal are used in order to avoid edge effects caused by stress induced when the crystal was cut, or light scattered off the edges. A point source will spread out to 16 mm at the modulator if the focal ratio is f/8.4 or less. If we wish to use a 1mm aperture without problems, f/8.9 is the minimum focal ratio. Since the modulator is not baffled on either side (see diagram) use of telescopes faster than given by this limitation will lead to light reaching the spectrometer without having passed through

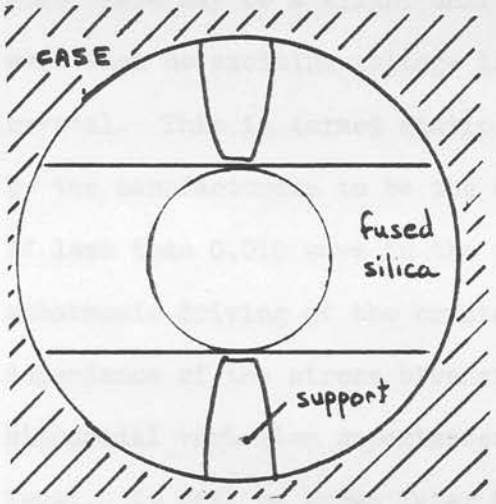

A photon's eye view of the modulator

the modulator, and hence to erroneous results. The instrument is seen not to be well suited to the larger telescopes ($\geqslant$ 90") that operate at f/9 or so. It will be recalled from a previous section discussing the polariser wheel, that waveplates are sensitive to the speed of the cone of light passing through them. However, as KEMP (1969) shows, a modulator, oscillating between $+\pi/2$ and $-\pi/2$ retardance, rather than $(N + \pi/2)$ and $-(N + \pi/2)$ is practically insensitive to the f-ratio.

Other small stress effects may affect the modulator. Any inhomogeneities in the fused silica crystal will affect the standing wave stress patterns and lead to further field dependence of the birefringence. Furthermore there may be a slight uniform stress in the crystal even when no exciting voltage is applied to the drive crystal. This is termed static stress, and is estimated by the manufacturers to be the equivalent of a retardation of less than 0.010 wave in the visual. A form of anharmonic driving of the crystal may lead to a time dependance of the stress birefringence equivalent to a sinusoidal variation superimposed on a non-zero constant level. It will be shown later (section A3) that both these effects are eliminated by taking measurements with the polarimeter in 0° and 90° orientations.

There are two sets of necessary calibration associated with the modulator. The first is to choose the size of the integration window within each half cycle. The second is to choose the excitation voltage to be used for each wavelength.

The first of these is preset in the present instrument. As will be discussed in the section on the counter, the window is set at 6.4μ sec (in a half cycle of 10μsec).

This is mainly for historical reasons and is not the optimum setting for this parameter. We should choose the integration window, 2Δ, such that the error in our measures of polarisation, σ, is minimised. Clearly, as Δ increases, the effective integration time increases, and σ decreases as more photons are counted. However, the larger the value of Δ, the worse is the fit of the sine wave to the ideal situation of square wave chopping from $+\pi/2$ to $-\pi/2$. The polarisation measured with the calibration filter, p_{CAL} or depolarisation factor, will hence decrease. This is our measure of efficiency of the polarimeter for the detection of polarised light, and each measure is subsequently corrected viz $p^1 = p/p_{CAL}$. Similarly, $\sigma' = \sigma/p_{CAL}$. Therefore we may say

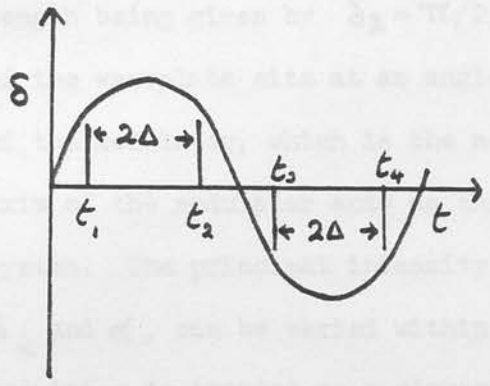

$$\sigma' \propto \frac{1}{p_{cal}\sqrt{\Delta}}$$

and this is the quantity to minimise.

A computer program was written to simulate the polarimeter in order to investigate this and other effects. The program uses the Mueller calculus to describe the various components in the optical train. The various

matrices are detailed in Appendix A1. Light, which is presumed unpolarised, is incident initially upon a calibration filter. This is modelled as a partial polariser, set with its axis at 45° to that of a waveplate which follows it. This waveplate gives $\pi/2$ retardance at wavelength, λ_Q, the dependence with wavelength being given by $\delta_\lambda = \pi/2 \times \lambda_Q/\lambda$. The fast axis of the waveplate sits at an angle α, to the stress axis of the modulator, which is the next component. The stress axis of the modulator acts as the defining axis for the system. The principal intensity coefficients, K_1 and K_2, λ_Q and α, can be varied within the program. The modulator is treated as a sinusoidally varying retardation plate, so:

$$\delta_t = \delta_{max} \sin\left(\frac{2\pi t}{T}\right) \qquad (2.3.2)$$

where: $T = 20$ μsec

$$\delta_{max} = \pi/2 \times \lambda_P/\lambda$$

λ_P can be set within the program. The final element is a further partial polariser (the analyser) which is set at either $\pm 45^{\circ}$ to the modulator stress axis. K_1^1 and K_2^1 for this polariser, and the sign of the angle are the variable parameters here. In matrix form, using the notation of Appendix A1, the optical train is represented as:

(2.3.3)

$$\begin{bmatrix} I' \\ Q' \\ U' \\ V' \end{bmatrix} = C_{\mp 45} A_{K_1' K_2'} C_{\pm 45} B_{\delta_t} C_{-\alpha} B_{\pi/2} C_{\alpha} C_{-(\alpha+45)} A_{K_1 K_2} C_{(\alpha+45)} \begin{bmatrix} I \\ Q \\ U \\ V \end{bmatrix}$$

The program acts as follows. After all parameters are set, including the wavelength under investigation, λ , the program works out the intensity transmitted through the system at each of twenty points in the modulator cycle (i.e. at 1 μsec intervals) and prints the values. The flux is then numerically integrated in the two windows, between t_1 and t_2 and between t_3 and t_4 and a polarisation and an intensity derived. t_{1-4} can be individually set. Figure 13 shows an example of the intensity waveform produced.

The program uses analytic expressions throughout, except for the numerical integration. For more complicated situations than the above, it would be easier and more flexible to allow the computer to multiply the various matrices together numerically. The numerical integration was done with a least square polynomial fit up to sixth order if necessary.

In the instrument we do not know the peak retardance δ_{max} to which the modulator is being driven. We know only the exciting voltage (MV) we are using. The relation between the two quantities should at least be roughly linear, but will depend on the exact properties of the two crystals. To choose the correct exciting voltage for a given value of Δ and λ , p_{CAL} is maximised with respect to MV. This was done with the program and the following table produced.

2Δ (μsec)	p_{CAL}(max)%	$\delta_{max}/\pi/2$	$(p_{CAL}(max)\sqrt{2\Delta})^{-1}$ *
5	98.5	1.09	1.114
6.5	96.2	1.16	1.000
7	94.8	1.18	.978
7.5	91.3	1.25	.952
(8.5)	interpolated		.950
9	85.8	1.27	.953

* normalised to 2Δ= 6.5μsec.

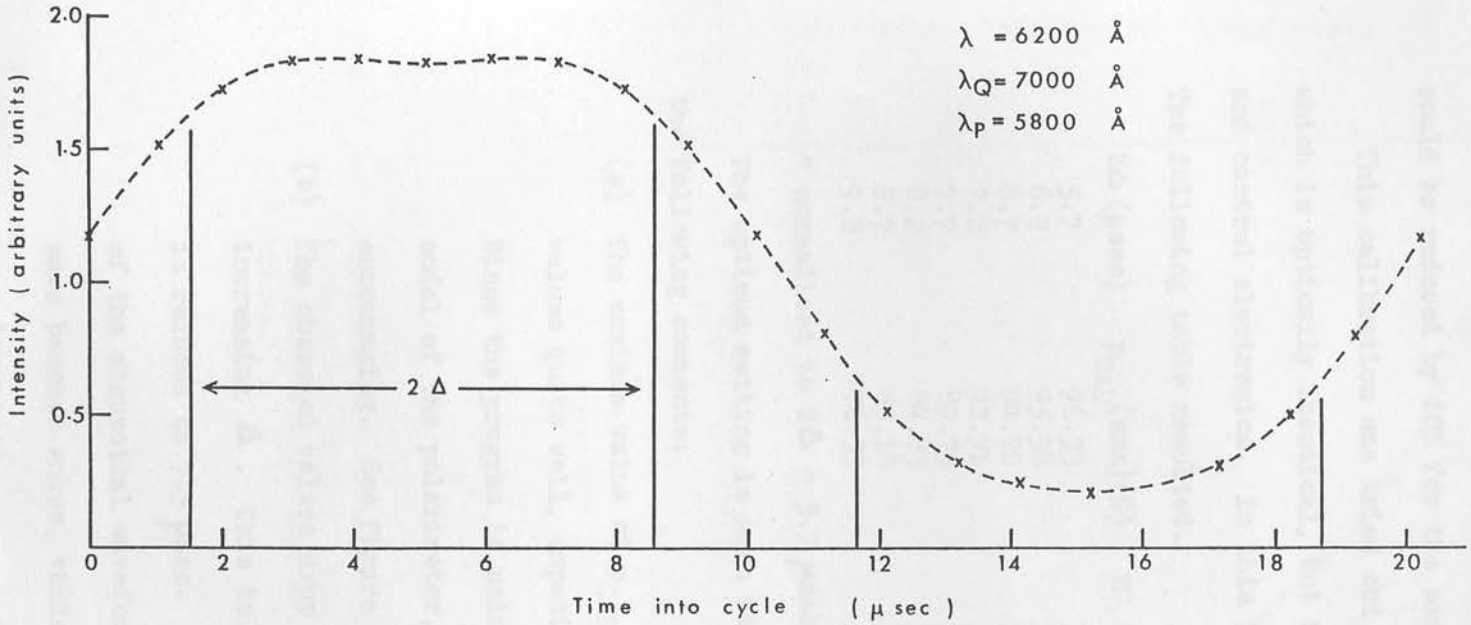

Figure A3: The Intensity waveform after the analyser, shown as a function of modulator phase. Results from a computer simulation with a calibration filter inserted in the beam. The integration windows of the two-channel counter are shown.

The optimum value of Δ is hence seen to be around 4.25 μsec. If Δ were changed in the ROE spectropolarimeter, according to these figures, integration times on objects could be reduced by 10% for the same error.

This calibration was tried out on another polarimeter which is optically identical, but has improved reduction and control electronics. In this instrument, Δ is adjustable. The following table resulted.

2Δ (μsec)	p_{CAL}(max)(%)	MV (volts)	$(p_{CAL}(\max)\sqrt{2\Delta})^{-1}$*
5.7	96.33	3.50	1.000
6.2	95.38	3.55	.968
6.7	94.20	3.65	.943
7.2	92.71	3.74	.925
7.7	89.73	3.77	.924
8.2	84.83	3.80	.947
8.7	80.18	3.79	.973
9.2	76.33	3.81	.993

* normalised to 2Δ = 5.7 μsec

The optimum setting is seen to be ~ 7.5μsec. We can make the following comments:

(a) The maximum value of p_{CAL} matches the theoretical values quite well, especially at lower values of Δ Since the program is using a reasonably crude model of the polarimeter, the agreement is encouraging. See figure A4.

(b) The observed values drop off more rapidly with increasing Δ . This is how the optimum setting is reduced to 7.5 μsec. It seems that as the fit of the sinusoidal waveform to the ideal square wave becomes worse, various non-idealities become more important.

(c) The ratios of values $(MV)_{\Delta_1}$ /$(MV)_{\Delta_2}$ do not agree

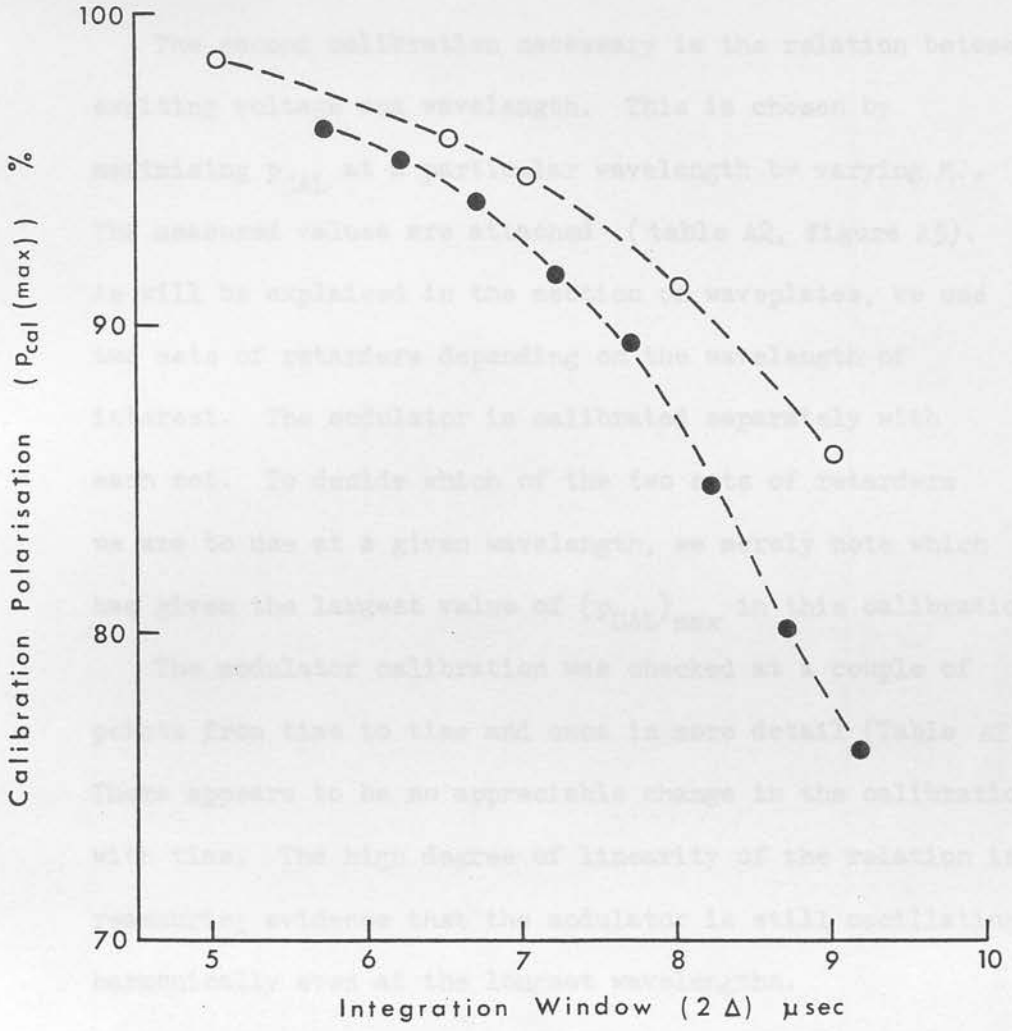

Figure A4: Dependence of calibration polarisation on width of the integration window. Open circles are predicted value (computer simulation) while filled circles are measured values.

well with $(\delta_{max})_{\Delta_1} / (\delta_{max})_{\Delta_2}$ found by the simulation.

The second calibration necessary is the relation between exciting voltage and wavelength. This is chosen by maximising p_{CAL} at a particular wavelength by varying M_1. The measured values are attached (table A2, figure A5). As will be explained in the section on waveplates, we use two sets of retarders depending on the wavelength of interest. The modulator is calibrated separately with each set. To decide which of the two sets of retarders we are to use at a given wavelength, we merely note which has given the largest value of $(p_{CAL})_{max}$ in this calibration.

The modulator calibration was checked at a couple of points from time to time and once in more detail (Table A2). There appears to be no appreciable change in the calibration with time. The high degree of linearity of the relation is reassuring evidence that the modulator is still oscillating harmonically even at the longest wavelengths.

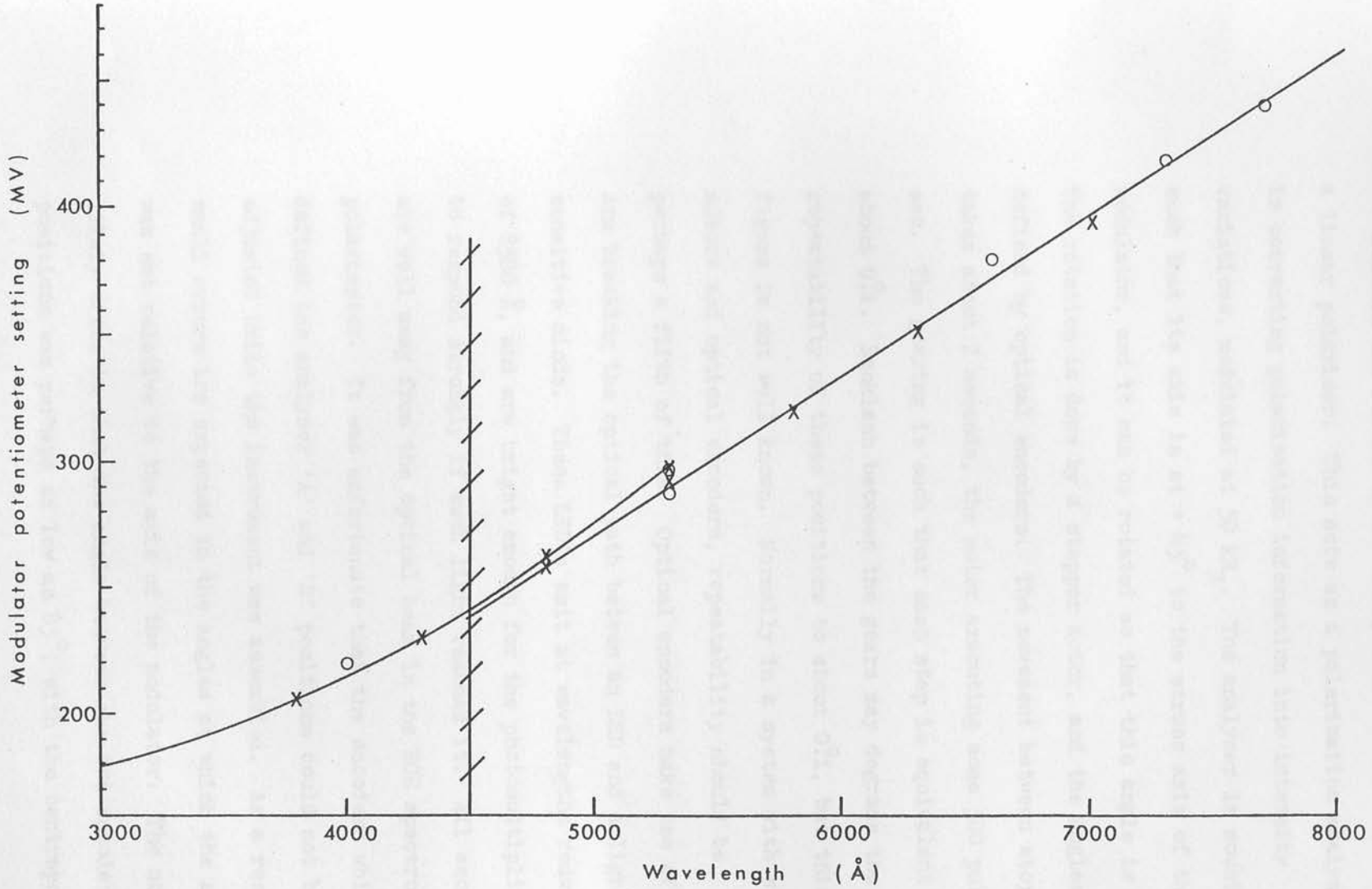

Figure A5: Adopted modulator calibration. For wavelengths below 4500 Å, the λ_0 = 3800 set of waveplates were normally used. Crosses refer to measurements made on 8th October, 1977, while open circles represent the measurements of 25th January, 1979.

2.4 The Analyser

Beneath the modulator in the optical train, there is a linear polariser. This acts as a polarisation analyser in converting polarisation information into intensity variations, modulated at 50 kH_Z. The analyser is mounted such that its axis is at + 45° to the stress axis of the modulator, and it can be rotated so that this angle is - 45°. The rotation is done by a stepper motor, and the angles are defined by optical encoders. The movement between stops takes about 2 seconds, the motor executing some 500 pulses/sec. The gearing is such that each step is equivalent to about 0°.1. Backlash between the gears may degrade the repeatability of these positions to about 0°.1, but this figure is not well known. Normally in a system with stepper motors and optical encoders, repeatability should be perhaps a fifth of this. Optical encoders make use of an arm breaking the optical path betwen an LED and a light sensitive diode. These LED's emit at wavelengths redward of 8500 Å, and are bright enough for the photomultiplier to respond strongly if such light reaches it. All encoders are well away from the optical beam in the ROE spectro-polarimeter. It was unfortunate that the encoders which defined the analyser 'A' and 'B' positions could not be adjusted while the instrument was assembled. As a result, small errors are expected in the angles at which the analyser was set relative to the axis of the modulator. The most likely error is that the angle between the two encoder positions was perhaps as low as 85°, with the centrepoint

displaced no more than a degree or so from the axis of the modulator.

The linear polariser is a piece of Polaroid Corporation's HNP'B polaroid. The material is available as a butyrate lamination which is only 150μ thick. The filter is cemented onto a metal ring. Almost inevitably, the filter warped badly during the cementing process, but even so no distortion of the image seems to arise. One unwelcome effect is the amount of light that is reflected from the upper (and lower) surface(s).

HNP'B becomes birefringent at wavelengths greater than $\sim$8200 Å. Measured polarisation with the calibration filter inserted is very low ($\sim$ 10%) at these wavelengths, and there are reasons to believe that some effect appears at shorter wavelengths than this. Consider the Figure A6. Here, measures of polarisation are recorded with the calibration filter inserted in the four states of the instrument, i.e. with the analyser lying at + 45° to the modulator ("A" position) and - 45° ("B" position) and with the polarimeter at 0°, and 90° positions. Note the increasing divergence between polarisations measured in the 0° and 90° positions. The difference between polarisation measured for different positions of the analyser are understandable, and will be dealt with in detail later. However, with the calibration filter in the beam, all polarisation information from the source of light (in this case Jupiter) is destroyed by the linear polariser which is the first optical element in the beam. Any difference between the polarisations measured in the 0° and 90° positions must arise therefore in the

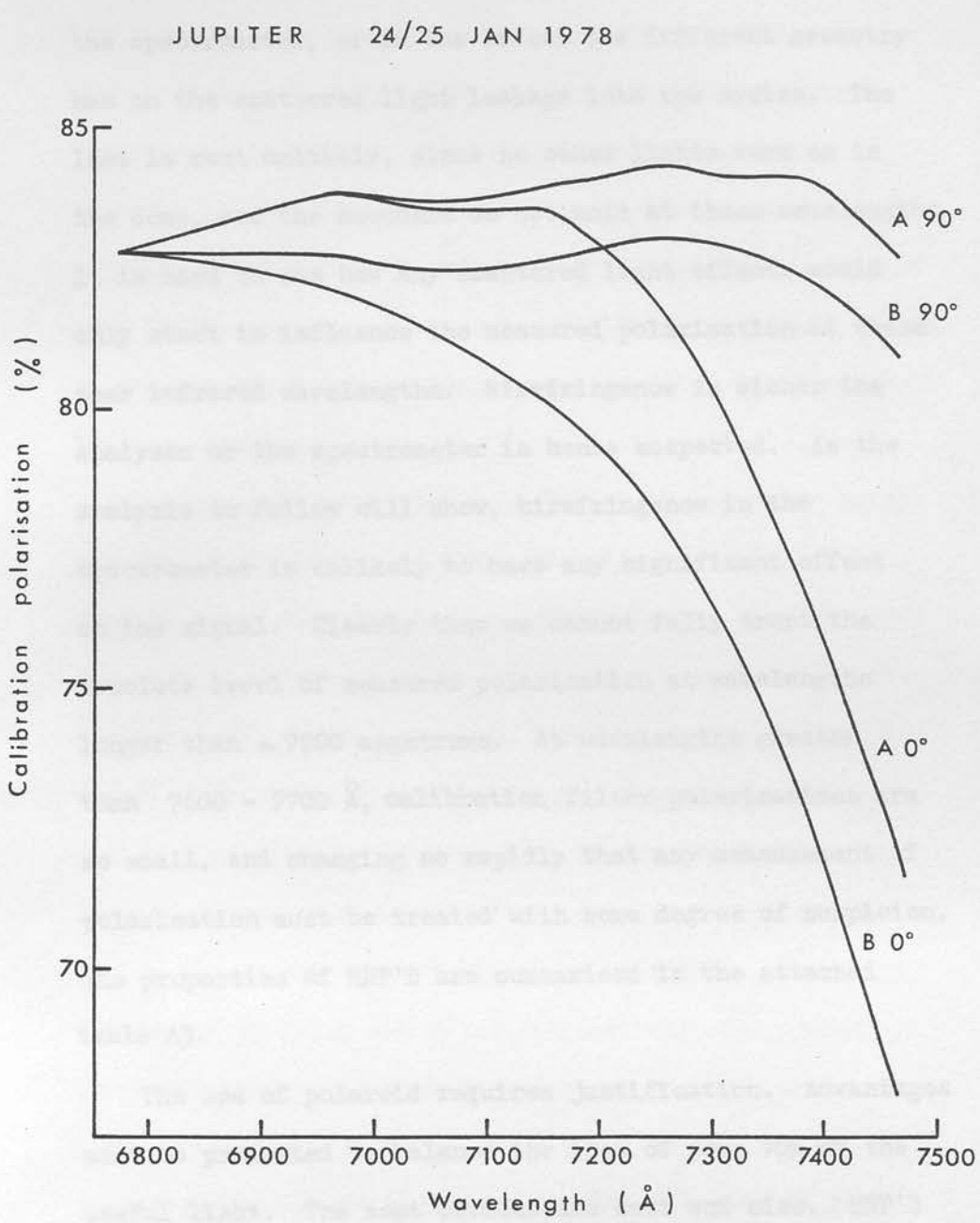

Figure A6: Measured calibration polarisations of Jupiter. 0° and 90° refer to orientation of polarimeter, while A and B refer to orthogonal positions of the analyser.

interaction of the light emerging from the polarimeter with the spectrometer, or in the effect the different geometry has on the scattered light leakage into the system. The last is most unlikely, since no other lights were on in the dome, and the encoders do not emit at these wavelengths. It is hard to see how any scattered light effects would only start to influence the measured polarisation at these near infrared wavelengths. Birefringence in either the analyser or the spectrometer is hence suspected. As the analysis to follow will show, birefringence in the spectrometer is unlikely to have any significant effect on the signal. Clearly then we cannot fully trust the absolute level of measured polarisation at wavelengths longer than ~ 7200 angstroms. At wavelengths greater than 7600 - 7700 Å, calibration filter polarisations are so small, and changing so rapidly that any measurement of polarisation must be treated with some degree of suspicion. The properties of HNP'B are summarised in the attached table A3.

The use of polaroid requires justification. Advantages must be presented to balance the loss of some 70% of the useful light. The most obvious are cost and size. HNP'B is still only about £5 per square inch, and its thickness means that it neither significantly affects the focus of the beam, nor causes image motion when rotated. Hence it does not have to be precisely flat. Its major advantage lies in its very wide field. Since there is no necessity to collimate the light for the modulator, the analyser, or any interference filters, we can dispense with the usual

collimating lens before the analyser. This lens can give instrumental polarisation through strain birefringence - particularly limiting in the measurement of very small circular polarisations. The chief drawback of using polaroid is the light loss. Its reflectivity can be countered by tilting it, though this is not (deliberately) done in the present instrument. The onset of birefringence in the red and the high opacity in the ultraviolet are both limiting factors.

A prism polariser such as a Rochon or Wollaston would be more difficult to use than polaroid. Rotation would require great care due to the prism's larger size and need for careful alignment. Its larger depth would remove the modulator yet further from the focus of the telescope (see above). While the field of view is nowhere as large as that for polaroid, values of 8° - 16° are usual which is about the angular aperture of the static waveplates we use in the measurement of linear polarisation. These correspond to f/7.1 and f/3.6 respectively, far faster than this instrument uses in practice. A prism could produce a beam of light at least 99.9% polarised (in both beams) over the entire wavelength interval to which the photomultiplier is sensitive, with little light loss ($K_1 \sim 0.9$). The use of both beams would be rather difficult as both the analyser and the entire polarimeter separately rotate. There are problems, too, in trying to put two beams through the spectrometer. Even so, an increase in the system throughput of 50% could be made by using just one beam of a polarising prism. The useful wavelength interval would also increase.

2.5 The Spectrometer

The grating spectrometer used is a GCA/McPherson, model 218, which employs the crossed Czerny-Turner configuration. The optical schematic is shown as figure A7 . Light is focussed by the telescope onto the entrance aperture A, and diverges again until it reaches the collimating mirror B, some 30 cm away. This mirror, roughly 55 mm square, produces a parallel beam of light for the grating (C). Depending on the angle at which the grating is sitting relative to the oncoming light, quasi-monochromatic light of a certain wavelength is diffracted, still parallel, to the camera mirror D which reimages it onto the exit slit E. B and D are identical aspheric mirrors in order that off-axis effects should disappear by symmetry. The entrance and exit slits, the grating and both mirrors are all coplanar. An eyepiece can be inserted into the optical train at F, in order to check that the object being observed is centred and in focus in the entrance aperture. Use of the crossed configuration leads to a compact design which is easier to baffle against stray light and does not call for the two subsidiary 45° mirrors just inside the exit slit and entrance apertures which other spectrometers use to direct the beam. This cuts down on light loss, but leaves the exit slit somewhat inaccessible. The spectrometer is in fact designed for work in the vacuum ultraviolet and is hence very rigid and was, originally, airtight. Wavelength scanning is performed by a lead screw acting on a sine bar and driven by a stepper motor. This tilts the grating and hence

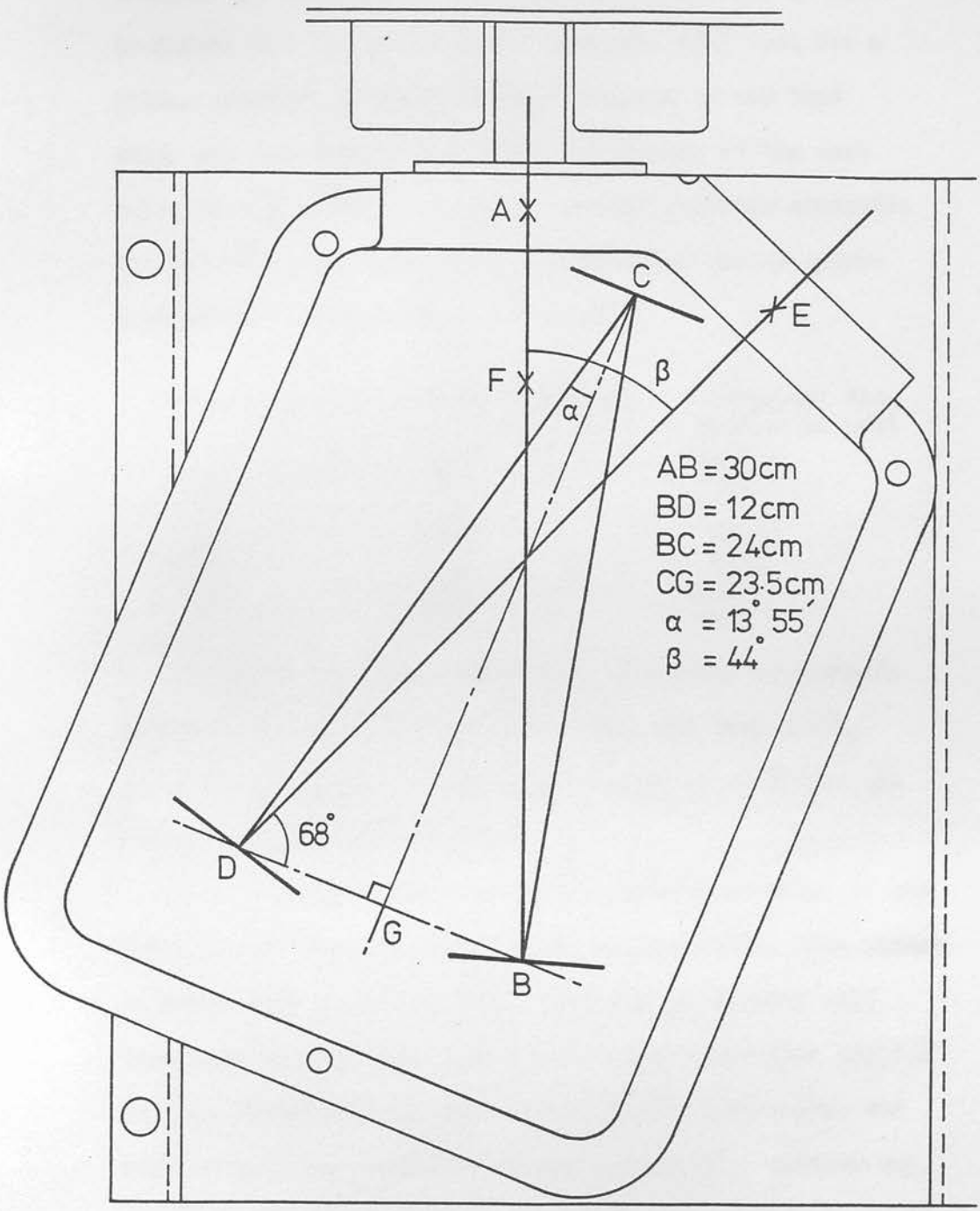

Figure A7: Schematic diagram of the McPherson monochromator, showing dimensions.

changes the wavelength. The driving arrangement is shown as figure A3. It can be shown (Appendix A3) that for a linear relation to exist between rotation of the lead screw and the central wavelength diffracted to the exit slit, $\alpha + \beta = 90^{\circ}$. There are several gratings available for use with this instrument, and they are easily interchangeable. Details are given below:

Ruling density grooves mm^{-1}	Blaze Wavelength (Å)	Reciprocal dispersion at exit slit Å mm^{-1}
1200	5000	26.5
1200	1200	26.5
300	5000	106.1
150	5000	212.2

If λ_B is the blaze wavelength, a grating is normally regarded as useful between $\lambda > 2/3\,\lambda_B$ and $\lambda < 3/2\,\lambda_B$. The grating with λ_B = 1200 Å is seen to be of little use for an astronomical instrument.

If a grating is inserted at an angle by mistake, or the angle is not correctly set by the manufacturers, this linear relation will no longer hold. The true wavelength will then vary by more than just a zero point correction applied to the counter mechanically linked to the lead screw, and will involve the cosine of an angle near 90°. Another way in which a wavelength error dependant upon wavelength could arise is a mismatch between the true and assumed proportionality constant between wavelength and the angle of the lead screw.

All the available gratings are 51 mm square. If the whole grating is to be used (for the highest resolution), the spot of light on the collimating mirror must be 51 mm in diameter, and hence the focal ratio of the incoming light

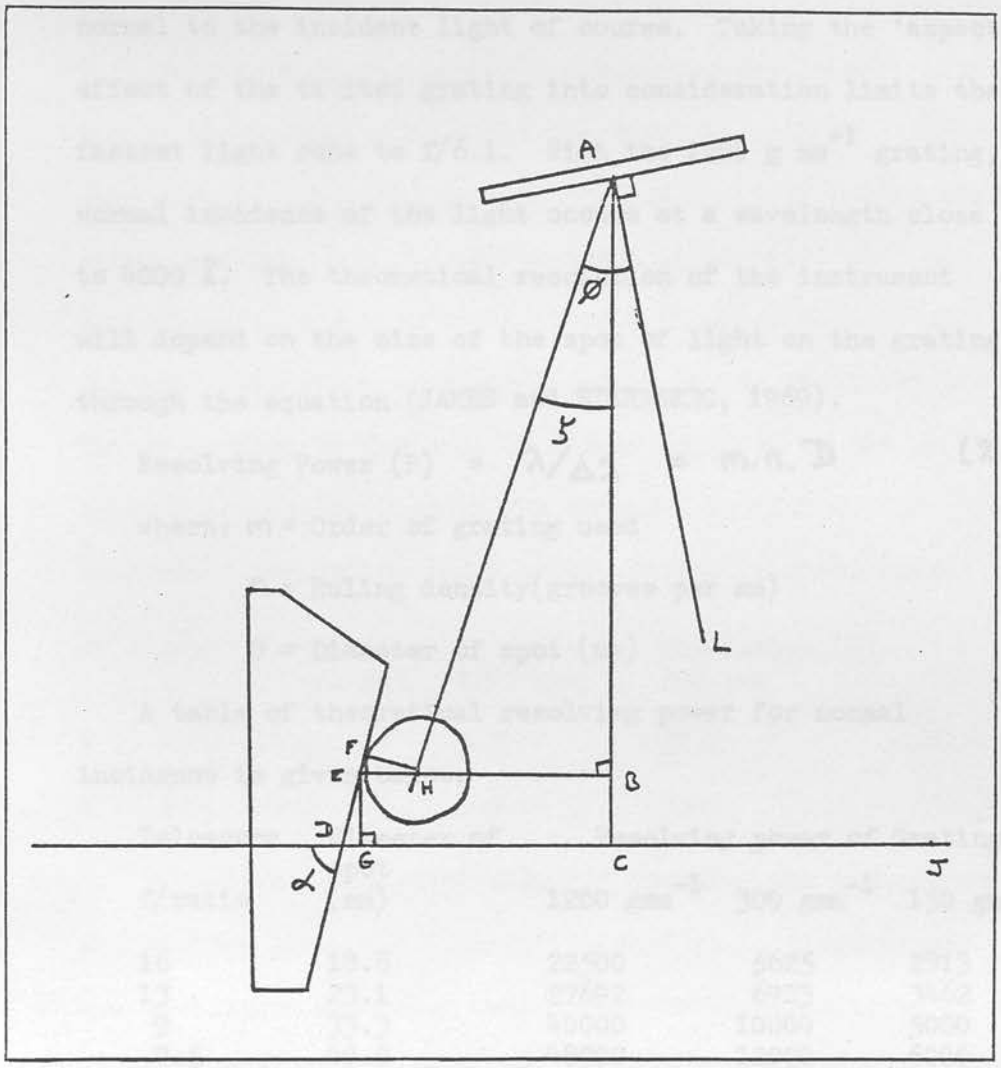

Figure A8: McPherson monochromator sine arm driving arrangement for the rotation of the grating. A = grating. DGCJ is a lead screw.

should be f/5.9. This is only for the case of the grating normal to the incident light of course. Taking the 'aspect' effect of the ti lted grating into consideration limits the fastest light cone to f/6.1. With the 1200 g mm^{-1} grating, normal incidence of the light occurs at a wavelength close to 4000 Å. The theoretical resolution of the instrument will depend on the size of the spot of light on the grating through the equation (JAMES and STERNBERG, 1969).

Resolving Power (R) = $\lambda/\Delta\lambda = m.n.D$ (2.5.1)

where: m = Order of grating used

n = Ruling density(grooves per mm)

D = Diameter of spot (mm)

A table of theoretical resolving power for normal incidence is given below:

Telescope f/ratio	Diameter of spot (mm)	Resolving power of Grating 1200 gmm^{-1}	300 gmm^{-1}	150 gmm^{-1}
16	18.8	22500	5625	2813
13	23.1	27692	6923	3462
9	33.3	40000	10000	5000
7.5	40.0	48000	12000	6000

When considering f/16 and incorporating the aspect effect, these figures correspond to the following resolutions ($\Delta\lambda$) at 3000 and 8000 angstroms:

Wavelength (Å)	Resolution for grating (Å) 1200 gmm^{-1}	300 gmm^{-1}	150 gmm^{-1}
3000	0.13	0.53	1.07
8000	0.37	1.48	2.96

The figures show that the spectral resolution is not limited by the gratings used, the following factor being more important. Consider again the optical schematic and consider the case of the grating acting merely as a mirror,

i.e. operating in zero order. Any motion of the star in the entrance aperture in the direction given by the arrow will lead to a corresponding displacement at the exit slit and as the McPherson is a 1 : 1 system, it will be of the same amount. When the grating is used in first order, the effect remains, but now any movement at the exit slit is equivalent to a change in wavelength. Hence bad guiding can lead to serious wavelength errors, as we shall see later. Our resolution in the case of a star is given by the apparent size of the seeing disc in the entrance aperture. The equivalent resolution for 2 arcsec seeing is given below:

Telescope	Platescale (" per mm)	Resolution (Å) 1200 gmm^{-1}	300 gmm^{-1}	150 gmm^{-1}
f/13 60") f/9 90")	10.0	5.3	21.2	42.4
f/16 60"	8.5	6.3	25.1	50.3

The above calculation was made assuming the reciprocal dispersions given previously. In fact these dispersions are wavelength dependant because of the aforementioned 'aspect' effect. In fact, if Δx is a displacement at the entrance aperture, and Δy the corresponding change at the exit slit, then:

$$\Delta y = \frac{\cos \theta_i}{\cos \theta_d} \Delta x = m \Delta x \qquad (2.5.2)$$

where θi = angle between incident light and grating normal

θd = angle between diffracted light and grating normal

The constant m is quite strongly dependant on wavelength

λ(Å)	m
3000	1.098
4000	1.135
5000	1.175
6000	1.220
7000	1.270
8000	1.328

In cases when the resolution is limited by the size of the image in the entrance aperture, this will imply a change in the resolution of over 20% over the spectrum for one setting of the exit slit. Calculations of the reciprocal dispersion using details given in the McPherson manuals gave 25.4 Å mm^{-1} at normal incidence (i.e. around 4000 Å). It is not clear to which wavelength the quoted reciprocal dispersion (26.5 Å mm^{-1}) referred and it may be that the published dimensions are approximate only. In other parts of this Thesis, when mention is made of resolution this is calculated from the manufacturer's figure and presumed wavelength independant. In critical cases, reference can be made back to the above table and the quoted resolution corrected.

The entrance apertures are circular and of diameters 8, 4, 2, 1 and ½ mm. Their cross-sections are illustrated in the diagram below. The diameters correspond to 68, 32, 16, 8 and 4 arcsecs for an f/16 60" telescope, and 80, 40, 20, 10 and 5 arcseconds for f/13, 60" or f/9, 90" telescopes. In the present configuration, then, the highest resolution that the instrument is capable of is about 5 angstroms. Very good guiding is necessary to maintain the position of the centre of the wavelength band at these relatively high resolutions. If a star had drifted across the smallest aperture, the wavelength selected by the exit

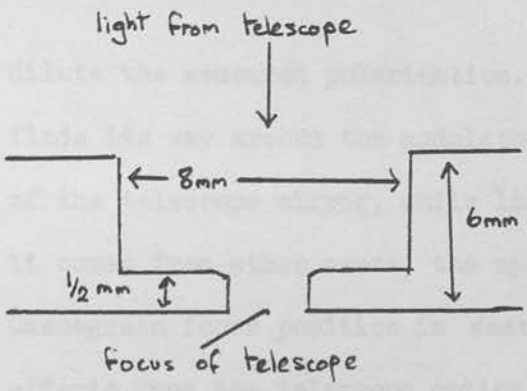

slit would have shifted by ~ 13 angstroms. A combination of poor illumination of the apertures and the low magnification (actually negative!) of the McPherson eyepiece meant that it was difficult to centre the star to an accuracy of, say, better than $\pm \frac{1}{4}$ mm, i.e. somewhere within the smallest aperture.

It was mentioned in the section on the modulator that the width of that component formed the limit to the speed of the light cone that could safely be put into the polarimeter. This limitation changes with aperture, as is given below. It can be seen that this instrument is not well suited to large (D > 1.5 m) telescopes which operate at ~ f/9.

Aperture	Minimum f/ratio
8mm	16.8
4mm	11.2
2mm	9.6
1mm	8.9
$\frac{1}{2}$mm	8.6
Point Source	8.4

If this limitation is exceeded, light will enter the spectrometer without passing through the modulator. This will dilute the measured polarisation. Since the light which finds its way around the modulator comes from certain areas of the telescope mirror, while light which does pass through it comes from other areas, the spherical symmetry of the Cassegrain focus position is destroyed and polarisational effects from the telescope optics may start to intrude.

The McPherson was calibrated in wavelength against a Helium spectral lamp before each observing run and this was redone if a grating was removed or replaced. The image of a pinhole illuminated by the spectral lamp - some 2 mm across - was focussed onto the smallest aperture.

Occasionally larger apertures were used to increase the flux. Measures of intensity were taken on either side of the peak of a spectral line, and averaged to give the instrumental wavelength of the line. This method (due to Mr A. Pickup) is more accurate than attempting to locate the maximum flux, as the gradient of flux against wavelength is steep at the measurement points. While the method assumes that the spectral lines are symmetric, slightly assymetric profiles were occasionally obtained with the spectral lamp. They would arise through miscentring of the image of the lamp in the aperture, leading to intensity variations across it. In such a case the zero point calibration will be in error too. In short, while the measurement accuracy was $\pm$ 1 Å, the precision of the correction would be more of the order $\pm$ 3 Å. On one run a dependence of the wavelength error with wavelength was found for the 1200 gmm^{-1} (Blaze 5000 Å) grating. This is shown as figure A9, and is attributed to the grating seating slightly differently in its holder (see appendix A3).

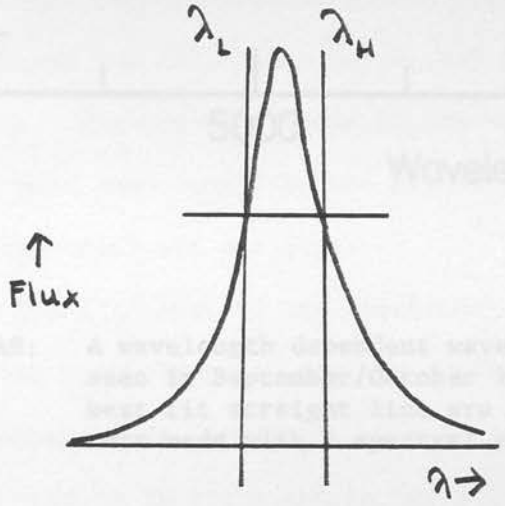

The exit slit is variable from zero (actually 5 microns) to 2 mm. The micrometer screws is marked in 10μ intervals and is backlash free to at least one interval. One complete revolution is equivalent to 200μ. 10μ would correspond

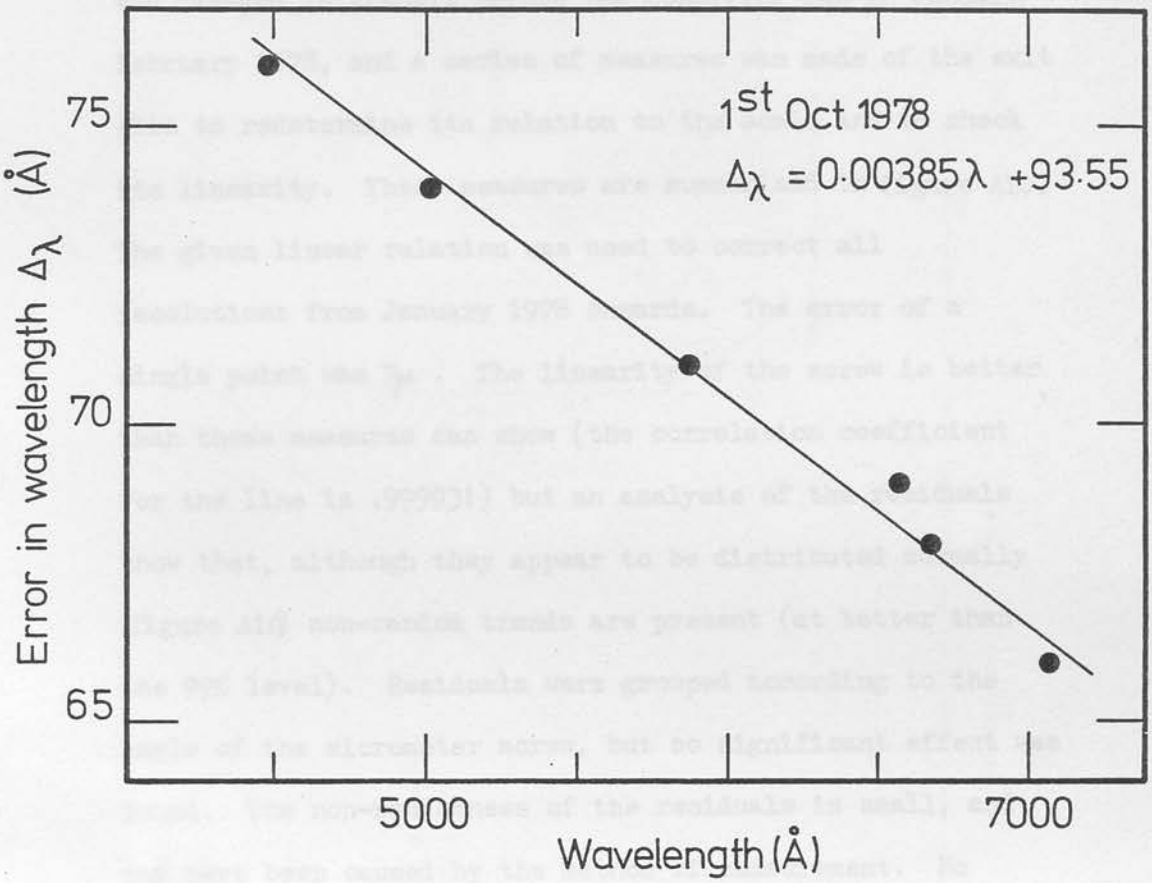

Figure A9: A wavelength dependent wavelength calibration error seen in September/October 1978. The equation of the best fit straight line are given. These measurements were made with a spectral source.

to 0.27 Å with the 1200 gmm^{-1} grating, 1.06 Å with the 300 gmm^{-1} grating, and 2.12 Å with the 150 gmm^{-1}. The micrometer screw was damaged in transit before the observing run in January/February 1978, and a series of measures was made of the exit slit to redetermine its relation to the scale and to check its linearity. These measures are summarised in figure A10. The given linear relation was used to correct all resolutions from January 1978 onwards. The error of a single point was 7μ . The linearity of the screw is better than these measures can show (the correlation coefficient for the line is .99993!) but an analysis of the residuals show that, although they appear to be distributed normally (figure A10) non-random trends are present (at better than the 99% level). Residuals were grouped according to the angle of the micrometer screw, but no significant effect was found. The non-randomness of the residuals is small, and may have been caused by the method of measurement. No further analysis was done.

The alignment of the spectrometer is quickly checked before each observing run, by confirming that, with the grating set to zero order, the image of the entrance aperture is in focus and is central in the exit slit. Adjustments of the collimating and focussing mirrors serve to correct any misalignment found.

The McPherson selects the 1st order spectrum produced by the grating. This is the order with the largest free spectral range, i.e. the part of the spectrum where no contamination by other orders is possible. In the astronomical context, some form of pre-filtering of the

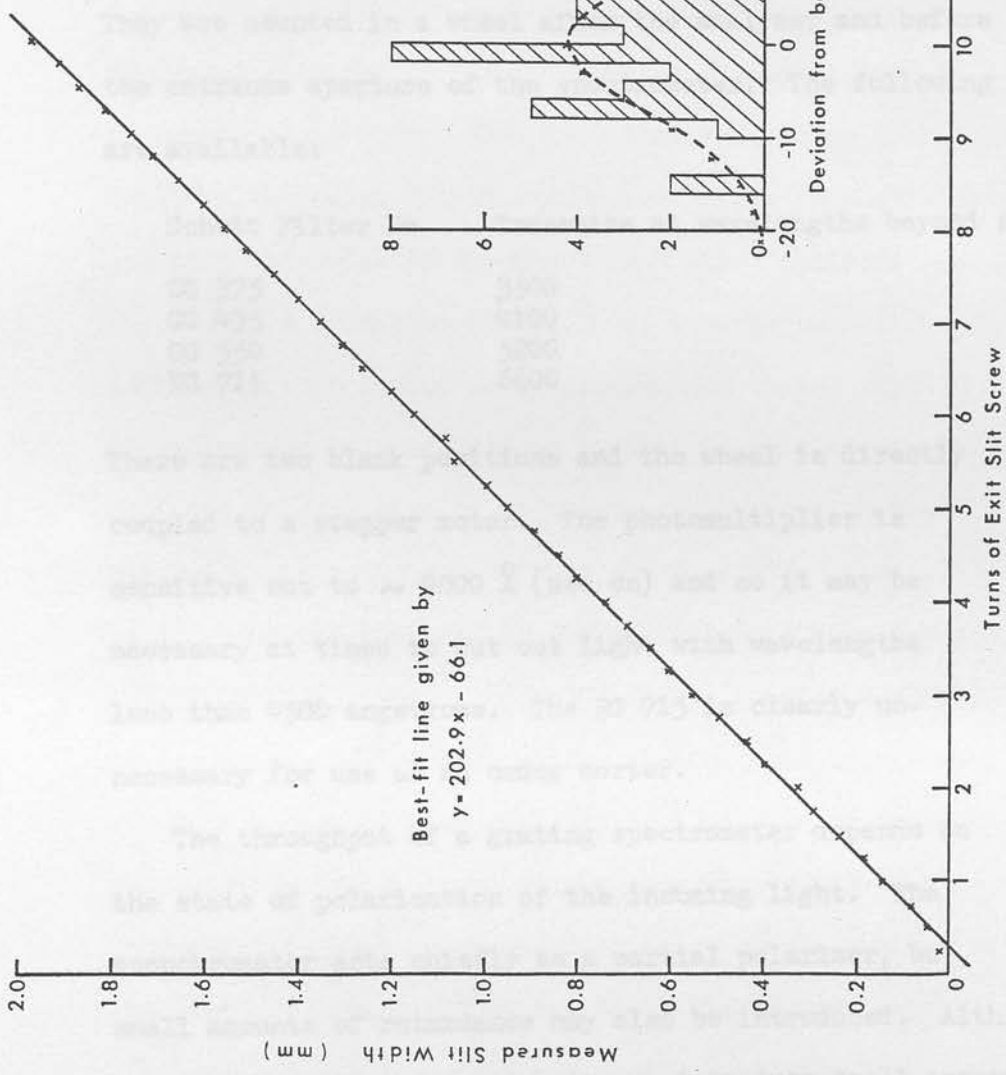

Figure A10 : Measurements of the width of the spectrometer exit slit, with best-fit straight line superimposed. The inset shows a histogram of the distribution of residuals with a gaussian curve of equal area.

light entering the spectrometer will be necessary when wavelength greater than 6000 angstroms are studied, as light at 3000 angstroms from the 2nd order spectrum will here start to contaminate the signal. To do this coloured glass Schott cut-on filters are used as order sorters. They are mounted in a wheel after the analyser and before the entrance aperture of the spectrometer. The following are available:

Schott Filter No	Transmits at wavelengths beyond :(Å)
GG 375	3500
GG 435	4100
OG 550	5200
RG 715	6600

There are two blank positions and the wheel is directly coupled to a stepper motor. The photomultiplier is sensitive out to $\sim$ 9000 Å (see on) and so it may be necessary at times to cut out light with wavelengths less than 4500 angstroms. The RG 715 is clearly unnecessary for use as an order sorter.

The throughput of a grating spectrometer depends on the state of polarisation of the incoming light. The monochromator acts chiefly as a partial polariser, but small amounts of retardance may also be introduced. Although both collimating and camera mirrors introduce small amounts of elliptical polarisation, the gratings act as the main source. There are several effects:

(a) A broadband polarisance, increasing away from the blaze wavelength.

(b) Narrowband effects at the Wood anomalies.

(c) A single broad peak in the polarisation.

(a) The broadband effect can easily polarise incoming light to 30 - 50% at large distances from the blaze wavelength, even in first order. The polarisation shifts in position angle by 90° at the blaze wavelength and this is probably the most accurate way of determining this quantity. A plot of polarisation against wavelength for the monochromator with the 1200 gmm^{-1} grating blazed at 5000 Å is presented as figure A11. Note that this graph also includes the polarisation dependance of the photomultiplier, and that this will be discussed in a later section.

(b) Wood's Anomalies (WOOD, 1902) are spurious light or dark bands that appear in a spectrum due to the rapid dependence of polarisation on wavelength in a narrow band. Only the transmission of light plane polarised in the direction perpendicular to that of the rulings (and slit) is affected and this can drop from 100% to 60% in 100 Å (BRECKINBRIDGE, 1971). RAYLEIGH (1907) pointed out that in his theory of the diffraction grating, his solutions showed a series of singular points. These would occur at wavelength at which light of the same wavelength is diffracted in another order so as to graze the surface of the grating. The wavelengths, the Rayleigh wavelengths (λ_R) were found to correspond to the Wood Anomalies. For a spectrometer of the design used in the ROE Spectropolarimeter, the Rayleigh wavelengths are given by the following expression:

$$\lambda_R = \frac{2a}{n+2R}\left\{\frac{1 \pm (2\sin\alpha\sqrt{R(n+R)}/(n+2R)}{1+(n\tan\alpha/(n+2R)^2}\right\} \quad (2.5.3)$$

Where a = grating spacing

n = order

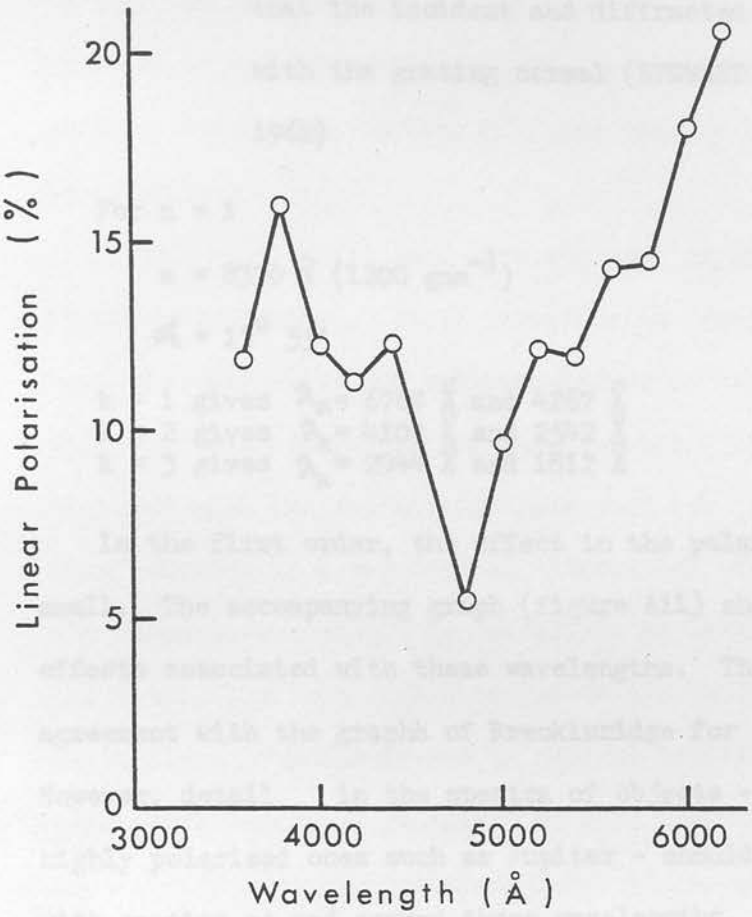

Figure A11 : The dichroic properties of the spectrometer. Unpolarised light entering the spectrometer is polarised to the amount shown. The grating used has 1200 grooves per millimetre, and is blazed at a nominal 5000Å.

$\alpha = \frac{1}{2}(\phi_i - \phi_d)$ and ϕ_i and ϕ_d are the angles that the incident and diffracted light make with the grating normal (STEWART and GALLAWAY, 1962)

For n = 1

a = 8330 Å (1200 gmm^{-1})

$\alpha = 13^\circ\ 55'$

k = 1 gives λ_R = 6769 Å and 4267 Å
k = 2 gives λ_R = 4109 Å and 2542 Å
k = 3 gives λ_R = 2944 Å and 1812 Å

In the first order, the effect in the polarisation seems to be small. The accompanying graph (figure A11) shows no obvious effects associated with these wavelengths. This is in agreement with the graphs of Breckinridge for zero order. However, detail in the spectra of objects - especially highly polarised ones such as Jupiter - should be treated with caution at and around these wavelengths.

(c) BRECKINRIDGE (1971) suggests that a single broad peak in polarisation (up to 90% in second order) might occur at a wavelength given by:

$$\lambda_p = 0.7\ a \cos\phi \qquad (2.5.4)$$

where $\phi = \frac{1}{2}(\phi_i + \phi_d)$

He appears to have been using a spectrograph arrangement, where wavelength scanning is achieved by moving the exit slit, and hence ϕ is held constant. In the case of the Czerny-Turner spectrometer, wavelength scanning is achieved by changing ϕ and we must solve with the grating equation:

$$n\lambda = 2a \sin\phi \cos\alpha \qquad (2.5.5)$$

Using the same values as above,

$\tan\phi = 0.35/\cos 13^\circ\ 55'$

Therefore $\phi = 19.^{\circ}8$ corresponding to a wavelength of 5487 Å. No peak appears in the attached graph (figure A11) and though it is possible that the specific blaze of this grating changes the factor, 0.7, the reality of the effect is questioned.

Finally, we shall deal with the problem of stray light in the spectrometer. It is necessary to consider the factor when discussing the ROE spectropolarimeter because of the wide spectral sensitivity of the detector (3000 to 9000 Å) compared with the small bandpasses used ($\leq$ 50 Å). The flux measured in a passband at ultraviolet wavelengths near the atmospheric cut-off can easily be as little as 10^{-4} of the total flux from that star detectable by the photo-multiplier. Monochromators in general exhibit relatively poor performances as isolators of pure spectral elements. An ordinary laboratory monochromator might have a rejection factor of only 10^{-3}, i.e. for $\lambda \neq \lambda$ SET, the transmitted intensity of wavelength λ is about 10^{-3} of the incident intensity. This compares with values of 10^{-4} to 10^{-5} and better for good interference filters. To reach these levels, two monochromators may be used, operating in "piggy-back" fashion, where one monochromator acts simply as a pre-disperser for the second. Some of this stray light arises because of the compactness and speed of the devices, since the wide beam and lack of room make effective baffling difficult. The McPherson 218 however is a large, relatively slow spectrometer, the crossed-beam design of which allows for efficient baffling against stray light. In this way, the effect of simple scattering by, for example, dust on the mirrors or grating, or reflectors from the inside of the

spectrometer has been reduced to at least the 10^{-4} level and probably even further. There is however a geometrical effect that allows certain wavelengths of light to be transmitted through the spectrometer besides the specific wavelength for which the instrument is set. The effect is known as 'double diffraction' and involves the light beam of a certain wavelength encountering the grating twice during its passage through the spectrometer. Suppose the grating is tilted at an appropriate angle to select a wavelength λ_o at the exit slit. Light of other wavelengths in this and other orders leaves the grating at various angles and in the main is absorbed by the blackened interior of the spectrometer or by the baffling provided. A proportion of this diffracted light will however strike the two mirrors (collimating and camera mirrors) and some of this, if certain geometrical conditions are satisfied, will be reflected back to the grating. Under these conditions, some of this light can be diffracted (for the second time) to the exit slit in a different order. The transmitted intensity of light at such a wavelength will however be greatly reduced in intensity. While the light beam is parallel when it encounters the grating for the first time, it will be focussed by the following mirror (whichever it might be) and will form an image on the grating at its second diffraction. Consequently the beam will not be focussed by the camera mirror onto the exit slit. A further reduction in the throughput for light of such a wavelength, as well as the extra losses from the extra components in the light path, will occur because the second

diffraction will not be in the same order as the first.

The problem has been investigated for this particular model of spectrometer (McPherson 218) by MARETTE (1969). His results indicate that no doubly-diffracted light can reach the exit slit when the spectrometer is set to a wavelength between 1600 Å and 4000 Å, while at 4500 Å (for example) light from wavelengths between 3350 Å and 4150 Å will contribute to the measured flux. Polarisation measurements collected on ζ Ophuichi at wavelengths near the ultraviolet atmospheric cut-off suggest that, on the contrary, stray light is important at 3000 Å (see Section 05). A simple experiment strongly supports the identification of double diffraction as the source of this stray light. If a light source illuminates the entrance aperture of the spectrometer, when the spectrometer is set to 3000 Å and one looks into the spectrometer through the exit slit, an image of the entrance aperture is clearly seen on the grating. The image appears deep blue in colour, suggesting that the mean wavelength of the light making up this image was $\sim$4000 Å. In conjunction with the discussion above, these observations suggest that light is reaching the exit slit after double diffraction. MARETTE (1969) only studied the doubly-diffracted light which follows the path entrance aperture - collimating mirror - grating - collimating mirror - grating - camera mirror - exit slit. The case where the light path included two reflections on the camera mirror was not covered. It is suggested therefore that this other case is important for the case of the McPherson 218 as it is in other spectrometers (e.g. PRIBRAM and PENCHINA, 1968).

The easiest way to avoid the problem of double difraction in the design stage of a new spectrometer is to arrange that the entrance aperture and exit slit are not in the same plane, tilting the collimating and camera mirrors to suit. When this is done, it is easy to see that no light diffracted from the grating can reach the collimating mirror, and any light reflected by the camera mirror cannot find its way back to the grating. In practice one has to make do with the instrument to hand. In this case, double diffraction can be eliminated at the cost of a lower transmission of the spectrometer. Light that reaches the grating for a second time is (nearly) focussed, and an image of the entrance aperture is formed on the grating. It follows therefore that if a mask is applied to the grating, as shown in the diagram below, this image cannot contribute to the flux reaching the exit slit. The height of the mask will be similar to the height of the exit slit. MARETTE (1969) gives a formula for the required dimensions of the mask.

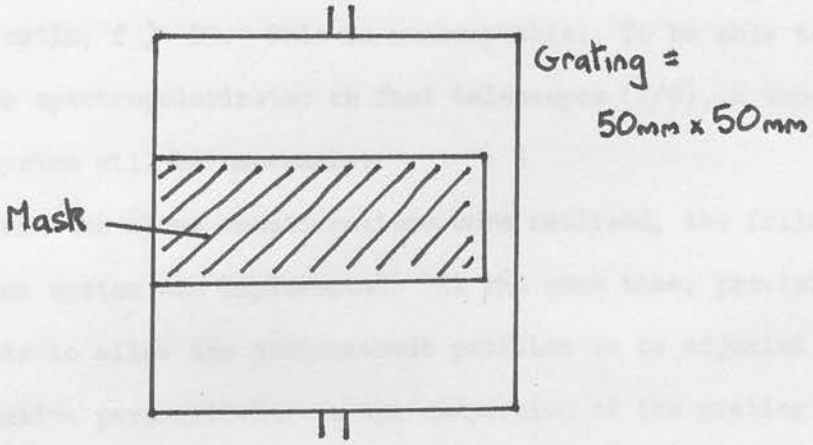

2.6 The detector

The image at the exit slit of the spectrometer is transferred to the photocathode of the photomultiplier by a system of Fabry lenses. The purpose of a Fabry lens is to produce an image of the telescope mirror on the photocathode, so that the photocathode will be uniformly illuminated wherever the star appears in the entrance aperture of the system. In order to do this, the Fabry lens (which need not be of high quality) must be its own focal length from the photocathode. In the present thermoelectric cooler, the physical layout of the device prevents the lens being closer than about 108 mm from the photocathode. The other limiting condition is that the size of the image produced on the photocathode must be smaller than the photocathode itself, for all telescopes on which the instrument is likely to be used. These two criteria give the following limitations on a single lens system:

(i) $F \lesssim 108$ mm (ii) $F/_f \lesssim 4$ mm

where F = focal length of the Fabry lens and f = focal ratio of the telescope. These conditions imply that an instrument with a single Fabry lens would be limited to telescopes with focal ratio, $f \gtrsim 29$. This is unacceptable. To be able to use the spectropolarimeter on fast telescopes (f/9), a two-lens system will be necessary.

When the above considerations were realised, the following two-lens system was implemented. At the same time, provision was made to allow the photocathode position to be adjusted in a direction perpendicular to the dispersion of the grating in

order that the most sensitive part of the photocathode could be used.

Lens	Diameter	Focal length	Type
1	25mm	30 mm	Planoconvex
2	50mm	60 mm	Biconvex

Both lenses are made of quartz and neither is anti-reflection coated. While an achromatic system would have been desireable, this would have lead to a severely reduced transmission of the system at wavelengths below 3500 Å. Achromatic ultraviolet-transmitting lenses can be obtained (they are made of magnesium fluoride and crystal quartz) but they are particularly expensive. Figure A13 shows the result of scanning a stellar image across the largest entrance aperture of the spectrometer. The scans are of the detected intensity against position in the aperture for three widely spaced wavelengths. The Fabry system is shown to be optimised for wavelengths near 5500 Å. At other wavelengths, the edges of the aperture appear to be somewhat vignetted. For the most accurate spectrophotometry, the Fabry system should be previously adjusted for the wavelength interval of interest. The lenses used are rather 'fast' (necessary to keep the unit compact) and will in consequence suffer enhanced light loss by reflection. This loss can be reduced dramatically by broad-band antireflection coating. Unfortunately the standard coatings (including multilayer coatings) lead to an increased light loss beyond the design range. While the wavelength interval 4000 - 7000 Å would have benefitted, the ultraviolet would again have suffered enhanced light losses.

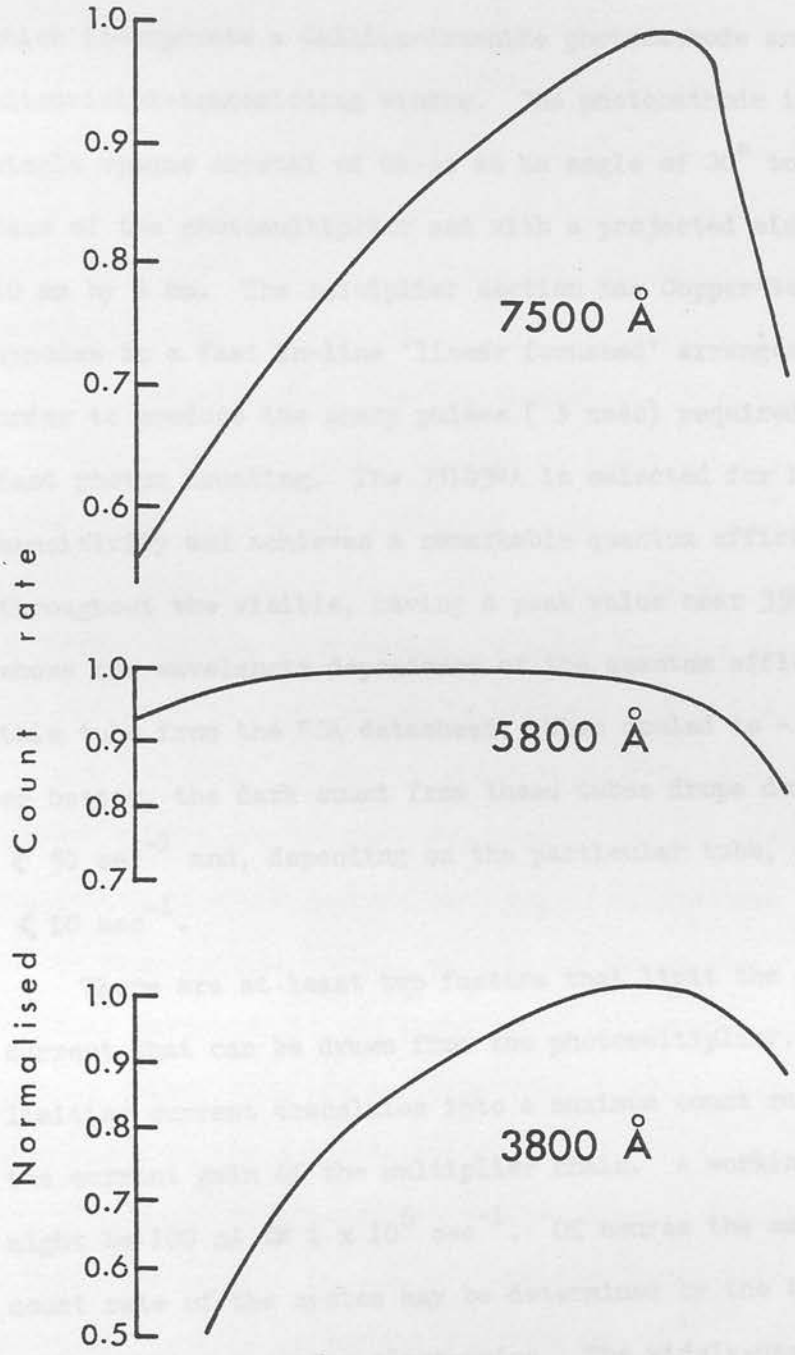

Figure A13 : Fabry scans. The effect of scanning a stellar image across the largest entrance aperture on the detected intensity. The image of the telescope mirror is seen not to be central on the photocathode.

The photomultipliers used are the RCA type C31034A which incorporate a Gallium-Arsenide photocathode and an ultraviolet-transmitting window. The photocathode is a single opaque crystal of Ga-As at an angle of 30^{o} to the face of the photomultiplier and with a projected size of 10 mm by 4 mm. The multiplier section has Copper-Beryllium dynodes in a fast in-line 'linear focussed' arrangement in order to produce the sharp pulses (5 nsec) required for fast photon counting. The C31034A is selected for high sensitivity and achieves a remarkable quantum efficiency throughout the visible, having a peak value near 35%. Table A6 shows the wavelength dependence of the quantum efficiency for this tube from the RCA datasheet. When cooled to - 20^{o}C or better, the dark count from these tubes drops down to $< 50\ sec^{-1}$ and, depending on the particular tube, sometimes $< 10\ sec^{-1}$.

There are at least two factors that limit the amount of current that can be drawn from the photomultiplier. This limiting current translates into a maximum count rate, given the current gain of the multiplier chain. A working figure might be 100 nA $\simeq 1 \times 10^{6}\ sec^{-1}$. Of course the maximum count rate of the system may be determined by the bandwidth of the photon counting electronics. The widely-used 1120 Princeton Applied Research preamplifier/discriminator is limited to about $2 \times 10^{6}\ sec^{-1}$ in actual operation by excessive counting losses (i.e. $>$ 10%). If the anode current taken from a photomultiplier exceeds $\sim 1\ \mu A$ (for tubes with roughly this number of dynodes) the response of

of the tube to incident light starts to become non-linear. Excessive exposure to light levels corresponding to anode currents in excess of 1 μA can lead to a permanent reduction in the sensitivity of the system. Simply put, the problem is in the cascade of photoelectrons onto the last dynode. If this becomes too great the dynode will literally start to evaporate under the bombardment and the performance of the tube will deteriorate. The RCA data sheets give the maximum safe anode current for the C31034A as 100nA but the limiting factor here is somewhat different. Gallium Arsenide photocathodes consist of a single crystal and are very sensitive to abuse. If too much current is taken from the photocathode, the structure of the crystal is affected and its performance suffers. Clearly, since the anode current is just the cathode current multiplied by the current gain, the corresponding limitation on anode current will depend on the gain and hence on the high-tension voltage applied to the dynode chain. The critical parameter is the light level illuminating the photocathode rather than the anode current, a point that is not made clear in the RCA datasheets.

Two coolers were used at various times. The first was a Princeton Applied Research thermoelectric cooler which was capable of cooling the tube to -20°C. In warm weather this cooler had some difficulty in maintaining the low temperature and some observations were made with an EMI-Gencom closed-cycle Freon cooler (model CH-1S). This is a powerful cooler capable of maintaining the tube at - 40°C, though in operation it was kept at around - 25°C. It is important with this highly efficient cooler that the tube

not be cooled too quickly, lest thermal stresses destroy it. A rate of between 10 - 15°C per hour is about the maximum safe speed. Both coolers incorporated quartz vacuum windows and the normal magnetic shielding for the photomultiplier. The values of the dynode chain resistors were set by the cooler manufacturers from recommendations for photon counting by RCA.

2.7 The Pulse Counting System

Current pulses corresponding to individual photons striking the photocathode of the photomultiplier pass through a preamplifier-discriminator and then to the two-channel counter. These are considered briefly in turn.

2.7.1

The preamplifier-discriminator used is a Princeton Applied Research (SSRI) model 1120. Its function is to amplify pulses from the photomultiplier for transmission to the remote counter and to reject smaller than normal pulses which are predominantly noise pulses originating in the multiplier chain. The 1120 is mounted at the telescope and connected to the base of the tube by the recommended short double-shielded coaxial cable. Little trouble with pick-up was observed. Occasionally the dome rotation motors produced spurious pulses. This was always checked before attempting to move the dome when observations were in progress.

The 1120 is a single level discriminator only and cannot reject the very large pulses that are caused by cosmic ray events and the like. It has a specified dead time of 30 nsec and pulse width of 30 nsec, giving a maximum counting speed of around 17 MHz. This was checked by using a signal generator. The discriminator level was set in accordance with the method of the PAR manual. This method aims to provide the lowest 'safe' discriminator level and does not purport to be an optimal setting. Since the HT supply to the tube was set to a level at the lower end of the 'plateau' region (to minimise the anode current

taken from the tube) the discriminator level should then be varied to optimise the signal-to-noise. The alternative method is to fix the discriminator setting and vary the supplied voltage to the tube. The aim in either case is to maximise the quantity

$$S/N = \frac{N\,(\text{Light} + \text{Dark}) - N\,(\text{Dark})}{\sqrt{N\,(\text{Dark})}}$$

where N (Dark) is the observed count rate (for some discriminator level) when no light is falling on the photomultiplier photocathode, and N (Light + Dark) is the corresponding value when a weak source (i.e. such that N (Light) is comparable with N (Dark)) illuminates the photocathode. Unfortunately with the adopted value of HT applied to the tube the height of the photon-generated pulses was not sufficiently separate from the mean of the dark pulses to enable this discriminator to be accurately optimised according to the above criterion.

2.7.2 The two-channel counter is a Princeton Applied Research (SSRI) Digital Synchronous Computer, model 1110. It has a maximum specified counting rate of 85 MHz and scaler capacities of up to 10^8 counts. The counter is located remote from the telescope, and accepts pulses from the preamplifier-discriminator down a shielded coaxial cable up to 10 metres long. The counter operates in two modes. In DUAL mode, used for photometry, pulses are gated to one of the two scalers (A) until a certain preset number of cycles of the internal (1 MHz) clock have elapsed. If necessary, a separate signal can be independantly gated

to the other (B) scaler. In the CHOP mode, used for polarimetry, the two counters are used sequentially, and pulses are gated to each in turn in accordance with an external chopping waveform, in this case the reference signal from the photoelastic modulator. Within the model 1110, adjustable level and slope detectors produce AGATE and BGATE windows in the positive and negative halves of the modulator cycle. After a delay, a DETECT window is opened, and counts are allowed to pass into one of the two counters depending on the AGATE and BGATE signals. The length of the DETECT window is determined by thumbswitches on the rear of the model 1110. The process continues until a preset number of modulator cycles (not internal clock cycles) has elapsed.

The counter has been modified somewhat from the basic instrument described in the PAR manual (by W. Cormack). 8-digit boards have been incorporated to allow the calculator to determine the polarisation and flux with full accuracy. Since the internal operation of the counter is synchronised to a 1 MHz internal clock and this is not synchronised to the modulator cycle, a 'jitter' appears on the DETECT window. While the length of the window is not affected, the position of the window within the modulator cycle becomes uncertain by $\pm \frac{1}{2}$ μsec. The effect should average out over the large number of cycles contributing to an integration (certainly $> 10^4$). However to make sure that no problems arose in the gating circuitry and to remove any possibility of consequential effects on the polarimetry, certain operations within the counter were altered (W. Cormack)

to run on a 4 MHz clock. The jitter is thereby reduced by a factor of 4. A troublesome counting bias appeared between the two counting channels from time to time. The above modification did little to reduce it. A new power supply was incorporated into the counter, and the DETECT window circuitry simplified in an attempt to reduce race hazards. The length of the DETECT window is now set by a simple monostable giving a fixed integration time of around 6.4 μsec. These modifications (by W. Cormack) helped to reduce the counting bias to tolerable levels (see below).

2.7.3 There are at least three effects in the photon counting system which can affect the measurement of polarisation. Any bias between the counting channels of the counter will clearly give an instrumental polarisation. A significant dark count from the photomultiplier will diminish the measured polarisation. Counting losses at count rates near to the maximum specified for the discriminator/counter combination will also affect the measured polarisation.

The counter bias was checked periodically using the photomultiplier as a source of pulses. Sources of regular pulses such as pulse generators could give misleadingly optimistic values for the bias up to an order of magnitude less than that observed with the irregular pulse strings from the photomultiplier. Despite frequent attempts to eliminate it, a bias remains which is dependant on count rate. If the counts collected in the two channels were N_1 and N_2 and we define the spurious

polarisation arising from the counting bias as:

$$p_s = (N_1 - N_2) / (N_1 + N_2) \qquad (2.7.3.1)$$

then values of p_s up to 0.05% were observed, with the average value being about 0.02%. The effect is eliminated by averaging together measurements made with the analyser orientated at $\beta = 45^\circ$ and 135°.

If in a particular counting interval, N_1 and N_2 counts are accumulated in the two channels of the counter, our basic measure of polarisation (be it linear or circular) would be:

$$p = (N_1 - N_2) / (N_1 + N_2) \qquad (2.7.3.2)$$

If in the same period of time, the photomultiplier contributed D dark counts to each channel, then the measured polarisation would be reduced to

$$p = (N_1 - N_2) / (N_1 + N_2 + 2D) \qquad (2.7.3.3)$$

Dark count is regularly monitored and subtracted from each channel before the polarisation is calculated.

The limiting count rate of the photon counting system is determined by the preamplifier-discriminator with an effective specified deadtime of 60 nsec. However in practice it is known that effective deadtimes larger than that specified by the manufacturer are observed. With the presently used photomultipliers this quantity is difficult to determine experimentally as we are limited to count rates less than about 1×10^6 sec^{-1}. Two methods were attempted. In the first the count rate from the brightening dawn sky is measured with a large and

with a small aperture. As the sky brightens the count rate observed with the large aperture will be affected by counting losses and the ratio of the count rates measured with large and small apertures will no longer remain constant. The second method is to measure the calibration polarisation with the brightening dawn sky as source. When measuring calibration polarisations, $N_1 \gg N_2$ in equation (2.7.3.2). As the dawn sky brightens, N_1 will be affected much more by counting losses than will N_2, and the calibration polarisation should decrease. Neither method turned out to be fully reliable. The best value obtained for the effective deadtime was $t = 70 \pm 10$ nsec. Using the standard linear correction for counting losses and applying it to equation (2.7.3.2) above we find

$$p^*/p = (1 + nt) / (1 + (1 + p^2)\, nt/2) \qquad (2.7.3.4)$$

where p = measured polarisation, p* = true polarisation and n = measured count rate. Therefore using the derived value for t, at a measured count rate of 1.0×10^6 sec^{-1}, a measured polarisation of 1% would imply a true polarisation of 1.043%. The effect has not be corrected for in measurements in the Thesis, although it is planned to incorporate such a correction into future software.

2.8 Control system

Certain aspects of the control system have been touched on elsewhere in this chapter. The treatment here is brief and User-orientated.

Figure A15 is a block diagram of the spectropolarimeter which illustrates the control hierarchy of this instrument. The calculator controls the cassette tape unit and plotter directly through interface cards. It is interfaced to the spectrometer control unit via a serial link and to the counter by a parallel link. In this way, photon counting can be initiated and the accumulated totals in the two scalars read under program control. By way of the hard-wired TTL logic spectrometer control unit, the analyser can be rotated between two positions, and the wavelength setting of the spectrometer can be selected. The analyser moves between two positions defined by optical encoders. When started up, the system automatically seeks one particular position, but after this the calculator may only change the position of the analyser and is not aware of which position the analyser is in. Two commands are necessary to change the wavelength setting of the spectrometer. Firstly the destination wavelength is loaded or 'latched' into the spectrometer control unit. This unit calculates the number of pulses that require to be sent to the stepper motor turning a lead screw in the spectrometer. On the second command, the spectrometer wavelength is changed. The destination wavelength then becomes the 'current' wavelength. When the system is powered up the current wavelength needs to

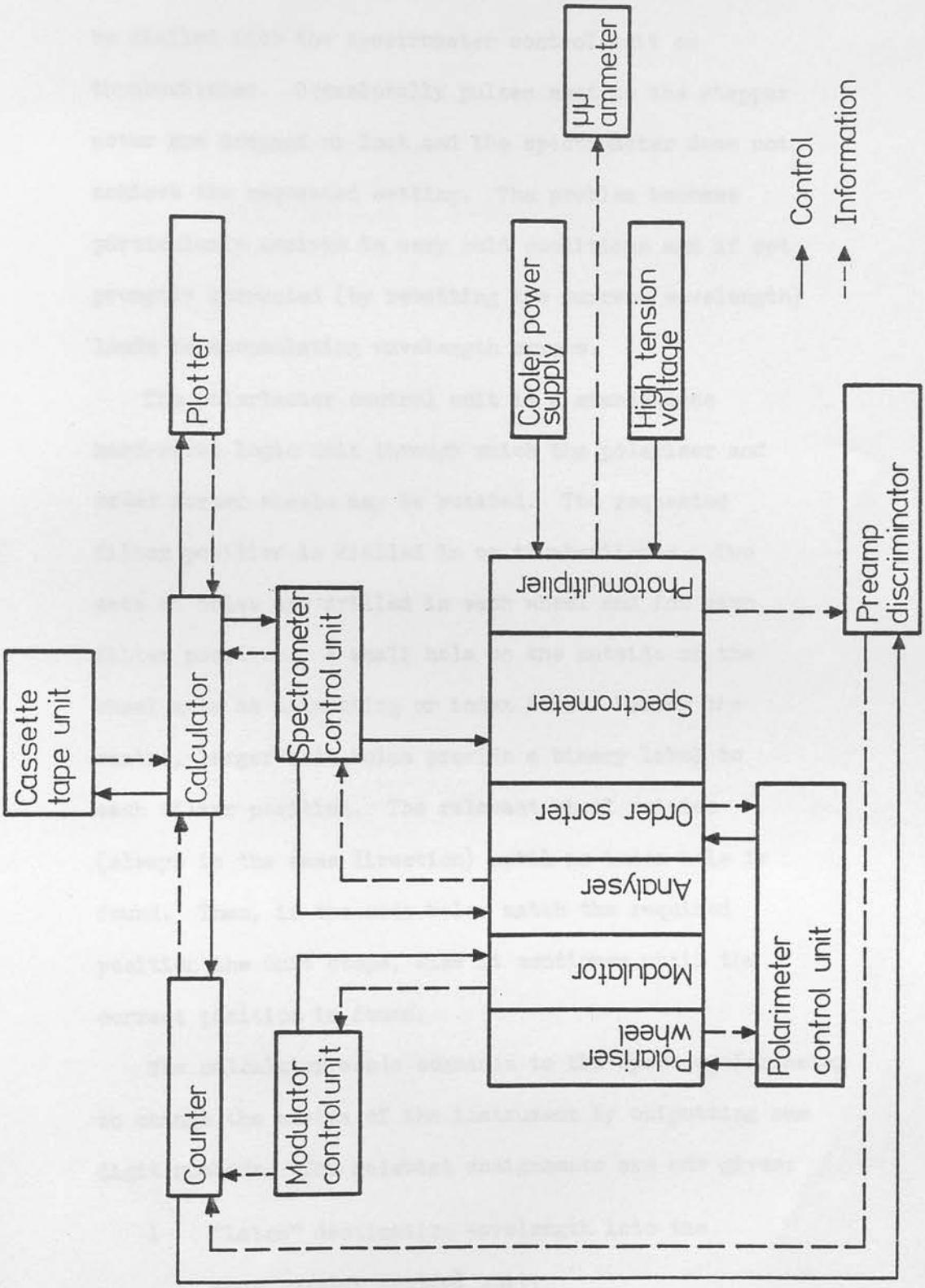

Figure A15 : The control and data handling system for the spectropolarimeter.

be dialled into the spectrometer control unit on thumbswitches. Occasionally pulses sent to the stepper motor are dropped or lost and the spectrometer does not achieve the requested setting. The problem becomes particularly serious in very cold conditions and if not promptly corrected (by resetting the current wavelength) leads to accumulating wavelength errors.

The polarimeter control unit is a stand-alone hard-wired logic unit through which the polariser and order sorter wheels may be rotated. The requested filter position is dialled in on thumbswitches. Two sets of holes are drilled in each wheel and for each filter position. A small hole on the outside of the wheel acts as a locating or index hole. Nearer the centre, larger code holes provide a binary label to each filter position. The relevant wheel rotates (always in the same direction) until an index hole is found. Then, if the code holes match the required position the unit stops, else it continues until the correct position is found.

The calculator sends commands to the spectropolarimeter to change the status of the instrument by outputting one digit numbers. The relevant assignments are now given:

1 "Latch" destination wavelength into the spectrometer control unit.

6 Move spectrometer to destination wavelength.

3 Start counter and, on completion of integration time, read foreground channel count into the

x-register of the calculator.

4 Read background channel count into the x-register of the calculator.

5 Change position of analyser.

2.9 Data Collection and Reduction

We have seen above how the calculator controls the instrument, and how it acquires data from the counter. In this section we are concerned with the order in which the information is gathered, and what the reduction system does with it.

2.9.1 The Reduction System

The system used consists of an Hewlett-Packard HP9810A calculator with added mathematical functions (a "Maths Block"), an HP9865A fast cassette tape store, and an HP9862A flat bed plotter. Each component will be quickly described.

The calculator in its modified form has 111 storage registers, and 1012 program steps. RPN logic is used, but operating on a three register stack - all of which are displayed simultaneously. The calculator can display up to ten digits plus a two digit exponent. Fixed format or floating format can be selected, but the number of digits in the floating format display is not under keyboard or program control. Display format does not affect the accuracy of the calculations which, with the help of two guard digits beyond the ten displayed, is kept to better than 5×10^{-10} for most operations. The calculator has a quiet thermal non-contact printer producing output with a field width of 14 characters, and also an integral magnetic card reader. A program is simply a list of key strokes such as the handheld HP calculators use, but for the 9810 there are no merged instructions or user-defineable keys. However, one flag is available and up to five levels of subroutines can be used. Indirect addressing and memory arithmetic are fully developed.

The basic calculator has the functions INT, $1/x$, x^2, $\sqrt{x}$, and π, and other functions are available with the plug-in "Maths Block". Trigonometric functions and their inverses, logarithmic functions and their inverses, and a number of interesting special functions then become available. Unfortunately, at the time of writing of the control programs to be described, no manual was available, and many of the cleverer functions could not be utilised.

The cassette unit can store up to 6000 data registers or 48000 program key strokes on a 300 foot length of magnetic tape. This equivalence of 1 data register ≡ 8 program steps is typical for most calculators (e.g. TI 58 and 59). Files on the cassette tape are labelled by numbers and can be of different lengths, so optimising tape use. The size of the files must be defined before recording any data or program steps onto the tape. A useful feature of the device is its technique for finding a specified file. The unit drives until it finds a file header, and having found out where it is, drives in the correct direction to reach the requested file. It moves at high speed but slows down when close to the file requested. While the cassette unit is relatively fast, having a search speed of 130 feet per minute, the large control programs used require a lot of tape movement, and some considerable amount of time is spent in this way. In a normal run, it is possible for up to 11 programs to be loaded, 18 data files to be loaded, and 17 data files to be stored. Each file must be found before any operation is performed upon it. Some typical time for these operations are given:

To find the next file on the tape	2 seconds
To load a program, having previously found it	3½ seconds
To find and store the first data file	26½ seconds
To find and store the next data file	3 seconds

To rewind from the last data file 19 seconds

(e.g. to load the next program)

All times are approximate. The cassette unit is somewhat sensitive to static. The discharge from a nearby astronomer can cause the unit to rewind to clear header erasing all programs and data on the way. The calculator itself is also vunerable to static. A discharge will completely clear the program memory and hence halt execution.

The plotter is capable of producing graphs up to 38 cm by 25 cm in size. Numerical resolution is 10000 i.e. each axis is internally divided by the plotter into 10000 units. Built-in software converts the user's unit into these basic plotter units. The plot accuracy is specified to be $< 0.3\%$ of full scale, with a resettability of $< .18$ mm. These figures are roughly in accord with our experience. Plot accuracy is at least as good as the thickness of the pen ($< .5$ mm). The pens can be changed quickly and are available in four colours. Graph paper is held to the platen electrostatically. This plotter will plot a 12 mm vector in approximately 90 msec. Axes can be drawn and fully annotated, points plotted and lines drawn by the built-in software provided.

By todays standards, the HP 9810A is a crude and rather limited device. It is fascinating indeed to realise this calculator was "state-of-the-art" in 1973, and to consider the vast progress which has taken place between then and now. In 1974/5 when this system was purchased, it cost between £6500 and £7000. In 1979, in a proposed update to the Spectropolarimeter, a vastly superior system using a PET microcomputer with twin floppy disc drives and a printer was costed at little more than half this amount. When inflation is taken into account, the real cost would probably be less than a quarter.

2.9.2 Previous Software

A control program was written for the Tenerife observing run in the Autumn of 1977. This program is known as SPC (for Spectro Polarimeter Control). It was written and tested with W. A. Cormack. It drew upon his experience and upon previous control software for this instrument. The reduction procedures implemented were derived by R. D. Wolstencroft. A spectrum scanning program and an Axes plotting program both written by Mr. Cormack were also available for this run.

SPC was a single wavelength, exclusively linear polarisation program. An outline flow chart is given as diagram A1 . For each waveplate, polarisation measure are made alternately in each of the analyser positions until four of each are obtained. From these values a mean value and an error are derived for both P_A and P_B. Besides spending a fair amount of time chopping from one position to the other, this procedure means that the mean and error calculated come from only four measures. Statistically such a procedure is not to be recommended. Notice that annotation is poor. Details such as modulator volts used, objects observed, resolution used, all have to be manually written onto the output. Trouble was also encountered with high dark counts, which as we have seen above, can seriously affect polarisation measurements. A large amount of manual offline reduction was necessary to correct for this. Finally, if a mistake were made during a measurement, or cloud extinguished the star, the program had to be restarted from the beginning, necessitating further offline reduction. The Axis plotting program and the spectrum scanning program were completely independant of SPC, and were run as stand-alone programs. All programs were recalled

Diagram A1 : A flow chart for SPC

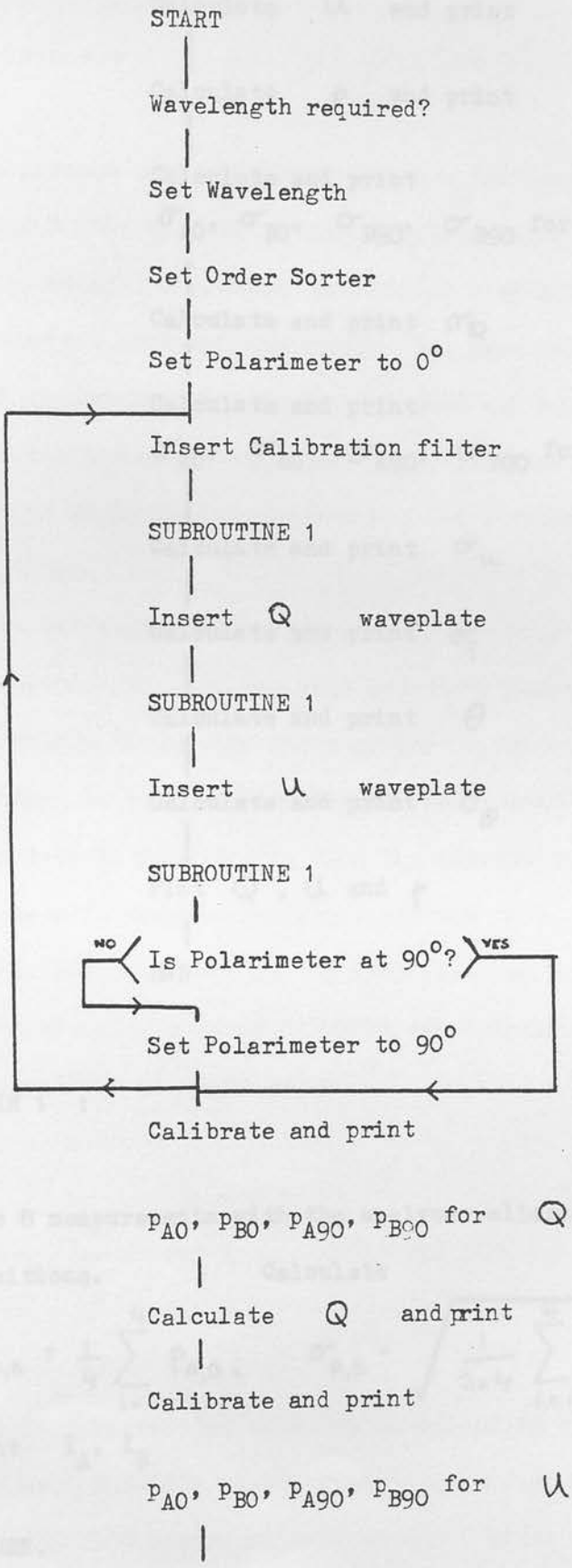

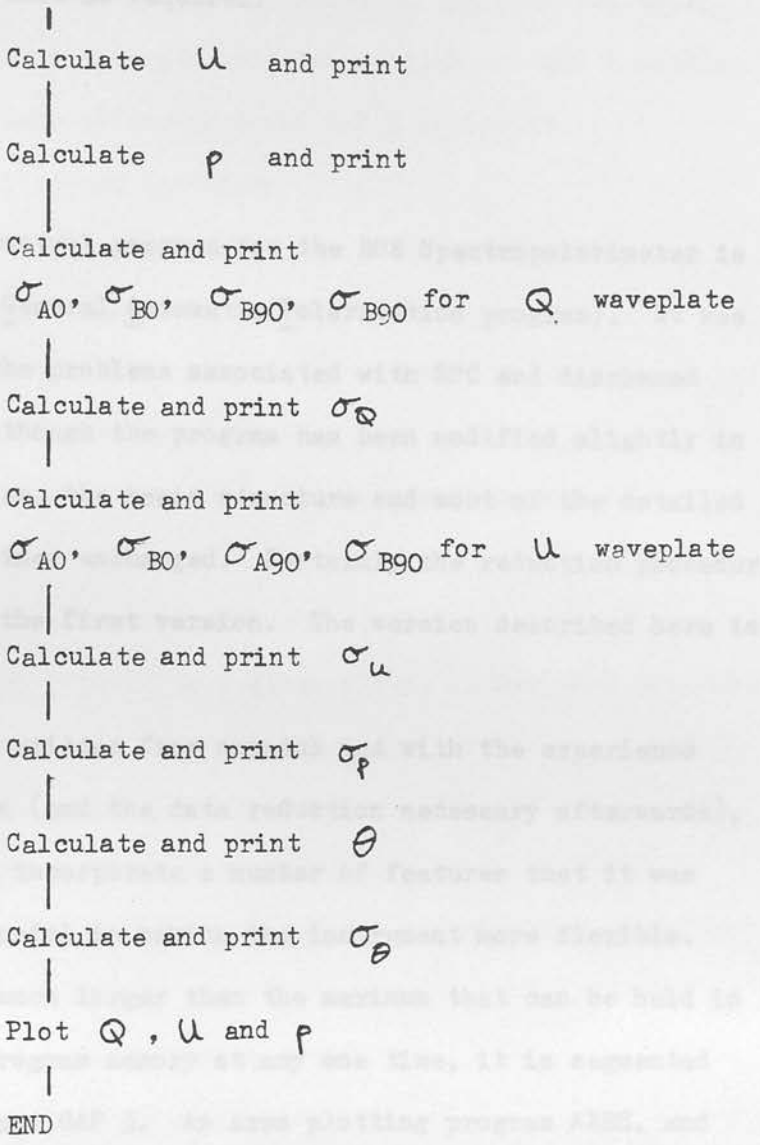

SUBROUTINE 1 :

Take 8 measurements with the analyser alternately in the A and B positions. Calculate

$$P_{A,B} = \frac{1}{4}\sum_{i=1}^{4} P_{A,B\,i} \qquad \sigma_{A,B} = \sqrt{\frac{1}{3\times 4}\sum_{i=1}^{4}(P_{A,B\,i} - P_{A,B})^2}$$

Print I_A, I_B

RETURN.

from the cassette unit as required.

2.9.3 Present Software

The present control program for the ROE Spectropolarimeter is known as GAP (for General Automatic Polarisation program). It was written to avoid the problems associated with SPC and discussed briefly above. Although the program has been modified slightly in line with experience, the basic structure and most of the detailed structure has remained unchanged. Certainly the reduction procedure is identical with the first version. The version described here is the latest one.

Since GAP was written from scratch and with the experience of an observing run (and the data reduction necessary afterwards), it was possible to incorporate a number of features that it was thought might be useful in making the instrument more flexible. As the program is much larger than the maximum that can be held in the calculator's program memory at any one time, it is segmented into GAP 1, GAP 2 and GAP 3. An axes plotting program AXES, and a spectrum scanning program SPECTRUM are incorporated into the program structive as shown below.

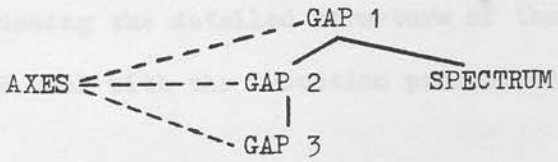

AXES is a Subroutine that can be called by any of the three GAP programs. SPECTRUM has its own axes plotting routines. Both GAP 3 and SPECTRUM return control to GAP 1 after execution. All

these programs are stored at the beginning of the cassette tape. Some offline reduction programs are also available. GAP 1 handles the collection of data while GAP 2 and GAP 3 reduce it.

GAP has the following features:

i) It is a multiwavelength program (up to 10 wavelengths).

ii) It prints plenty of logging information.

iii) It can select and reduce linear or circular polarisation - or both - or take a spectral scan.

iv) The errors produced are from a statistically acceptable size of sample.

v) Integration time is under software control.

vi) Integration can be made to a given error, rather than for just a fixed interval.

vii) Sections of the program can be repeated if a bad measurement, an error or sky conditions warrant it.

viii) Wavelengths to be studied can be spaced at equal intervals or selected individually.

ix) Dark count is (correctly) subtracted.

x) All data can be plotted on-line

We have seen in a previous section how we should combine information taken in different states of the instrument. Before discussing the detailed structure of the programs listed above, we shall deal with the reduction procedures used.

2.9.4 Reduction procedure

Our basic polarisation measurement comes from two integer counts, accumulated in some time interval in the two channels of the

counter. Let us call these two numbers F and G. Then,

$$p = \frac{F - G}{F + G} \qquad \text{and} \qquad I = F + G$$

As mentioned above, the calculator has no control over the integration time of the counter. This is set by thumb switches on the front of the counter. However, taking twenty one-second integrations is the equivalent of one twenty-second integration, and also gives us the possibility of extracting an error measure. Extending the definitions above, we may say:

$$p_i = \frac{F_i - G_i}{F_i + G_i} \qquad \text{and} \qquad I_i = F_i + G_i$$

where $i = 1, \ldots\ldots, N$

and, instead, define

$$p = \frac{1}{N} \sum_{i=1}^{N} p_i \quad , \qquad \sigma^2(p) = \frac{1}{N(N-1)} \left(\sum_{i=1}^{N} p_i^2 - Np^2 \right)$$

and $I = \sum I_i$

Note that $\sigma(p)$ is the error of the mean, namely p. Now, if the photomultiplier is giving a high dark count, these measurements will be distorted. We would obtain

$$p_i = \frac{F_i - G_i}{F_i + G_i + 2D}$$

i.e. the measured polarisation is reduced. To eliminate the effect of dark count, we first of all find its magnitude for the interval of time set on the counter. This value is then subtracted from F and G before any further reduction is done on them.

These dark count corrected values of p and $\sigma(p)$ are collected for various combinations of waveplates, polarimeter and analyser. For each waveplate, we have four possibilities.

Polarimeter	0^o	0^o	90^o	90^o
Analyser	A	B	A	B

and so we define p_{AO}, p_{BO}, p_{A90} and p_{B90}, and similarly for errors and intensities. There are up to four waveplates (or rather three and a blank), and we need to define p_{CalAO}, p_{VAO}, p_{QAO}, p_{UAO} etc.

The first stage of reduction is to divide each of the polarisation (and errors) obtained for each of three waveplates with the appropriate calibration value. This is p_{Cal}. When we insert the calibration filter we are introducing 100% linearly polarised light into the instrument. The measured value of the polarisation is p_{Cal} and is normally around 90%. Hence by dividing by p_{Cal} we are correcting for this 90% instrument efficiency in the detection of polarisation. Note the implicit assumption of linearity in this efficiency. We obtain

$$p'_{VAO} = p_{VAO} / p_{CalAO} \qquad \sigma'_{VAO} = \sigma_{VAO} / p_{CalAO}$$

$$p'_{QBO} = p_{QBO} / p_{CalBO} \qquad \sigma'_{QBO} = \sigma_{QBO} / p_{CalBO}$$

etc. etc.

There is an assumption here that σ_{VA0} etc. will dominate σ_{CalAQ}.

If $z = xy^{-1}$, then, ignoring covariance,

$$\sigma^2(z) = \left(\frac{\partial z}{\partial x}\right)^2 \sigma^2(x) + \left(\frac{\partial z}{\partial y}\right)^2 \sigma^2(y)$$

and hence $$\sigma^2(z) = \frac{\sigma^2(x)}{y^2} + \frac{x^2\,\sigma^2(y)}{y^4}$$

Applied to the present case, where $y \sim 1$ and $x \sim .01$, it is clear that the second term on the right hand side of the equation is indeed negligeable. If we take especially unfavourable conditions - low y (50%) and high x (5%) - we still find that $\sigma(y)$ can be up to ten times the size of $\sigma(x)$ before the two terms are comparable in size. In practice, a rough ratio of 5 : 1 in integration times was kept between measurements with waveplates and calibration filter. Since the transmission of the polaroid (to unpolarised light) is $\sim 30\%$, the difference in errors between calibration filter and waveplate measurements was not normally more than a factor of 4 - 5.

After correction for instrumental efficiency, all the measures for the same waveplate can be combined.

$$p_V = \frac{1}{4}\left(p'_{VA0} + p'_{VB0} + p'_{VA90} + p'_{VB90}\right)$$

$$\sigma_V = \frac{1}{4}\sqrt{\left(\sigma'^2_{VA0} + \sigma'^2_{VB0} + \sigma'^2_{VA90} + \sigma'^2_{VB90}\right)}$$

$$p_{Q,U} = \frac{1}{4}\left(p'_{Q,UA0} + p'_{Q,UB0} - p'_{Q,UA90} - p'_{Q,UB90}\right)$$

$$\sigma_{Q,U} = \frac{1}{4}\sqrt{\left(\sigma^2_{Q,UA0} + \sigma^2_{Q,UB0} + \sigma^2_{Q,UA90} + \sigma^2_{Q,UB90}\right)}$$

p_V, p_Q and p_U are reduced Stokes parameters in the instrumental system. Parameters Q, and U change sign on a 90^o rotation, while V is unchanged. This explains the different form for the three waveplates.

Degree of linear polarisation and position angle, p and θ, can now be calculated by the standard equations for conversion to polar coordinates.

$$p = \sqrt{p_Q^2 + p_U^2} \qquad \theta = \tfrac{1}{2}\arctan p_U/p_Q$$

$$\sigma(p) = \sqrt{\left(\frac{p_Q}{p}\sigma_Q\right)^2 + \left(\frac{p_U}{p}\sigma_U\right)^2}$$

$$\sigma(\theta) = \frac{180}{\pi}\cdot\frac{1}{2p}\sqrt{\left(\frac{p_U}{p}\sigma_Q\right)^2 + \left(\frac{p_Q}{p}\sigma_U\right)^2} \quad \text{(in degrees)}$$

The circular polarisation, p_V, requires one futher step. The implicit assumption in the procedure of dividing by p_{CAL} is that 100% linearly polarised light is produced by the HNP'B filter. This is to all extents and purposes true (see Table A3). For the calibration of circular polarisation we require a source of 100% circularly polarised light. At any wavelength but the quarterwavelength of the waveplate, light passing through the calibration filter will not be 100% circularly polarised. It is necessary to correct for this by multiplying p_V and σ_V by $\sin(90^o \times \lambda_Q/\lambda)$ where λ_Q will be 3800 or 5825 (Å). As discussed above, this is an approximate formula.

Therefore $$q = p_V \sin\left(\frac{\lambda_0}{\lambda} \times 90^\circ\right)$$

$$\sigma_q = \sigma_V \sin\left(\frac{\lambda_0}{\lambda} \times 90^\circ\right)$$

The reduction procedure is somewhat different for Zeeman polarimetry within a spectral line. If the line is centred at a wavelength λ_0, and the circular polarimetry obtained at $\lambda_0 + \Delta\lambda$ and $\lambda_0 - \Delta\lambda$, call these polarisation q_+ and q_-. Then our measure is

$$\langle q \rangle = \tfrac{1}{2}(q_+ + q_-)$$

Since we are dealing with a differential measure, and do not need to know q_+ and q_- to great precision, we can relax some of the procedures above for the elimination of instrumental effects. These effects will not vary significantly over (say) 10 Å. Atmospheric effects (such as a highly polarised dawn sky) will also be eliminated to first order, as long as they are not changing faster than the time taken to obtain a single pair of measures, q_+ and q_-. The following procedure is followed when reducing Zeeman polarimetry. This is not done by GAP.

Integration time is kept short (100 seconds maximum) in order to minimise wavelength shifts caused by guiding errors. The quantity $\langle q \rangle$ is calculated for each setting of the instrument (that is, A0, B90 etc.), and these values combined to form a weighted mean - weighted that is by the errors of the individual $\langle q \rangle$'s. Normally the same order of instrumental settings would be followed as the procedures above, but the complete series might not be completed.

2.9.5 The detailed descripton of GAP

We deal with each program in turn. Flow charts are given where such a format is more appropriate than an extended description of program function and method.

a) GAP 1

This program is organised on three levels:

i) Control level. This level interacts with the astronomer, logs information and structures the collection of data.

ii) Subroutine 1. This level is responsible for scanning in wavelength, and the temporary storage of the data on tape.

iii) Subroutine 2. This level takes data in both analyser positions and calculates polarisations, errors and intensities.

Flow charts are given as Diagrams A2 , A3 and A4. The numbers on the right of the flow chart refer to notes below.

1. The program requires the following information of the astronomer, but doesn't use any of it. These details are invaluable six months later in trying to deduce what exactly was happening on that particular night. Typical and limiting values of the various parameters are given in Table A4.

Diagram A2 : A flow chart for GAP 1 , Control level

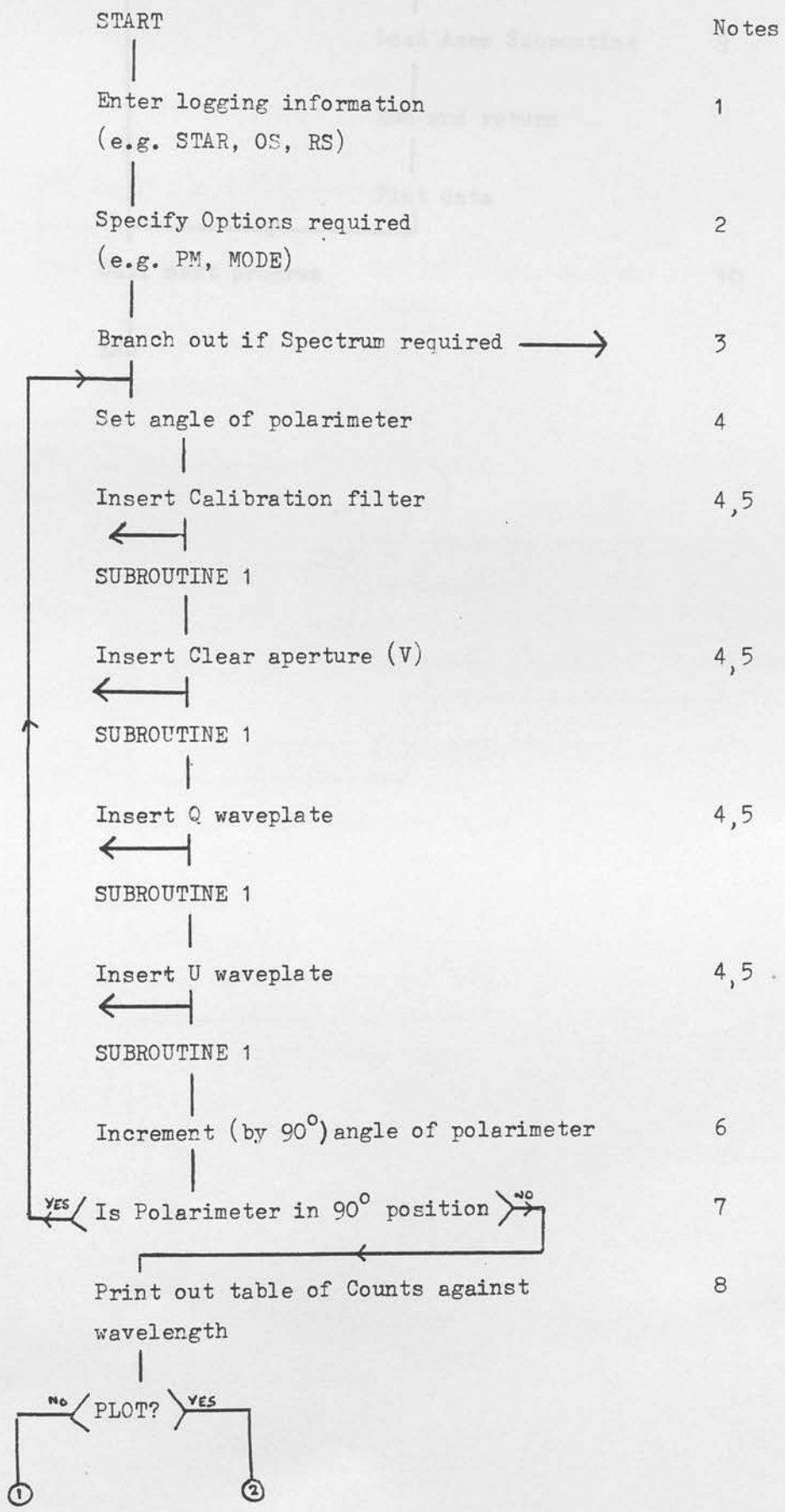

Notes

1

2

3

4

4,5

4,5

4,5

4,5

6

7

8

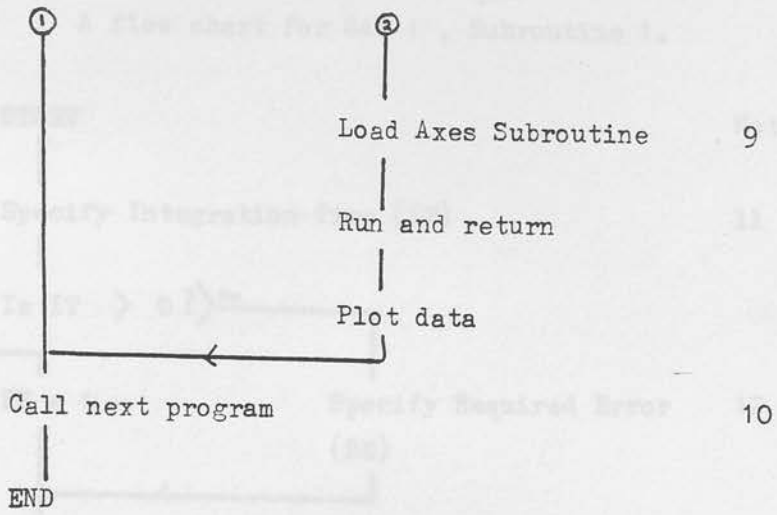
1
2
Load Axes Subroutine
9
Run and return
Plot data
Call next program
10
END

Diagram A3 : A flow chart for GAP 1 , Subroutine 1.

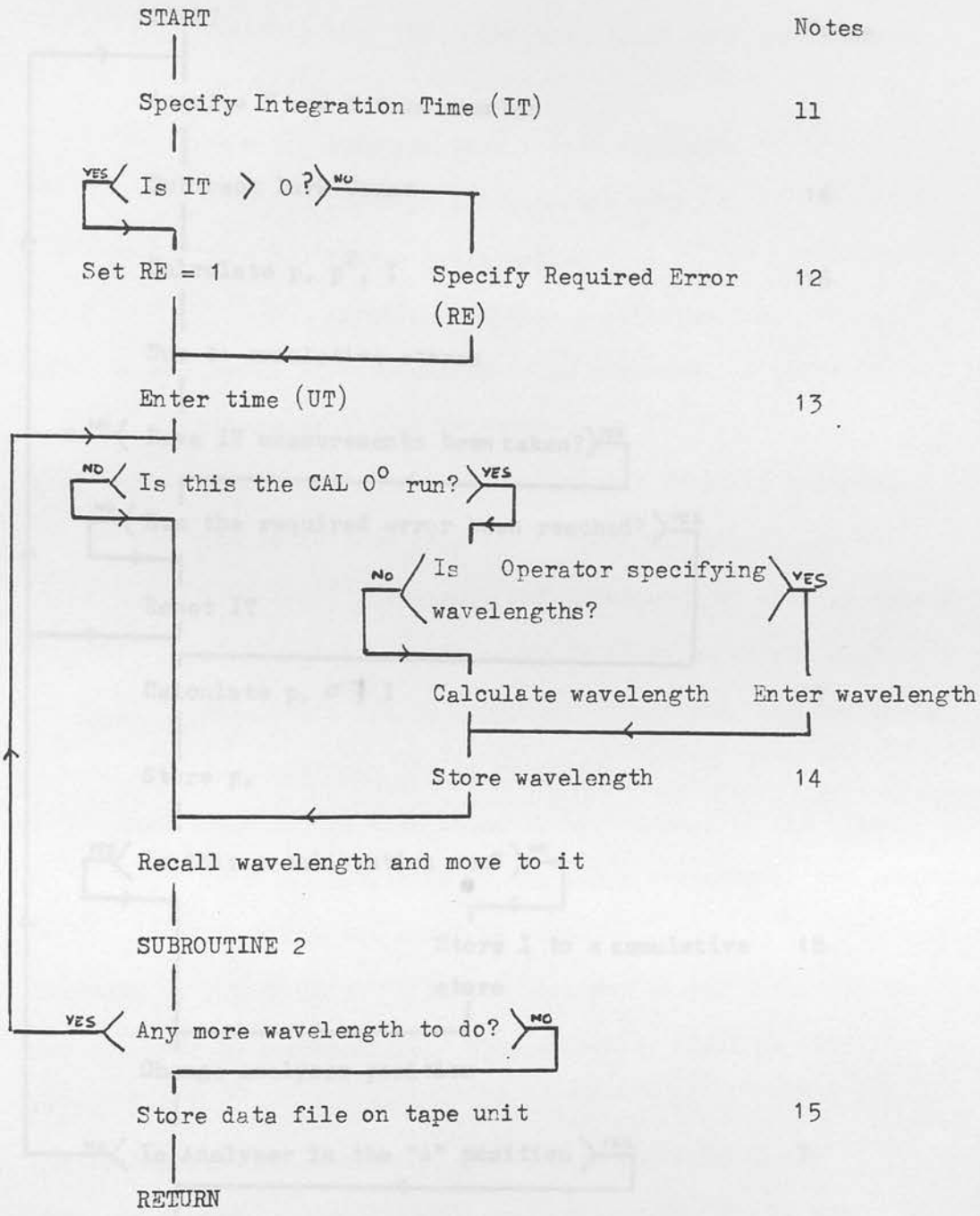

Diagram A4 : A flow chart for GAP 1 , Subroutine 2

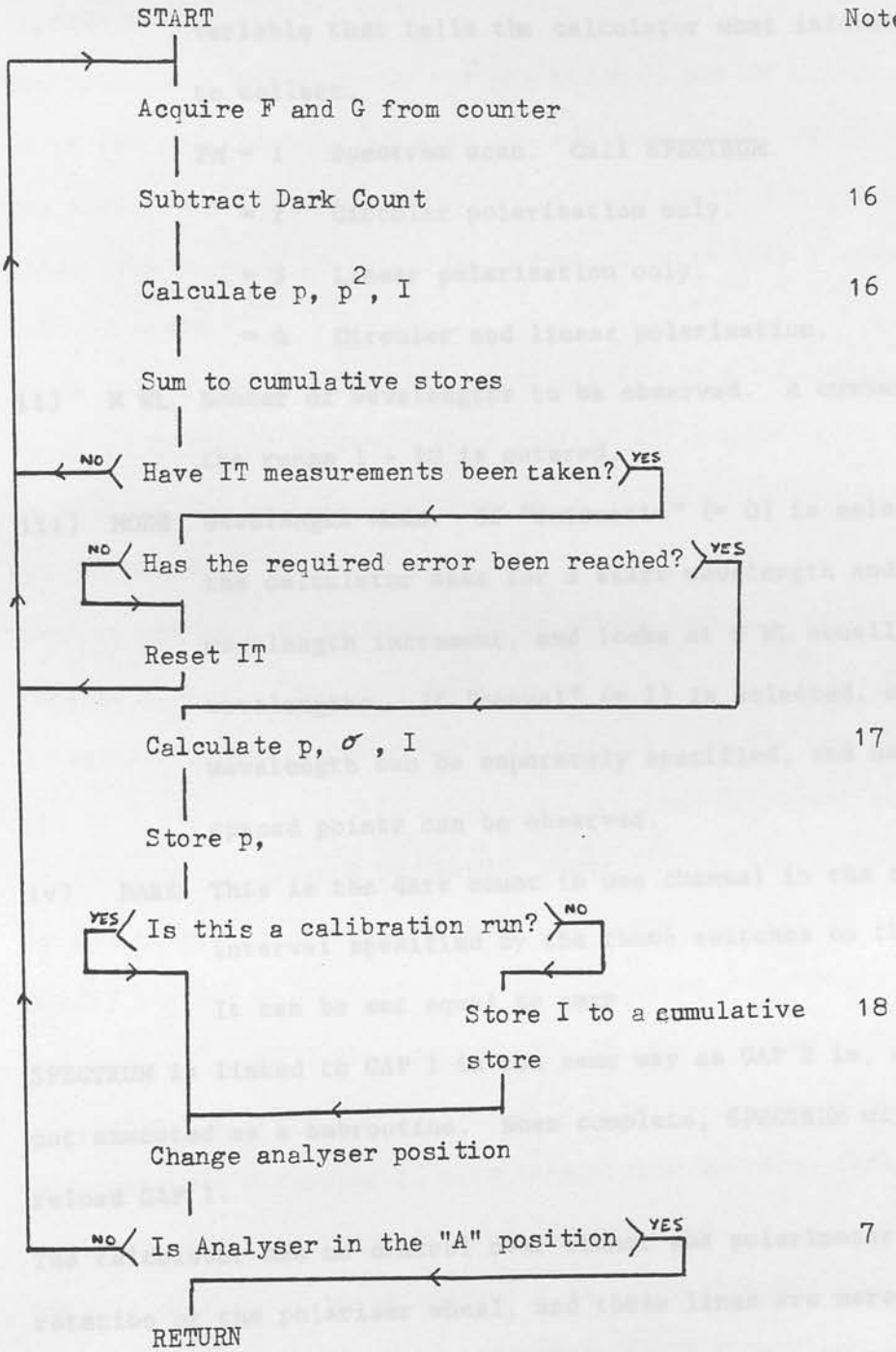

2. GAP is flexible in the options it offers.

   i) PM Polarisation Mode takes the values 1 - 4, and is the variable that tells the calculator what information to collect.

      PM = 1 Spectrum scan. Call SPECTRUM.

         = 2 Circular polarisation only.

         = 3 Linear polarisation only.

         = 4 Circular and linear polarisation.

   ii) N WL Number of wavelengths to be observed. A number in the range 1 - 10 is entered.

   iii) MODE Wavelength Mode. If "automatic" (= 0) is selected, the calculator asks for a start wavelength and a wavelength increment, and looks at N WL equally spaced wavelengths. If "manual" (= 1) is selected, each wavelength can be separately specified, and unequally spaced points can be observed.

   iv) DARK This is the dark count in one channel in the time interval specified by the thumb switches on the counter. It can be set equal to zero.

3. SPECTRUM is linked to GAP 1 in the same way as GAP 2 is, and is not executed as a subroutine. When complete, SPECTRUM will reload GAP 1.

4. The calculator has no control over either the polarimeter rotation or the polariser wheel, and these lines are merely prompts to the operator. For the polariser wheel, the operator enters the actual wheel number of the waveplate inserted as a double check for errors.

5. If, upon the prompt "Insert ..... waveplate", a - 1 is entered, the program will jump to the last prompt printed, so that the

last waveplate polarisations can be repeated. Multiple recycling is allowed. The position in the program jumped to depends on PM.

6,7. The calculator cannot sense the positions of any of the wheels or of the polarimeter, not even the analyser wheel, which it can move. Hence any knowledge of the position of any component comes from keeping track of the number of moves from a prescribed initial state.

8. It is rarely necessary to plot this table. If intensities are required SPECTRUM is used. Note that if RE is used (Note 18), or a waveplate position repeated (Note 5), these counts will not be correct.

9. AXES is run as a subroutine. It is called from a tape file.

10. This is a simple link for GAP 2.

11. Integration time is under software control. If the counter is set to 1 second (Note 1), an integration time of twenty seconds is achieved by integrating twenty times for one second each.

12. If a negative integration time is specified, the RE (Required Error) feature is entered. If, say, -20 were entered for IT, and 2×10^{-4} (.02%) were entered for RE, the program would initially integrate for 20 secs. If this target error had not been reached, a further 20 secs integration would be made, and repeated until the required error is achieved.

13. This is useful for investigating time lost, calculating mean times of observations - and inferring cloudy weather when it is not elsewhere stated!

14. Note that even if the wavelengths are set by the operator, they are entered only once, during the Cal 0^{o} run. Henceforward they are recalled from store. If Cal 0^{o} is repeated (Note 8), it is not necessary to re-enter the wavelengths.

15. No malfunction of the tape unit during operation has ever been noticed. Since program and data files are well separated on the tape, storing away the first data file takes some 20 seconds.

16. If required for debugging, or higher time resolution, the individual counts, polarisations and intensities can be printed as they are obtained / calculated.

17. The actual integration time is used for these calculations even if the RE feature (Note 12) is used.

18. Summing in intensities from Calibration runs might distort the measures. These intensities should be at least as good measures of the spectrum as the program SPECTRUM could produce.

(b) GAP 2

GAP 2 (with GAP 3) is a stand-alone reduction program. Usefully it can be used independantly of GAP 1 to reduce data offline. The program makes a lot of use of the tape files, firstly to obtain the data that GAP 1 has collected, for reduction, and subsequently to store intermediate steps in the calculations. The initial allocation of tape files is now shown.

File No	11	12	13	14	15	16	17	18
PM								
2	Cal 0	V0	Cal 90	V 90				
3	Cal 0	Q0	U0	Cal 90	Q 90	U 90		
4	Cal 0	V0	Q0	U0	Cal 90	V 90	Q 90	U 90

The GAP programs are stored in files 0 - 4. By knowing PM, the program knows where to find a particular set of data. The table above looks unnecessarily complex, but the format adopted does

minimise the number of files used, and hence cuts down on tape movement. Note that the total number of files used is 2 x PM.

In order to manipulate or operate upon the tape files it is necessary to hold two files in core at the same time. Since each wavelength requires five pieces of information to be stored this limits the program to a maximum of ten wavelengths. Even with ten, very few stores are left for program control.

GAP 2 also makes heavy use of subroutines, with the main program merely controlling loops and recalling and restoring data files. All the reduction is done by subroutines into which one or two data files are input. These subroutines are:

i) Subroutine 1 : Calibration

ii) Subroutine 2 : Collection

iii) Subroutine 3 : Sine Factor

iv) Subroutine 4 : Print out

v) Subroutine 5 : Plot data

Flow charts for GAP 2 are given. The Subroutines are not flow charted, but notes on their operation are given below.

i) Subroutine 1 : Calibration

As this Subroutine is entered, the base file and top file contain data in the format

..... λ , P_A, σ_A, P_B, σ_B ..... and .... λ , P_{ACAL}, σ_{ACAL}, P_{BCAL}, σ_{BCAL}

respectively, for 0° or 90° (and some waveplate in the case of the

Diagram A5 : A flow chart for GAP 2

Data files stored on tape are called "tapefiles"

The storage locations 1 - 50 inc. are called the " basefile"

The storage locations 51 - 100 inc. are called the "topfile"

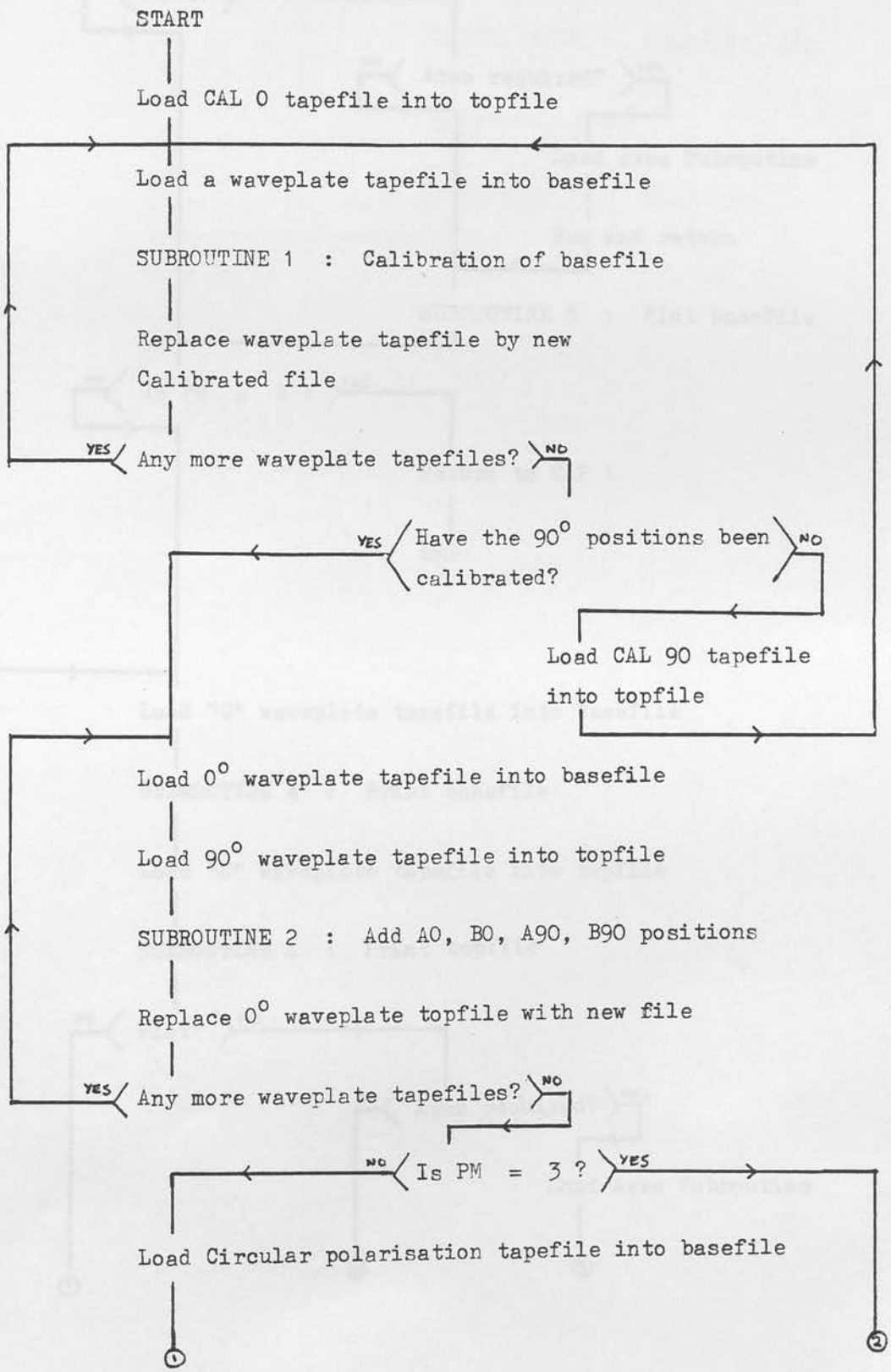

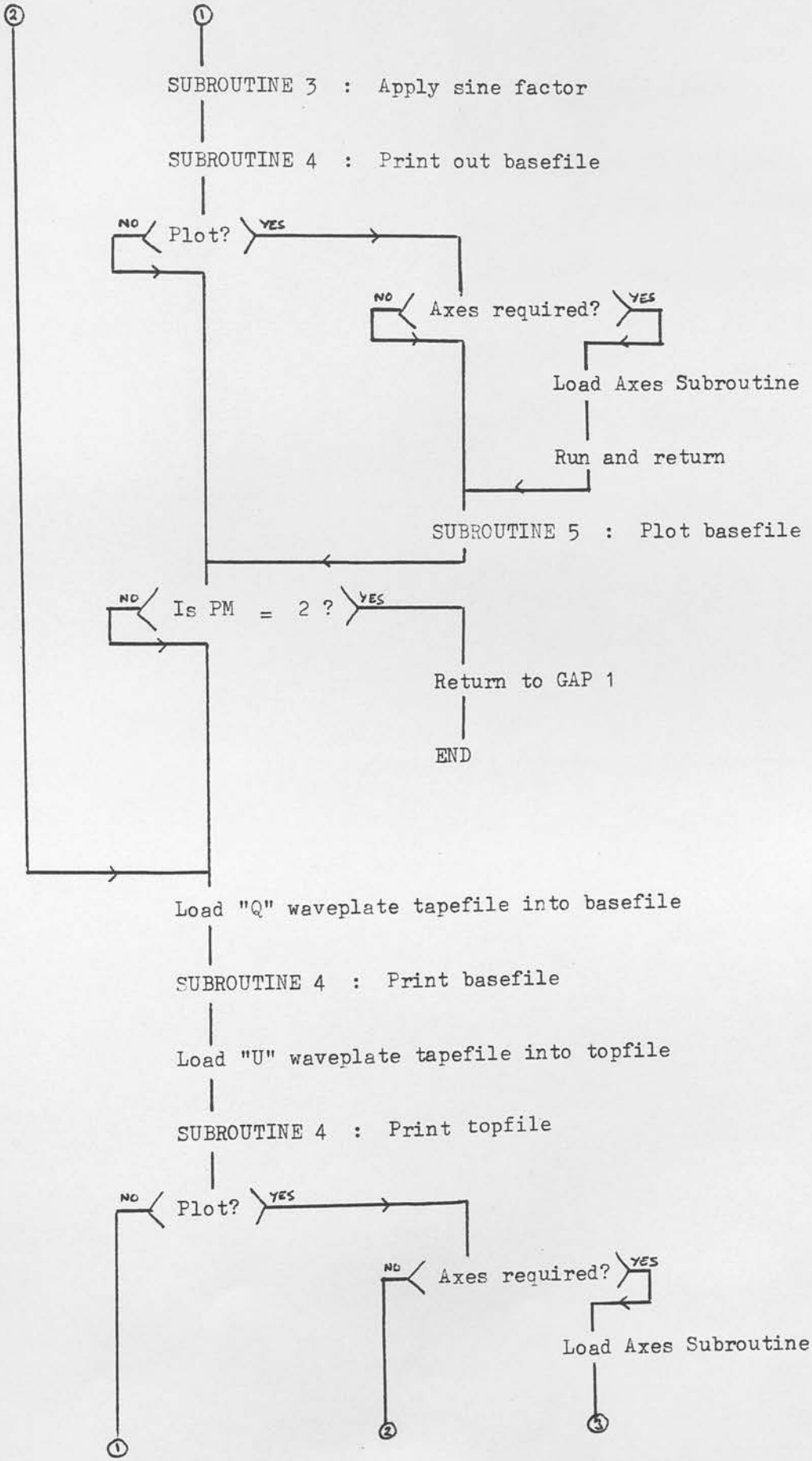
SUBROUTINE 3 : Apply sine factor
SUBROUTINE 4 : Print out basefile
Plot?
NO
YES
Axes required?
NO
YES
Load Axes Subroutine
Run and return
SUBROUTINE 5 : Plot basefile
Is PM = 2 ?
NO
YES
Return to GAP 1
END
Load "Q" waveplate tapefile into basefile
SUBROUTINE 4 : Print basefile
Load "U" waveplate tapefile into topfile
SUBROUTINE 4 : Print topfile
Plot?
NO
YES
Axes required?
NO
YES
Load Axes Subroutine

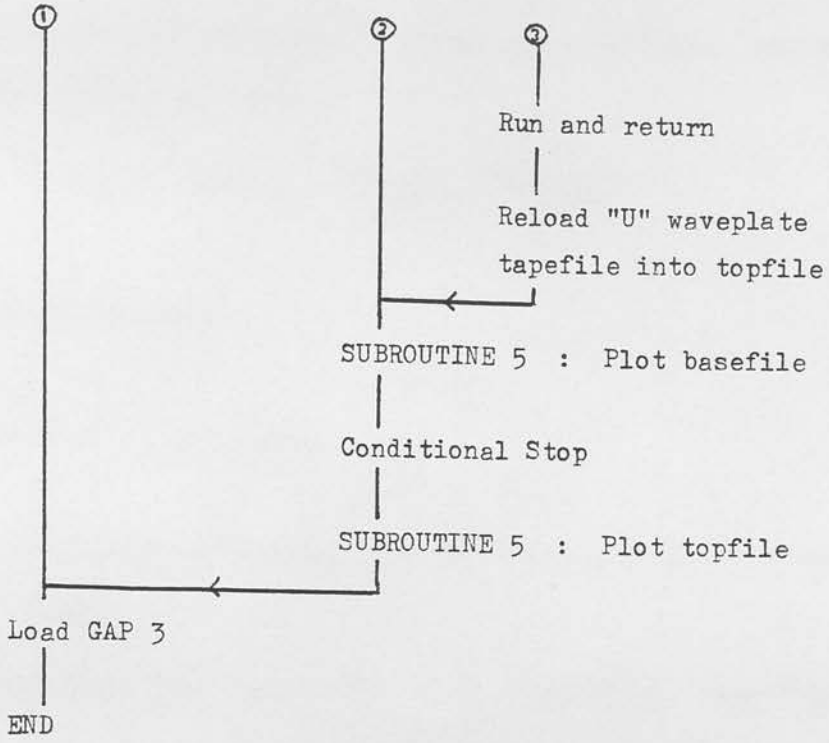
①
②
③
Run and return
Reload "U" waveplate
tapefile into topfile
SUBROUTINE 5 : Plot basefile
Conditional Stop
SUBROUTINE 5 : Plot topfile
Load GAP 3
END

base file) and for each wavelength. After the subroutine, the base file contains data in the form

$$\ldots\lambda,\ p_{A/p_{ACAL}},\sigma_{A/p_{ACAL}},\ p_{B/p_{BCAL}},\sigma_{B/p_{BCAL}}\ \ldots\ldots$$

for each wavelength.

ii) Subroutine 2 : Collection

As the subroutine is entered, the base file and top file contain data in the format

$$\ldots\lambda, p_{A0}, \sigma_{A0}, p_{B0}, \sigma_{B0}\ldots \text{ and } \ldots\lambda, p_{A90}, \sigma_{A90}, p_{B90}, \sigma_{B90}\ \ldots$$

respectively where these p and σ's are already calibrated and could be Q,U or V. First of all, "A" and "B" positions are combined...

$$\ldots\lambda,\ p_{A0}+p_{B0},\ \sigma^2_{A0}+\sigma^2_{B0},\ p_{B0},\ \sigma_{B0}\ \ldots$$

for each of the files, and then and 0° and 90° information is combined into the base file...

$$\ldots\lambda,\ (p_{A0}+p_{B0}+p_{A90}+p_{B90}),(\sigma^2_{A0}+\sigma^2_{B0}+\sigma^2_{A90}+\sigma^2_{B90}),-,-,\ \ldots$$

for circular, and

$$\ldots\lambda,\ (p_{A0}+p_{B0}-p_{A90}-p_{B90}),(\sigma^2_{A0}+\sigma^2_{B0}+\sigma^2_{A90}+\sigma^2_{B90}),-,-,\ldots$$

for linear. Finally, the mean values are obtained, leaving

$$\ldots\lambda,\ p,\sigma,-,-\ \ldots$$

where $p = \frac{1}{4}(p_{A0} + p_{B0} \pm p_{A90} \pm p_{B90})$

and $\sigma = \frac{1}{4}\sqrt{\left(\sigma^2_{A0} + \sigma^2_{B0} + \sigma^2_{A90} + \sigma^2_{B90}\right)}$

iii) Subroutine 3 : Sine Factor

The base file is changed from

$\ldots\lambda,\ p_V,\ \sigma_V,\ -,\ -\ldots$ to $\ldots\lambda,\ Kp_V,\ K\sigma_V,\ -,\ -\ \ldots$

where $K = \sin\left(90^\circ \times \frac{\lambda_a}{\lambda}\right)$

iv) Subroutine 4 : Print out

The Subroutine prints out data of the form λ, p, σ. It can print out base file or top file, or a portion of either.

v) Subroutine 5 : Plot data

The Subroutine plots polarisations against wavelength, and also draws 1σ error bars. Axes must have already been drawn. It can plot base file or top file, or a portion of either.

c) GAP 3

This program is merely a continuation of GAP 2. All the reduced Stokes parameters have been calculated in GAP 2, and this program merely calculates p, θ, prints and plots them. It uses some of the same subroutines as GAP 2, plus one of its own. A flow chart is given.

vi) Subroutine 6 : Polar coordinates

With $\ldots\lambda,\ p_Q, \sigma_Q, -,\ -\ \ldots$ in the base file and $\ldots\lambda,\ p_u, \sigma_u, -, -$

Diagram A6 : A flow chart for GAP 3

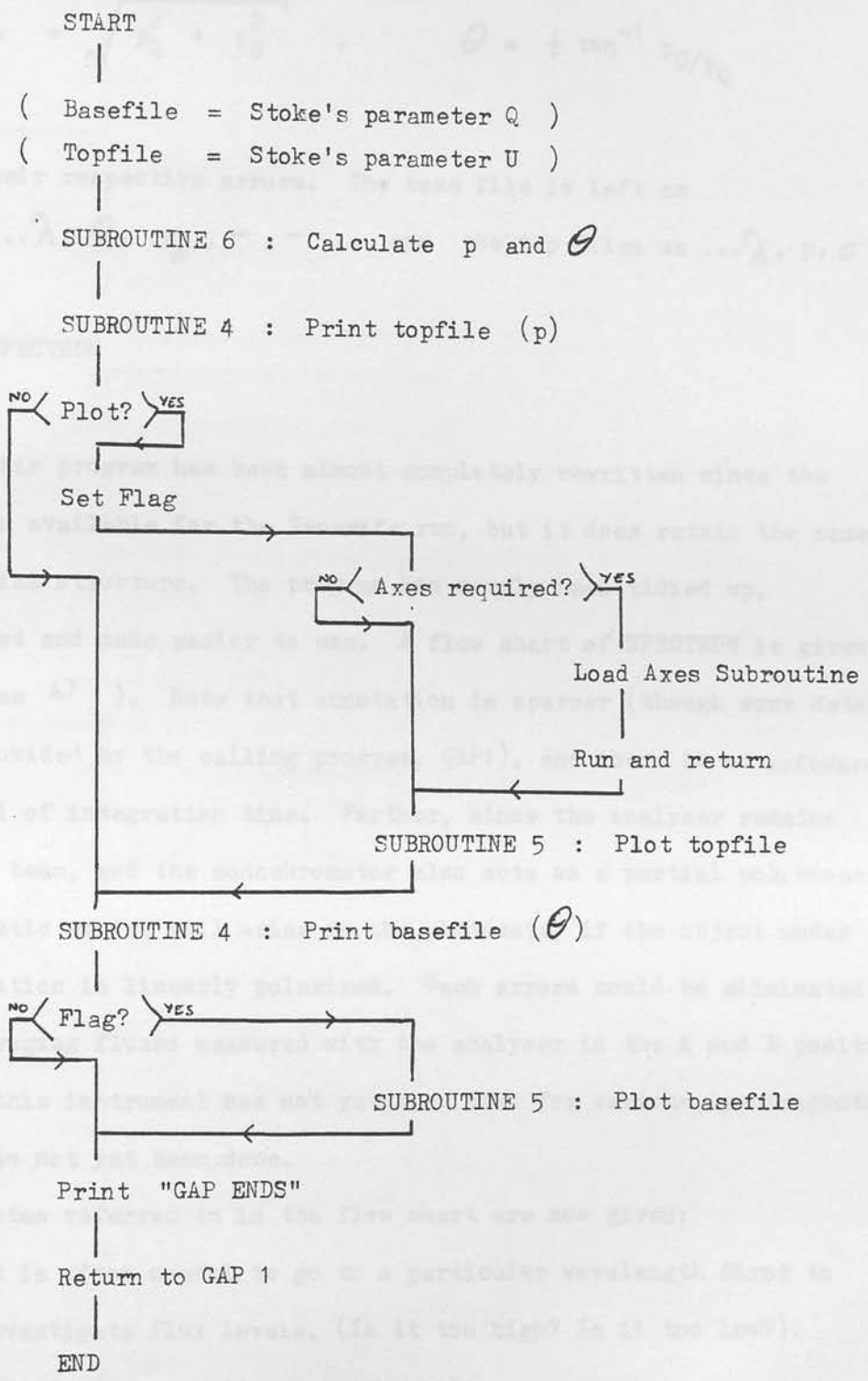

in the top file, this Subroutine calculates

$$p = \sqrt{p_Q^2 + p_U^2} \quad , \qquad \theta = \tfrac{1}{2} \tan^{-1} p_U/p_Q$$

and their respective errors. The base file is left as

$\ldots\lambda, \theta, \sigma_\theta, -, - \ldots$ and the top files as $\ldots\lambda$, p, σ, —, —...

d) SPECTRUM

This program has been almost completely rewritten since the version available for the Tenerife run, but it does retain the same essential structure. The program has merely been tidied up, enhanced and made easier to use. A flow chart of SPECTRUM is given (Diagram A7). Note that annotation is sparser (though some details are provided by the calling program, GAP1), and there is no software control of integration time. Further, since the analyser remains in the beam, and the monochromator also acts as a partial polariser, systematic errors will arise in the photometry if the object under observation is linearly polarised. Such errors could be eliminated by averaging fluxes measured with the analyser in the A and B positions. Since this instrument has not yet been used for serious spectrophotometry, this has not yet been done.

Notes referred to in the flow chart are now given:

1) It is often useful to go to a particular wavelength first to investigate flux levels. (Is it too high? Is it too low?). This feature provides a quick probe.

2) "Resolution" is defined as in GAP 1 (Table A4). The maximum number of wavelengths it is possible to investigate in one run is 80.

Diagram A7 : A flow chart for SPECTRUM

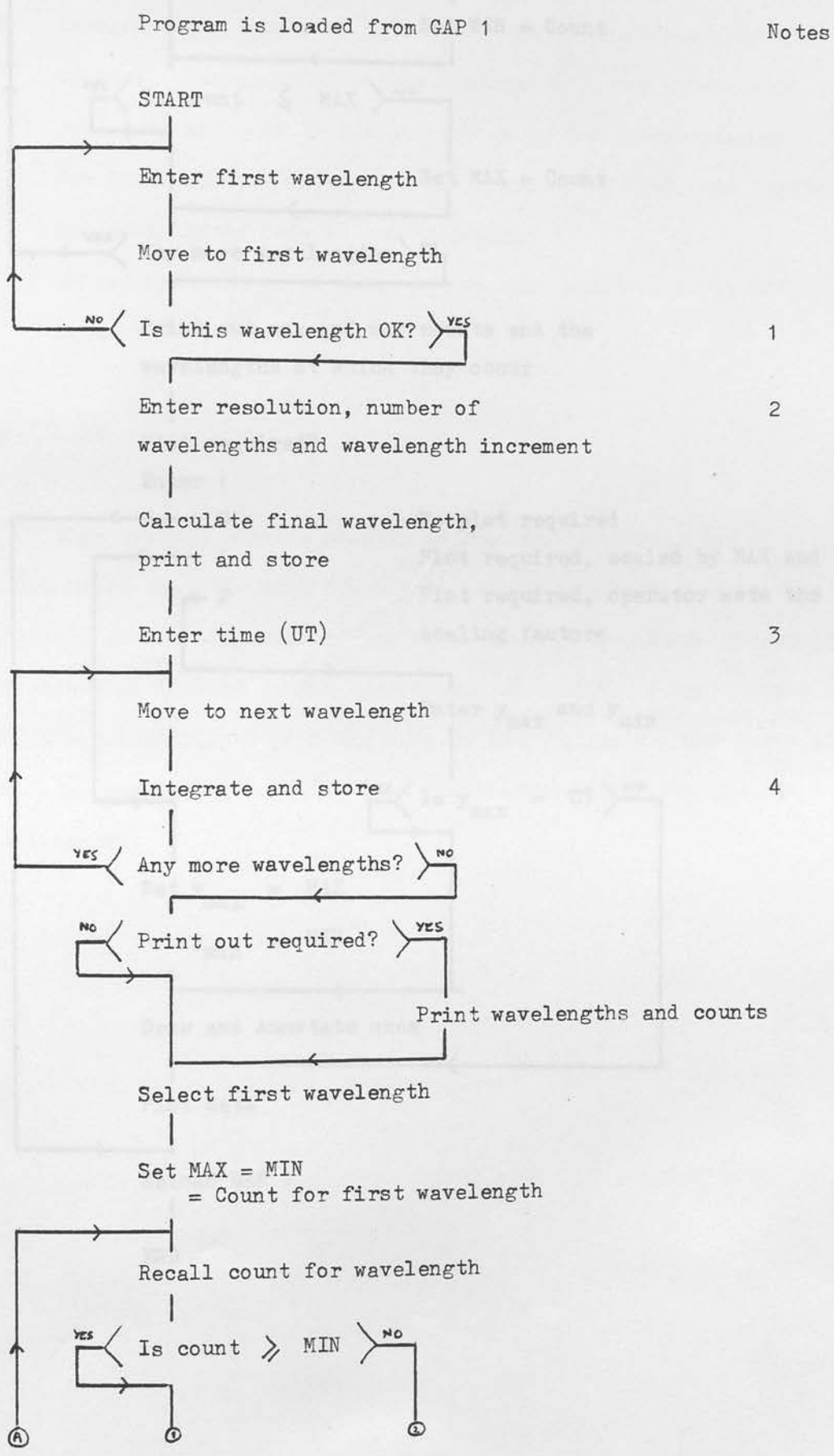

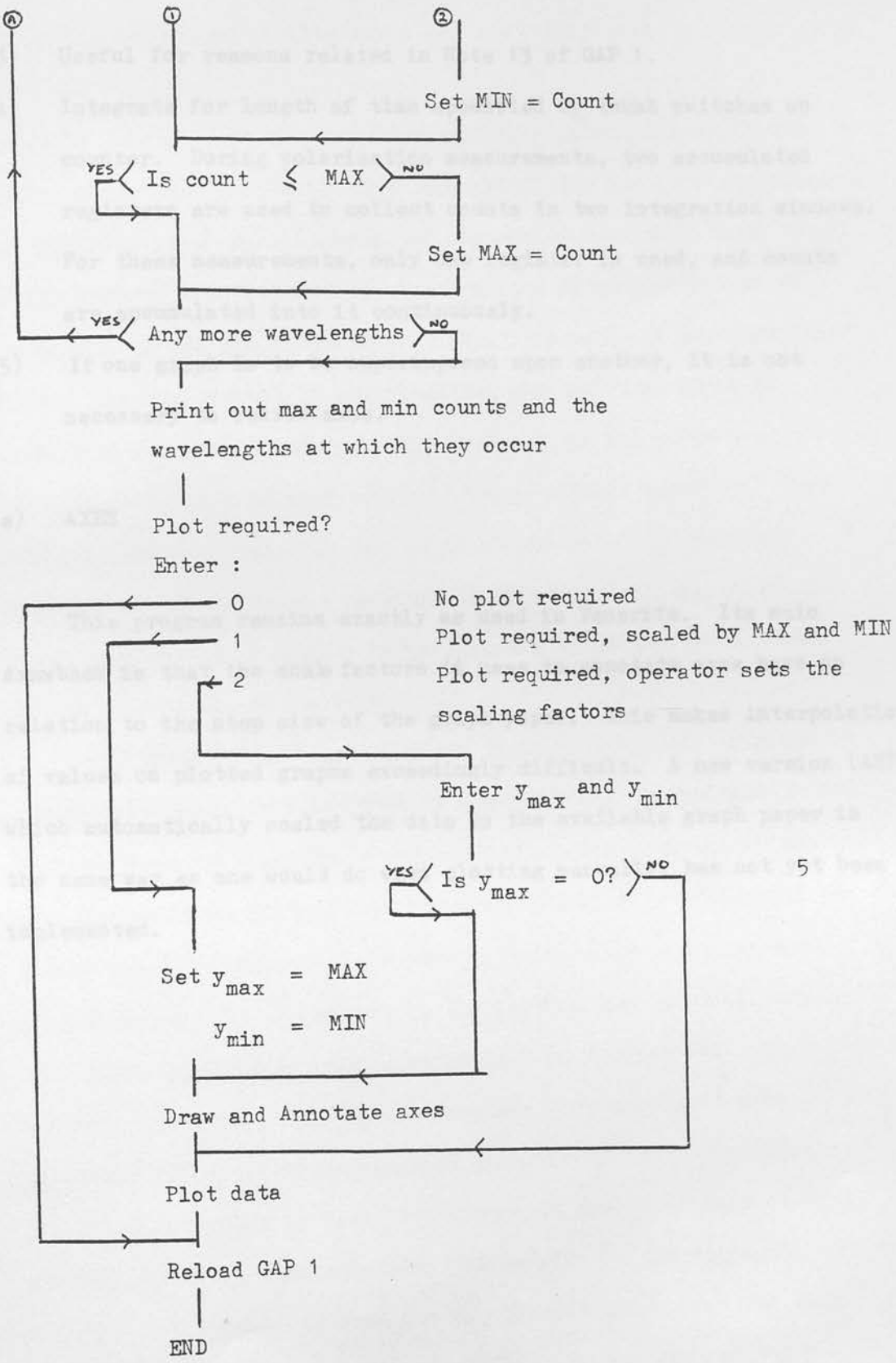
A
1
2
Set MIN = Count
YES
Is count ≤ MAX
NO
Set MAX = Count
YES
Any more wavelengths
NO
Print out max and min counts and the wavelengths at which they occur
Plot required?
Enter :
0
No plot required
1
Plot required, scaled by MAX and MIN
2
Plot required, operator sets the scaling factors
Enter y_{max} and y_{min}
YES
Is y_{max} = 0?
NO
Set y_{max} = MAX
y_{min} = MIN
Draw and Annotate axes
Plot data
Reload GAP 1
END

3) Useful for reasons related in Note 13 of GAP 1.

4) Integrate for length of time specified by thumb switches on counter. During polarisation measurements, two accumulated registers are used to collect counts in two integration windows. For these measurements, only one register is used, and counts are accumulated into it continuously.

5) If one graph is to be superimposed upon another, it is not necessary to redraw axes.

e) AXES

This program remains exactly as used in Tenerife. Its main drawback is that the scale factors it uses to annotate axes have no relation to the step size of the graph paper. This makes interpolation of values on plotted graphs exceedingly difficult. A new version (ASP) which automatically scaled the data to the available graph paper in the same way as one would do when plotting manually, has not yet been implemented.

3. The effect of misalignments and non-idealities

It has been demonstrated above that most components in the polarimeter have properties that can affect the accurate measurement of polarisation. Misalignments of components that were ideal would still lead to differences from the analysis given above. It is necessary to see how these various misalignments and non-idealities affect the measurement of polarisation, and how they might be accounted for in the reduction procedures. In the pages that follow, no attempt is made to deal with all these effects together. This would be neither practical nor particularly helpful. Instead, simplified situations are examined in order to obtain a physical 'feel' for what is actually happening, and to obtain rough ideas of the magnitudes of the effects.

The analysis is based upon the Mueller calculus. A guide to commonly used matrices is given in Appendix A1. Quoted and derived there is a matrix not normally included in compilations of these matrices (Clarke and Grainger, Shurcliff). This will be termed the dichroic waveplate matrix, and its use requires some justification. It was stated in the section upon the analyser that HNP'B polaroid becomes birefringent in the far red. It becomes, in effect, a dichroic waveplate. Obversely, a mica waveplate tends to become somewhat dichroic in the ultraviolet. The important point is that both dichroism and birefringence are the result of the same molecular assymetries in the compound. As a result, both the dichroism and the birefringence have the same reference axis, with the axis of maximum transmission of the dichroism normally corresponding with the 'fast' axis of the birefringence. The dichroic waveplate matrix presented in the

appendix assumes this conaxial property, and will be suitable for modelling both a birefringent analyser and a slightly dichoic waveplate. In the present instrument, however, the waveplates are of quartz and show no appreciable dichroism in the wavelength interval of interest.

We deal with the following cases:

3.1 Imperfect analyser

3.2 Imperfect calibrator

3.3 Misaligned waveplates

3.4 The modulator

3.5 Effect of the spectrometer

3.6 Telescope dependant polarisation.

3.1 Imperfect analyser

The simplest model of the polarimeter has only two components: a photoelastic modulator; and an analyser mounted with its axis at 45° to the fast axis of the modulator. In this section, we consider the consequence of a birefringent and/or misaligned analyser with dichroic efficiency less than one. The matrix equivalent of the optrical train, and the System matrix are given in Appendix A2.

The instantaneous detected intensity at the photocathode is:

$$I_t = \tfrac{1}{2}\left((K_1 + K_2)\, I + (K_1 + K_2)\, Q \cos 2\beta + (K_1 - K_2)\, U \sin 2\beta \cos \delta t + (K_1 - K_2)\, V \sin 2\beta \sin \delta_t\right) \qquad (3.1.1)$$

where K_1 and K_2 are the intensity transmission coefficients for the analyser.

Note that the retardance introduced by the analyser does not appear in this equation, and hence cannot affect the measurement of polarisation. Consider first of all the case of a perfectly aligned analyser, i.e. $\beta = 45^\circ$ or 135°. The equation above becomes:

$$I_t = \tfrac{1}{2}\left(K_1 + K_2\right) I \pm (K_1 - K_2)\, U \cos \delta_t \pm (K_1 - K_2)\, V \sin \delta_t) \qquad (3.1.2)$$

where upper signs refer to $\beta = 45^\circ$ and lower signs to $\beta = 135^\circ$. This equation leads to a measure of polarisation that differs from the ideal case only by a factor $(K_1 - K_2)/(K_1 + K_2)$. If we calibrate by passing 100% circularly polarised light through the system, this factor is eliminated. If the analyser orientation is not exactly 45° or 135°, a dependence on instrumental Stokes parameter Q can arise. Putting realistic values into (3.1.1) leads to the following table which illustrates the size of the effect.

β (°)	q' (%)		
	Q = 0.20	Q = 0.35	Q = 0.50
40	0.967	0.943	0.920
41		0.954	
42	0.980	0.965	0.950
43		0.976	
44	0.993	0.988	0.983
45	1.000	1.000	1.000
46	1.007	1.012	1.018
47		1.025	
48	1.021	1.038	1.055
49		1.051	
50	1.036	1.065	1.095

Here $q' = q/q_{CAL}$, $K_1 = 0.70$, $K_2 = 0.0007$. Input Stokes parameters were I = 1, U = 0, V = 0.01, Q as shown. This table is also shown as figure A16. While the actual misalignments of the Analyser were unfortunately not measured, the mechanical arrangement should lead to the encoder positions being accurate to better than 2°. The table illustrates that in situations where circular polarisation is measured in the presence of strong linear (i.e. the measurement of calibration polarisations at wavelengths far from that at which the waveplates are quarterwave), the perceived polarisation can be affected by up to 2% of its value. With the reduction procedure in operation, these effects are greatly reduced by the analyser and polarimeter rotations. To see this consider the following case. If the orientations of the polarimeter are denoted 0° and 90°, and those of the analyser A and B, where A corresponds to setting $\beta = 45^\circ + \varepsilon$, and B to

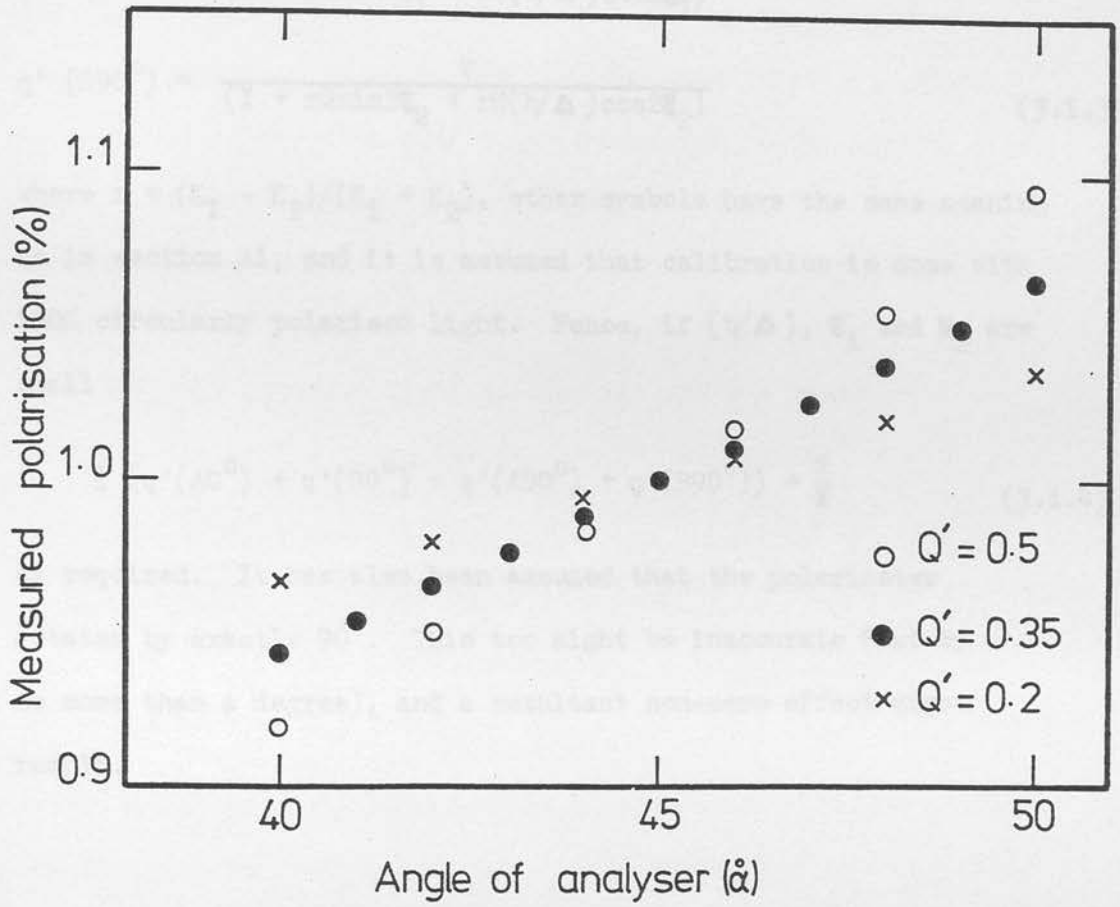

Figure A16 : The effect of a misaligned analyser. When the analyser is not at 45^{o} to the system axis, the measured circular polarisation (1%) is affected by any linear polarisation of the incoming beam. Specifically the measurement is affected by the size of the Q Stokes parameter. Three cases are shown, where Q' = Q/I = 50%, 35% and 20%.

$= 135^{\circ} + \varepsilon_2$, then

$$q'(A0^{\circ}) = \frac{V}{(I + rQ\sin 2\varepsilon_1 + rU(b/\Delta)\cos 2\varepsilon_1)}$$

$$q'(B0^{\circ}) = \frac{V}{(I - rQ\sin 2\varepsilon_2 - rU(b/\Delta)\cos 2\varepsilon_2)}$$

$$q'(A90^{\circ}) = \frac{V}{(I - rQ\sin 2\varepsilon_1 - rU(b/\Delta)\cos 2\varepsilon_1)}$$

$$q'(B90^{\circ}) = \frac{V}{(I + rQ\sin 2\varepsilon_2 + rU(b/\Delta)\cos 2\varepsilon_2)} \qquad (3.1.3)$$

where $r = (K_1 - K_2)/(K_1 + K_2)$, other symbols have the same meaning as in section A1, and it is assumed that calibration is done with 100% circularly polarised light. Hence, if (b/Δ), ε_1 and ε_2 are small

$$\frac{1}{4}(q'(A0^{\circ}) + q'(B0^{\circ}) + q'(A90^{\circ}) + q'(B90^{\circ})) = \frac{V}{I} \qquad (3.1.4)$$

as required. It has also been assumed that the polarimeter rotates by exactly 90°. This too might be inaccurate (but by no more than a degree), and a resultant non-zero effect might result.

3.2 Imperfect calibration filter

The calibration filter consists of a linear polariser at 45° to the axis of a quarter wave retarder. If the polariser is birefringent, misaligned or of dichroic efficiency less than one, the fractional circular polarisation of the light leaving the filter will not be the assumed value. The proportion of linearly polarised light in the beam may also increase leading to enhanced interaction with other components in the optical train. The system matrix for an imperfect calibration filter is given in Appendix A2, where the retardance of the waveplate is assumed to be 90°.

If the incoming light is unpolarised, the state of polarisation of the light leaving the filter is:

$$\begin{aligned} I' &= (K_1 + K_2)\, I \\ Q' &= (K_1 - K_2)\, I\cos^2 2\alpha \\ U' &= (K_1 - K_2)\, I\cos 2\alpha \sin 2\alpha \\ V' &= (K_1 - K_2)\, I\sin 2\alpha \end{aligned} \qquad (3.2.1)$$

where α is the angle at which the waveplate is orientated, and the linear polarisation axis is assumed to be at 0°. It is clear that if the linear polariser is misaligned, equivalent to $\alpha \neq 45^{\circ}$, V'/I' will decline and linear polarisation will appear in the beam (mainly in Stokes parameter, U). Any misalignment of this component should be small and comparable to the error in aligning the two components of (each of) the waveplates (about 1 arcminute - see section A3.3). The factor $(K_1 - K_2)/(K_1 + K_2)$ also appears. This factor is not eliminated in the reduction, but will not seriously affect the calibration within the wavelength range

3000 - 7500 Å. It is tabulated in table A3.

If the light falling upon the calibrator is polarised, the non-ideality of the polaroid can affect the measurements by a small amount. It is the information in Stokes parameter U that has the greatest effect. The following table is calculated from the expressions shown in the appendix, and presumes $\alpha = 45^{\circ}$, $K_1 = 0.7$, $K_2 = 0.0007$, $Q/I = 0.3$ and $V/I = 0$. χ is the retardance of the polariser.

χ	Q'/I'	U'/I'	V'/I'
0	0.000	0.019	0.998
10	0.003	0.019	0.998
20	0.006	0.018	0.998
30	0.009	0.016	0.998
45	0.013	0.013	0.998
60	0.016	0.009	0.998

These figures for high χ's are a little misleading. There appears to be so little difference because K_1 and K_2 remain at values characteristic of the non-birefringent wavelengths of the polaroid. If K_1 and K_2 are chosen such that a beam of light would be 50% polarised (i.e. $K_1 = 0.7$, $K_2 = 0.23$), and a couple of options from the last table are repeated, it is found that:

χ	Q'/I'	U'/I'	V'/I'
0	0.000	0.259	0.505
30	0.129	0.224	0.505
45	0.183	0.183	0.505
60	0.224	0.129	0.505

To summarise: the most important non-ideality of the calibration filter is the loss of dichroic efficiency. The calibration procedure is such that 100% linearly polarised light is always assumed to be produced by the polaroid. If the dichroic efficiency is only 50%, we overestimate polarisation by a factor of 2. By comparison any birefringence of the polaroid is unimportant, since it only makes a significant difference when the dichroic efficiency is also degraded. Since dichroic efficiency only starts to fall off in the red as the polaroid becomes birefringent, by avoiding one evil, we succeed in avoiding both.

3.3 Non-ideal, misaligned and non-identical waveplates

The measurement of linear and circular polarisation involves three waveplates. It is assumed that: the waveplates are in fact quarter wave at the wavelength stated; the two waveplates for linear polarisation measurements are exactly at 45°; all three waveplates are identical.

If the polarimeter measures a calibration polarisation of 90% rather than 100%, this reflects both the effect of a sinusoidal rather than a squarewave modulation of retardance by the photoelastic modulator, as well as a waveplate which at wavelengths $\lambda \neq \lambda_{Q}$ is not a quarter wave retarder. Both these effects are taken out by multiplying by the factor (1.0/0.9). As the calibration polarisation is a measure of the efficiency of the polarimeter as a detector of polarisation, it is important to be able to maintain a high value across the spectrum. A further consideration is the proportion of linearly polarised flux in the light after the calibration filter. It has been shown above that the sinusoidal oscillation of the Modulator birefringence leads to a sensitivity to linear polarisation when measuring circular polarisation (section A1.3). Since misalignments may occur in the various positions of analyser and polarimeter used to eliminate this dependence, it is preferable to have only a small proportion of linearly polarised light in the light after it has passed through the calibration filter. If light 100% linearly polarised is incident upon a waveplate at 45° to its fast axis, the resultant Stokes vector is $(I, -I\cos\delta, 0, -I\sin\delta)^{T}$, where δ is the retardance of the waveplate. If p and q represent the linear and circular polarisations of the beam respectively,

then $q = \sin\delta$ and $p = \cos\delta$. To obtain the following table, it is also assumed that:

$$\delta = \delta(\lambda) = \pi/2 \times \lambda_Q/\lambda \qquad (3.3.1)$$

where λ_Q is the wavelength for which the waveplate exhibits quarter wave retardance. Signs have been dropped.

λ(Å)	λ_Q = 3800 Å		λ_Q = 5825 Å	
	q	p	q	p
3000	0.914	0.407		
3500	0.991	0.134		
4000	0.997	0.078	0.754	0.657
4500	0.970	0.242	0.895	0.446
5000	0.930	0.368	0.967	0.256
5500			0.996	0.093
6000			0.999	0.046
6500			0.987	0.162
7000			0.965	0.261
7500			0.939	0.344
8000			0.910	0.414
8500			0.880	0.474

The waveplates with λ_Q = 3800 Å were normally used when wavelengths $\lambda \leq$ 4600 Å were studied. Above this, the other set was used. Equation (3.3.1) is a good approximation to the true wavelength dependence of δ, except for wavelengths below 3200 Å. See figure A12. The table shows that, in normal use, light up to 40% linearly polarised is present in the measurement of calibration polarisations at both ends of the wavelength range.

Polarisation measures are taken in both analyser positions for the waveplate and for the calibration filter. If these are

denoted P_A, P_B, P_{ACal}, P_{BCal} (A and B being the two analyser positions) then it can be argued that a better way to calibrate the waveplate measurements would be:

$$p^1 = (P_A + P_B)/(P_{ACal} + P_{BCal}) \qquad (3.3.2)$$

The justification for this is clear. Any difference in the polarisation registered in the two analyser positions caused by the presence of linearly polarised flux will be different in the two cases. Some numerical tests were carried out to compare this method of reduction with that actually used. It was found that the difference in the average calibrated polarisation was only of the order of 1% of the polarisation (except when the calibration polarisation was low).

In each set of retarders, the two waveplates may not be mounted with their fast axes exactly 45° apart, and also the mean angle of each set may be different. The second point is overcome by separately calibrating position angles measured with each set of optics on standard objects. If the axes of the two waveplates are not at 45°, "crosstalk" between the Stokes parameters will result. If the angle between them is γ, Q and U are the true Stokes parameters and q and u the measured values, then:

$$q = Q \qquad u = Q\cos 2\gamma + U\sin 2\gamma \qquad (3.3.3)$$

The above quotation shows that for a linearly polarised source, (p, θ), the measured values (p_1, θ_1) will depend on both p and θ. The dependence is illustrated in figures A17 and A18. Please note the following points.

i) The amplitude of $\Delta\theta$ (= measured - true) is equal to the misalignment angle, i.e. $(45 - \gamma)$.

ii) The displacement of the maximum in $\Delta\theta$ from 90° also approximates to $(45 - \gamma)$.

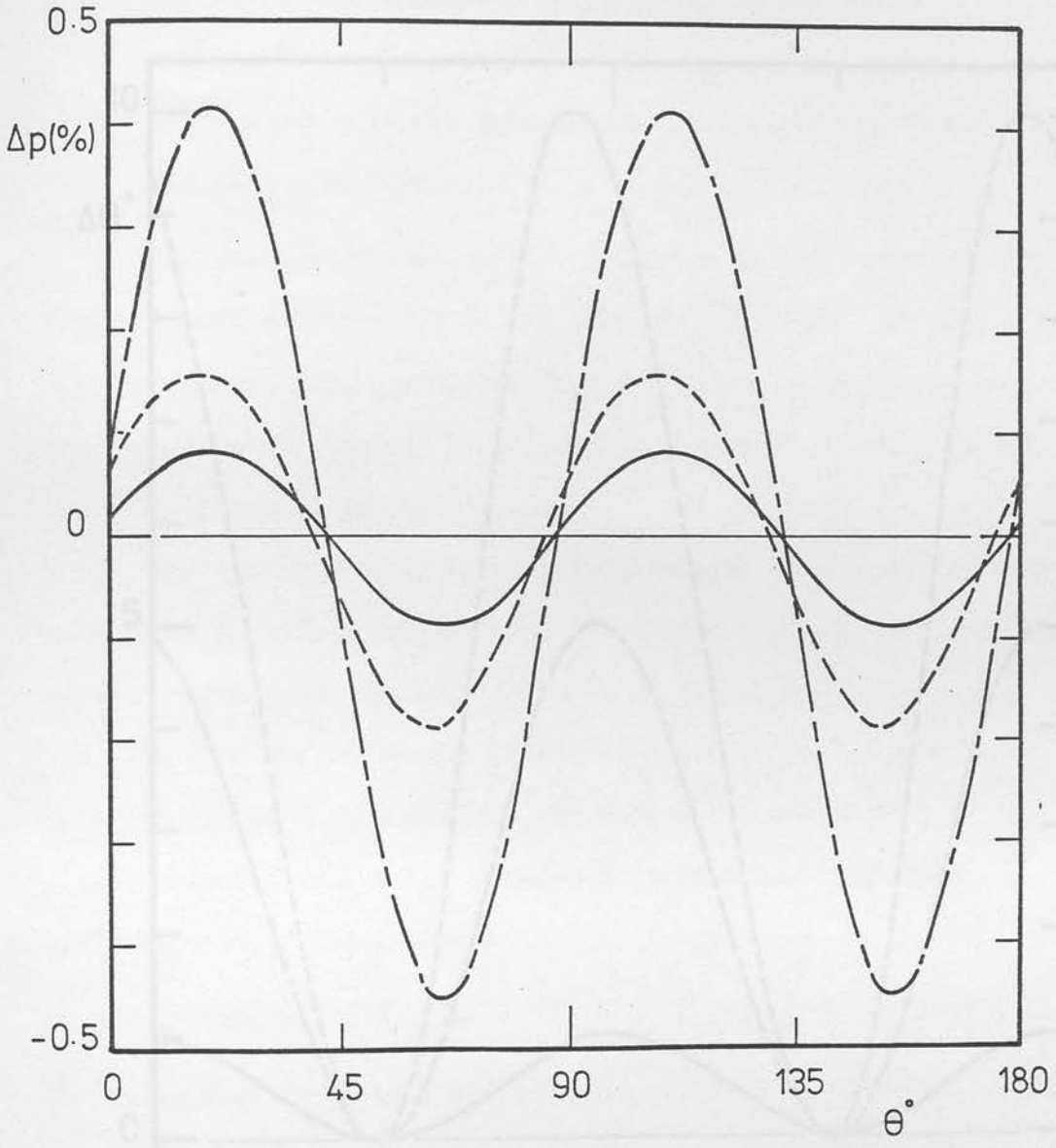

Figure A17 : Effect on the measured degree of linear polarisation of waveplate fast axes being $\nu \neq 45^{o}$ apart. Δp = measured polarisation - true polarisation. Solid line is case of $\nu = 40^{o}$ and true polarisation of 1%. Dashed line is case of $\nu = 35^{o}$ and true polarisation of 1%.

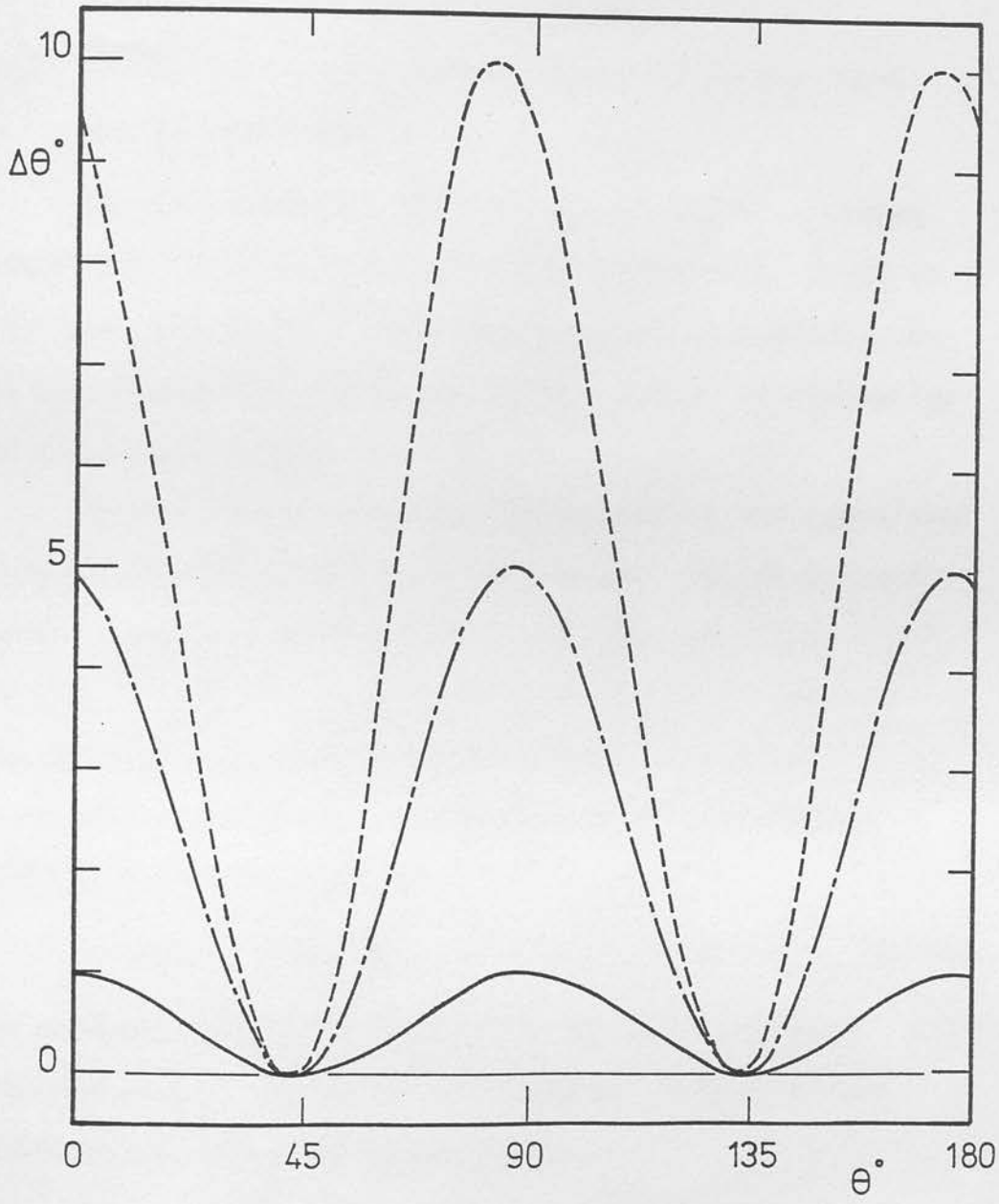

Figure A18 : Effect on the measured position angle of waveplate fast axes being $\nu \neq 45^{o}$ apart. $\Delta\theta$ = measured position angle - true position angle (both in the instrumental system). Solid line is case of $\nu = 44^{o}$ chained line is case of $\nu = 40^{o}$, and dashed line is case of $\nu = 35^{o}$. Degree of polarisation has no effect on these graphs.

iii) The degree of polarisation has no effect on $\Delta\sigma$.

iv) Increasing p increases the amplitude of Δ p to scale.

v) Increasing misalignments displace the curves towards smaller σ and increase the amplitude.

vi) The Δ p curve is not symmetric about the x-axis. There has been a dc level shift.

The measured values of γ for the two sets of waveplates were $\gamma(3800) = 47.^{\circ}8 \pm 0.3$ and $\gamma(5825) = 50.^{\circ}0 \pm 0.3$. It can be seen from these graphs and from figure C15 that measurements with the 5825 Å waveplates may be affected by up to 9% in polarisation and 5° in position angle.

The two sets of waveplates are designed to give quarterwave retardance at 3800 Å and 5825 Å respectively. The manufacturer's quoted tolerance on the waveplates is $\lambda/300$, i.e. $1.^{\circ}2$ or $\pm$ 50 Å and $\pm$ 80 Å on the two wavelengths quoted above. Any departure from the quoted wavelength will not affect the measurement of linear polarisation, while circular polarisation is slightly affected through the factor:

$$K = \sin 90^{\circ} \times \lambda_0/\lambda \qquad (3.3.4)$$

The propagated error in K and hence in the derived circular polarisation is $2\frac{1}{2}\%$ of the polarisation. An error on the retardance may arise for several reasons.

i) The thickness of the two components of the waveplate are not accurately controlled.

ii) During the cementing process, one of the components has been tilted with respect to the other.

iii) The sample of crystal quartz from which the two components were cut may differ somewhat in birefringence from the

laboratory values used to calculate the necessary thickness of the components.

iv) The optic axes of the two components may not be accurately crossed.

v) The effect of multiple internal reflections within a waveplate is to give a retardance strongly dependant on its exact thickness (to better than the wavelength of light) (see HOLMES, 1964).

The first and last two effects should be negligeable. The thicknesses of the components are controlled to 0.2 μ, while the optic axes are crossed to 1 arcminute. The effect of internal reflections being so critically dependent on thickness should lead to it cancelling across the waveplate. The importance of factor (iii) is difficult to judge but one component could be tilted with respect to the other by almost a degree because causing a 1% change in retardance.

More important than whether a certain waveplate exhibits a specific retardance is whether each of the three waveplates is identical to the others. Since they are all made from the same batch of material and are polished together, effects (i) and (iii) should not be important. Perhaps most important is the possibility that one or more of the filters could be tilted in its holder. A $\frac{1}{2}^{\circ}$ tilt would give a 1% change in retardance with larger tilts having a proportionately larger effect. Visual observation of the filters was used to ensure that the filters were normal to the beam and not tilted with respect to each other, though small tilts (1° - 2°) would not have been detected. A displacement of images observed through the waveplates would not arise unless the tilt was gross. However such a displacement was

seen with the 5825 Å calibration filter in the optical train. The most likely cause of this is that the calibration filter was made wedge-shaped when the difficult task of attaching the polariser to the waveplate was carried out. This is unlikely to detectably affect the polarimetry.

3.4 The photoelastic modulator

Reference was made to the phenomenon of 'static stress' in section A2.3. The effect is eliminated by taking measurements at positions of the polarimeter 90° apart, as will now be demonstrated.

Consider the measurement of circular polarisation, where, for the polarimeter in its 0° orientation:

$$I_t = \tfrac{1}{2} (I \pm U\cos\delta_t \pm V\sin\delta_t) \qquad (3.4.1)$$

If we represent the instantaneous modulator retardance, δ_t, by

$$\delta_t = \eta + A\sin\omega t \qquad (3.4.2)$$

where η represents a mean d.c. level of retardation, and then integrate in the normal manner, between $\omega t = \pi/2 \pm \Delta$ and $3\pi/2 \pm \Delta$, we find

$$P_{A,BO} = \frac{\pm a\,(V\cos\eta - U\sin\eta)}{I\Delta \pm b\,(V\sin\eta + U\cos\eta)} \qquad (3.4.3)$$

where positive signs refer to P_{AO} and negative ones to P_{BO}, and a,b have been defined above. For the calibration measurement, assuming the retardance of the waveplate to be 90° for simplicity,

$$P_{CalA;BO} = \frac{\pm a\cos\eta}{\pm b\sin\eta} \qquad (3.4.4)$$

and it can be shown that, ignoring terms in $(b/\Delta)^2$,

$$\frac{1}{2}\left(\frac{P_{AO}}{P_{CalAO}} + \frac{P_{BO}}{P_{CalBO}}\right) \simeq \left(\frac{V}{I} - \frac{U}{I}\right)\tan\eta \qquad (3.4.5)$$

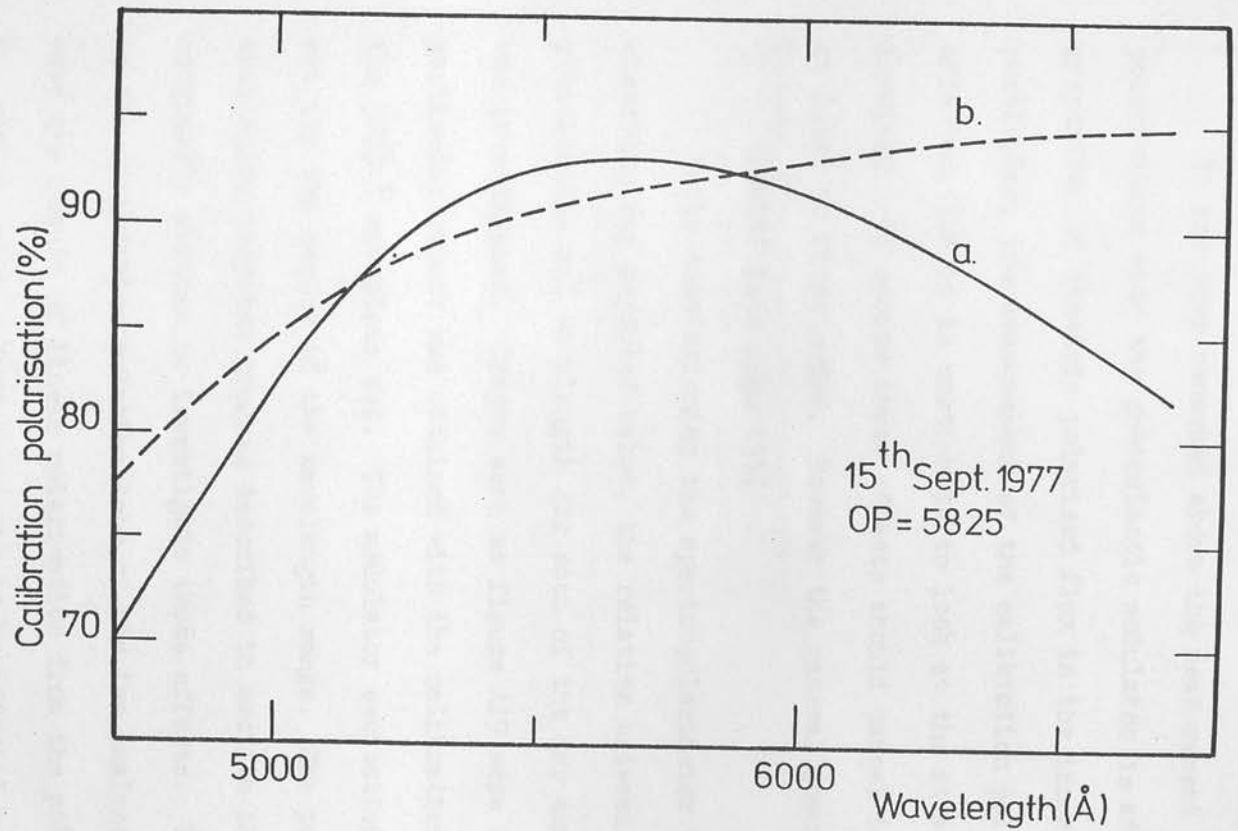

Figure A19 : Calibration polarisations measured in each of the two analyser positions A (=a) and B (=b). Obtained using a light source and with the modulator optimised for the centre of the wavelength range.

The corresponding expression for the polarimeter at 90° is

$$\frac{1}{2}\left\{\frac{P_{A90}}{P_{CalA90}} + \frac{P_{B90}}{P_{CalB90}}\right\} = \frac{V}{I} + \frac{U}{I} \tan \eta \qquad (3.4.6)$$

Hence averaging these two orientations will eliminate the effect.

It has been remarked above the measurement of circular polarisation with the photoelastic modulator is affected by the proportion of linearly polarised flux in the incoming light. In particular, the measurement of the calibration polarisation is affected, and it is worthwhile to look at the size of the effects involved. Of course these effects should cancel in the analysis, at least to first order. However the general assumption above

INSERT (see page 133)

While commissioning the spectropolarimeter before the first observing run reported below, the relation between calibration polarisation and wavelength for each of the two analyser positions was investigated. Graphs such as figure A19 were obtained. This particular result was obtained with the calibration filter of the 5325 Å waveplate set. The modulator excitation voltage was set for the centre of the wavelength range. The polarimeter simulation computer program described in section A2.3 was originally written to investigate these effects. If the difference in the calibration polarisations of the two analyser positions were the result of linear polarisation from the polaroid part of the filter, such a difference should be affected by rotating the calibration filter. It was found by runs with the simulation program that if the angle of the polaroid axis to the modulator axis was $\phi = 0°$, polarisations with the analyser in either position were identical. However, as ϕ increased, a greater difference was seen until $\phi = 45$ where a maximum effect occurs. Figure A20

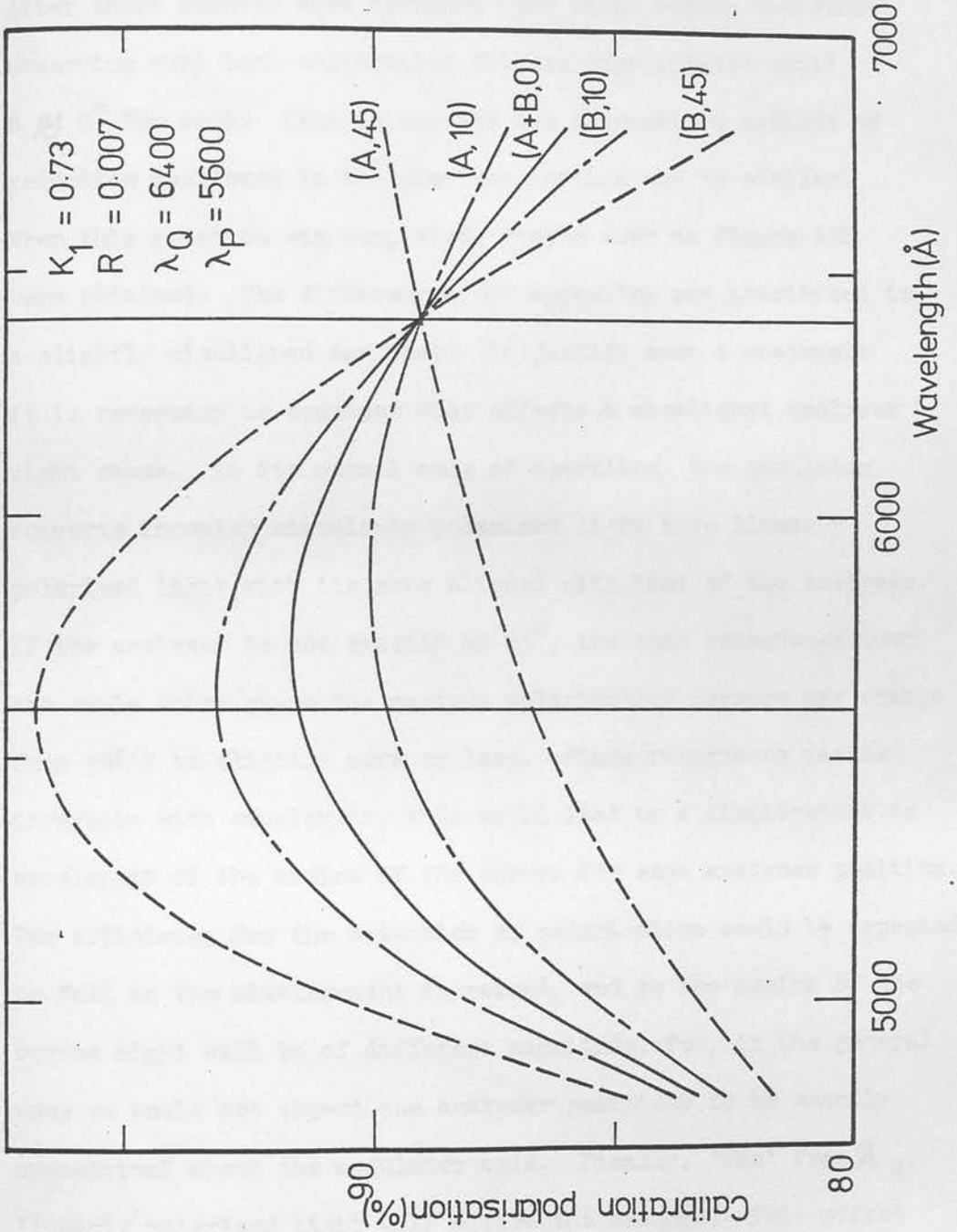

Figure A20 : The effect of rotating the calibration filter on the measured polarisation in each analyser position. Each line is labelled with an analyser position (A or B) and an angle (0^o, 10^o, 45^o). The angle is of the polaroid in the filter to the system axis. Note that when this angle is zero, and the axis of the polaroid is midway between the two analyser positions, polarisations measured in the two analyser positions are identical.

illustrates this. The angle of the polaroid of the calibration filter that was used to obtain figure A19 was $\phi \simeq 40^{\circ} \pm 2^{\circ}$. After these results were obtained (and again before the first observing run) both calibration filters were rotated until $\phi \approx 0^{\circ}$ for each. This is why the two alternative methods of reduction mentioned in the previous section are so similar. When this rotation was completed, graphs such as figure A21 were obtained. The differences now appearing are attributed to a slightly misaligned analyser. To justify such a statement it is necessary to consider what effects a misaligned analyser might cause. In its normal mode of operation, the modulator converts incoming circularly polarised light into linearly polarised light with its axis aligned with that of the analyser. If the analyser is not exactly at 45°, the mean retardance over the cycle which gives the maximum polarisation measure may change from $+\pi/2$ to slightly more or less. Since retardance varies inversely with wavelength, this would lead to a displacement in wavelength of the maxima of the curves for each analyser position. The efficiency for the detection of polarisation would be expected to fall as the misalignment increased, and so the maxima of the curves might well be of different magnitude, for, in the general case we would not expect the analyser positions to be exactly symmetrical about the modulator axis. Finally, 'far' from λ_{Q}, linearly polarised light will affect the measure. This effect will be zero at λ_{Q} and will increase faster on the blue side than on the red.

Inspection of figure A21 shows that all of these effects are seen. The displacement of the maxima in wavelength is 450° or about 7%. The difference in maximum polarisations is small

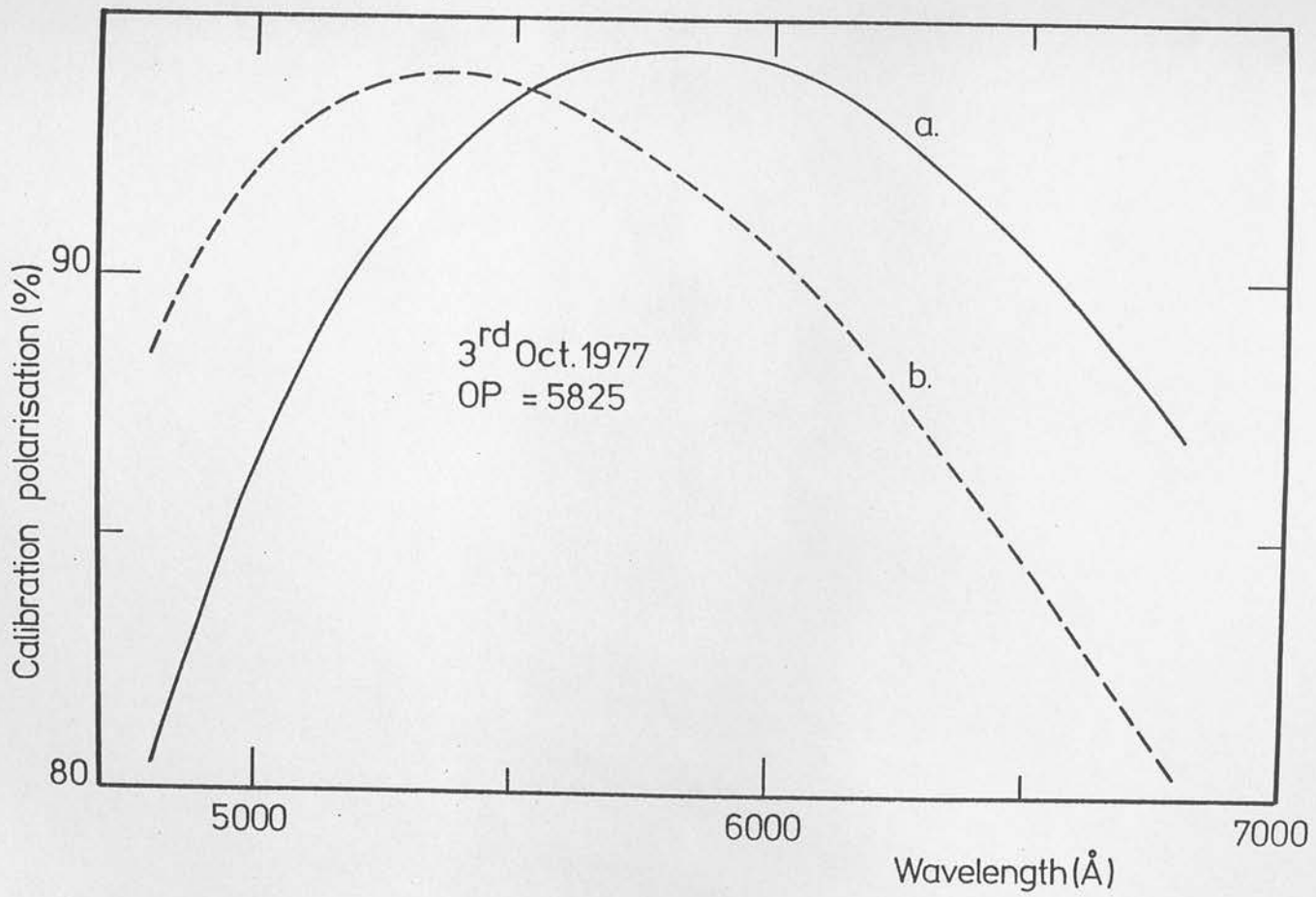

Figure A21 : Calibration polarisations measured in each of the two analyser positions A (=a) and B (=b). The axis of the polaroid in the calibration filter is midway between the two analyser positions.

(only $\frac{1}{2}\%$ - but see the comment on the alignment of the analyser in section A2.4). Figure A22 shows the situation when these differences are eliminated by simple zero-point scale shifts.

INSERT (page 129)

that $(b/\Delta)^2$ is negligeable may fail in certain cicumstances - in particular when the modulator is optimised at a wavelength at some distance from the wavelength of interest. At a wavelength 500Å from that for which the modulator is set, $(b/\Delta)^2$ can be 0.03.

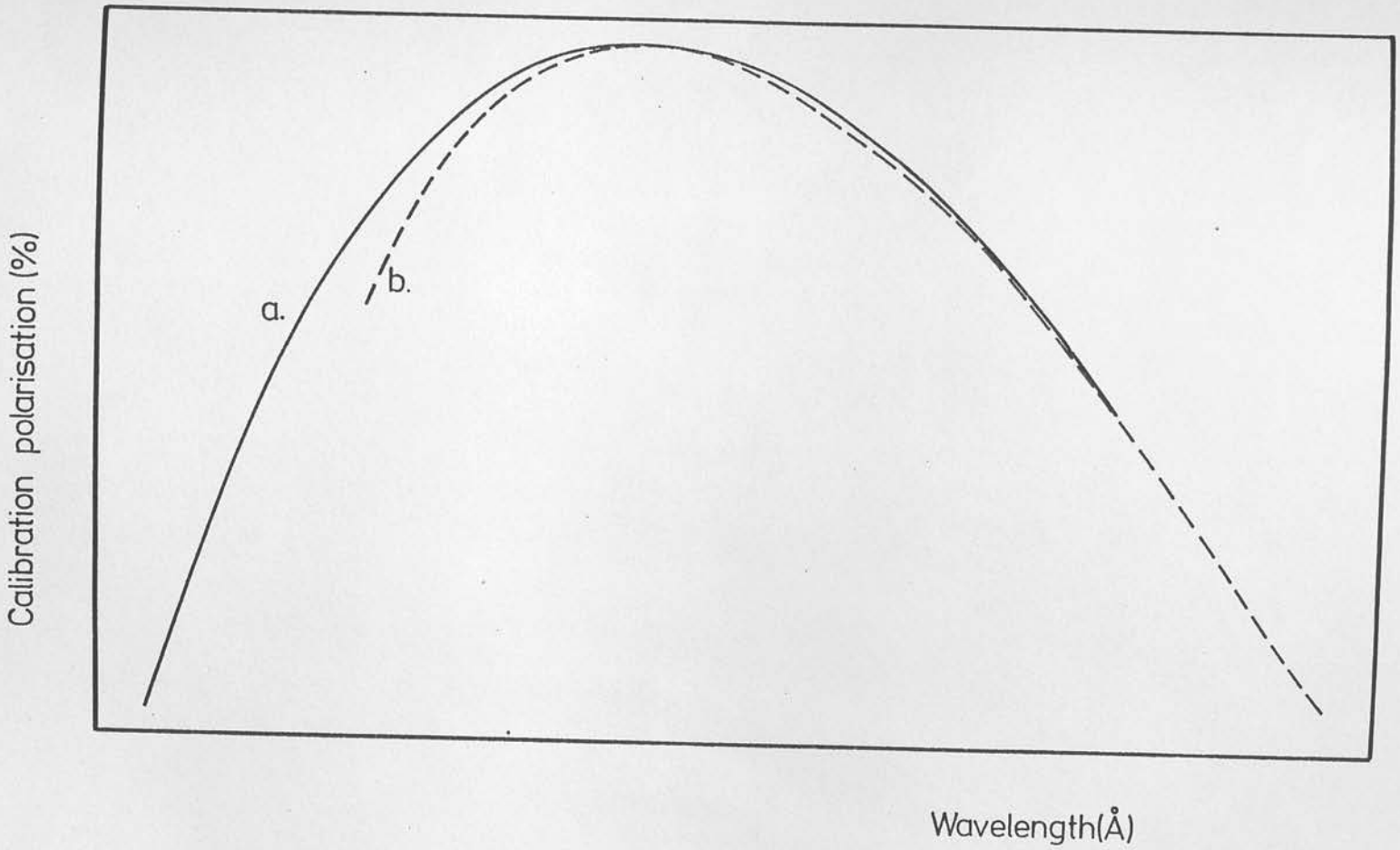

Figure A22 : As figure A21, where the two curves have been moved (by zero-point corrections only) until their maxima coincided.

3.5 The effect of the spectrometer and photocathode

It was considered above how an imperfect analyser would affect themeasurement of polarisation, and in particular how any birefringence in the analyser had no effect. When other polarisation sensitive elements following the analyser are also considered these conclusions may be altered. Narrow slits, tilted mirrors and gratings can all polarise light incident on them, as can the photomultiplier photocathode, since this is inclined. It is intended to model all these components using just one dichroic waveplate matrix, an approach requiring justification. Note initially that the "characteristic axes" of the slits, mirrors and grating are the same, probably to better than a degree. Further, the axis of the photocathode is also the same, since it is aligned along the spectrum. It will now be shown that the product of two dichroic waveplate matrices with the same orientation is simply another dichroic waveplate matrix.

Define two such matrices:

$$M_{1,2} = \begin{bmatrix} K & k & 0 & 0 \\ k & K & 0 & 0 \\ 0 & 0 & a\cos\Delta & a\sin\Delta \\ 0 & 0 & -a\sin\Delta & a\cos\Delta \end{bmatrix}_{1,2}$$

where, for convenience, the notation has been changed somewhat. Note that $a = \sqrt{(K^2 - k^2)}$.

If we define:

$$\bar{K} = K_1K_2 + k_1k_2 \qquad \bar{\Delta} = \Delta_1 + \Delta_2$$

$$\bar{k} = K_1k_2 + k_1K_2 \qquad \bar{a} = a_1 + a_2$$

Then $\bar{W} = W_1 \times W_2 = \begin{bmatrix} \bar{K} & \bar{k} & 0 & 0 \\ \bar{k} & \bar{K} & 0 & 0 \\ 0 & 0 & \bar{a}\cos\bar{\Delta} & \bar{a}\sin\bar{\Delta} \\ 0 & 0 & -\bar{a}\sin\bar{\Delta} & \bar{a}\cos\bar{\Delta} \end{bmatrix}$.

and $\bar{a} = \sqrt{(\bar{K}^2 - \bar{k}^2)}$.

Hence by suitable choice of K, k and Δ above, all six components after the analyser may be represented by one matrix.

The case of the measurement of circular polarisation is considered, including the effect of components after the (imperfect) analyser. The matrix representation of the optical train and the system matrix are given in appendix A2 . For clarity, γ is set to zero, and β to 45°, when:

$$I_t = 1/4\ ((K_1 + K_2)(L_1 + L_2)I + (2\sqrt{K_1K_2}\cos\chi)(L_1 - L_2)Q$$
$$+((L_1 + L_2)(K_1 - K_2)\cos\delta_t + 2\sqrt{K_1K_2}\,(L_1 - L_2)\sin\chi\sin\delta_t)U$$
$$+((L_1 + L_2)(K_1 - K_2)\sin\delta_t - 2\sqrt{K_1K_2}\,(L_1 - L_2)\sin\chi\cos\delta_t)V)$$

where (L_1, L_2) are the intensity transmission coefficients for the spectrometer/detector combination (with γ the orientation of the associated polarisation axis), and χ is the retardance produced by the birefringence of the analyser. From this we obtain

$$p_A = \frac{a}{\Delta}\ \frac{(mU\sin\chi+(L_1+L_2)(K_1-K_2)V)}{(K_1+K_2)(L_1+L_2)I+mQ\cos\chi+(b/\Delta)((L_1+L_2)(K_1-K_2)U-mV\sin\chi))}$$

where $m = 2\sqrt{K_1K_2}\,(L_1-L_2)$

If 100% circularly polarised light passed through this system, we find

$$P_{ACal} = \frac{+a}{\Delta} \frac{(L_1 + L_2)(K_1 - K_2)}{(K_1 + K_2)(L_1 + L_2) - (b/\Delta)m\sin\chi}$$

After averaging the measures between the two analyser positions, we obtain

$$\frac{1}{2}\left(\frac{P_A}{P_{ACal}} = \frac{P_B}{P_{BCal}}\right) = \left(\frac{m\sin\chi}{(L_1+L_2)(K_1-K_2)} \quad \frac{U}{I} + \frac{V}{I}\right)\left(1 + \frac{m\cos\chi}{(L_1+L_2)(K_1+K_2)} \quad \frac{Q}{I}\right)^{-1}$$

and hence, provided that $m/(L_1 + L_2)(K_1 - K_2)$ and $m/(L_1 + L_2)(K_1 + K_2)$ are small, averaging 0° and 90° orientations of the polarimeter will result in an accurate measurement of the circular polarisation. Typical values in the above equation might be $L_1 = 0.6$, $L_2 = 0.4$, $m = 0.01$ and $(K_1 - K_2) \simeq (K_1 + K_2) \simeq 0.7$. These values imply an error in V/I of less than 10^{-6} through the values assumed small above.

3.6 Other factors influencing the measurement of polarisation

Before starlight enters the polarimeter it is reflected by the telescope mirrors and this will affects its state of polarisation. When working at the Cassegrain focus, any linear polarisation introduced is usually small because of the symmetry of the optical arrangement. Larger effects (0.1%) may occur: there may be vignetting of the beam in the polarimeter; the aluminium coatings may have aged differently across the mirrors; or different weights may be given to different regions of the primary by the spatially variable sensitivity of the photocathode. The retardance caused by the telescope mirrors should also be small (see Kemp et al. (1972)). Both effects can be enhanced if the instrument is slightly off-axis with respect to the telescope. Observations were made of bright unpolarised stars in order to determine the importance of the polarisation introduced by each telescope. Some of these measurements are listed here as table A5. Only on the Mauna Kea 24" telescope have large effects been seen. This telescope contributes a linear polarisation of around 0.1%. The instrumental polarisation is well determined, and then subtracted to give the presented measurements. Some planetary measurements were taken with this telescope (1980 measurements, chapter B).

Some factors that may affect the measurement of polarisation have been dealt with only briefly in the last three sections. A number of these are discussed more fully in following sections where they appear to be relevant to the data being presented. In particular, the following are discussed later: the effect of an extended image in the entrance aperture (section B5); the accuracy of sky polarisation measurements (section B6); the effect

of misaligned and possibly tilted waveplates (section 04.3.2); and the problem of stray light (section 05.4).

4. Recent modifications to the spectropolarimeter

The previous sections have made clear the limitations of the ROE Spectropolarimeter. When a new spectropolarimeter was built at ROE, the experience gained with this instrument allowed many of the problems occuring in the optical system to be eliminated. The MkII spectropolarimter is controlled by an hierarchical system of two microprocessors and a minicomputer, and uses both hard and floppy discs for non-volatile memory. Most instrumental functions are automated, including guiding, which is implemented by having a SIT-vidicon camera looking at the offset guide mirror. The present instrument has recently been modified to improve its flexibility and reliability. Hand-wired logic has been replaced by a system of two microprocessors, carried across practically unchanged from the MkII instrument. These give improved control and display of status information, though final control still remains with the programmable calculator. The waveplate and order sorter wheels are now under the control of the calculator, as is the entrance aperture wheel of the spectrometer. This aperture wheel has both slits and circular apertures. The optical train remains identical to that of the instrument described in this paper. However modifications have been made to allow more accurate setting up and adjustment of the various components. These modifications should lead to further reduction in the importance of instrumental effects in our polarimeter. Some of the modifications and improvements will now be detailed. The offset guide mirror has been realuminised, the illumination improved and the problem of focussing resolved. Guiding is now relatively easy. The

quarterwave retardation plates have been put into proper filter holders and are held in by silicone rubber. These waveplates can now be rotated in situ by up to $\pm 2^{\circ}$. A mask has now been affixed to the waveplate side of the photoelastic modulator such that, while some of the beam may still be vignetted at the modulator, light that does not pass through the modulator can no longer reach the photomultiplier. The analyser is now removeable and held in place in such a way that it does not warp. The encoders that determine the two analyser positions are now adjustable in situ (by almost $\pm 5^{\circ}$). As yet a prism has not been installed. A new viewing eyepiece has been designed and incorporated into the spectrometer. With better illumination, centring is now quick and efficient. The slits in the aperture wheel allow high resolution (5 Å) work such as Zeeman polarimetry. The order sorter filters have been antireflection coated, with the exception of the RG 715. The multilayer coating is optimised for the visual region and would have led to increased reflection losses for the filter. Finally, the instrument has also been upgraded by the provision of a photometer section which optionally replaces the spectrometer. Broad band interference filters are mounted in a filter wheel and are selected by the calculator. The full range of resolutions is now available - from 5 to 5000 angstroms.

Engineers involved in this update were A.J. Hutton (electronic), T.A. McKie (mechanical) and J.T. Herd (microprocessor software).

Appendix A1 : The mathematical description of light.

This appendix is split into several sections, detailed below:

1. Definition of linearly, circularly and elliptically polarised light.
2. Introducing the Stokes parameters.
3. The Mueller Calculus. Listing of matrices used in various parts of this thesis. Derivation of one of them.

1. Circular, linear and elliptical polarisation

It was stated in the General Introduction that any beam of light might be regarded as a mixture of unpolarised light, of linearly polarised light, and of circularly polarised light. First of all, we shall make these concepts clearer.

Experiment shows that in circumstances where light is satisfactorily described by the mathematics of a wave model, then that wave is transverse to the direction of propagation. Solution of the classical Maxwell equations describing the magnetic and electric fields

$$\text{curl } \underline{E} = -\mu\mu_o \frac{\partial \underline{H}}{\partial t} \qquad \text{curl } \underline{H} = \sigma E + \varepsilon_o \varepsilon \frac{\partial \underline{E}}{\partial t}$$

$$\text{div } \underline{H} = 0 \qquad \text{div } \underline{E} = 0 \qquad \text{(A1)}$$

gives the wave equations

$$\nabla^2 \underline{E} - \sigma\mu\mu_o \frac{\partial \underline{E}}{\partial t} - \varepsilon\varepsilon_o\mu\mu_o \frac{\partial^2 \underline{E}}{\partial t^2} = 0$$

and

$$\nabla^2 \underline{H} - \sigma\mu\mu_o \frac{\partial \underline{H}}{\partial t} - \varepsilon\varepsilon_o\mu\mu_o \frac{\partial^2 \underline{H}}{\partial t^2} = 0 \qquad \text{(A2)}$$

These equations are linear, and show that the electric and magnetic vectors are at right angles to each other, in phase, and are both perpendicular to the direction of propagation.

A simple sinusoidal wave is a solution to these equations. Such a wave must necessarily be linearly polarised. That is to say, the plane of vibration of the electric vector is constant, and is inclined at an angle θ to some reference direction. When talking of light, we always refer to the electric vector, as it is this component that causes most of the effects we observe. Now consider coherent addition of a second sinusoidal wave of equal amplitude to the first, and whose electric vector oscillates in a plane orthogonal to that of the first. If the two are in phase, a linearly polarised beam results, whose angle to the reference direction is 45^{o}. If there is a phase difference of $\pi/2$ between the beams, the electric vector will appear to rotate about the direction of propagation at a frequency equal to the frequencies of the component waves. Such a beam is termed circularly polarised. If the phase difference is anything else, the electric vector will be seen to execute an ellipse, forming so-called elliptically polarised light.

Consider now the macroscopic case. A beam of light is a collection of these waves, put together with no regard to phase. Furthermore, the quantum theory predicts that even the light from one oscillator will be subject to random phase shifts, breaking down the continuous waves into 'photons'. If, in fact, the photons have randomly orientated electric vectors, the light is said to be unpolarised, or 'natural'. On the other hand, if phase relations do manage to persist over long time scales, due to the nature of the emission or the nature of the light path, we shall obtain elliptically polarised light. In general this light will only be partially polarised. It is clear that linearly polarised light and circularly

polarised light can be regarded as special cases of elliptically polarised light.

2. The Stokes Parameters

Consider a beam of completely elliptically polarised light. To describe the ellipse that the tip of the electric vector is, on average, tracing out, we need four parameters. We need to know the size and shape of the ellipse, its orientation with respect to the reference axes, and in which way it is rotating.

We may resolve this ellipse into two orthogonal sinusoids, with phase differences, δ , and represent them as:

$$E_x = E_{x_o} \cos \omega t \quad \text{and} \quad E_y = E_{y_o} \cos (\omega t - \delta) \qquad \text{(A3)}$$

Note that these are averaged over all photons in the beam. Eliminating time dependence between these gives the ellipse:

$$E_x^2/E_{x_o}^2 + E_y^2/E_{y_o}^2 - 2 E_x E_y \cos \delta / E_{x_o} E_{y_o} = \sin^2 \delta \qquad \text{(A4)}$$

Hence we have specified the ellipse by the parameters E_{x_o} , E_{y_o} , δ and the sign of δ. The sign of δ determines the direction of rotation of the vector, and is a matter of convention. We shall return to this point later.

A more convenient representation suggests itself. It is possible to define the elliptically polarised light by its intensity, I_p, the axial ratio of the ellipse, η , and its azimuth, or angle between the major axis and reference direction, ϕ. The fourth parameter we may take to be the sign of ϕ . These can be found from the relations:

$$I_p = E_{x_o}^2 + E_{y_o}^2$$

$$\tan 2\phi = 2E_{x_o} E_{y_o} \cos\delta / (E_{x_o}^2 - E_{y_o}^2)$$

$$2\eta/(1+\eta^2) = 2E_{x_o} E_{y_o} \sin\delta / (E_{x_o}^2 + E_{y_o}^2) \qquad (A5)$$

To make this simpler, we could define:

$$M = E_{x_o}^2 - E_{y_o}^2$$

$$C = 2 E_{x_o} E_{y_o} \cos\delta$$

$$S = 2 E_{x_o} E_{y_o} \sin\delta \qquad (A6)$$

and hence write (A5) as:

$$\tan 2\phi = C/M \quad \text{and} \quad \frac{2\eta}{1+\eta^2} = S/I_p \qquad (A7)$$

The quantities M, C, S just defined in (A6) turn out to be rather interesting. Note firstly that

$$M^2 + C^2 + S^2 = E_{x_o}^4 + E_{y_o}^4 - 2 E_{x_o}^2 E_{y_o}^2 + 4 E_{x_o}^2 E_{y_o}^2 \cos^2\delta$$

$$+ 4 E_{x_o}^2 E_{y_o}^2 \sin^2\delta$$

$$= E_{x_o}^4 + E_{y_o}^4 + 2 E_{x_o}^2 E_{y_o}^2$$

$$= (E_{x_o}^2 + E_{y_o}^2)^2$$

Therefore $M^2 + C^2 + S^2 = I_p^2$ (A8)

If E_{x_o} and E_{y_o} are equal and $\delta = \pi/2$, the case of perfectly circularly polarised light, then, using (A8)

$$M = C = 0 \qquad S = I_p \tag{A9}$$

The parameter S seems to characterise circularly polarised light. Further, if the light is linearly polarised parallel to the x-axis (and hence E_{y_o} is zero).

$$C = S = 0 \qquad M = I_p \tag{A10}$$

M has also a physical significance. If the light were polarised parallel to the y-axis, M would be negative. The significance of C can be seen by setting E_{x_o} equal to E_{y_o}, and δ to zero. This is the case of linearly polarised light at 45^o to the reference axes. Then

$$M = S = 0 \qquad C = I_p \tag{A11}$$

The above representation of polarised light is termed the Stokes representation, and the parameters I_p, M, C, S, the Stokes parameters. The notation is that of JONES (1941) and PERRIN (1942). Modern astronomical usage tends to follow CHANDRASEKHAR (1950) and WALKER (1954) , in which

$$I_p \equiv I_p \qquad U \equiv C$$
$$Q \equiv M \qquad V \equiv S \tag{A12}$$

We follow their usage from here on.

When writing equations (A3), we noted that we were dealing with quantities averaged over the beam. For unpolarised light, there are no long lasting phase relations, and so M, C and S when averaged over the beam are zero. Therefore the Stokes representation for

unpolarised light is:

$$I_u = I_p \qquad U_u = C_u = 0$$

$$Q_u = M_u = 0 \qquad V_u = S_u = 0$$

Now, the major advantage of the Stokes representation is that "when several independant streams of light are combined, the Stokes parameters for the mixture is the sum of the respective Stokes parameters of the separate streams" (CHANDRASEKHAR, 1950). Hence the most general case of partially elliptically polarised light can be treated as a mixture of purely elliptically polarised light and unpolarised light, and, when we seek to investigate the effect of somemedium or element on the Stokes parameters of a beam of light, the unpolarised and the polarised parts can be treated separately, and simply summed to provide the final result.

We return now to the problem of the description of the direction of rotation of the electric vector in elliptically polarised light. Notice that in the Stokes representation, this reduces to the question of the physical meaning of the sign of V, since $\cos\delta$ is on even function (see equation (A6)). Even when we have decided which direction we shall denote as positive and which negative, it is still necessary to decide which to call "right-handed" and which "left-handed".

The standard convention is given by GEHRELS (1974) . Positive circular polarisation is when the electric vector has increasing θ with time. With this definition, positively circularly polarised light carries positive angular momentum. This means that if an observer who is looking towards the source sees the electric vector rotating in a counterclockwise direction, he is observing positive circularly polarised light. This leads to a resolution of the

second point. In radio-astronomy such a positively circularly polarised wave would be termed right-handed, by reference to the Institute of Radio Engineers definitions of terms (IRE, 1942). All measurements of circular polarisation reported in this thesis are corrected in accord with this convention. CLARKE & GRAINGER (1971) have pointed out that if one looks at the locus of the tip of the electric vector along the direction of propagation, one sees a helix. The handedness of this helix can also be used to define the handedness of the light and this leads to the opposite convention.

3. The Mueller Calculus

The additivity of the Stokes parameters was commented on above. Note however that 'this additivity of the Stokes paramters holds only so long as the component streams forming a mixture have no permanent phase relations between themselves.' (CHANDRASEKHAR, 1950). That is, they are incoherent. For coherent beams, the Stokes parameters cannot be used to describe the sum of several beams, and a form known as the Jones calculus is used. For Stokes parameters the appropriate calculus is the Mueller calculus. In this , the effect of an optical element on a beam is calculated using matrix techniques. First of all, the beam is split into unpolarised and completely polarised light, and the Stokes vectors formed, using (A13).

$$\begin{bmatrix} I \\ Q \\ U \\ V \end{bmatrix} = \begin{bmatrix} I_u \\ 0 \\ 0 \\ 0 \end{bmatrix} + \begin{bmatrix} I_p \\ Q \\ U \\ V \end{bmatrix} \qquad \text{(A14)}$$

Now, operations are performed using 4 x 4 matrices. The usual matrices are given in table A7 . By combining these matrices, any polarimetric system can be modelled, and represented by one matrix.

$$\begin{bmatrix} I' \\ Q' \\ U' \\ V' \end{bmatrix} = \begin{bmatrix} & S & \end{bmatrix}_{4 \times 4} \begin{bmatrix} I \\ Q \\ U \\ V \end{bmatrix} \qquad \text{(A15)}$$

As an example, the matrix for a dichroic waveplate (or any optical element which is simultaneously dichroic and birefringent) will now be derived. Consider the case of a general completely elliptically polarised beam. This beam has the following components when resolved along the axes of the dichroism.

$$E_x = E_{xo} \cos (wt + \delta_x)$$

$$E_y = E_{yo} \cos (wt + \delta_y)$$

Such a beam will have Stokes parameters:

$$I = E_{xo}^2 + E_{yo}^2$$

$$Q = E_{xo}^2 - E_{yo}^2$$

$$U = 2 E_{xo} E_{yo} \cos (\delta_y - \delta_x)$$

$$V = 2 E_{xo} E_{yo} \sin (\delta_y - \delta_x)$$

The beam then passes through the optical element. This has the effect of reducing the amplitude of the 'x'-component by a factor k_1 , of the y-component, by k_2. It also retards the y-component by a retardance, Δ .

Hence the beam now appears:

$$E'_x = k_1 E_{xo} \cos (wt + \delta_x)$$

$$E'_y = k_2 E_{yo} \cos (wt + \delta_y - \Delta)$$

This beam has Stokes parameters as follows:

$$I' = k_1^2 E_{xo}^2 \; k_2^2 E_{yo}^2$$

$$= k_1^2 \frac{I + Q}{2} + k_2^2 \frac{I - Q}{2}$$

$$= \tfrac{1}{2}\left\{ (k_1^2 + k_2^2)\, I + (k_1^2 - k_2^2)\, Q \right\}$$

$$Q' = k_1^2 E_{xo}^2 - k_2^2 E_{yo}^2$$

$$= k_1^2 \frac{I + Q}{2} - k_2^2 \frac{I - Q}{2}$$

$$= \tfrac{1}{2}\left\{ (k_1^2 - k_2^2)\, I + (k_1^2 + k_2^2)\, Q \right\}$$

$$U' = 2k_1 k_2 E_{xo} E_{yo} \cos (\delta_y - \Delta - \delta_x)$$

$$= k_1 k_2 (2 E_{xo} E_{yo} \cos (\delta_y - \delta_x) \cos \Delta)$$

$$+ k_1 k_2 (2 E_{xo} E_{yo} \sin (\delta_y - \delta_x) \sin \Delta)$$

$$= k_1 k_2 U \cos \Delta + k_1 k_2 V \sin \Delta$$

$$V' = 2 k_1 k_2 E_{xo} E_{yo} \sin (\delta_y - \Delta - \delta_x)$$

$$= k_1 k_2 (2 E_{xo} E_{yo} \sin (\delta_y - \delta_x) \cos \Delta)$$

$$- k_1 k_2 (2 E_{xo} E_{yo} \cos (\delta_y - \delta_x) \sin \Delta)$$

$$= k_1 k_2 V \cos \Delta - k_1 k_2 U \sin \Delta$$

Therefore, the matrix for this situation, is:

$$\begin{bmatrix} I' \\ Q' \\ U' \\ V' \end{bmatrix} = \frac{1}{2} \begin{bmatrix} k_1^2 + k_2^2 & k_1^2 - k_2^2 & 0 & 0 & I \\ k_1^2 - k_2^2 & k_1^2 + k_2^2 & 0 & 0 & Q \\ 0 & 0 & 2k_1k_2\cos\Delta & 2k_1k_2\sin\Delta & U \\ 0 & 0 & -2k_1k_2\sin\Delta & 2k_1k_2\cos\Delta & V \end{bmatrix}$$

It is normal practice to replace k_1^2 by k_1 and k_2^2 by k_2. These variables, k_1, k_2 are known as the principal intensity transmission coefficients. The form shown in table A8 is derived by the further substitution, $k_1 = k$, and $k_2 = rk$.

The quoted form for the standard Mueller matrices is derived from CLARKE & GRAINGER (1971). Unfortunately, the matrices imply the opposite convention for circular polarisation. This should be borne in mind when considering the algebra presented at various places in this thesis. The convention for the positive direction of rotation of the linear polarisation vector is in accord with normal usage.

Appendix A2: System matrices for both the real and the ideal spectropolarimeter.

We give here the matrix representations for the various cases described in the text (sections A 1.3 and A 3). Angles are defined in and by Fig. A1.

1. The ideal instrument

1.1 Determination of circular polarisation

Matrix representation of the system is

$$\begin{bmatrix} I' \\ Q' \\ U' \\ V' \end{bmatrix} = C_{-\beta}\, A_{K_1 K_2}\, C_{+\beta}\, B_{\delta_t} \begin{bmatrix} I \\ Q \\ U \\ V \end{bmatrix}$$

where δ_t = instantaneous retardance of the modulator

β = angle of the analyser (i.e. = 45° or 135°)

$K_1 = 1$

$K_2 = 0$

Hence the system matrix is

$$\begin{bmatrix} 1 & 0 & \pm\cos\delta & \pm\sin\delta \\ 0 & 0 & 0 & 0 \\ \pm 1 & 0 & \cos\delta & \sin\delta \\ 0 & 0 & 0 & 0 \end{bmatrix}$$

where upper signs apply in the case β = 45°, and lower signs β = 135°. This matrix represents the system when the polarimeter is orientated at 0°, while at 90° the matrix representation is:

$$\begin{bmatrix} I' \\ Q' \\ U' \\ V' \end{bmatrix} = C_{-90}\ C_{-\beta}\ A_{K_1K_2}\ C_{+\beta}\ B_{\delta_t}\ C_{90}\ \begin{bmatrix} I \\ Q \\ U \\ V \end{bmatrix}$$

and the system matrix becomes (signs as before)

$$\begin{bmatrix} 1 & 0 & \mp\cos\delta & \pm\sin\delta \\ 0 & 0 & 0 & 0 \\ \mp 1 & 0 & \cos\delta & -\sin\delta \\ 0 & 0 & 0 & 0 \end{bmatrix}$$

1.2 Determination of linear polarisation

In this case the matrix representation of the system is

$$\begin{bmatrix} I' \\ Q' \\ U' \\ V' \end{bmatrix} = C_{-\beta}\ A_{K_1K_2}\ C_{+\beta}\ B_{\delta_t}\ C_{-\psi}\ B_{\tau}\ C_{\psi}\ \begin{bmatrix} I \\ Q \\ U \\ V \end{bmatrix}$$

where β, K_1, K_2 and δ_t are defined above.

ψ is the angle which the fast axis of the waveplate makes with the x-axis.

τ is the retardance of the waveplate.

If the system matrix is represented as $\frac{1}{2}[a_{ij}]$, then

$a_{11} = 1$ $\qquad a_{12} = \pm\sin2\psi\cos2\psi(1-\cos\tau)\cos\delta_t \pm \sin2\psi\sin\tau\sin\delta_t$

$a_{21} = 0$ $\qquad a_{22} = 0$

$a_{31} = \pm 1$ $\qquad a_{32} = +\sin2\psi\cos2\psi(1-\cos\tau)\cos\delta_t + \sin2\psi\sin\tau\sin\delta_t$

$a_{41} = 0$ $\qquad a_{42} = 0$

$$a_{13} = \pm(\sin^2 2\psi + \cos^2 2\psi\cos\tau)\cos\delta_t \mp \cos 2\psi\sin\tau\sin\delta_t$$

$$a_{23} = 0$$

$$a_{33} = +(\sin^2 2\psi + \cos^2 2\psi\cos\tau)\cos\delta_t - \cos 2\psi\sin\tau\sin\delta_t$$

$$a_{43} = 0$$

$$a_{14} = \pm\cos 2\psi\sin\tau\cos\delta_t \pm \cos\tau\sin\delta_t$$

$$a_{24} = 0$$

$$a_{34} = \cos 2\psi\sin\tau\cos\delta_t + \cos\tau\sin\delta_t$$

$$a_{44} = 0$$

Again, upper signs are for the case $\beta = 45°$, and lower for $\beta = 135°$. This is the case of the polarimeter at 0°. For the case of the polarimeter at 90°, the only difference is that the following terms change sign: a_{21}, a_{31}, a_{12}, a_{13}, a_{42}, a_{43}, a_{24}, a_{34}.

1.3 Determination of calibration polarisation

The matrix representation of the system is

$$\begin{bmatrix} I' \\ Q' \\ U' \\ V' \end{bmatrix} = C_{-\beta}\, A_{K_1K_2}\, C_{\beta}\, B_{\delta_t}\, C_{-\alpha}\, B_{\tau}\, C_{\alpha}\, C_{-\alpha+45}\, A_{K_1K_2}\, C_{+\alpha-45} \begin{bmatrix} I \\ Q \\ U \\ V \end{bmatrix}$$

where K_1, K_2, β, δ_t, τ are defined above;

α is the angle at which the calibration waveplate is orientated.

For simplicity we define

$$a_2 = \sin 2\alpha\cos 2\alpha(1 - \cos\tau)\cos\delta_t + \sin 2\alpha\sin\tau\sin\delta_t$$

$$a_3 = (\sin^2 2\alpha + \cos^2 2\alpha\cos\tau)\cos\delta_t - \cos 2\alpha\sin\tau\sin\delta_t$$

i.e. $a_2 = a_{32} = \pm a_{12}$ and $a_3 = a_{33} = \pm a_{13}$ in case (b) above.

Further, we define $d = a_2 \sin 2\alpha - a_3 \cos 2\alpha$

Now the system matrix for the polarimeter in the 0° position, may hence be written:

$$\frac{1}{4}\begin{bmatrix} (1\pm d) & (1\pm d)\sin 2\alpha & -(1\pm d)\cos 2\alpha & 0 \\ 0 & 0 & 0 & 0 \\ (\pm 1+d) & (\pm 1+d)\sin 2\alpha & -(\pm 1+d)\cos 2\alpha & 0 \\ 0 & 0 & 0 & 0 \end{bmatrix}$$

where upper signs apply for $\beta = 45°$ and the lower for $\beta = 135°$.

For the polarimeter in the 90° position:

$$\frac{1}{4}\begin{bmatrix} (1\pm d) & -(1\pm d)\sin 2\alpha & +(1\pm d)\cos 2\alpha & 0 \\ 0 & 0 & 0 & 0 \\ -(\pm 1+d) & (\pm 1+d)\sin 2\alpha & -(\pm 1+d)\cos 2\alpha & 0 \\ 0 & 0 & 0 & 0 \end{bmatrix}$$

2. The real instrument

2.1 Imperfect analyser

Consider the case of the measurement of circular polarisation, where the analyser is birefringent, not perfectly dichroic ($K_2 \neq 0$) and not at 45° to the axis of the modulator ($\beta \neq 45$). Then the matrix representation of the system is:

$$\begin{bmatrix} I' \\ Q' \\ U' \\ V' \end{bmatrix} = C_{-\beta}\, D_{K_1 K_2 \chi}\, C_{\beta}\, B_{\delta_t} \begin{bmatrix} I \\ Q \\ U \\ V \end{bmatrix}$$

where χ is the retardance introduced by the analyser.

If the system matrix is written as $\frac{1}{2}[c_{ij}]$, then:

$$c_{11} = (K_1 + K_2) \qquad c_{12} = (K_1 - K_2)\cos 2\beta$$

$$c_{21} = (K_1 - K_2)\cos 2\beta \qquad c_{22} = (K_1 + K_2)(1-\sin^2 2\beta) + 2\sqrt{K_1 K_2}\cos\chi \sin^2 2\beta$$

$$c_{31} = (K_1 - K_2)\sin 2\beta \qquad c_{32} = (K_1 + K_2 - 2\sqrt{K_1 K_2}\cos\chi)\sin 2\beta\cos 2\beta$$

$$c_{41} = 0 \qquad c_{42} = 2\sqrt{K_1 K_2}\sin\chi \sin 2\beta$$

$$c_{13} = (K_1 - K_2)\sin 2\beta\cos\delta_t$$

$$c_{23} = (K_1 + K_2 - 2\sqrt{K_1 K_2}\cos\chi)\sin 2\alpha\cos 2\alpha\cos\delta_t + 2\sqrt{K_1 K_2}\sin\chi \sin 2\alpha \sin\delta_t$$

$$c_{33} = (K_1 + K_2)\cos\delta_t - (K_1 + K_2 - 2\sqrt{K_1 K_2}\cos\chi)\cos^2 2\beta\cos\delta_t - \\ - 2\sqrt{K_1 K_2}\sin\chi\cos 2\beta\sin\delta_t$$

$$c_{43} = -2\sqrt{K_1 K_2}(\sin\chi\cos 2\beta\cos\delta_t + \cos\chi\sin\delta_t)$$

$$c_{14} = (K_1 - K_2)\sin 2\beta\sin\delta_t$$

$$c_{24} = (K_1 + K_2 - 2\sqrt{K_1 K_2}\cos\chi)\sin 2\beta\cos 2\beta\sin\delta_t - 2\sqrt{K_1 K_2}\sin\chi\sin 2\beta\cos\delta_t$$

$$c_{34} = (K_1 + K_2)\sin\delta_t - (K_1 + K_2 - 2\sqrt{K_1 K_2}\cos\chi)\cos^2 2\beta\sin\delta_t + \\ + 2\sqrt{K_1 K_2}\sin\chi\cos 2\beta\cos\delta_t$$

$$c_{44} = -2\sqrt{K_1 K_2}(\sin\chi\cos 2\alpha\sin\delta_t - \cos\chi\cos\delta_t)$$

2.2 Imperfect calibration filter

The matrix representation of an imperfect polarisation calibration filter, where the linear polariser is not completely dichroic, is slightly birefringent, and not exactly at -45° to the waveplate, is:

$$\begin{bmatrix} I' \\ Q' \\ U' \\ V' \end{bmatrix} = C_{-\alpha}\ B_{\tau}\ C_{\alpha}\ C_{-\rho}\ D_{K_1K_2\chi}\ C_{\rho} \begin{bmatrix} I \\ Q \\ U \\ V \end{bmatrix}$$

where ρ is the angle at which the linear polariser is orientated. We simplify by setting $\rho = 0$ and $\tau = 90°$. If the system matrix is then written as $\frac{1}{2}[d_{ij}]$ it is found that:

$d_{11} = (K_1 + K_2)$ $\qquad$ $d_{12} = (K_1 - K_2)$

$d_{21} = (K_1 - K_2)\cos^2 2\alpha$ $\qquad$ $d_{22} = (K_1 + K_2)\cos^2 2\alpha$

$d_{31} = (K_1 - K_2)\sin 2\alpha\cos 2\alpha$ $\qquad$ $d_{32} = (K_1 + K_2)\sin 2\alpha\cos 2\alpha$

$d_{41} = (K_1 - K_2)\sin 2\alpha$ $\qquad$ $d_{42} = (K_1 + K_2)\sin 2\alpha$

$d_{13} = 0$ $\qquad$ $d_{14} = 0$

$d_{23} = 2\sqrt{K_1K_2}\sin 2\alpha(\cos\chi\cos 2\alpha + \sin\chi)$ $\qquad$ $d_{24} = 2\sqrt{K_1K_2}\sin 2\alpha(\sin\chi\cos 2\alpha - \cos\chi)$

$d_{33} = 2\sqrt{K_1K_2}(\cos\chi\sin^2 2\alpha - \sin\chi\cos 2\alpha)$ $\qquad$ $d_{34} = 2\sqrt{K_1K_2}(\cos\chi\cos 2\alpha + \sin\chi\sin^2 2\alpha)$

$d_{43} = -2\sqrt{K_1K_2}\cos\chi\cos 2\alpha$ $\qquad$ $d_{44} = -2\sqrt{K_1K_2}\sin\chi\cos 2\alpha$

2.3 Effect of spectrometer and photomultiplier

All components after the analyser are modelled with just one dichroic waveplate matrix, $D_{L_1L_2\sigma}$. We consider the case of measurement of circular polarisation. In this case:

$$\begin{bmatrix} I' \\ Q' \\ U' \\ V' \end{bmatrix} = C_{-\gamma}\ D_{L_1L_2\sigma}\ C_{\gamma}\ C_{-\beta}\ D_{K_1K_2\chi}\ C_{\beta}\ B_{\delta_t} \begin{bmatrix} I \\ Q \\ U \\ V \end{bmatrix}$$

where γ is the angle between the x axis (see Fig.A1) and the polarisation of the spectrometer. This matrix may be written as EF where $E = C_{-\gamma} D_{L_1 L_2 \sigma} C_{\gamma}$, that is

$$E = \frac{1}{2}\begin{bmatrix} (L_1 + L_2) & (L_1 - L_2)\cos 2\gamma & (L_1 - L_2)\sin 2\gamma & 0 \\ (L_1 - L_2) & (L_1 + L_2)\cos 2\gamma & (L_1 + L_2)\sin 2\gamma & 0 \\ 0 & -2\sqrt{L_1 L_2}\cos\sigma\sin 2\gamma & 2\sqrt{L_1 L_2}\cos\sigma\cos 2\gamma & 2\sqrt{L_1 L_2}\sin\sigma \\ 0 & 2\sqrt{L_1 L_2}\sin\sigma\sin 2\gamma & -2\sqrt{L_1 L_2}\sin\sigma\cos 2\gamma & 2\sqrt{L_1 L_2}\cos\sigma \end{bmatrix}$$

If $EF = 1/4[g_{ij}]$ and $F = C_{-\beta} D_{K_1 K_2 \chi} C_{\beta}$ is derived in section 4(a) then the detected intensity may be written

$$I'_t = 1/4\{g_{11} I + g_{12} Q + g_{13} U + g_{14} V\}$$

For simplicity, we give only these four coefficients:

$$g_{11} = (K_1 + K_2)(L_1 + L_2) + (K_1 - K_2)(L_1 - L_2)\cos 2(\gamma - \beta)$$

$$g_{12} = (K_1 - K_2)(L_1 + L_2)\cos 2\beta + (K_1 + K_2)(L_1 - L_2)\cos 2\gamma + \\ + (K_1 + K_2 - 2\sqrt{K_1 K_2}\cos\chi)(L_1 - L_2)\sin 2\beta \sin 2(\gamma - \beta)$$

$$g_{13} = [(K_1 - K_2)(L_1 + L_2)\sin 2\beta + (K_1 + K_2)(L_1 - L_2)\sin 2\gamma - \\ - (K_1 + K_2 - 2\sqrt{K_1 K_2}\cos\chi)(L_1 - L_2)\cos 2\beta \sin 2(\gamma - \beta)]\cos\delta_t - \\ - 2\sqrt{K_1 K_2}(L_1 - L_2)\sin\chi \sin 2(\gamma - \beta)\sin\delta_t$$

$$g_{14} = [(K_1 - K_2)(L_1 + L_2)\sin 2\beta + (K_1 + K_2)(L_1 - L_2)\sin 2\gamma - \\ - (K_1 + K_2 - 2\sqrt{K_1 K_2}\cos\chi)(L_1 - L_2)\cos 2\beta \sin 2(\gamma - \beta)\sin\delta_t + \\ + 2\sqrt{K_1 K_2}(L_1 - L_2)\sin\chi \sin 2(\gamma - \beta)\cos\delta_t$$

In practice, γ is no greater than a few degrees.

Appendix A3 : The wavelength scanning system of the McPherson monochromator.

The drive arrangment of the grating in the McPherson is shown in figure A8 , which also defines the various angles and dimensions referred to. The grating is free to rotate about the axis into the paper at 'A'. An arm is attached to the grating which ends in a polished metal ball. The angle between the normal to the grating and this arm is 'ϕ'. DGCJ is a lead screw with a block attached to it. The polished face of the block, at an angle 'α' to the lead screw, bears onto the ball. Light from the collimating mirror travels along the path KA. The angle $\angle$ KAC is fixed, and equal to about 14°. To reach the exit slit, light must also leave at this angle. Motion of the block in the direction DJ hence rotates the grating normal AL, and in this way longer wavelengths are conducted to the exit slit. It is required to demonstrate under what conditions the wavelength selected is linearly dependant on the distance DC.

The grating equation describes the relation between angle and wavelength selected.

$$\lambda = \frac{2d}{m} \sin \tfrac{1}{2} (\theta_d - \theta_i) \cos \tfrac{1}{2} (\theta_d + \theta_i)$$

where: d = grating spacing

m = order

θ_i = angle of incident light to grating normal

θ_d = angle of diffracted light to grating normal

Since $\theta_d + \theta_i = 28^{\circ}$ and defining $\Delta\theta = \tfrac{1}{2} (\theta_d - \theta_i)$

we have: $\lambda = \frac{2d}{m} \cos 14^{\circ} \sin \Delta\theta$

Define $x = DC$ $r = FH$

$a = HA$ $b = AC$

Then $HB = a \sin \xi$ $DC = EG \cot \alpha = BC \cot \alpha$

$EH = r \operatorname{cosec} \alpha$ $BC = AC - AB = AC - a \cos \xi$

Hence $x = DG + EH + HB$

$= (b - a \cos \xi) \cot \alpha + r \operatorname{cosec} \alpha + a \sin \xi$

$= \frac{1}{\sin \alpha} (b \cos \alpha + r - a \cos (\xi - \alpha))$

Now $\theta_i + \phi - \xi = 14$

Hence $x = \frac{(b \cos \alpha + r)}{\sin \alpha} - \frac{a}{\sin \alpha} \cos (\theta_i + \phi - 14 - \alpha)$

and since $\Delta\theta = 14 - \theta_i$

$x = \frac{(b \cos \alpha + r)}{\sin \alpha} - \frac{a}{\sin \alpha} \cos (\Delta\theta + \alpha - \phi)$

$x = \frac{b \cos \alpha + r}{\sin \alpha} - \frac{a}{\sin \alpha} \sin (\Delta\theta + \alpha - \phi - 90)$

Therefore the required condition for linearity is that $\alpha = \phi + 90^\circ$. The setting of this condition must be left to the manufacturer as no adjustment is provided. The constant term can be eliminated by setting the wavelength counter to zero when the grating is set up in zero order (i.e. as a simple mirror). In this case $\Delta\theta = 0$. The multiplicative factor is accounted for in the gearing to the lead screw. There is some adjustment here through 'a', which it will be recalled is the length of the arm attached to the grating. This is slightly adjustable. If the grating is seating slightly incorrectly in its holder, then the condition $\alpha = \phi + 90$ might be destroyed. This is equivalent to a small error in $\Delta\theta$.

Since $\lambda = \frac{2d}{m} \cos 14^\circ \sin \Delta\theta$

Then $\delta\lambda = \frac{2d}{m} \cos 14^\circ \cos \Delta\theta \; E$

where E = error in $\Delta\theta$ (radians)

Putting in values for the 1200 gmm^{-1} grating, and converting E to degrees gives:

$$\delta\lambda = 282 \; E^\circ \cos \Delta\theta$$

This relation would look linear over quite large ranges of wavelength, since at 5000 Å, $\cos \Delta\theta = 0.95$. In fact, the difference in wavelength error between 5000 Å and 7000 Å is given by the expression:

$$\varepsilon(\text{Å}) = 14.11 \; E^\circ$$

Applying this approximation to the observed results (figure A9), we derive $E^\circ = 0^\circ.55$. Such an error in inserting a grating is not unreasonable.

Literature cited:

Allen, C.W.: 1973, "Astrophysical Quantities", Athlone Press, London, p243

Breckenbridge, J.B : 1971, App. Optics, 10, 286

Chandrasekhar, S.: 1950, "Radiative Transfer", Clarendon Press, London

Clarke, D.; Grainger, J.F.: 1971, "Polarized Light and Optical Measurement", Pergamon Press, London

Gehrels, T.: 1974, in "Planets, Stars and Nebulae, studied with photopolarimetry", ed. T. Gehrels, University of Arizona Press, Tucson, p53

James, J.F.; Sternberg, R.S.: 1969, "The Design of Optical Spectrometers", Chapman & Hall, London

Jones, R.C.: 1941, J. Op. Soc. Amer., 31, 488

Kemp, J.C.: 1969, J. Op. Soc. Amer., 59, 955

Marette, G.: 1969, Bull. Soc. Roy. Sci. Liege, 38, 687

Perrin, F.: 1942, J. Chem. Phys., 10, 415

Pribram, J.K.; Penchina, C.M.: 1968, App. Optics, 7, 2005

Rayleigh (J.W. Strutt, 3rd Baron): 1907, Phil. Mag., 14, 60

Serkowski, K.: 1974, in "Planets, Stars and Nebulae, studied with photopolarimetry", ed. T. Gehrels, University of Arizona Press, Tucson, p53

Stewart, J.E.; Galloway, W.S.: 1962, App. Optics, 1, 421

Walker, M.J.: 1954, Amer. J. Phys., 22, 170

Wood, R.W.: 1902, Phil. Mag., 4, 396

Table A1 : The variation of the birefringence of crystal quartz with wavelength

λ	$(n_e - n_o)$ (10^{-5})	τ_1	τ_2
3000	1045	2.225	1.369
3500	984	1.796	1.105
4000	958	1.530	0.941
4500	940	1.334	0.821
5000	927	1.184	0.729
5500	918	1.066	0.656
6000	911	0.970	0.597
6500	903	0.887	0.546
7000	898	0.819	0.504
7500	893	0.760	0.468
8000	889	0.710	0.437
8500	886	0.666	0.410

The birefringence of crystal quartz is given in the first column. The second and third columns are retardation, normalised for $\pi/2$ at 5825 Å and 3800 Å respectively.

e.g. A zero-order waveplate that exhibits $\pi/2$ retardance at 3800 Å will exhibit a retardance of 0.437 x $\pi/2$ at 8000 Å

A comparison of the actual retardance at a certain wavelength and the approximation obtained by ignoring the wavelength dependence of the birefringence of crystal quartz is shown in figure A12.

Table derived from American Institute of Physics Handbook, 1972.

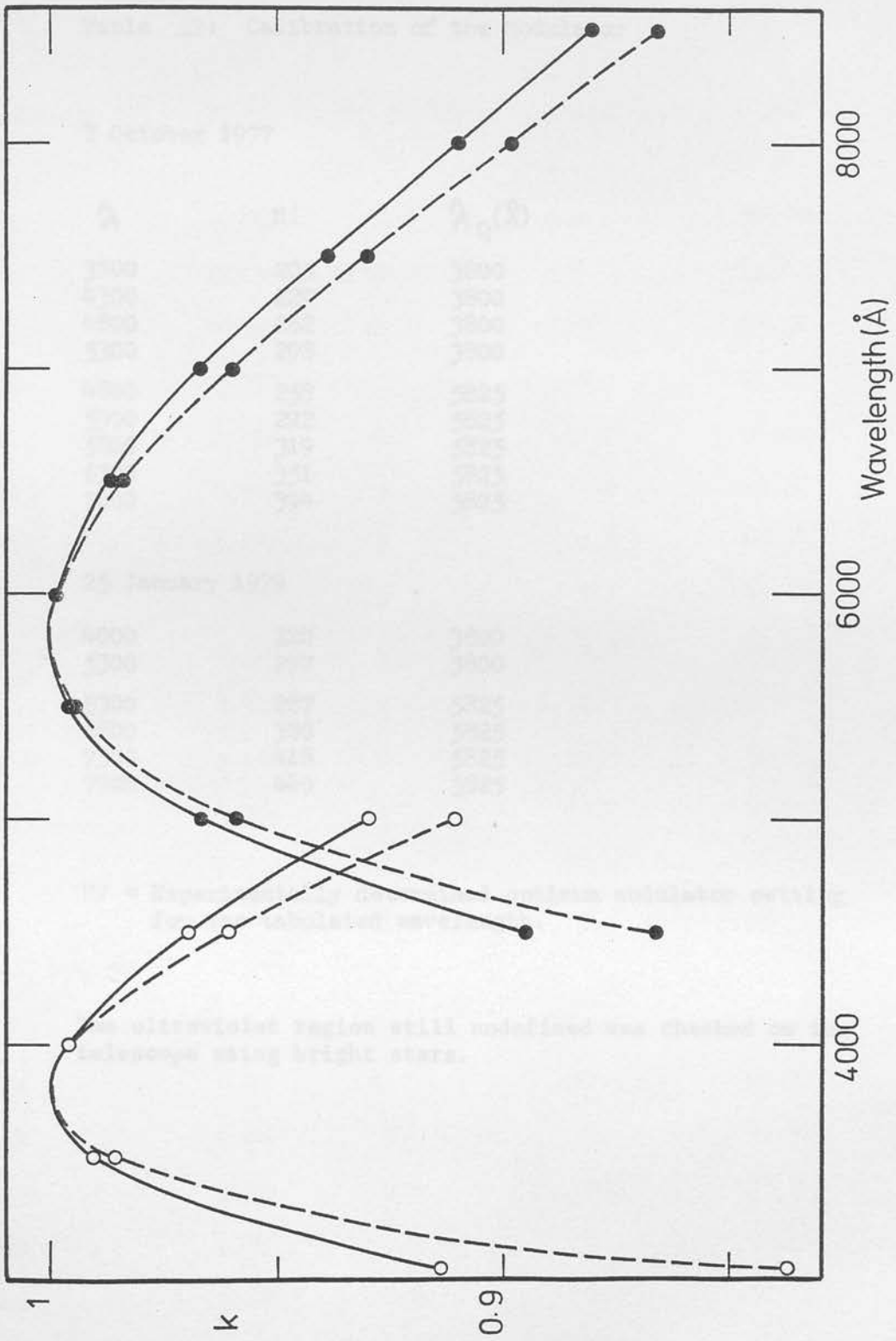

Figure A12 : The solid lines represent the quantity $\kappa = \sin(90^{\circ} \times \lambda_{\alpha}/\lambda)$ used in the reduction procedure. The case of $\lambda_{\alpha} = 3800\text{Å}$ is shown by open circles, that of $\lambda_{\alpha} = 5825\text{Å}$ by filled circles. The dashed lines give the quantity κ' of which κ is an estimate. κ' includes the effect of the variation with wavelength of the birefringence of crystal quartz.

Table A2: Calibration of the Modulator

8 October 1977

λ	MV	λ_Q(Å)
3800	205	3800
4300	229	3800
4800	262	3800
5300	298	3800
4800	258	5825
5300	292	5825
5800	319	5825
6300	351	5825
7000	394	5825

25 January 1979

4000	220	3800
5300	297	3800
5300	287	5825
6800	380	5825
7300	418	5825
7700	440	5825

MV = Experimentally determined optimum modulator setting for the tabulated wavelength.

The ultraviolet region still undefined was checked on the telescope using bright stars.

Table A3 : The polarising properties of HNP'B.

Wavelength (Å)	K_1	K_2 (10^{-4})	r (10^{-4})	p (%)
2750	0.250	126	504	90.40
2800	0.328	110	335	93.51
2900	0.340	40	118	97.67
3000	0.372	17	45.7	99.09
3100	0.448	9	20.1	99.60
3200	0.546	6	11.0	99.78
3300	0.611	3	4.9	99.90
3400	0.602	2	3.3	99.93
3500	0.568	1	1.8	99.96
3600	0.550	3	5.5	99.89
3700	0.568	7	12.3	99.75
3800	0.604	9	14.9	99.70
3900	0.644	8	12.4	99.75
4000	0.688	5	7.3	99.85
3750	0.33	10	30.3	99.40
4000	0.47	30	63.8	98.73
4500	0.68	5	7.4	99.85
5000	0.75	0.5	0.7	99.99
5500	0.70	0.2	0.3	99.99
6000	0.67	0.2	0.3	99.99
6500	0.70	0.2	0.3	99.99
7000	0.77	0.3	0.4	99.99

The upper part of the table are the quoted values for HNP'B.

Beyond 4000 Å it behaves as HN 32, whose properties are listed in the second half of the table.

K_1 and K_2 are the principal intensity transmission coefficients, i.e. the transmittance of the polaroid to linear polarised light parallel and perpendicular to its axis. In the alternative formulation used in the appendix, $k = K_1$, and r is defined through the expression $K_2 = rK_1$. p is the degree of linear polarisation of an unpolarised beam after having passed through the filter. It is calculated from

$$p = \frac{K_1 - K_2}{K_1 + K_2}$$

Table derived from the American Institute of Physics Handbook, 1972

Table A4 : Logging information requested by GAP 1

Mnemonic	Description	Limiting values	Typical value
STAR	Name of object being observed.	-	-
OS	Order Sorter filter used.	1 to 6	5
HT	High tension voltage applied to Photomultiplier.	1000 - 2000 V	1500 V
AP	Aperture used (wheel number).	1 - 5	3
CS	Counter Setting, as determined by thumb switches on the counter. Enetered in units of seconds.	1 - 100	1
MV	Modulator Volts set. In units of centivolts.	180 - 500	300
OP	Set of optics used. Which set of waveplates?	5825 or 3800 Å	-
RS	Resolution used. Effective width of exit slit in terms of resolution. Depends on grating being used.	5 - 400 Å	50 Å

Table A5 : Unpolarised star measurements.

Unpolarised star measurement

1. Linear polarisation

Object (Date)	Wavelength (Å)	Q/I (%)	σ	U/I (%)	σ
β Vir	4500	-0.024	0.028	-0.005	0.032
(May 1978)	5000	+0.047	0.023	+0.032	0.025
	5500	+0.020	0.024	+0.029	0.028
	6000	-0.013	0.029	-0.028	0.030
	6500	+0.014	0.033	-0.050	0.028
	7000	-0.016	0.031	+0.045	0.029
β Cas	5500	-0.002	0.021	-0.002	0.021
(Oct 1978)	5800	+0.013	0.021	+0.029	0.024
	6100	-0.004	0.022	-0.029	0.027
	6400	-0.012	0.024	-0.015	0.024
	6700	-0.013	0.026	+0.013	0.029
	7000	-0.026	0.026	+0.017	0.030
α CMa	3200	+0.006	0.012	-0.011	0.012
(Feb 1979)	3400	-0.015	0.011	-0.011	0.011
	3600	-0.013	0.010	-0.005	0.011
α Aur	Hα	-0.004	0.004	-0.003	0.004
(Oct 1978)	Hβ	+0.002	0.007	+0.002	0.007

2. Circular polarisation

Object (Date)	Wavelength (Å)	V/I (%)	σ
α Aur	Hα	-0.004	0.007
(Oct 1978)	Hβ	-0.005	0.007
λ And	Hα	+0.017	0.014
(Oct 1978)			
ε UMa	Hβ red wing	-0.007	0.015
(Feb 1979)	Hβ blue wing	-0.019	0.015

Measurements on β Vir and β Cas were made at 50Å resolution; while those on α CMa are at 100Å resolution. Points on α Aur and λ And are averages of data at various resolutions between 5 and 25Å across spectral lines. ε UMa was studied at 5Å resolution. These measurements were taken with the 1.0m and 1.5m telescopes of the University of Arizona at Mt. Lemmon, and the 1.55m telescope at the Catalina outstation.

Table A6 : The quantum efficiency of the RCA C31034A photomultiplier.

This table is extracted from the RCA data sheet.

Wavelength (Å)	Quantum Efficiency (%)
2500	34
3000	36
3500	35
4000	30
4500	28
5000	26
5500	24
6000	22
6500	21
7000	20
7500	19
8000	18
8400	17
8800	12
8900	7.5
9000	0

Table A7 : Mueller matrices

1. Partial polariser

$$A_{k,r} = \frac{1}{2}\begin{bmatrix} k(1+r) & k(1-r) & 0 & 0 \\ k(1-r) & k(1+r) & 0 & 0 \\ 0 & 0 & 2kr^{\frac{1}{2}} & 0 \\ 0 & 0 & 0 & 2kr^{\frac{1}{2}} \end{bmatrix}$$

This is a slightly different representation to that normally quoted. An equivalent form is $A_{K_1K_2}$ where

$$K_1 = k \qquad \text{and} \qquad K_2 = rk$$

and K_1 and K_2 are the intensity transmission coefficients of the optical element to perfectly linearly polarised light in two orthogonal directions (chosen such that $K_1 - K_2$ is maximised). Hence 'k' characterises the transmittance of the element and 'r' characterises the degree to which it polarises light. 'r' is the inverse of the extinction ratio. Unpolarised light falling onto the element is linearly polarised to an extent. $p = \frac{(1 - r)}{(1 + r)}$

2. Pure retarder

$$B_{\delta} = \begin{bmatrix} 1 & 0 & 0 & 0 \\ 0 & 1 & 0 & 0 \\ 0 & 0 & \cos\delta & \sin\delta \\ 0 & 0 & -\sin\delta & \cos\delta \end{bmatrix}$$

δ is the differential retardation (of the y - axis with respect to the x - axis) or retardance.

3. Rotation

$$C_{\alpha} = \begin{bmatrix} 1 & 0 & 0 & 0 \\ 0 & \cos 2\alpha & \sin 2\alpha & 0 \\ 0 & -\sin 2\alpha & \cos 2\alpha & 0 \\ 0 & 0 & 0 & 1 \end{bmatrix}$$

This matrix is equivalent to a rotation of the coordinate axes by an angle α , anticlockwise.

4. Dichroic waveplate.

This matrix represents an optical element which is both dichroic and birefringent. It is assumed that the axis of the birefringence is parallel to that of the dichroism.

$$D_{k,r,\delta} = \frac{1}{2} \begin{bmatrix} k(1+r) & k(1-r) & 0 & 0 \\ k(1-r) & k(1+r) & 0 & 0 \\ 0 & 0 & 2kr^{\frac{1}{2}}\cos\delta & 2kr^{\frac{1}{2}}\sin\delta \\ 0 & 0 & -2kr^{\frac{1}{2}}\sin\delta & 2kr^{\frac{1}{2}}\cos\delta \end{bmatrix}$$

As for the case of a partial polariser, there is an equivalent form, $D_{K_1K_2\delta}$.

Chapter B

Spectropolarimetry of Jupiter and Saturn

1. Introduction

Jupiter and Saturn have been studied since ancient times. Their brightness and readily detectable motions attracted the interest and study of many of the early astronomers. In those times, when the terms astronomer, scientist and priest were often indistinguishable, these planets were reckoned of great importance. They were associated with the most powerful of the gods - Zeus/Jupiter and Chronos/Saturn in the graecoroman pantheon. These planets have affected the history of civilisation on this planet in a number of ways, and probably more through astrology than astronomy. Was the Bethlehem star a conjunction of Jupiter and Saturn? Do conjunctions of the planets trigger earthquakes here on Earth? (GRIBBIN and PLAGUEMANN, 1974). Is one's future career affected by the planetary configurations at birth? (GAUQUELIN, 1969) (These questions are not to be answered here!) These things aside, the major planets have certainly been great spurs to research. The discovery of the satellites of Jupiter by Galileo (GALILEO, 1610), or possibly Marius (see OWEN (1976) and references therein), was instrumental in the conversion from a geocentric to a heliocentric view of the solar system (or perhaps more exactly, the Universe). The nature of Saturn's rings was a problem which required the development of better telescopes for its solution (HUYGENS, 1649).

Planetary polarimetry can be said to have started with Bernard Lyot in the 1920's. His visual polarimeter could be read to 0.1% and was applied to the study of the dependence of linear polarisation with phase angle of the Moon, Venus, Mars, Jupiter

and Saturn. In this pioneering work (LYOT, 1929), the centre-to-limb and latitudinal variations of Jupiter and Saturn were studied, along with the phase dependence. The centre-to-limb and phase dependencies were interpreted as being caused by a 'fog' or distribution of aerosols suspended in a gaseous atmosphere. The latitudinal variations were explained as an increasing transparency of the atmosphere from the equator towards the poles. Besides Öhman, another pioneer in many fields of polarimetry, in the 1940's, the field then lay dormant until A. Dollfus (DOLLFUS, 1961) began detailed study of the nearby planets. He studied the wavelength dependence of some areas of Jupiter, and looked closely at the variations in polarisation around the rings of Saturn. He used visual, photographic and photoelectric polarimeters, and even designed an infrared polarimeter (sensitive to 2.6μ). Both Lyot and Dollfus made extensive laboratory measurements on various terrestrial materials.

This chapter reviews the standard references on the polarimetry of Jupiter and Saturn (section 2) and gives a brief description of our current understanding of the atmosphere of these two planets (section 3). Having stated the model, the justification for the present observations will be explained (section 4). The polarisation data for Jupiter will then be presented (section 5), followed by that for Saturn (section 6). After the discussion of other relevant information drawn from the literature (section 7), the polarisation data is interpreted (section 8). This chapter ends with a conclusion, and with suggestions for future work (section 9). While figures are incorporated into the text, the tables are collected together at the end of the chapter.

2. Previous Polarimetry of Jupiter and Saturn

The planets are complex objects for polarimetric study, but fruitful ones. There are a number of variables upon which the polarisation may depend. We may summarise them under four headings:

i) Dependence on phase angle;

ii) Dependence on wavelength;

iii) Dependence on position on the planetary disc;

iv) Dependence on time.

These headings relate to the ways in which the polarisation is studied. More physically meaningful headings would be: geometry of illumination, composition, size and shape of the scattering particles and structure of the atmosphere. Early observational work is summarised by DOLLFUS (1961). The summary of the observational evidence below is intended to include work published up to mid-1980. Since most of these studies were made in the 1960's and early 1970's comments are made on the polarimeters and on their probable accuracies.

The dependence of linear polarisation on phase and wavelength for both Jupiter and Saturn has been studied by Russian groups. BUGAENKO et al (1971) studied the phase dependence for selected areas of Saturn using twelve filters which covered the range 3600-7500 Å, and had passbands of 2% of their peak wavelength. Two of the filters were centred on methane bands (at 6190 and 7250 Å). The variation of linear polarisation with wavelength for two runs on the South pole of the planet at a phase angle of about $3^{\circ}.5$ is shown here as figure B1. The quoted error for the Russian measures is 0.12%. On the basis of these results, the authors ruled out any variation of polarisation between the methane bands and the continuum. Despite the size

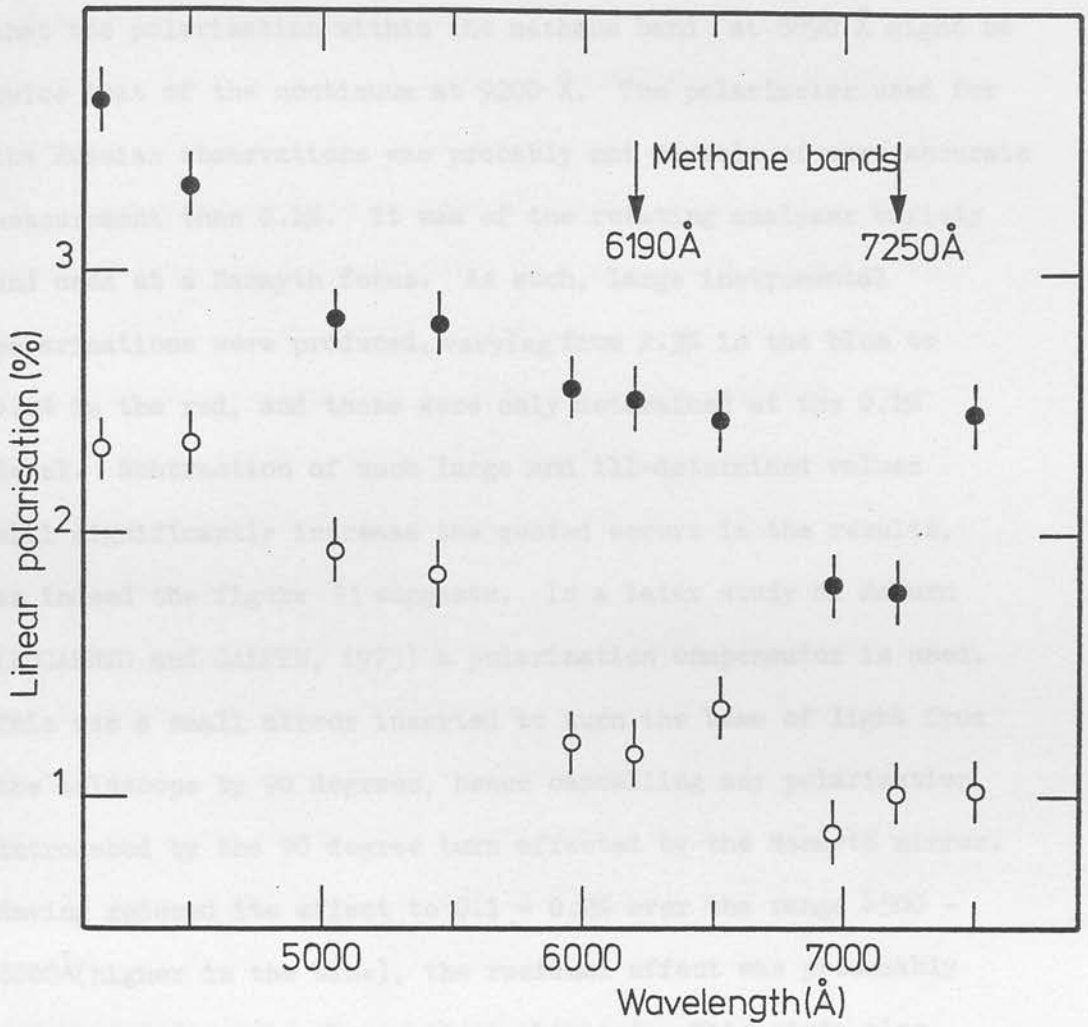

Figure B1: Linear polarisation of the South pole of Saturn (wavelength dependence), according to BUGAENKO et al (1971). Two nominally identical runs are shown. Phase angle 3°.5.

of the errors no further investigation of this possible variation has been made, though COFFEEN & HANSEN (1974) have suggested since that the polarisation within the methane band at 8890 Å might be twice that of the continuum at 9200 Å. The polarimeter used for the Russian observations was probably not capable of more accurate measurement than 0.1%. It was of the rotating analyser variety and used at a Nasmyth focus. As such, large instrumental polarisations were produced, varying from 2.3% in the blue to 4.6% in the red, and these were only determined at the 0.1% level. Subtraction of such large and ill-determined values will significantly increase the quoted errors in the results, as indeed the figure B1 suggests. In a later study on Saturn (BUGAENKO and GALKIN, 1973) a polarisation compensator is used. This was a small mirror inserted to turn the beam of light from the telescope by 90 degrees, hence cancelling any polarisation introduced by the 90 degree turn effected by the Nasmyth mirror. Having reduced its effect to 0.1 - 0.2% over the range 4500 - 8000Å(higher in the blue), the residual effect was presumably subtracted from the observations obtained. This study also used markedly better observational techniques and better guiding. Unfortunately as a consequence of the earlier study, the 7200 Å filter was not used.

The phase dependence of the linear polarisation of Jupiter has been studied with the same polarimeter by MOROZENKO (1973). Here, the whole planet was observed with seven filters including two centred at 6200 Å and 7200 Å. However, no variation across the methane bands could be studied with such sparse and widely spaced data. The scatter again is quite high, and is presumably

due to imperfections in the polarimeter, though for these observations it was being used at a Cassegrain focus. The rather large zenith distances (up to 70°!) at which the planet was of necessity observed might also have contributed. The phase dependence found for the 5050 Å filter is shown as figure B2.

The wavelength dependence of linear polarisation was extended into the infrared for both Jupiter and Saturn by KEMP et al (1978). Instrumental polarisation for the photoelastic modulator polarimeter used by this group was certainly below 0.05%. Other notable studies of the phase or wavelength dependence of Jupiter and Saturn are DOLLFUS (1961), GEHRELS et al (1969) and DOOSE (1973).

In both Jupiter and Saturn, the linear polarisation does not disappear at zero phase angle, as expected. In Jupiter, the polarisation is about +0.4% at phase angle 0°, and decreases with increasing phase. The polarisation drops with wavelength and becomes negative in the red at large (i.e. > 6°!) phase angles. In Saturn, the polarisation is again small at small phase angles, but then increases with phase. As with Jupiter the linear polarisation decreases with wavelength, but does not become negative until ~1μ.

Most of the papers referred to above have discussions and/or measurements of the dependence of polarisation across the planetary disc. The most comprehensive measurements however, are those of Hall and Riley, both on Jupiter (HALL and RILEY, 1968; HALL and RILEY, 1974a) and Saturn (HALL and RILEY, 1974b). Using a scanning polarimeter, diagrams such as the one reproduced here as figure B3 were obtained in the ultraviolet (UG1 filter, 3760 Å) and in the visible (OG5 filter, 5740 Å). The polarimeter is described by HALL (1968). Scanning is performed by moving an

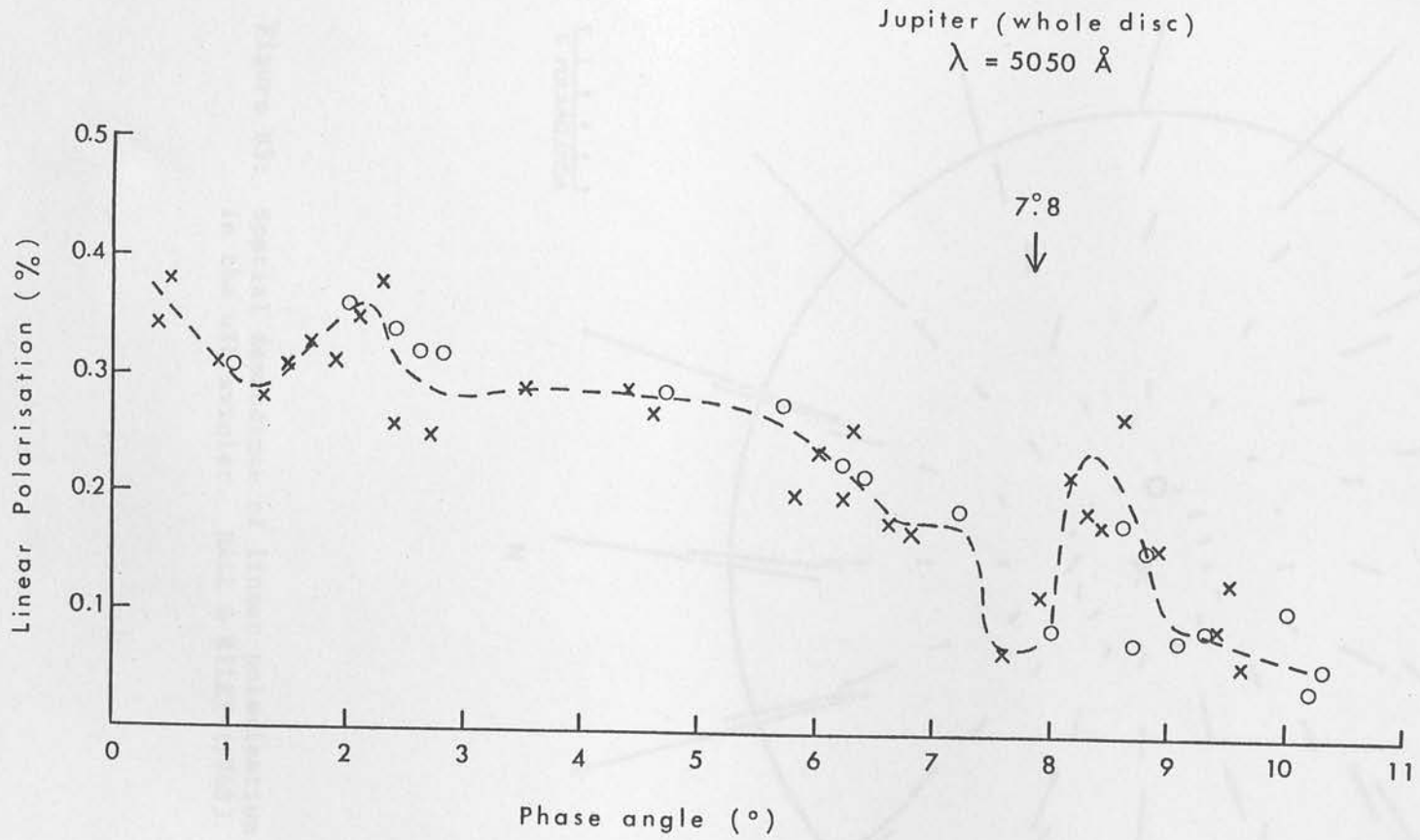

Figure B2: Linear polarisation of the whole disc of Jupiter at 5050 Å (phase dependence), according to MOROZHENKO (1973).

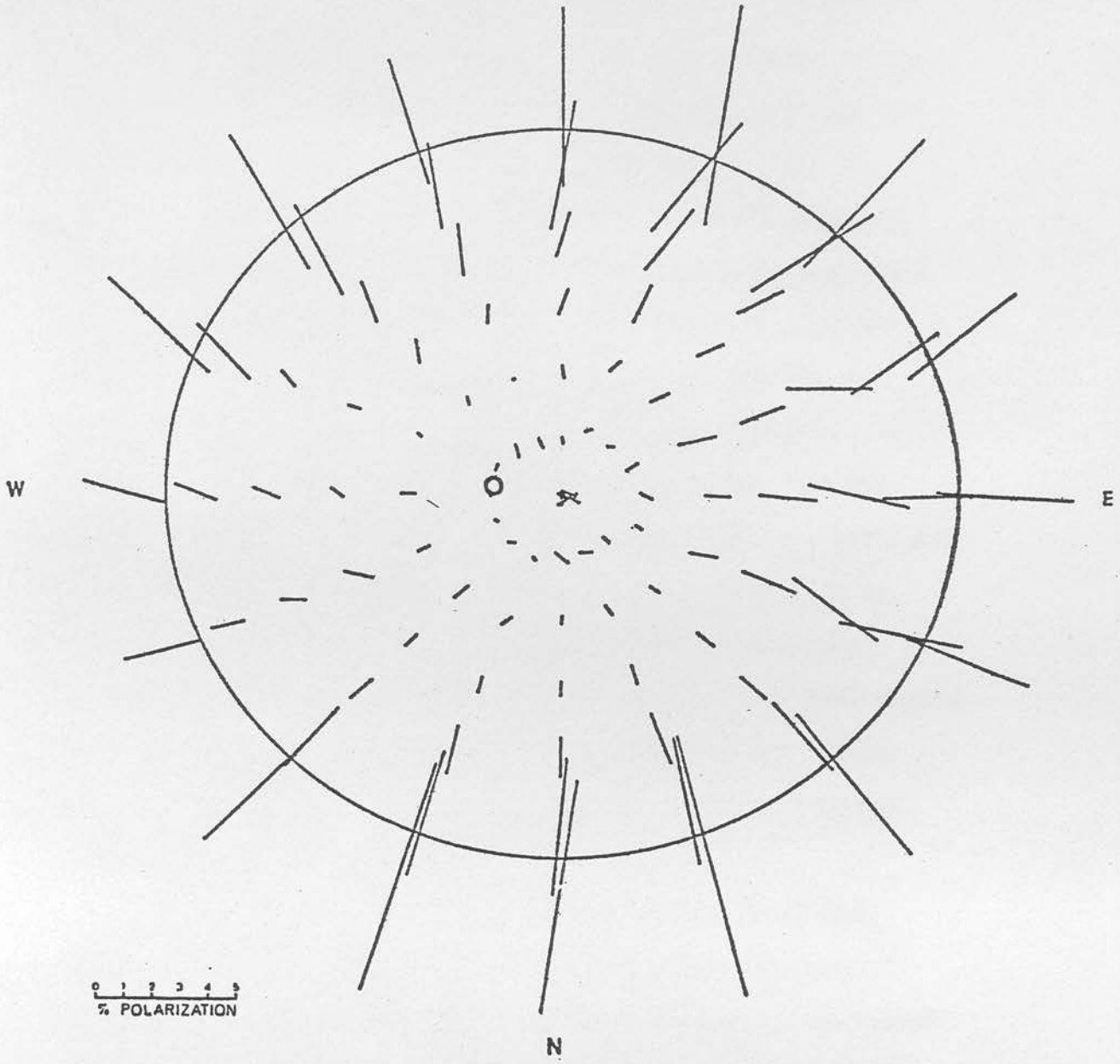

Figure B3: Spatial dependence of linear polarisation on the disc of Jupiter in the ultraviolet. HALL & RILEY (1968).

aperture smoothly with a linear cam, and gives good positional accuracy. The polarimeter consists simply of a Wollaston prism. Separate photomultipliers look at the two emerging beams and the measure of polarisation is derived from the ratio of the two signals. The whole polarimeter is rotated to measure position angle, and the scanning aperture stage can be rotated separately. Instrumental polarisation is found to be ~ 0.3%. One can make three comments on the instrument. Firstly, the apertures are metallic, and can polarise light at their edges (SERKOWSKI, 1974). Secondly, since it is the aperture that moves rather than the image of the star, each point measured is seen through a different part of the Wollaston prism. Hence any inhomogeneities in the prism will affect the measured distribution of polarisation. Thirdly, there is no time modulating element. In all, observations made with this polarimeter should be dependable to 0.1 - 0.2%. This is perfectly adequate for observations in the ultraviolet (Figure B3).

The pattern of polarisation on both planets is chiefly radial. At phase angles $\neq 0^{\circ}$, a phase dependant component of polarisation is introduced, which is more important in the visual than in the ultraviolet. In both planets, the polarisation of the polar regions seems less phase dependant than the centre of the disc. On Saturn in the ultraviolet the polarisation at the limbs on the equator is about the same as at the poles, while in Jupiter it is only about half as much. Infrared scans of Jupiter (at 1.6μ) show a tangential pattern (KEMP et al 1978). As the polarisation decreases with wavelength on this planet, this is perhaps not surprising.

Time variations in the polarisation of the light from these two Major planets have been remarked on by several of the authors mentioned above. It is clear that much of this is simply due to poor seeing and/or guiding (HALL and RILEY, 1974). See, for example, the two runs shown in figure B1 which were nominally of the same area of the planet at near identical phases. However, since the axis of rotation of both planets is inclined to the equator, variations might well be expected if latitudinal variations in cloud structure occur (as has been suggested for example by GEHRELS, 1969). Similarly polarisation variations might occur associated with the appearance and disappearance of specific surface features as the planets rotate. HALL and RILEY (1976) have looked for polarisational structure associated with discrete features on the disc of Jupiter, but have found no evidence for any such variation. The Great Red Spot in particular seemed not to affect the polarisational structure (HALL and RILEY, 1974a).

The linear polarisation of the rings of Saturn has been studied by LYOT (1929), summarised in DOLLFUS (1961), KEMP and MURPHY (1973), HALL and RILEY (1974), KEMP et al (1978), and JOHNSON et al (1980). Dollfus interpreted his measurements of linear polarisation in terms of two components. The position angle of one of these was parallel to the scattering phase, while that of the other remained parallel or perpendicular to the radius vector. The latter component could change in a rapid and unpredictable manner. The polarisation associated with the scattering phase was thought to imply a mixture of solid particles of albedo similar to "dirty ice" with diameters of at least a few millimetres, and of smaller, darker grains which dominated the polarisation in the ultraviolet. The

polarisation component associated with the ring phase arose from illumination of the rings by reflected light from the planet. Multiple scattering between 'blocks' of particles could cause the variability of this component even to the extent of changing its sign. Kemp and collaborators do not see the ring phase component of polarisation. Measurements around opposition, where such a component would be most obvious, were used to put an upper limit on any ring phase associated polarisation at the ansae of 0.1%.

The dependence of the circular polarisation of several regions of Jupiter with phase has been studied by KEMP et al. (1971a), KEMP et al (1971b) and MICHALSKY and STOKES (1974). As yet this seems only to have been done at red wavelengths 6100 - 6800 Å. Saturn has been studied in more detail by SWEDLUND et al (1972), who covered both the wavelength dependence (at phase angles $0^{\circ}.6$ and $6^{\circ}.3$) and the phase dependence at the poles of the planet. Circular polarisation is of opposite signs and roughly equal magnitude at the two poles of a planet. The polarisation also changes sign through opposition. These effects are termed the 'polar' and 'opposition' effects respectively. The wavelength dependence for Saturn is mainly independant of phase in the red, but the polarisation changes sign in the blue ($\sim$ 5000 Å). Such a change of sign has been predicted for Jupiter (KAWATA, 1978). In both planets, a sharp increase in the circular polarisation has been found at a specific phase angle - $7^{\circ}.8$ in Jupiter and $2^{\circ}.7$ in Saturn. The enhancement lasts for about $\frac{1}{2}^{\circ}$ in phase (MICHALSKY and STOKES, 1974). KEMP et al (1971b) studied Jupiter continuously for a five hour period and found no dependence of the circular polarisation on the rotation of Jupiter on its axis.

3. The Atmospheres of Jupiter and Saturn.

This section describes the model for the atmospheres of Jupiter and Saturn that is generally accepted at present. The photometric and polarimetric basis for the model will be briefly reviewed. Most work on the atmospheres of the Outer planets has concentrated on Jupiter. Accordingly when details are quoted below, these will refer to Jupiter. Saturn is contrasted at the end of this section.

The portion of the (Jovian) atmosphere available for photometric investigation is shown diagrammatically as figure B4. The major features of this model were put forward by LEWIS (1969a, b). Deep in the atmosphere ($P \sim 1$ atm., $T \sim 210K$), are clouds of water and of aqueous NH_3 and NH_4SH. These clouds are effectively semi-infinite to visual and infrared photometry (COCHRAN and SLAVSKY, 1979). Above these clouds there is a layer of clear gas (20 - 30 km?) before an upper cloud layer is reached ($P \sim \frac{1}{2}$ atm., $T \sim 145K$. DANIELSON and TOMASKO, 1969). The clear gas layer may have a significant haze suspended in it. Such a haze, made up of solid NH_4OH and NH_4SH, is predicted by Lewis. The upper cloud layer is composed of ammonia crystals a few microns in diameter, which is optically thick at visual wavelengths ($\tau \sim 2 - 4$), but semi-transparent to the infrared. The ammonia clouds are identified with the bright white cloud layer observed on both planets, and would not have a sharply defined upper boundary. Ultraviolet observations suggest a further layer of particles high up in the atmosphere around the tropopause. (In a planetary atmosphere, as the distance from the planetary 'surface' increases, temperatures decrease up to a certain point,

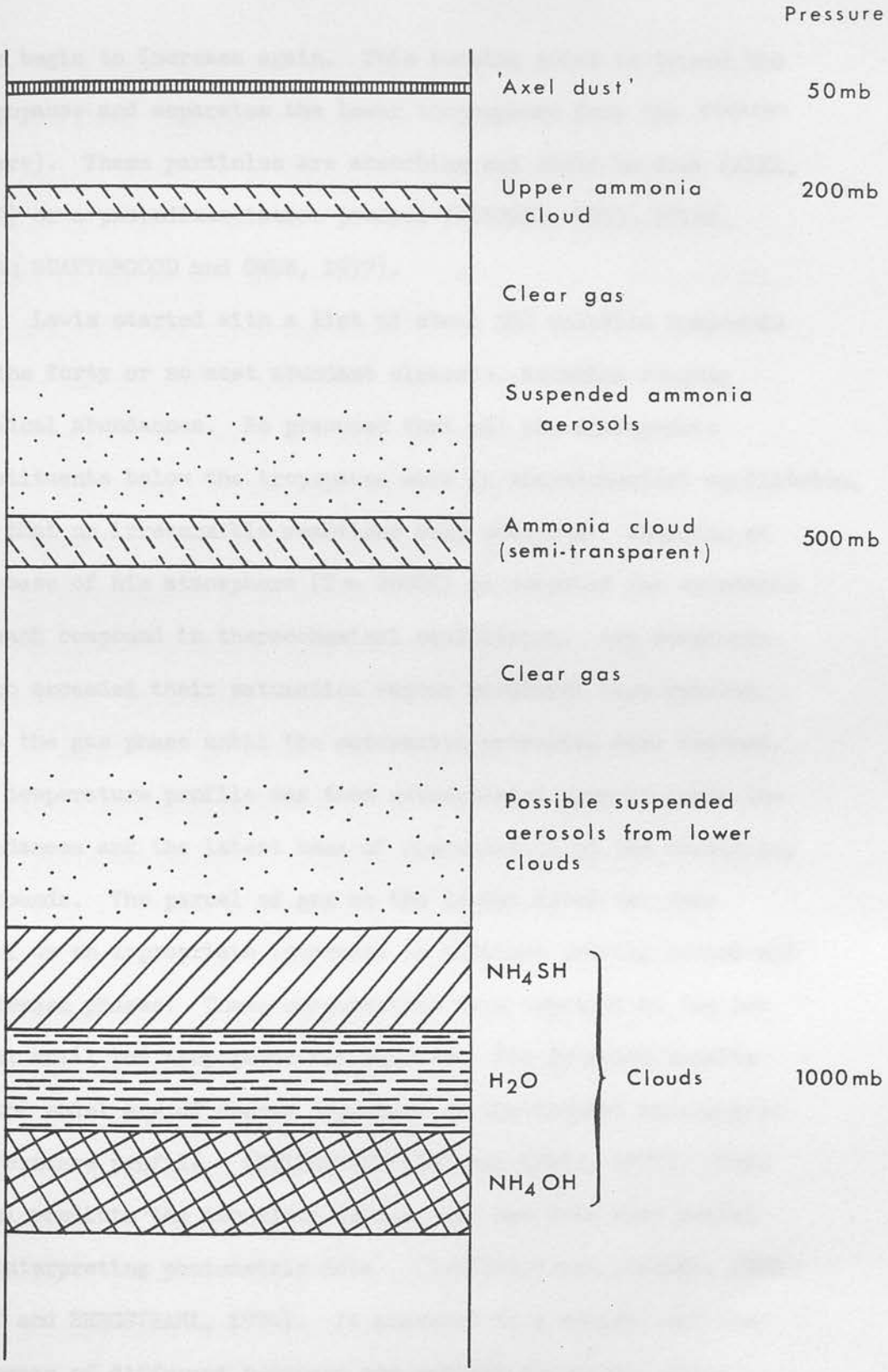

Figure B4: General purpose Jovian atmosphere. Diagrammatic only.

then begin to increase again. This turning point is termed the tropopause and separates the lower troposphere from the stratosphere). These particles are absorbing and could be dust (AXEL, 1972) or a photodissociation product (STROBEL, 1973; PRINN, 1974; SCATTERGOOD and OWEN, 1977).

Lewis started with a list of about 500 volatile compounds of the forty or so most abundant elements, assuming roughly cosmical abundances. He presumed that all the atmospheric constituents below the tropopause were in thermochemical equilibrium, and that no irreversible reactions were occuring. Starting at the base of his atmosphere ($T \sim 2000K$) he computed the abundance of each compound in thermochemical equilibrium. Any compounds which exceeded their saturation vapour pressures were removed from the gas phase until the saturation pressures were reached. The temperature profile was then extrapolated upwards using the abundances and the latent heat of condensation of the condensing compounds. The parcel of gas at the lowest level was then moved up an appropriate increment in altitude leaving behind all condensed phases. These computations were repeated at the new level until the tropopause was reached. The detailed results of the model are of course dependant on the assumed atmospheric temperature profile (WEIDENSCHILLING and LEWIS, 1973). This model predicts the two cloud levels, and has been very useful in interpreting photometric data (DANIELSON and TOMASKO, 1969; HUNT and BERGSTRAHL, 1974). It answered in a natural way the dilemmas of different hydrogen and methane abundances being derived from strong and weak absorption lines, and from infrared and visual measurements. In the weak lines and in the infrared, we are sampling a much larger depth of the atmosphere. Spatially resolved measurements of Jupiter at 5μ (KEAY et al 1973, WESTPHAL

et al 1974) show that most emission at these wavelengths comes from localised 'hot spots' strongly correlated with visually dark belts. Hence it is suggested that above these bands the upper cloud layer is absent (or mostly absent) and the colouring is that of the deeper layers below. Both organic and inorganic colourants for the cloud layers have been suggested (see SILL, 1976). The absence of the cloud layer is supposed to be due to convection, belts (dark, latitudinal markings) being descending regions and zones (bright, latitudinal markings) ascending ones.

Determinations of the ultraviolet albedo of Jupiter have lead to the suggestion of a very high absorbing aerosol layer. The planet should become brighter into the ultraviolet (because of Rayleigh scattering) but the opposite occurs. A thin layer of very small dust particles was suggested (AXEL, 1972) to darken the planet in the ultraviolet - particles now called 'Axel dust'. Later calculations (PRINN, 1974) showed that photodissociation of ammonia could produce a thin ($\tau \sim 0.2$) layer of small hydrazine (NH_2NH_2) particles ($r \ll 1\mu$) which fitted the observation rather well. Photodissociation products of methane have also been suggested (SCATTERGOOD and OWEN, 1977).

Let us see how this model can be used to interpret the polarisation observations of Jupiter and, indeed, what extra information or constraint such observations provide. The features to interpret are an increasingly negative polarisation of the whole disc with increasing phase angle, the wavelength dependence and spatial dependences of the linear polarisation. MOROZHENKO and YANOVITSKII (1973) interpreted the linear polarisation data of MOROZHENKO (1973) using a model of an optically thin layer of gas above a cloud layer. The observations were normalised by subtracting the residual polarisation found

when phase angle was less than $0^{\circ}.5$. This component was attributed to the "optical inhomogeneity of the planetary disc". If the cloud structure varies with latitude, and one pole is tilted towards the observer, it is feasible that the integrated linear polarisation of the planet would not fall to zero at zero phase angle. These authors used Mie scattering models and derived the radius of the aerosols to be $\sim 0.2\mu$ and their refractive index to be 1.36. This they claimed was in full agreement with the ammonia cloud model, since ammonia has a refractive index of 1.36 at around $T = 200^{\circ}K$. However this is the refractive index of liquid ammonia, while other authors have suggested that ammonia crystals form the clouds. The refractive index of solid ammonia, at its melting point ($195^{\circ}K$), is 1.42. Further, while liquid ammonia aerosols might be expected to be spherical (allowing Mie scattering calculations) there is no a priori reason to suppose that ammonia crystals would be. If temperature is such a critical parameter, we must consider at what level of the atmosphere the polarisation data is sampling. The calculations of Morozhenko and Yanovitskii are most strongly constrained by their ultraviolet and blue ($\sim$4000 Å) data. This and the small particle size derived might suggest that it is very much the upper layers of the ammonia clouds that are being modelled - where temperatures would be expected to be considerably lower than $200^{\circ}K$ (say, $150^{\circ}K$). COFFEEN and HANSEN (1974) point out that, in the Mie theory, the broad glory that gives rise to negative polarisation at small phase angles (as seen in Jupiter) persists for indices of refraction from 1.25 to 2.00. Hence the refractive index is not well determined from this property.

KAWABATA and HANSEN (1975) compare linear polarisation phase and wavelength dependence data with models calculated using the more refined 'doubling and adding' method. They found that the derived cloud phase matrix is suggestive of non-spherical aerosols larger than the wavelength, (they studied wavelengths up to 8μ). KAWATA and HANSEN (1976) calculate the circular polarisation of Jupiter implied by Morozhenko and Yanovitshii's aerosol particles and find it opposite in sign to the observed values. Solid ammonia particles of about 25% larger radius would fit the observed circular polarisation. The wavelength dependence of linear polarisation is partially attributable to the diminishing importance of Rayleigh scattering towards longer wavelengths. The fractional importance of the Rayleigh component in the scattering process can determine the sign of the circular polarisation produced (KAWATA and HANSEN, 1976). (We are dealing with at least second-order scattering when considering the origin of circularly polarised light. The first scattering produces linearly polarised light, which then illuminates other aerosols. Total internal reflection within these secondary aerosols introduces a phase difference between orthogonal modes of polarisation, and hence circular polarisation is produced from linear. The first scattering may be in the gas or by another aerosol, and in fact under identical scattering geometries, these give opposite signs of linear polarisation. Hence circular polarisation produced by a Rayleigh-aerosol scattering scheme is opposite in sign to that produced in an aerosol-aerosol scattering event.)

The spatial dependence of the linear polarisation can, in general terms, be explained by the same sorts of mechanisms as those above. GEHRELS (1969), interpreting his linear polarisation

data for the poles and limbs of Jupiter (GEHRELS et al 1969), suggested that the clouds are a lot lower over the poles than over the equator (as of course had Lyot before him). However, photographs in the 8890 Å methane band (OWEN, 1969; FOUNTAIN and LARSON, 1973), show bright areas over the poles. It is tempting to associate these high atmosphere scatterers (the methane band is very strong) with the linear polarisation of the polar regions, which is about twice as strong as at the limbs on the equator. There could be a number of reasons why the latitudinal variation occurs. LEWIS (1969a) pointed out that the adiabatic lapse rate is dependant on g - the gravitational acceleration - and would hence lead to latitudinal variations. At high latitudes, g will be larger, and this would give a steeper temperature gradient in the atmosphere and hence thinner clouds. BUSSE (1976) has suggested that large scale convection is responsible for the visible bands and zones on the planet, and that this ceases at latitudes $\geq 45^{\circ}$. Without convection the cloud level would be less disturbed and hence lower.

The structure of the atmosphere on Saturn is presumed to be rather similar to that of its larger neighbour. However on this planet the clouds appear to be relatively more extensive, though of the same composition. Ammonia is just detectable spectroscopically on Saturn, the equivalent width of the ammonia lines at 6450 Å being a factor of between 3 - 15 smaller than that for Jupiter (WOODMAN et al, 1977; SMITH et al 1980). Our best estimate of its abundance comesfrom the spectral distribution of the brightness temperature of the planet in the microwave regions (KUZMIN et al 1972). A fractional abundance of about $3 - 5 \times 10^{-5}$ is derived for ammonia in the undercloud atmosphere of Saturn. Infra-red

measurements at 5μ give another contrast with Jupiter. On Saturn there are none of the 'hot spots' found on Jupiter (LOW and DAVIDSON, 1969; WESTPHAL, 1971). Hence the upper cloud layers must be thick enough to be opaque at 5μ wavelengths and we do not see the water clouds on Saturn. The decrease of albedo into the ultraviolet is present in Saturn as in Jupiter and so a high layer of small absorbing aerosols is also required in the atmosphere of Saturn (BUGAENKO, 1972; PODOLAK and DANIELSON, 1971). The colours apparent on the disc of Saturn are not as striking as those of Jupiter. Saturn appears with cream or yellow colourings which could be due to sulphurous compounds brought up by convection from deeper clouds. There also appear to be latitudinal variations of cloud heights on Saturn. The region around the equator ($\pm$ 30°) appears to be optically distinct (TEIFEL', 1974). The polar regions are also more restricted on Saturn, possibly because of the smaller metallic hydrogen core in this planet (BUSSE, 1976).

As described in the previous section, the state of polarisation of the reflected light from Saturn is somewhat different to that of the light from Jupiter. Linear polarisation increases with phase for Saturn and the circular polarisation is also of a different sign. COFFEEN and HANSEN (1974), fitting Lyot's visual polarisation measurements, concluded that aerosol particles of diameter 1.5 to 3μ and of refractive index n = 1.3 to 1.5 were present. KAWATA (1978) using just the wavelength dependence of the sign of both linear and circular polarisation derived an aerosol diameter of about 3μ for a refractive index of 1.44, or lower and upper limits of 4 and 10μ respectively when n = 1.6.

These results show that the aerosols present in the Saturnian atmosphere are somewhat larger than those on Jupiter, at least in the part of the atmosphere probed by polarimetry. Of course, all these calculations have assumed spherical particles and may not therefore be accurate. The greater density and extent of the ammonia clouds may also lead to a larger or smaller contribution by molecular scattering on Saturn, depending on how diffuse the upper levels of the cloud are. Depending on the fractional importance of Rayleigh scattering in the atmosphere, the circular polarisation at small phase angles can be positive or negative (KAWATA and HANSEN, 1976).

Recently, data from spaceprobes have started to become available. The Pioneer and Voyager satellites have allowed study of both the Jovian and Saturnian atmospheres at large phase angles and high spatial resolution. Pioneers 10 and 11 carried two-colour photopolarimeters while Voyagers 1 and 2 could study polarisation in eight wavelength bands from 2350 Å to 7500 Å (LILLIE et al, 1977).

Reduction of Pioneer images of Jupiter has been carried out by Tomasko and his collaborators (eg, TOMASKO et al 1978; STOLL and TOMASKO, 1980). At large phase angles (up to 150°) the information given by these measurements relates mainly to the highest levels of the atmosphere. The lack of contrast between belts and zones at high phase angles confirms the necessity for a population of aerosols high in the atmosphere. Such aerosols had been suggested by ultraviolet limb darkening measurements. STOLL and TOMASKO (1980), suggest a scattering haze of optical depth around 0.13 (at 4400 Å) at the 200mbar level. The aerosols of this haze would, if spherical, have

diameters of ~ $\frac{1}{3}\mu$ and a refractive index close to 1.5. They would be strongly forward scattering and of high albedo, but would only be weakly backscattering. The upper (ammonia) cloud would have an optical depth greater than 2 and be situated at the 500 mbar level. These particles are larger than the haze aerosols, and are also moderately efficient backscatters. West has used a similar model to interpret spatial resolved photometry within strong methane bands and in the nearby continuum, (WEST, 1979a; WEST, 1979b; WEST and TOMASKO, 1980). However he finds it necessary to use a backscattering aerosol for the high level haze over the polar regions to give the bright 'hoods' over the poles seen in photographs taken through a filter isolating the 8890 Å methane band. The connection between the high 'shiny' aerosol haze and the strongly absorbing 'Axel' dust at similar heights is not clear. Imaging at 2400 Å with the photopolarimeter on Voyager 2 (HORD et al, 1979) has shown the absorbing particles must be near the top of the atmosphere (say, at 40 mbar) over the poles.

On Saturn, the contrast between the zones and belts persists to large phase angles, unlike the situation seen on Jupiter (TOMASKO et al, 1980). Hence there is no requirement to postulate a concentration of aerosols high in the atmosphere and distinct from the ammonia cloud. In Saturn, optical depth $\tau = 1$ in the cloud corresponds to 750 mbar level and is lower than on Jupiter because of the lower temperature.

The polarisation recorded by the photopolarimeters is dominated by Rayleigh scattering. As a first approximation, a model of Rayleigh scattering above a Lambertian reflector is moderately successful in explaining the general dependence on latitude, with the detailed structure being interpreted as

variations in the height of the cloud-tops (BAKER et al, 1975; GEHRELS, 1976). This statement implies of course that such measurements give little information on the deeper levels. In order to probe these regions we shall need absorption band studies and infrared measurements. The Voyager photopolarimeters contain filters centred at 7270 Å and 7500 Å and, although of low accuracy ($\pm$0.5%), polarisation measurements with these filters will be most interesting. Voyager also carries an infrared spectrometer - IRIS.

A good review of planetary polarimetry is given by COFFEEN and HANSEN (1974). Very full information on the atmosphere of Jupiter is given in another textbook by Gehrel, 'Jupiter', especially the articles by TOMASKO (1976), TEIFEL' (1976), SILL (1976), PRINN and OWEN (1976) and RIDGWAY et al (1976). Recent discussions of the atmosphere of Saturn include TEIFEL' (1974) and MACY (1977). TOMASKO et al (1978), TOMASKO (1976) and GEHRELS (1976) discuss Pioneer results. Preliminary results from the Voyager spacecraft can be found in SMITH et al (1979a) and SMITH et al (1979b).

4. The case for spectropolarimetry of the Major planets.

The discussion of the literature on the polarisation of Jupiter and Saturn (in section 2) makes the point that no accurate study has been done on either planet to seek polarisational effects within spectral lines or bands. One reason to do so immediately suggests itself. When we look at a planet in the wavelength of a strong absorption band, we are looking at the topmost levels of its atmosphere, while in weaker bands we are looking at intermediate levels. Hence in defining the dependence of polarisation within spectral lines, we are studying the vertical structure of the atmosphere. FYMAT (1974) has made detailed predictions of the polarisation profiles of spectral lines expected in planetary atmospheres using both Rayleigh and Mie scattering models. He finds that polarisation always arises in spectral lines formed in a scattering atmosphere. The polarisation increases with the strength of the line up to a certain point and then decreases again as saturation is approached. Polarisation reversals are predicted during scans along the meridian and possibly also along the equator. (By polarisation reversal, we mean that the polarisation in the line changes sign, ie its position angle rotates through 90°.) However, the polarisation is always positive for weak bands. Spectropolarimetry of Venus was attempted in the region 1.6μ - 1.7μ with a Fourier Interferometer Polarimeter (FORBES and FYMAT, 1974). Polarisation effects were observed, though these were not convincing, and were not interpreted. BURIEZ et al (1979) made calculations of the information that could be derived from the equivalent widths of the polarisational profiles of lines. They did this by generalising

the curve of growth procedure for all four Stokes parameters. From this technique can be derived the atmospheric levels at which the polarisation arises. This is done by determining the rotational temperatures from the polarisation equivalent widths for several lines. The ratio of the scale height of a compound gas (eg methane) to that of the cloud particles can be found, and hence the ratio of the scale heights of different gasses. Finally, if spatially resolved spectropolarimetry is possible, the different angles of incidence will allow investigation of yet higher levels of the atmosphere, as would studying the phase dependence of any effect.

Broadly speaking, visible and ultraviolet photometry and polarimetry give information on the part of the atmosphere in the region $0.05 \lesssim P \lesssim 0.5$ bar, while infrared data are useful in the range $0.5 \lesssim P \lesssim 4$ bar. Absorption band studies cover the interval $0.1 \lesssim P \lesssim 3$ bar. Such studies, sounding levels at the top of and within the upper ammonia cloud, are complementary to polarisation measures taken at large phase angles from spacecraft, as the latter are most useful for deriving information on the gas above the cloud.

We therefore conclude that spectropolarimetry of absorption bands can give information on a part of the planetary atmosphere not well covered by other techniques. It is considered that the case for spatially resolved spectropolarimetry is made. However, as with all novel fields, the effect has to be shown to be detectable before a detailed program is attempted. This is done in the following sections and is the major result of this section of the Thesis.

5(a) Measurements of the polarisation of Jupiter

In this section the new observations of Jupiter are described. After the various tables and figures are presented, a commentary is given, identifying notable features in the polarisation. These features will be the subject of the discussion and interpretation sections to follow.

Measurements of the whole disc of Jupiter were obtained with the ROE Spectropolarimeter in 1978 January at the Mount Lemmon Observatory in Arizona and in 1980 April at the Mauna Kea Observatory in Hawaii. Observing logs are presented as Tables B1 and B4.

The observed spectrum of Jupiter in the interval 6700 - 8500 Å is shown in figure B5. The 6190 Å and 7250 Å methane bands are shown in more detail in figures B12 and B6 respectively. The 6450 Å ammonia band is shown in figure B13. The linear polarisation measurements given in Table B2 , and the circular polarisation measurements in Table B3, were collected in January 1978. These measurements of linear and circular polarisation are displayed, day-by-day as figures B7 (linear polarisation), B8 (position angle), and B9 (circular polarisation). The complete set of observations is shown in figure B10. The linear and circular polarisation measurements collected in April 1980 are tabulated in Tables B5 and B6, and displayed in figures B11 (7250 Å methane band), B12 (6190 Å methane band) and B13 (6450 Å ammonia band).

The accuracy of the quoted wavelength depended on how well the planet could be set in the centre of a large aperture and is about $\pm$ 5 Å. The effective resolution of these observations was determined by the (intensity-weighted) size of the planetary disc and is probably around 75 Å for the January 1978 data,

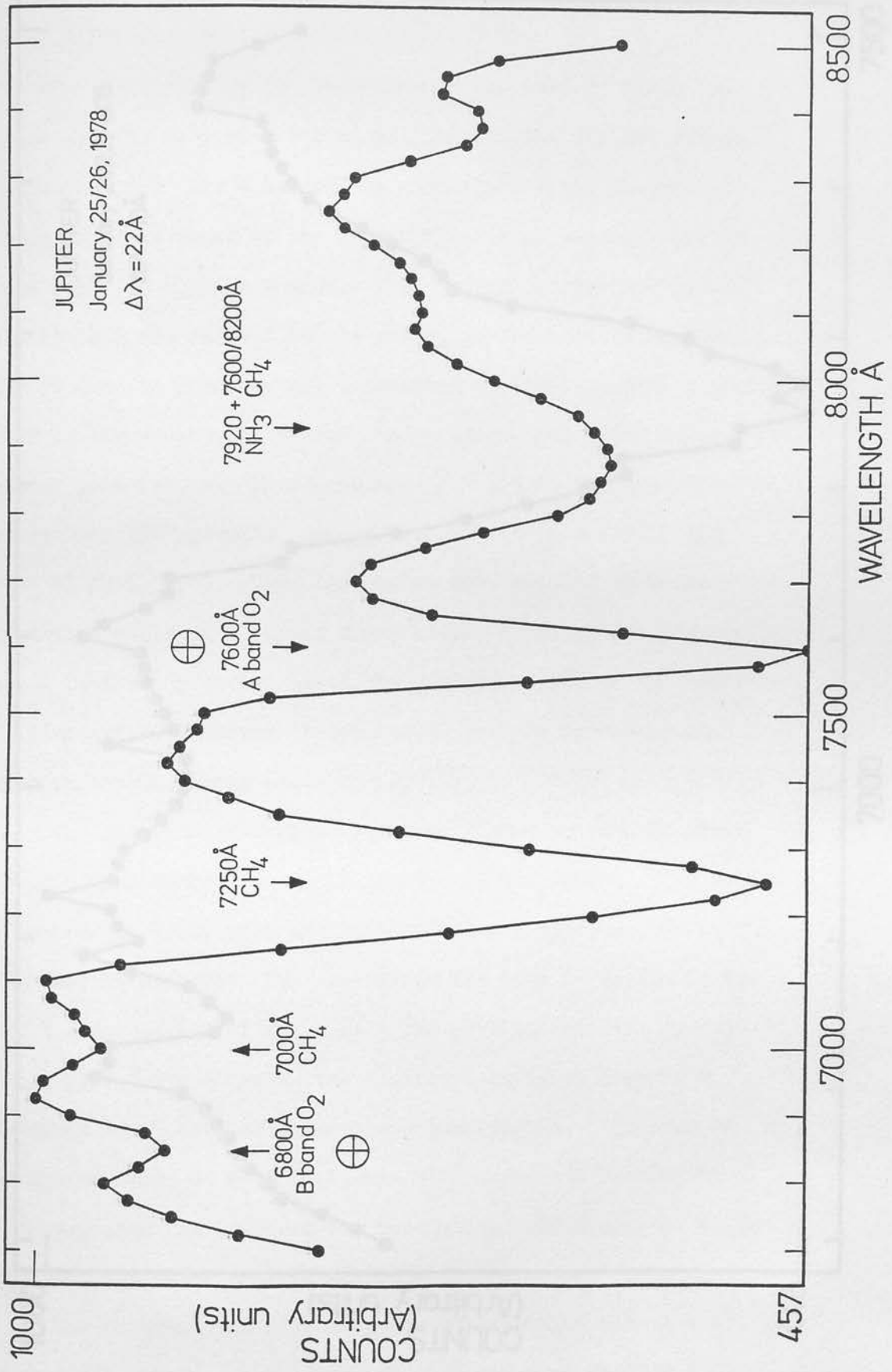

Figure B5: Observed spectrum of Jupiter. (1978)

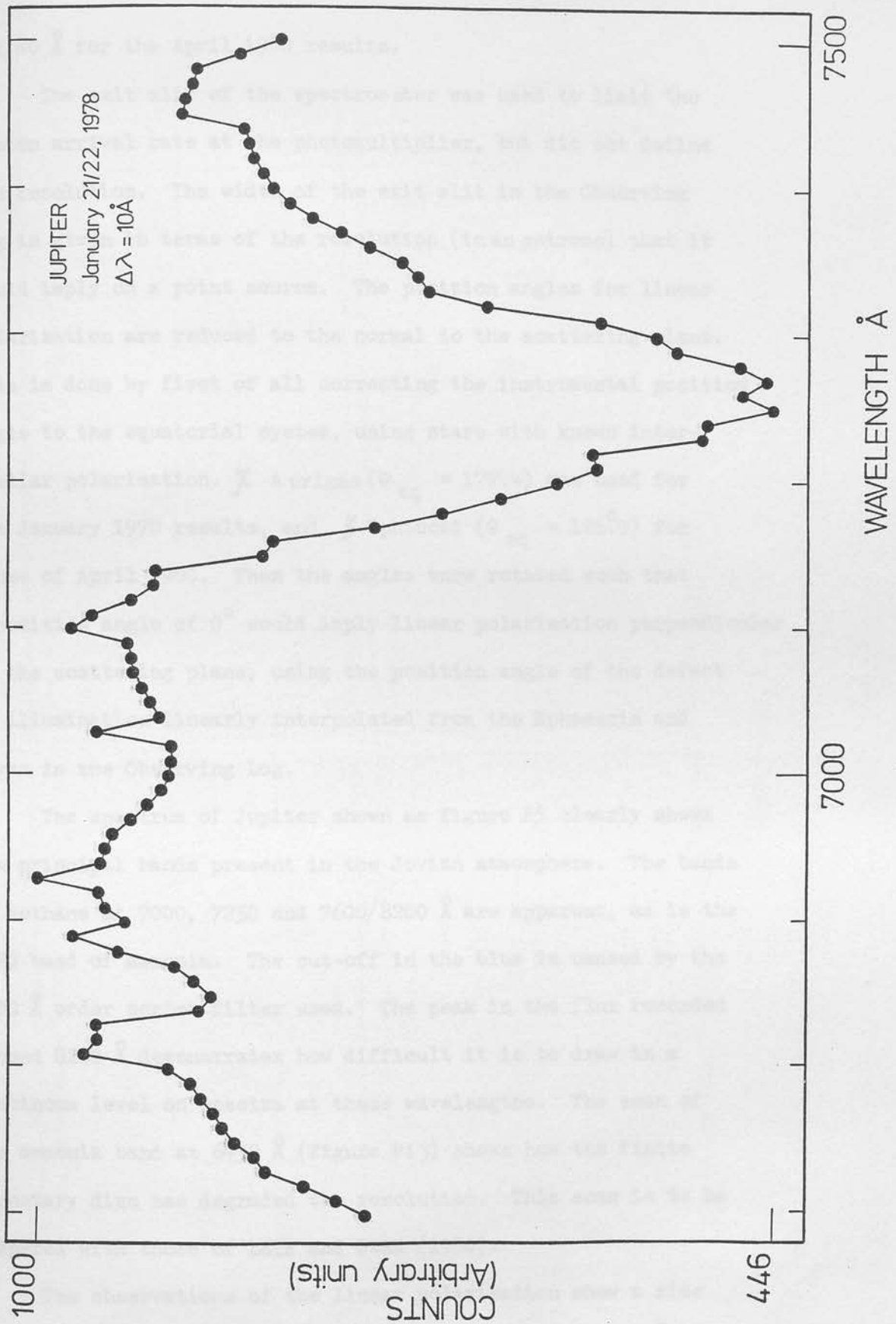

Figure B6: The 7250 Å methane band: the observed profile on Jupiter (1978).

and 40 Å for the April 1980 results.

The exit slit of the spectrometer was used to limit the photon arrival rate at the photomultiplier, but did not define the resolution. The width of the exit slit in the Observing Log is given in terms of the resolution (in angstroms) that it would imply on a point source. The position angles for linear polarisation are reduced to the normal to the scattering plane. This is done by first of all correcting the instrumental position angle to the equatorial system, using stars with known interstellar polarisation. χ Aurigae (θ_{eq} = 177.4) was used for the January 1978 results, and ζ Ophiuchi (θ_{eq} = 126.°0) for those of April 1980. Then the angles were rotated such that a position angle of 0° would imply linear polarisation perpendicular to the scattering plane, using the position angle of the defect of illumination linearly interpolated from the Ephemeris and given in the Observing Log.

The spectrum of Jupiter shown as figure B5 clearly shows the principal bands present in the Jovian atmosphere. The bands of methane at 7000, 7250 and 7600/8200 Å are apparent, as is the 7920 band of ammonia. The cut-off in the blue is caused by the 6600 Å order sorter filter used. The peak in the flux recorded around 8200 Å demonstrates how difficult it is to draw in a continuum level on spectra at these wavelengths. The scan of the ammonia band at 6450 Å (figure B13) shows how the finite planetary disc has degraded the resolution. This scan is to be compared with those of LUTZ and OWEN (1980).

The observations of the linear polarisation show a rise in measured polarisation across the methane band at 7250 Å (figure B10). For the January 1978 data, the polarisation is

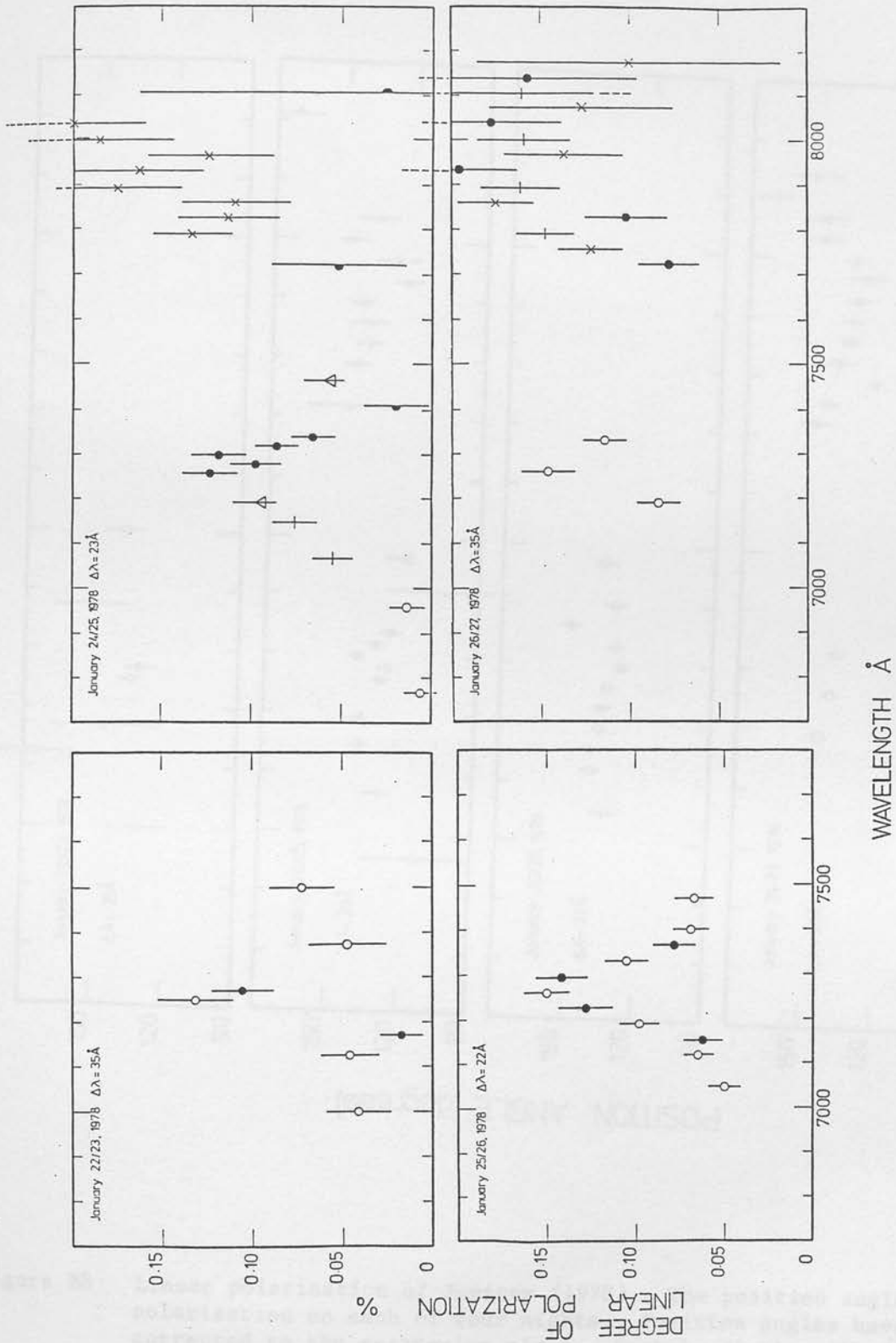

Figure B7: Linear polarisation of Jupiter (1978). The degree of polarisation on each of four nights in 1978. Symbols distinguish different runs on a given night.

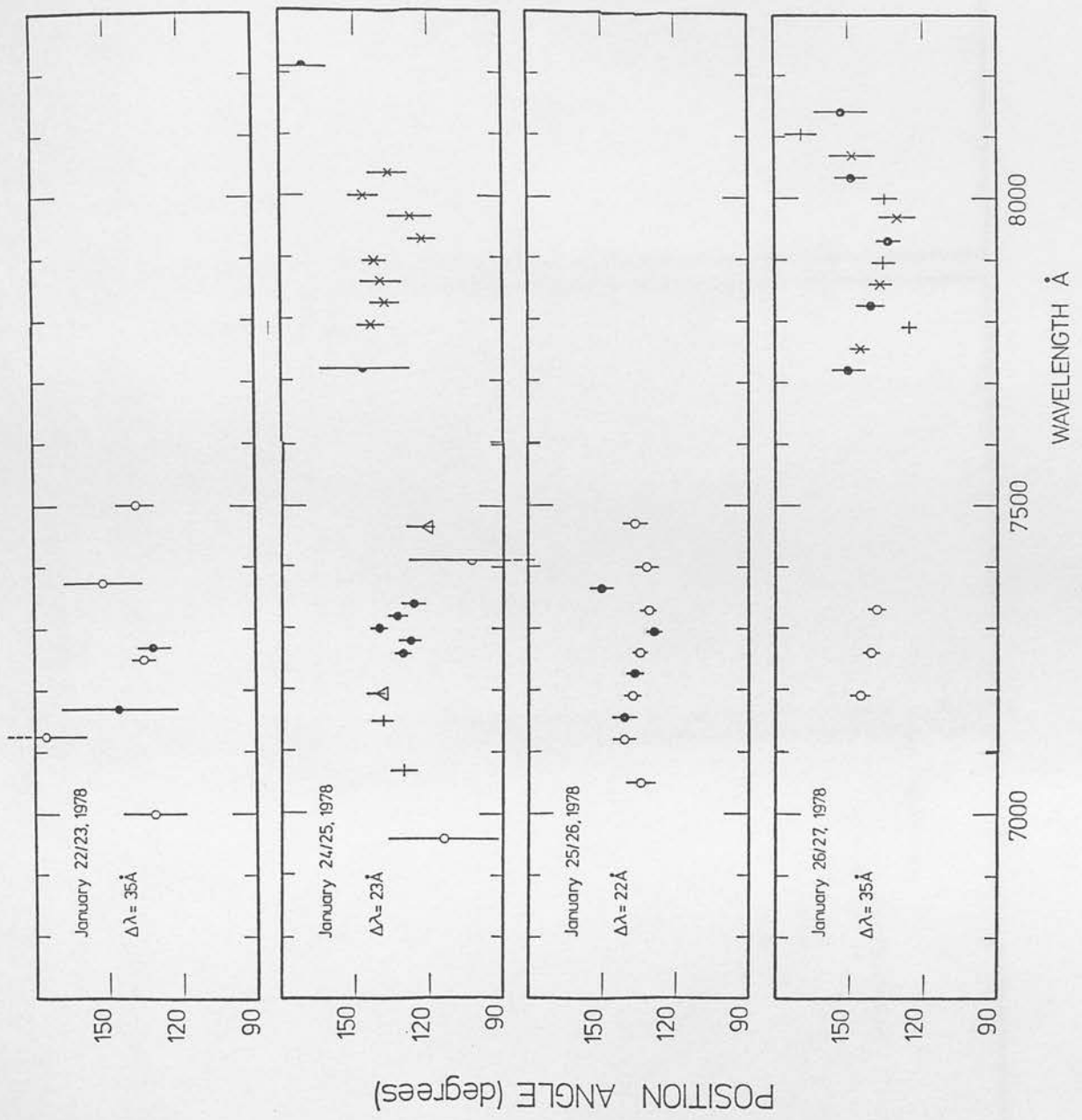

Figure B8: Linear polarisation of Jupiter (1978). The position angle of polarisation on each of four nights. Position angles have not been corrected to the scattering plane. Symbols distinguish different runs on a given night.

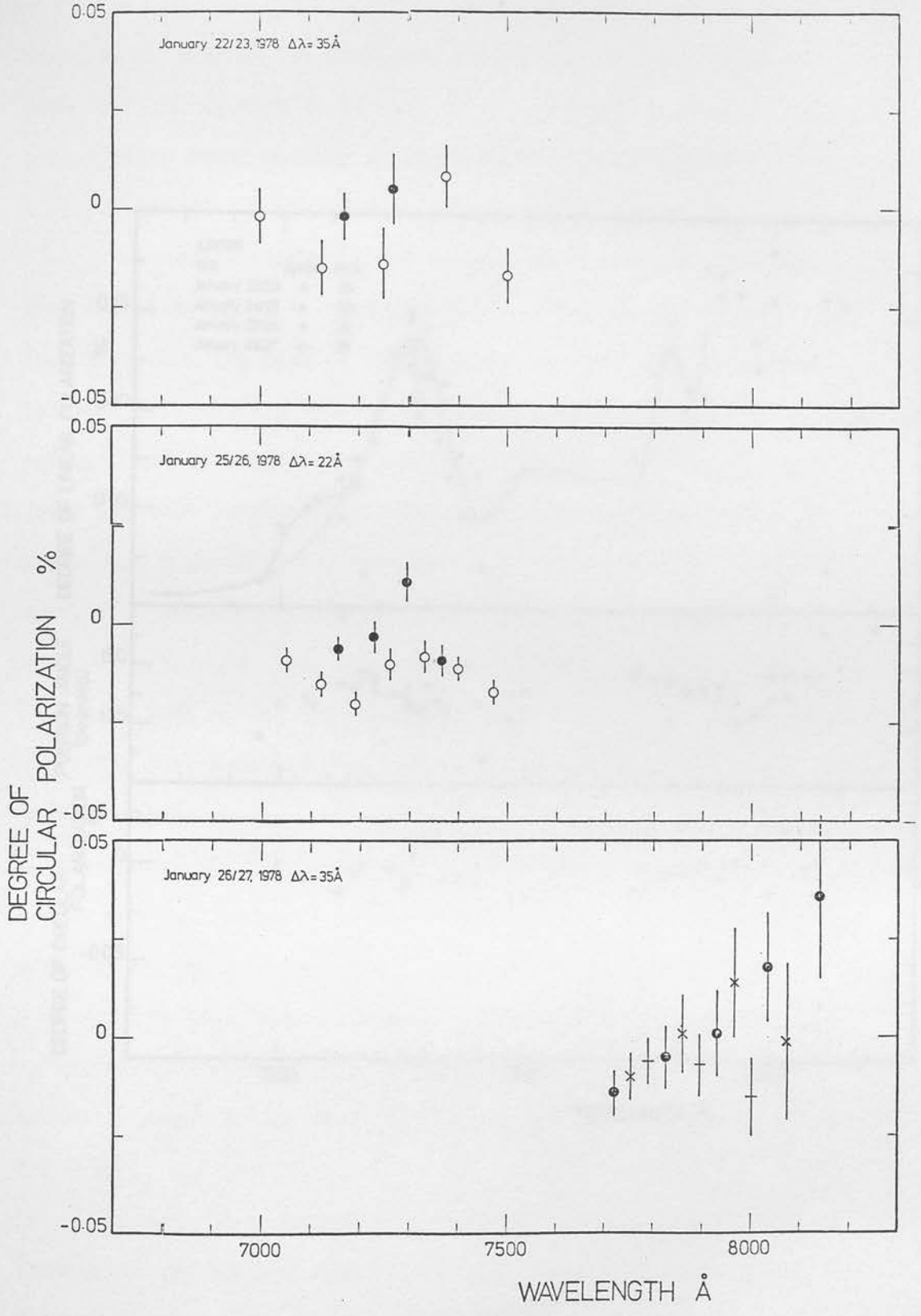

Figure B9: Circular polarisation of Jupiter (1978). Symbols distinguish different runs on a given night.

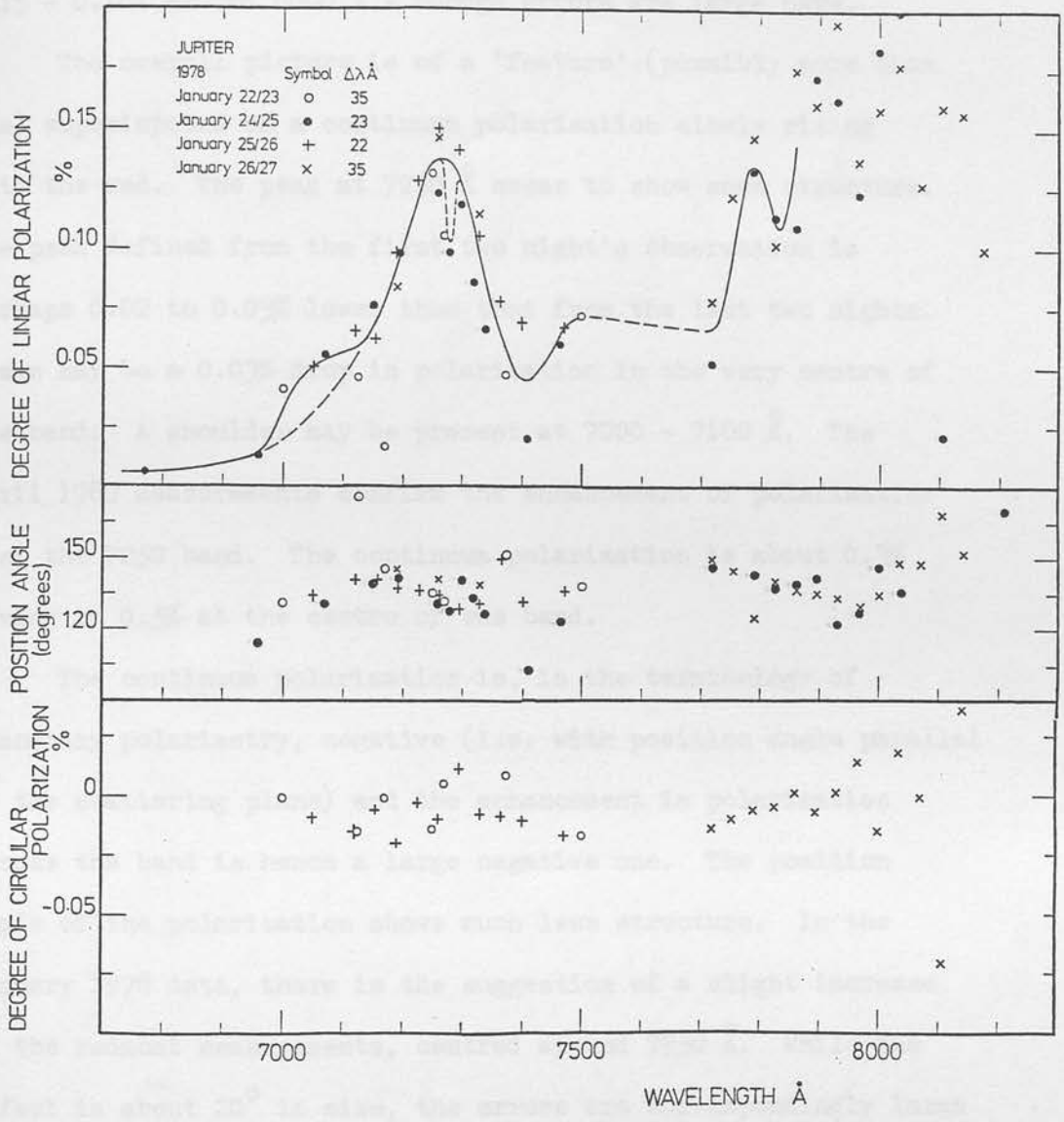

Figure B10: Linear and circular polarisation of Jupiter in January 1978.

very low (0.01%) in the continuum before 7000 Å. then rises to a peak of 0.14% at 7250 Å, to fall to around 0.04% at 7400 Å. The polarisation rises rapidly at wavelengths longer than 7750 Å to 0.15 - 0.18% around 8000 Å - though errors are large here.

The overall picture is of a 'feature' (possibly more than one) superimposed on a continuum polarisation slowly rising into the red. The peak at 7250 Å seems to show some structure. The peak defined from the first two night's observation is perhaps 0.02 to 0.03% lower than that from the last two nights. There may be a 0.03% drop in polarisation in the very centre of the band. A shoulder may be present at 7000 - 7100 Å. The April 1980 measurements confirm the enhancement of polarisation over the 7250 band. The continuum polarisation is about 0.3% rising to 0.5% at the centre of the band.

The continuum polarisation is, in the terminology of planetary polarimetry, negative (i.e. with position angle parallel to the scattering plane) and the enhancement in polarisation across the band is hence a large negative one. The position angle of the polarisation shows much less structure. In the January 1978 data, there is the suggestion of a slight increase in the redmost measurements, centred around 7950 Å. While the effect is about 20° in size, the errors are correspondingly large (5° - 10°).

The data of January 25/26 show a slight dispersion shape centred on the methane band at 7250, possibly confirmed by the January 24/25 points. Again, the size of the effect (10°) is small compared to the error obtained (3° - 4°).

Observations, in April 1980, of linear polarisation across the 6450 Å band of ammonia show no enhancement of the polarisation greater than or equal to 0.05% (above a continuum of 0.2%).

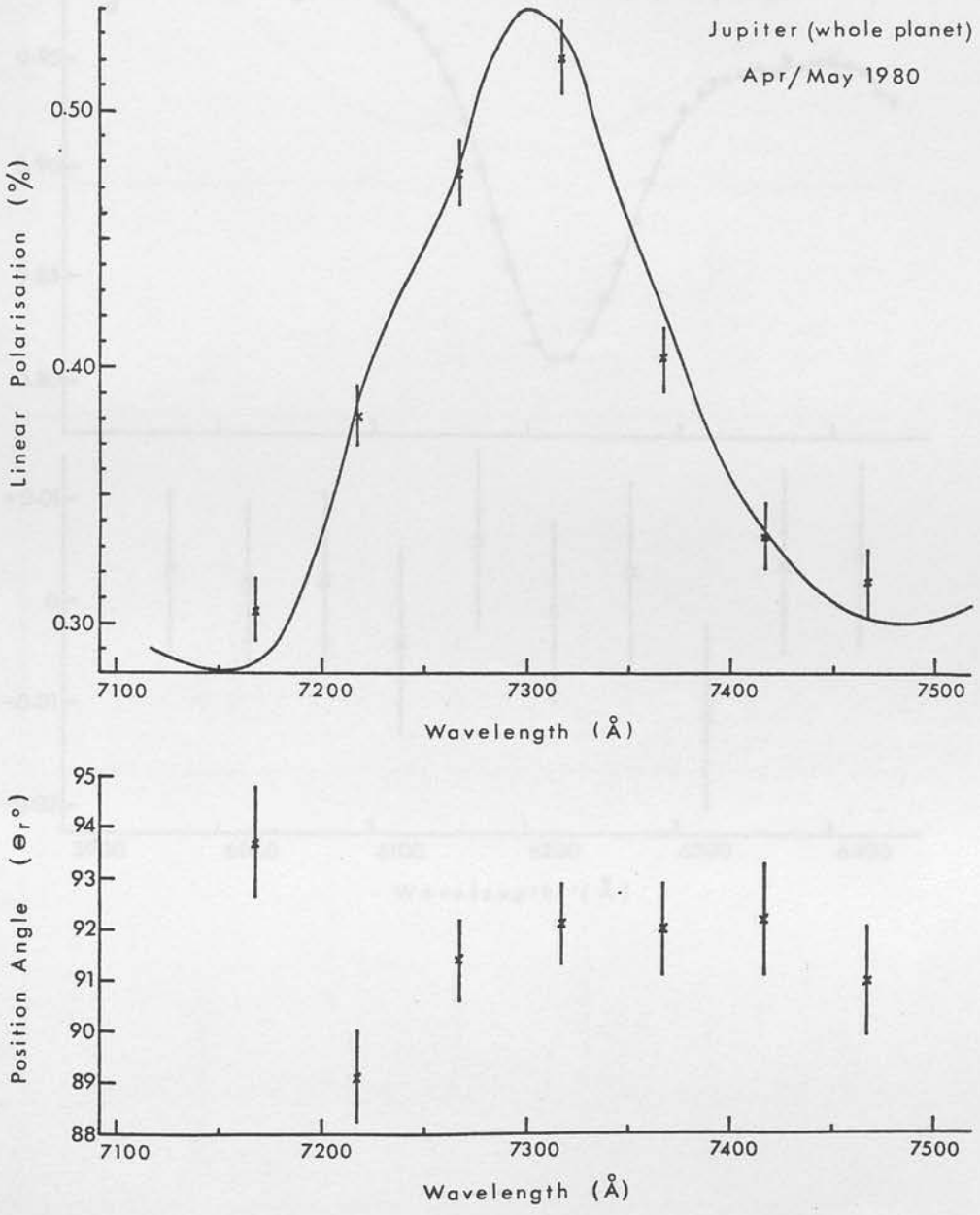

Figure B11: Linear polarisation of Jupiter, 1980. Degree of polarisation shown with inverted intensity profile of the 7250 Å methane band, scaled to the polarisation measurements. Position angles are measured from the normal to the scattering place.

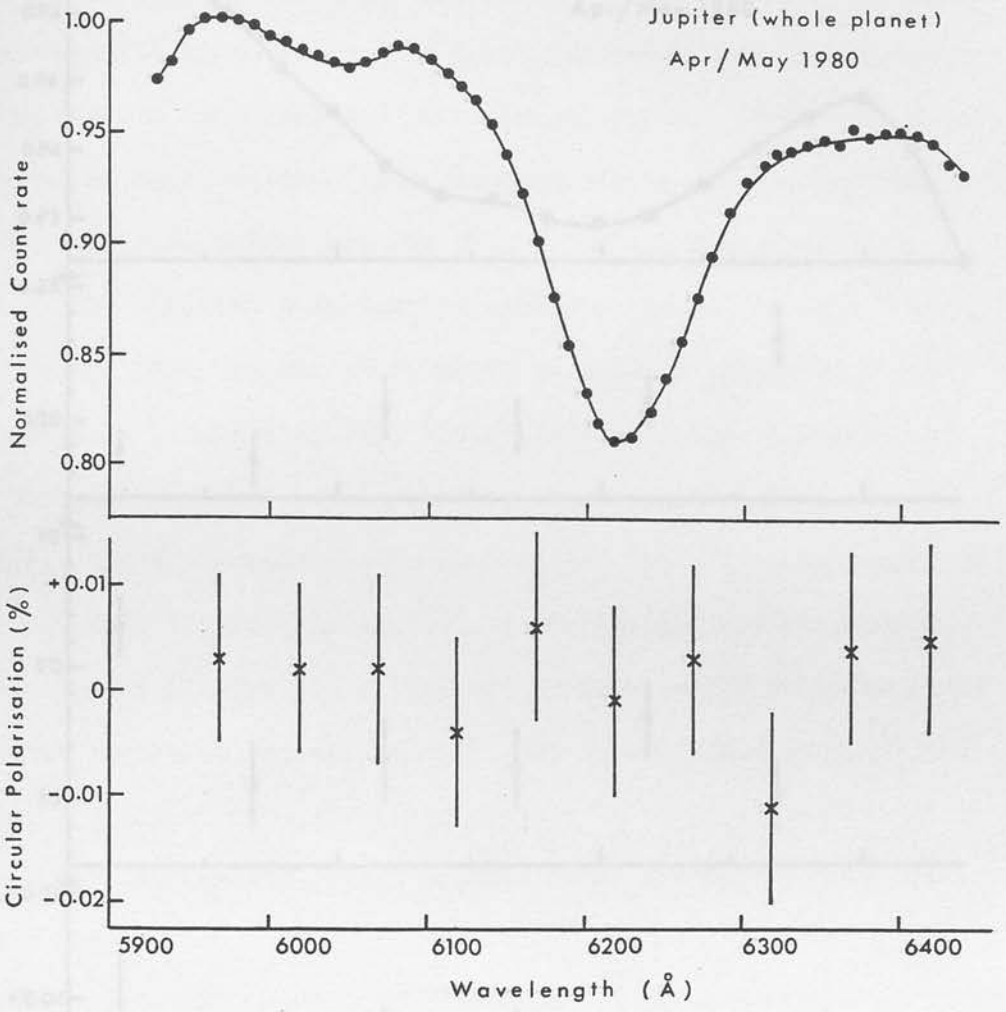

Figure B12: Circular polarisation of Jupiter, 1980. An intensity profile of 6190 Å methane band is also shown.

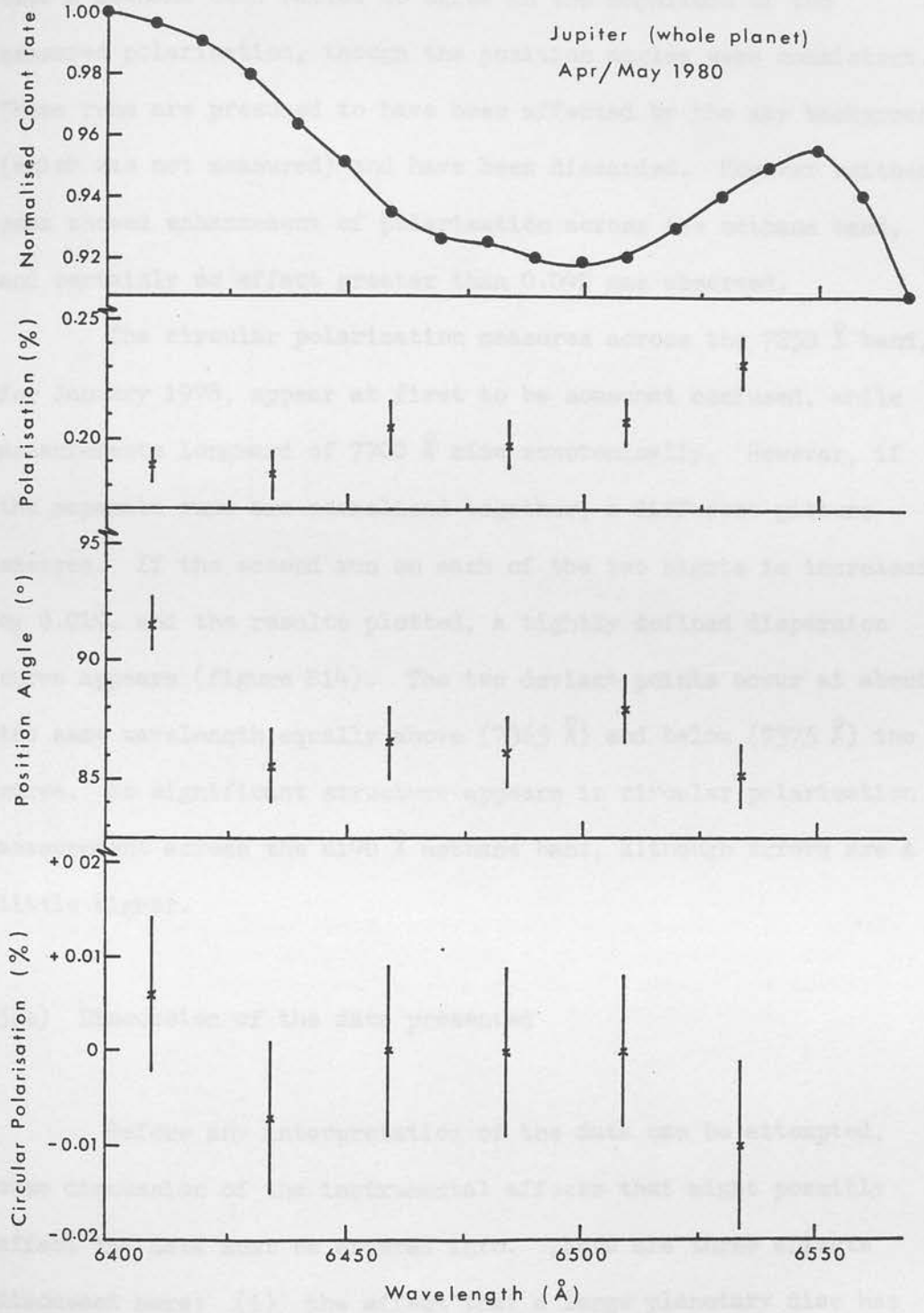

Figure B13: Measurements across the 6450 Å ammonia band in 1980. Position angle of linear polarisation measured from the normal to the scattering plane.

In 1980 May, two scans of linear polarisation across the 6190 Å methane band failed to agree in the magnitude of the measured polarisation, though the position angles were consistent. These runs are presumed to have been affected by the sky background (which was not measured) and have been discarded. However neither scan showed enhancement of polarisation across the methane band, and certainly no effect greater than 0.04% was observed.

The circular polarisation measures across the 7250 Å band, for January 1978, appear at first to be somewhat confused, while measurements longward of 7700 Å rise monotonically. However, if the separate runs are normalised together, a different picture emerges. If the second run on each of the two nights is increased by 0.01%, and the results plotted, a tightly defined dispersion curve appears (figure B14). The two deviant points occur at about the same wavelength equally above (7365 Å) and below (7375 Å) the curve. No significant structure appears in circular polarisation measurement across the 6190 Å methane band, although errors are a little higher.

5(b) Discussion of the data presented

Before any interpretation of the data can be attempted, some discussion of the instrumental effects that might possibly affect the data must be entered into. There are three effects discussed here: (i) the effect that a large planetary disc has on the operation of the spectrometer; (ii) whether the errors presented are realistic; and (iii) the ability of the polarimeter to measure polarisations at wavelengths in excess of 7500 Å.

(i) At several points in this Thesis (but especially in section A2.5) the effect of an extended image in the entrance

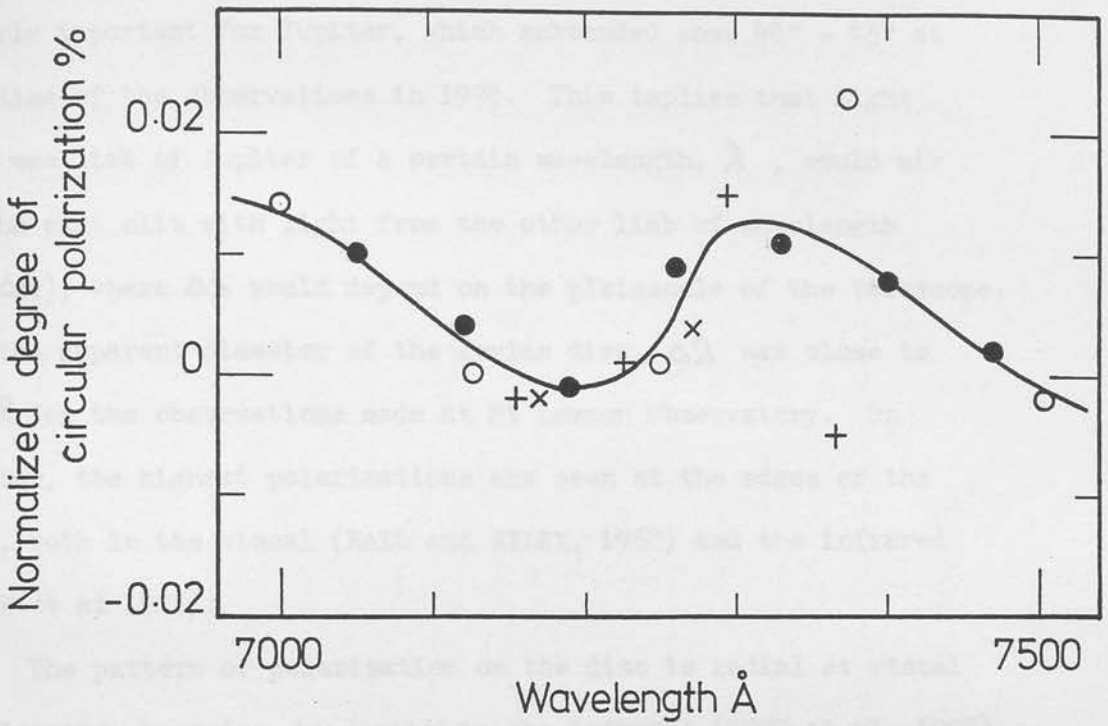

Figure B14: Normalised degree of circular polarisation of Jupiter (1978), $q(\lambda) - q(7200\ \text{Å})$. Open circles and crosses refer to the first and second runs on January 22/23, and filled circles and plus signs to the first and second runs on January 25/26.

aperture of the spectrometer has been commented on. The effect is clearly important for Jupiter, which subtended some 40" - 45" at the time of the observations in 1978. This implies that light from one limb of Jupiter of a certain wavelength, λ , would mix at the exit slit with light from the other limb of wavelength $(\lambda+\Delta\lambda)$, where $\Delta\lambda$ would depend on the platescale of the telescope, and the apparent diameter of the Jovian disc. $\Delta\lambda$ was close to 100 Å for the observations made at Mt Lemmon Observatory. On Jupiter, the highest polarisations are seen at the edges of the disc, both in the visual (HALL and RILEY, 1968) and the infrared (KEMP et al 1978).

The pattern of polarisation on the disc is radial at visual wavelengths, becoming tangential in the infrared (KEMP et al, 1978). Polarisation is stronger at the poles than at the east and west limbs and when we look at the whole planet the relatively large local polarisations almost cancel out. As the polarisation of the poles (or one pole) determines the overall value for the integrated disc at zero phase angle, the observed negative polarisation at these wavelengths implies a tangential pattern on the disc.

Consider now what will happen as we scan across the band. The contribution in intensity from the West limb declines before that for other parts of the planet, and hence the contribution from the two poles dominates the integrated polarisation of the planet, and an increasingly negative polarisation results. At the centre of the band, the polarised intensity from the poles would be diminished more than that from the two limbs, and the polarisation would turn positive. Towards the red wing of the band, the polarisation would again turn positive before returning to a continuum level. Some

simple modelling was carried out using the intensity profile of the 7250 Å band observed in April 1980. Four profiles were added together corresponding to the two poles and both limbs. The poles were given a positive polarisation and the limbs a slightly larger negative one. The profiles for the East and West limbs were

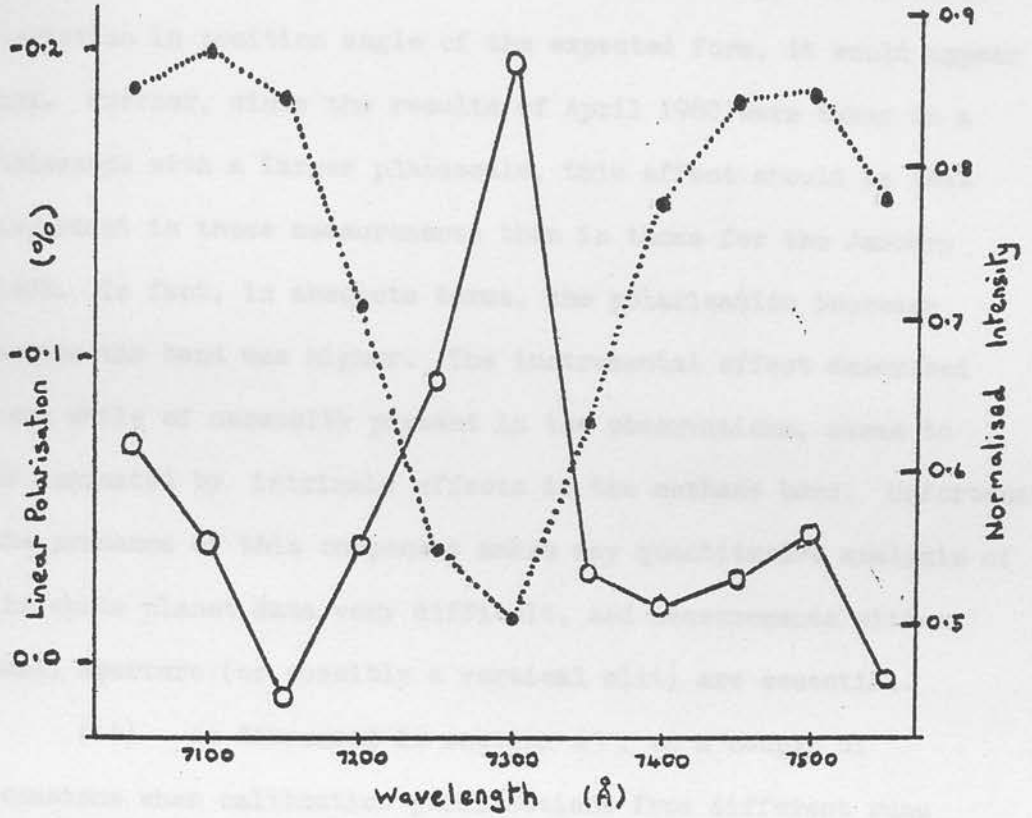

Diagram B1 Possible profile across the methane band. p (Pole) = 1%, p (Limb) = 1.1%. Full line is polarisation; dotted line, intensity.

displaced by $\pm$50 Å respectively before adding. The resulting intensity and polarisation scans are shown as diagram B1. The enhancement in polarisation at the band centre is large, but the effect in the wings less obvious than might be expected. Note that the polarisation profile is hence much narrower than the intensity profile. A position angle variation would only occur if a non-radial component in the polarisation was also present - which is indeed usually the case. Qualitatively such a variation would

look similar to that for the magnitude of the polarisation, since both mirror the intensity profile. Could this instrumental effect be the cause of the observed polarisation enhancement? Since the observed polarisation profile is a little wider rather than narrower than the intensity profile, and there appears to be no variation in position angle of the expected form, it would appear not. Further, since the results of April 1980 were taken on a telescope with a larger platescale, this effect should be less important in these measurements than in those for the January 1978. In fact, in absolute terms, the polarisation increase across the band was higher. The instrumental effect described here while of necessity present in the observations, seems to be dominated by intrinsic effects in the methane band. Unfortunately, the presence of this component makes any quantitative analysis of the whole planet data very difficult, and measurements with a small aperture (or possibly a vertical slit) are essential.

(ii) As discussed in section A3 , on a couple of occasions when calibration polarisations from different runs were compared for nominally identical conditions, differences of many times the calculated errors were found. This effect might change polarisation measures by a few percent of the polarisation, but not more except for far red wavelengths. Since calibration values are low in the far red, a change in the calibration polarisation of a few percent is more important. Errors might arise of up to 6 - 8% of the measured polarisation at wavelengths around 8000 Å. Hence the change in the height of the peak in polarisation at 7250 Å is unlikely to have been caused by this instrumental effect.

(iii) In the section on the analyser (section A2.4) graphs of calibration polarisations were presented. The measures were

obtained on Jupiter. As the present waveplates produce a reduced birefringence at these wavelengths, and there is evidence that the analyser may well be becoming seriously birefringent, any measurement taken at a wavelength greater than 7700 Å must be treated with suspicion.

6(a) Measurements of the polarisation of Saturn

In this section the new observations of Saturn are described. As in the previous section this is then followed by a commentary describing the principal features.

Measurements of Saturn using an aperture large enough to accept the rings as well as the whole disk were made in May 1978 and in January/February 1979. Various telescopes of the University of Arizona were used at Tucson., Arizona. The observing logs for the two sessions are given here as tables B7 and B12. An explanation of the abbreviations used follows as table B8. In May 1978 the dependence of linear and circular polarisation was followed across the methane band at 7250 angstroms. In the 1979 run, two methane bands were studied, the 7250 Å band again and also the 6190 Å band. The broadband wavelength dependence of the circular polarisation was also obtained, from 3500 to 7000 angstroms. Further data were obtained on the 24" telescope of the University of Hawaii in May 1980, over the 7250 Å band. (Table B19).

A composite spectrum of the planet and rings from the University of Arizona runs is given as figure B15. The 7250 Å band is shown in more detail in figure B16 and the 6190 Å band in figure B17. As in the presented spectra of Jupiter, figures B5, 6 etc, the plots are not corrected for instrumental efficiency or atmospheric transmission, nor is the intensity scale intended to relate to any continuum level. The accuracy of the wavelength scale should be comparable to that for Jupiter i.e. $\pm$ 5 Å. The comments on the effective resolution of the data given in section 5(a) are also applicable here. The estimated resolution is 30 - 40 Å.

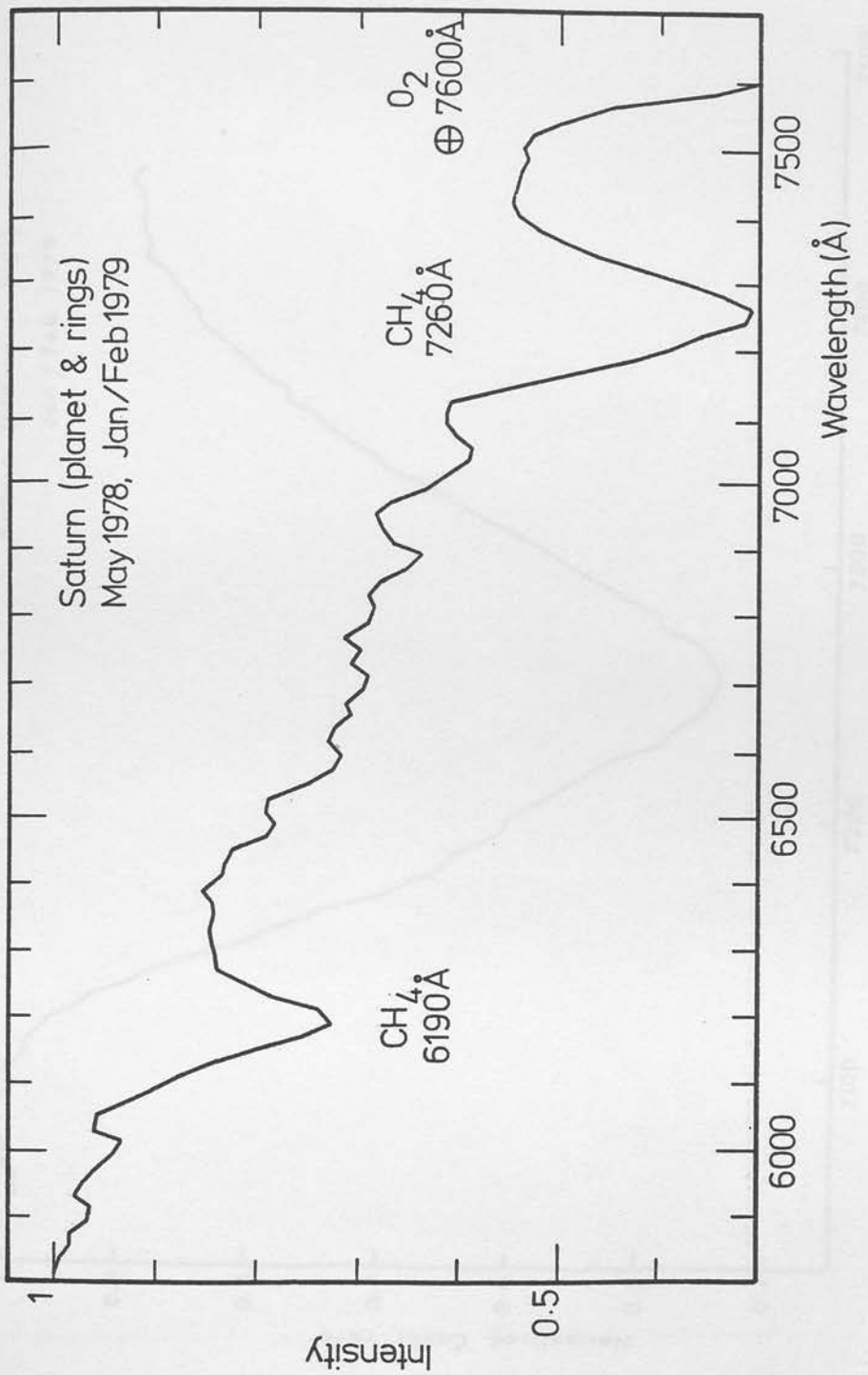

Figure B15: Observed spectrum of Saturn (1978).

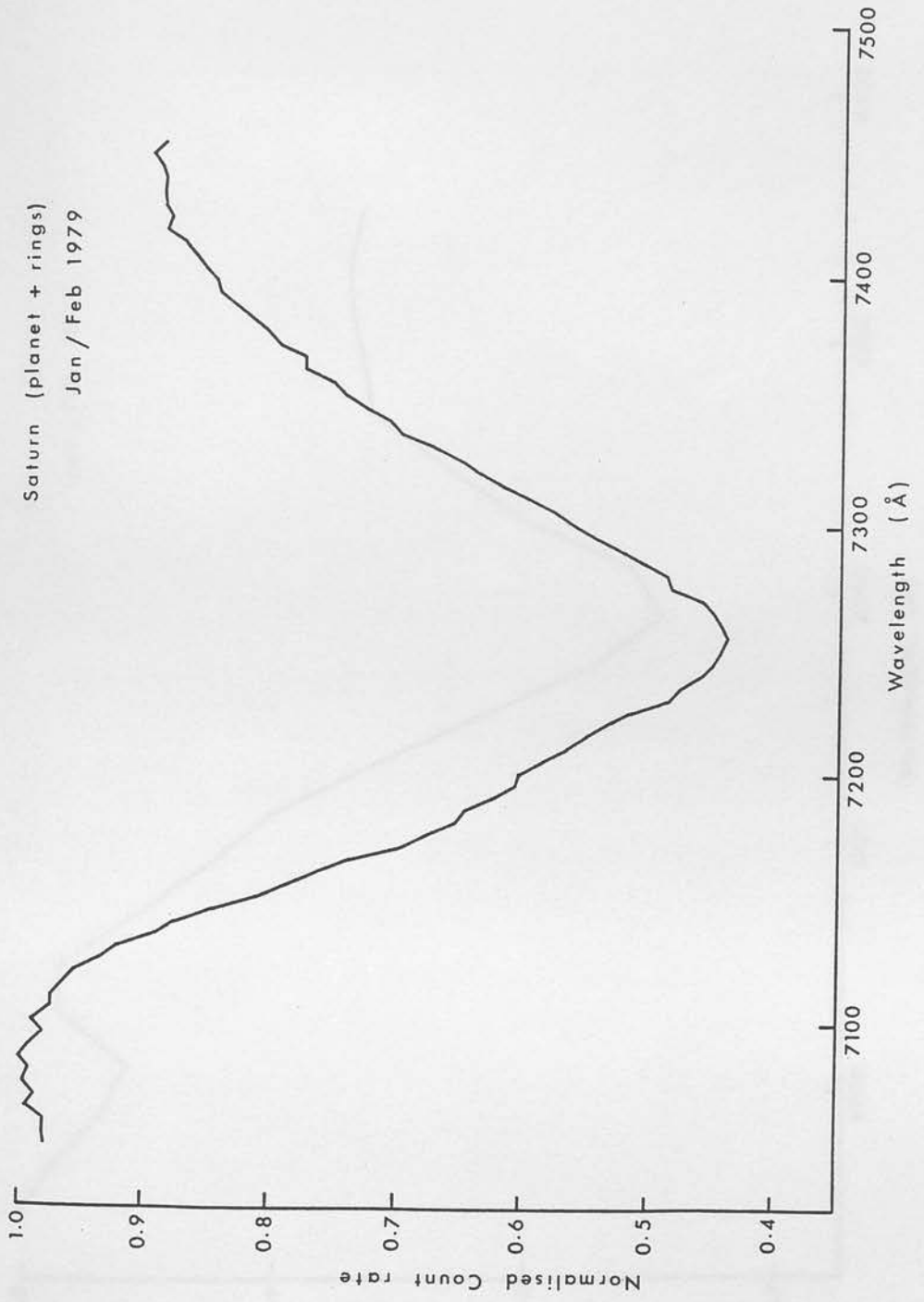

Figure B16: The 7250 Å methane band: the profile on Saturn (1979).

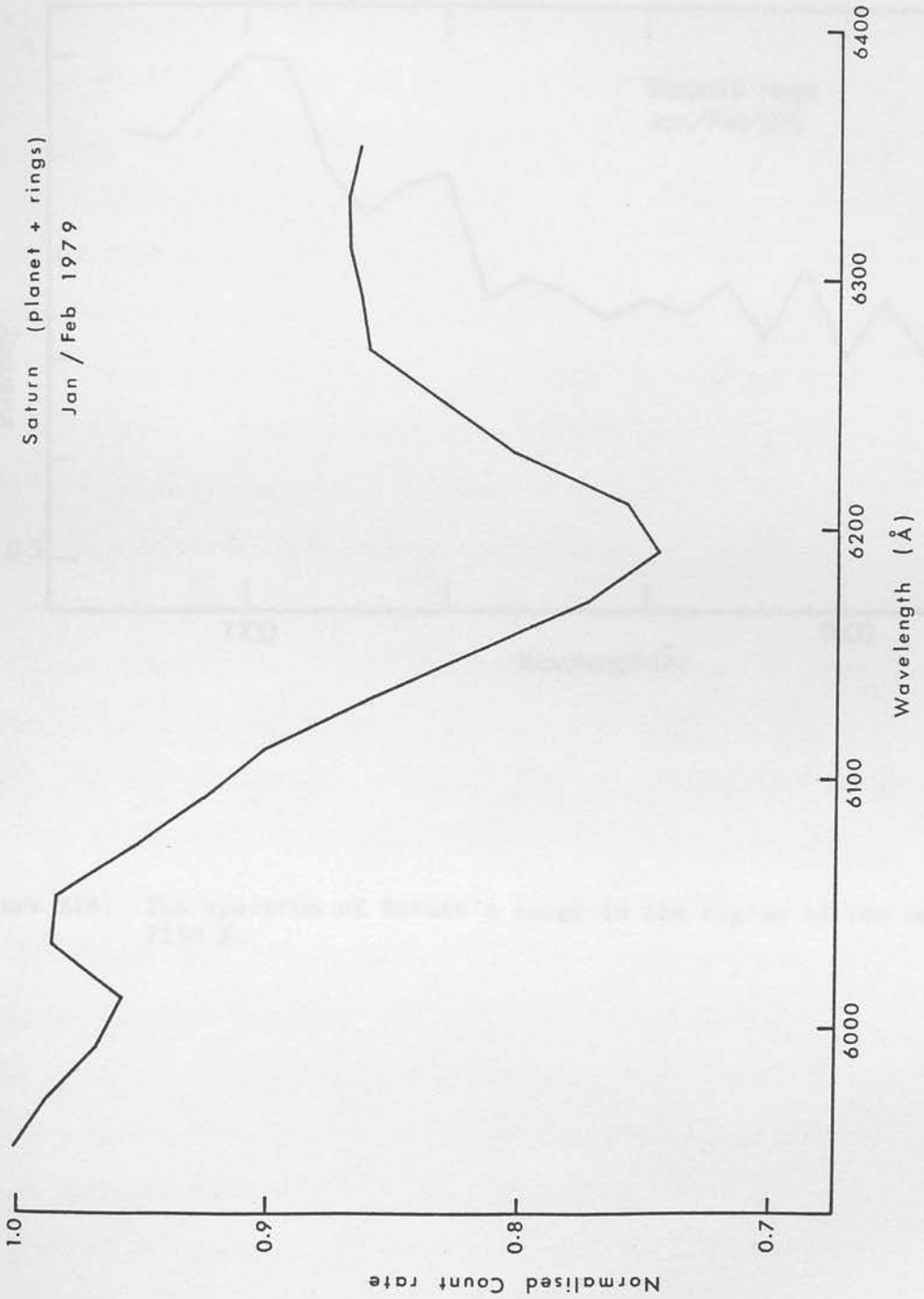

Figure B17: The 6190 Å methane band: the observed profile on Saturn (1979).

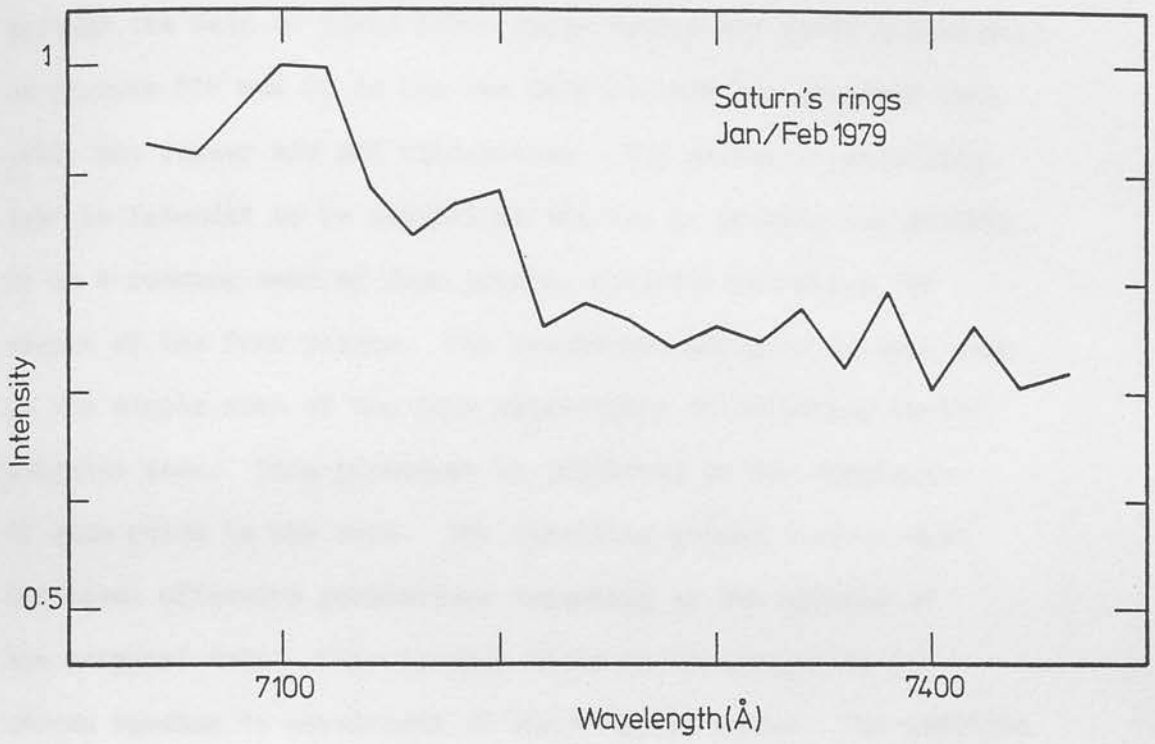

Figure B18: The spectrum of Saturn's rings in the region of the methane band at 7250 Å.

The linear polarisation measurements obtained in 1978 May are presented as table B9. This data has been smoothed to produce the data of table B10. These tables are shown graphically as figures B19 and 20. As the raw data follows the smoothed data well, the former are not illustrated. The method of smoothing used is intended to be helpful to the eye in picking out details. It is a running mean of four points, weighted according the errors of the four points. The wavelength assigned to this mean is the simple mean of the four wavelengths contributing to the weighted mean. This procedure is justified as the resolution of each point is the same. The resulting graphs however have different effective resolutions depending on the spacing of the original data. This is made clear on the graphs by the uneven spacing in wavelength of the weighted means. The position angles have been corrected as described for Jupiter. First of all, position angles are converted from the instrumental system to the equatorial system using observations of interstellar polarisation standards. ζ Ophiuchi (assumed position angle = $126^{\circ}.0$) was used for the 1978 May and 1980 May data and χ Aurigae (assumed position angle = $177^{\circ}.4$) for the 1979 run. The applied correction was redetermined for each telescope. (These values for the interstellar polarisation standards come from SERKOWSKI et al (1975)). Then using the tabulated values of the position angle of the defect of illumination, the angles were corrected to the normal of the scattering plane. The linear polarisation measures for 1979 January/February are presented as tables B13 and B14. Observations taken on 11/12 February required correction for Sky background. The corrected values are shown as table B15. Measurements obtained in 1980 May are displayed in table B20 and plotted in figures B21 and B22.

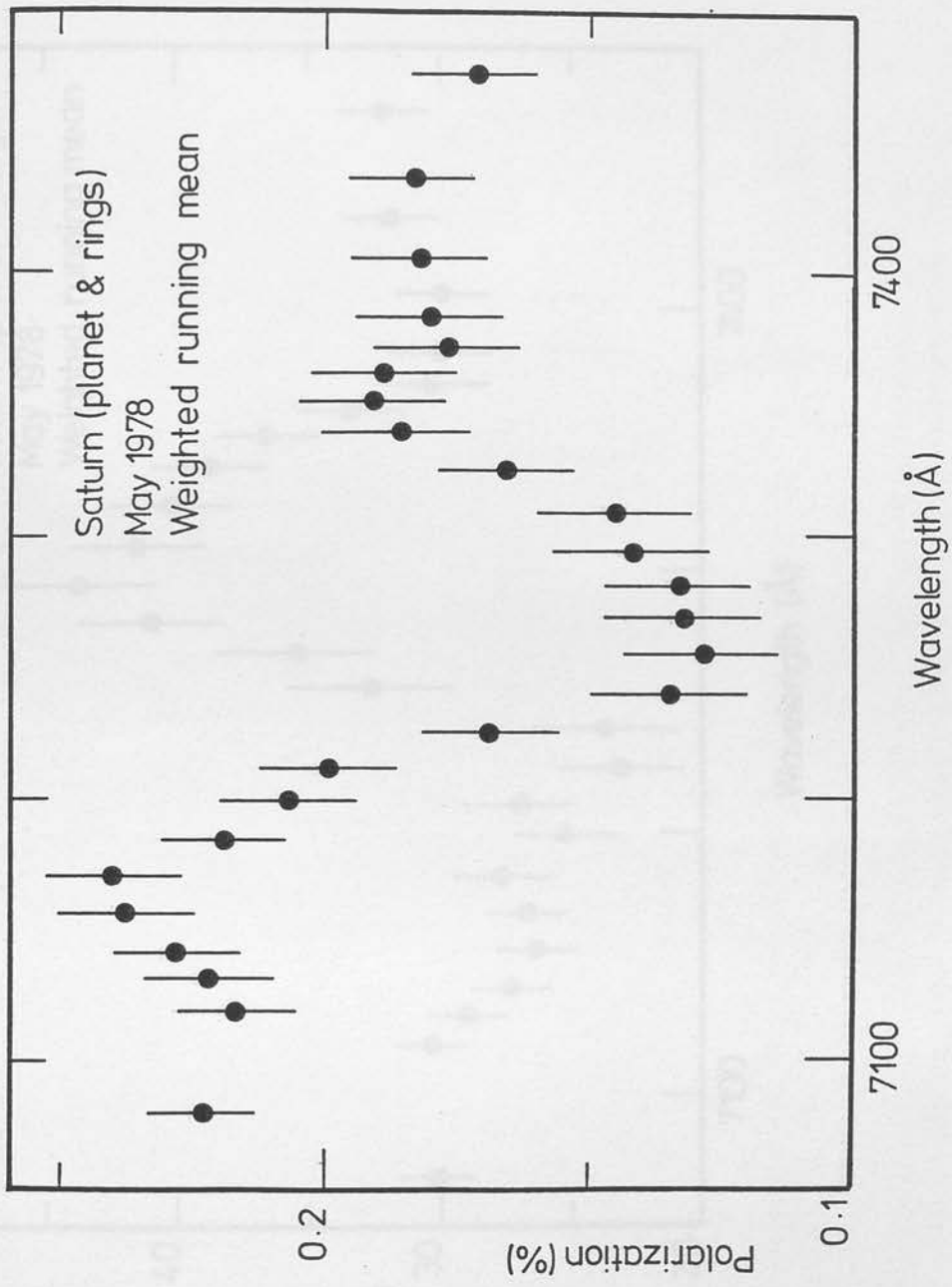

Figure B19: Linear polarisation of Saturn (1978). The points plotted here are weighted running means of four measurements.

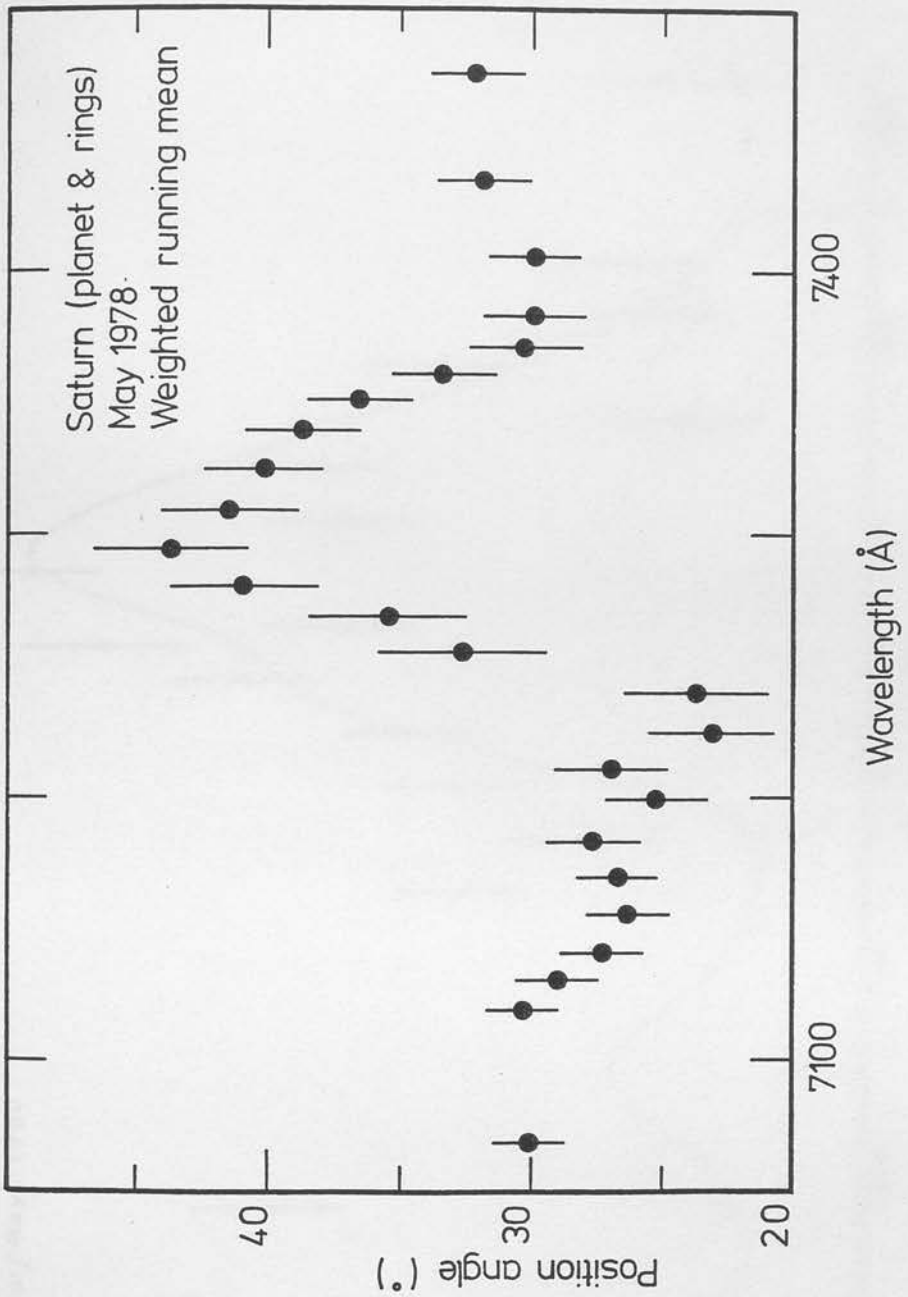

Figure B20: Linear polarisation of Saturn (1978). The position angles plotted here are weighted running means of four measurements.

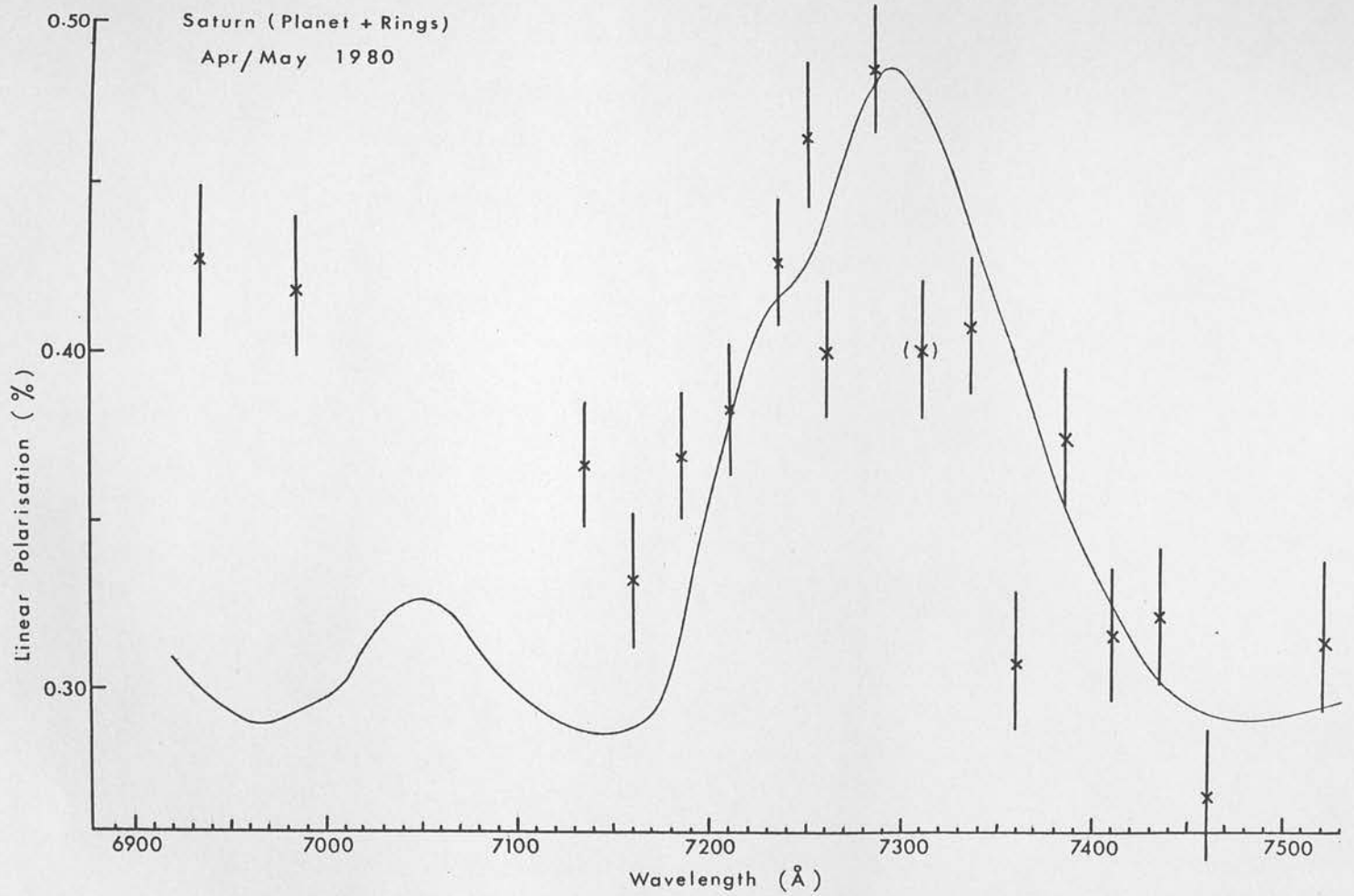

Figure B21: Linear polarisation of Saturn (1980). An inverted intensity profile of the 7250 Å methane band is also shown, scaled to the polarisation measurements.

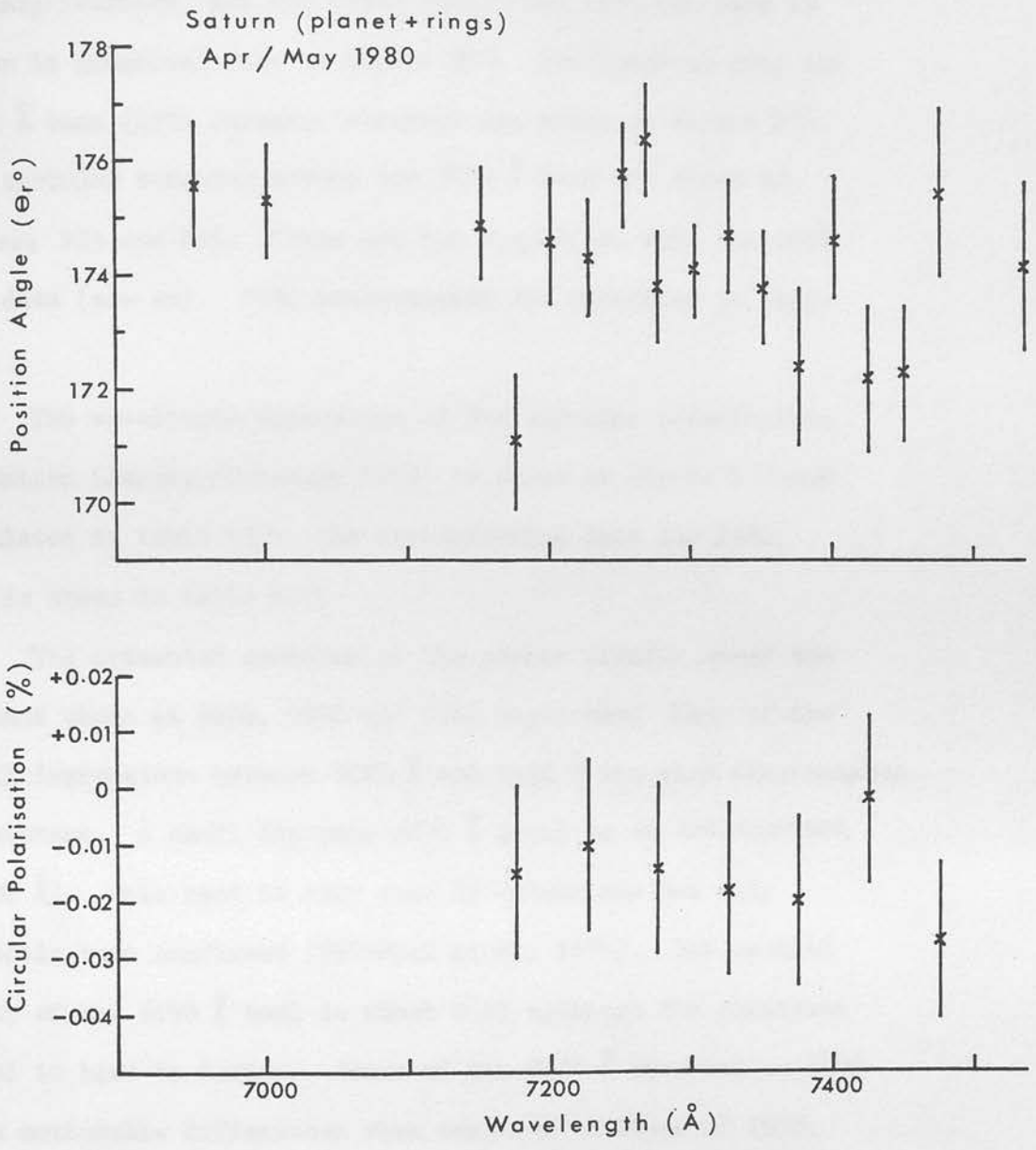

Figure B22: Linear and circular polarisation of Saturn (1980). The position angles of the linear polarisation points plotted in figure B21 are shown, corrected to the normal to the scattering plane. Circular polarisation measurements are also shown.

The circular polarisation measurements across the methane bands are given as tables B11 (1978 May), B16 and B17 (1979 January/February, and B21 (1980 May). The 1978 May data is shown in graphical form as figure B23. The measures over the 6190 Å band (1979 January/February) are shown as figure B24. The circular measures across the 7250 Å band are shown as figures B25 and B26. These are for comparison with the 1978 May data (see on). 1980 measurements are tabulated in table B21.

The wavelength dependence of the circular polarisation of Saturn (January/February 1979) is shown as figure B27 and tabulated in table B18. The corresponding data for 1980, May is shown in table B22.

The presented spectrum of the planet clearly shows the methane bands at 6190, 7050 and 7260 angstroms. Many of the small depressions between 6190 Å and 7050 Å are also attributable to methane. A small dip near 6470 Å could be an ammonia band (6450 Å). This band is very weak in Saturn and has only recently been confirmed (ENGRENAZ et al, 1974). The central depth of the 6190 Å band is about 0.15 although the continuum level is hard to define. Scans of the 7250 Å obtained in 1979 show noticeable differences when compared to those of 1978. The central depth, which lies in the region of 0.50 to 0.55, is at least 5% deeper. The spectrum of the rings is featureless in the region 7100 - 7400 angstroms (figure B18). The apparent structure is probably just photon noise. The spectrum was obtained by centring a small aperture on one of the ansae of the rings. The lack of any depression at 7250 Å suggests that scattered light from Saturn has not seriously affected the

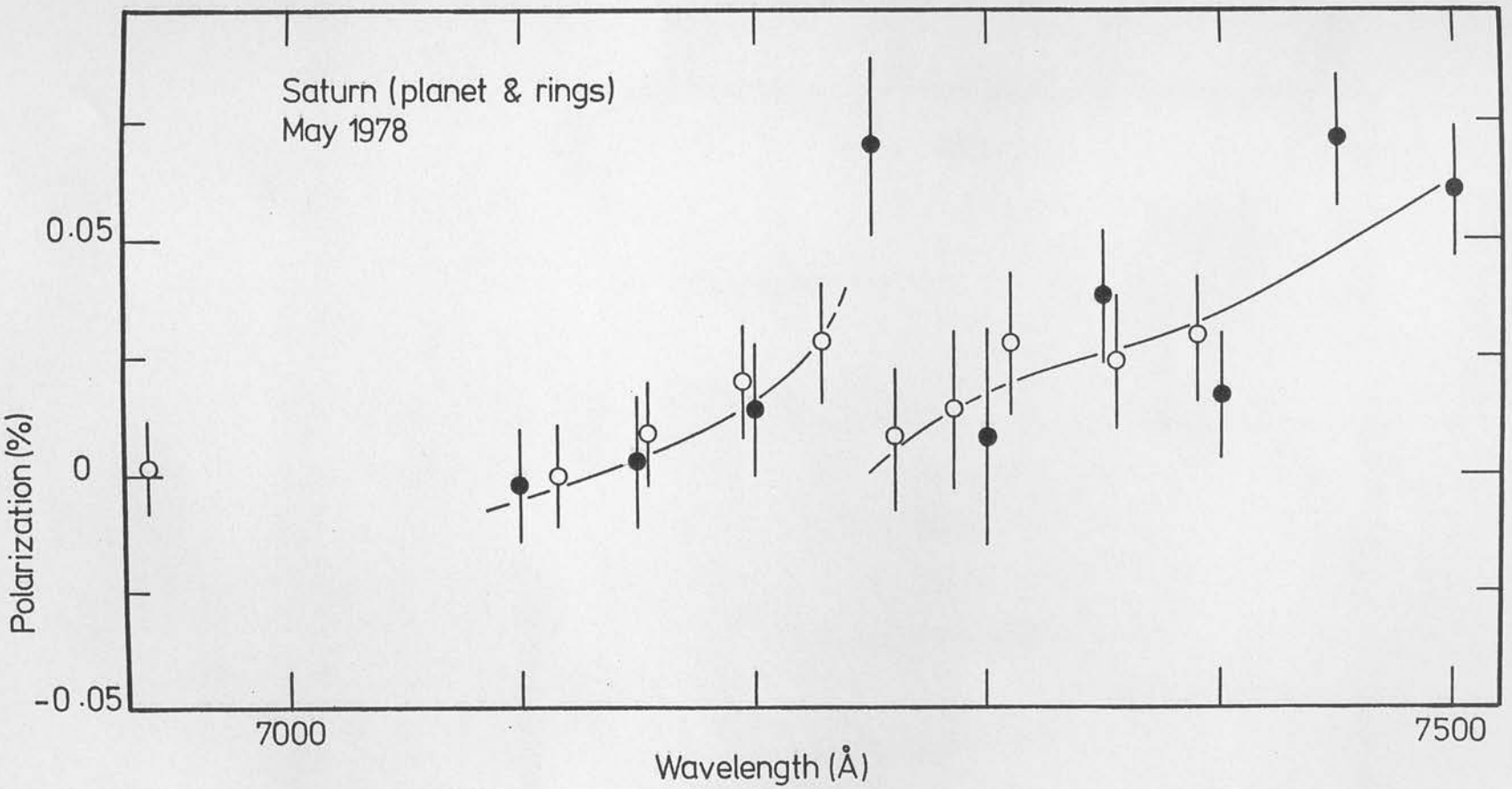

Figure B23: Circular polarisation measurements across the 7250 Å methane band of Saturn (1978). Symbols distinguish measurements made on different nights.

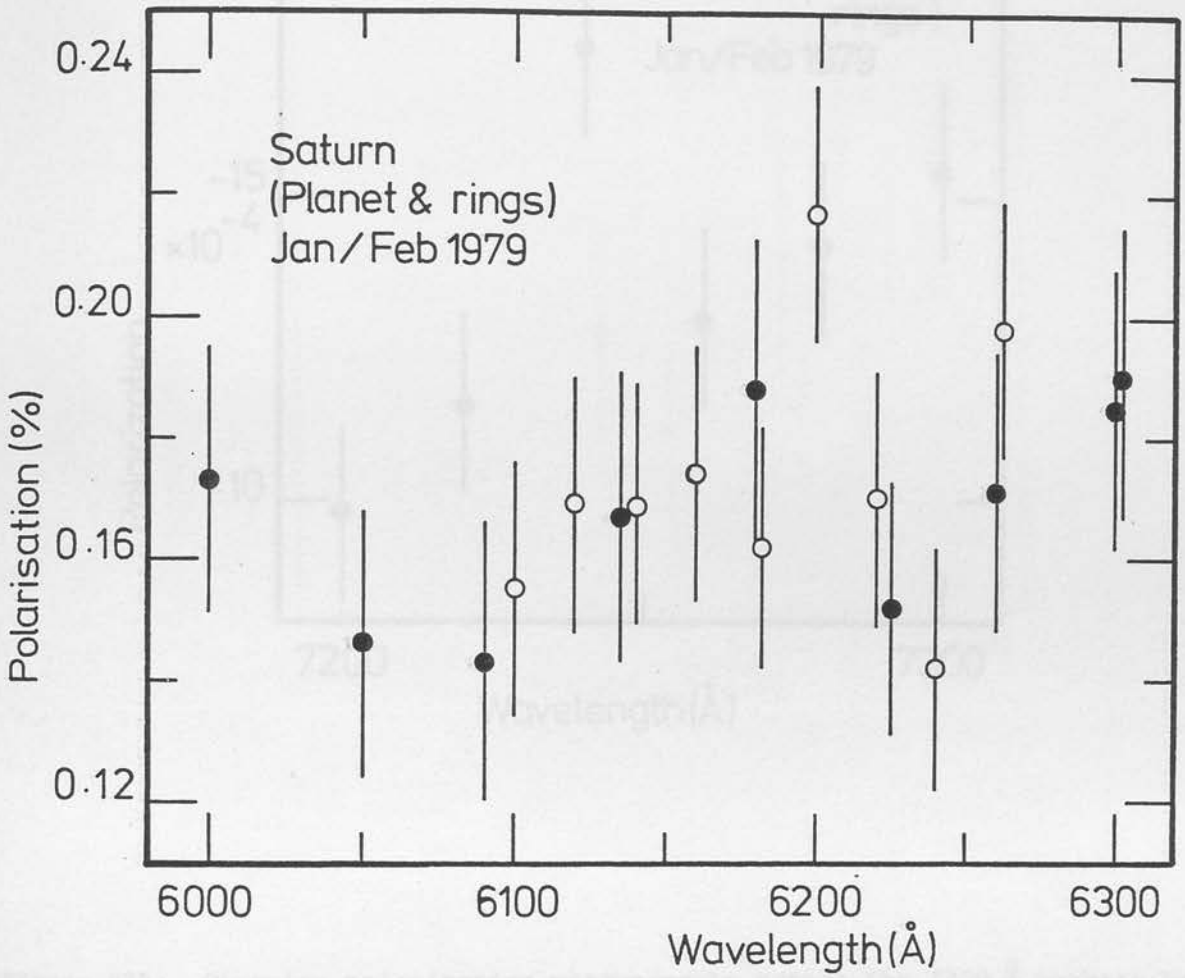

Figure B24: Circular polarisation measurements across the 6190 Å methane band of Saturn (1979). Symbols distinguish measurements made on different nights.

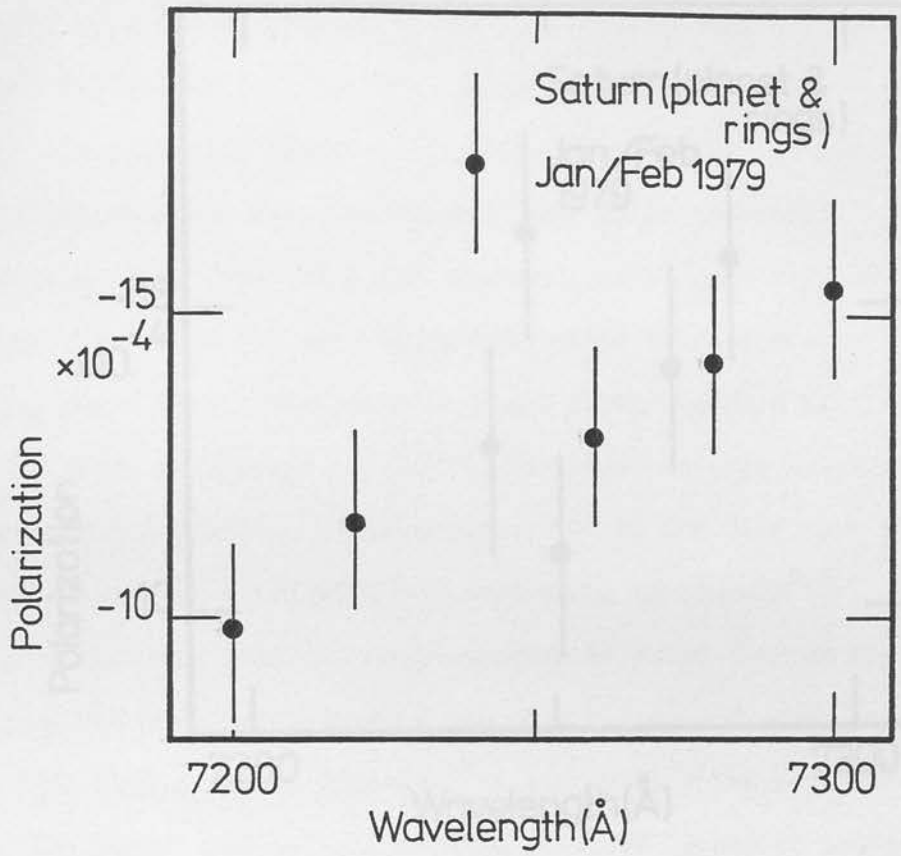

Figure B25: Circular polarisation measurements across the 7250 Å methane band of Saturn (1979). Measurements taken on the night 9/10 February.

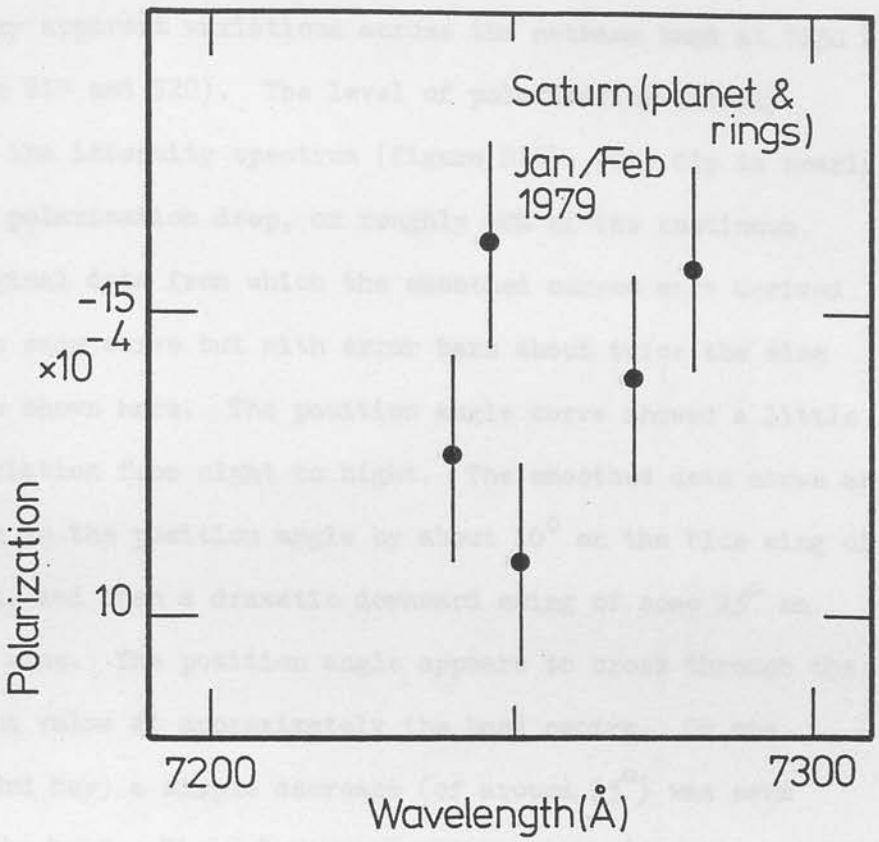

Figure B26: Circular polarisation measurements across the 7250 Å methane band of Saturn (1979). Measurements taken on the night 11/12 February.

spectrum of the rings.

The smoothed curves of the linear polarisation for 1978 May show very apparent variations across the methane band at 7250 Å (figures B19 and B20). The level of polarisation closely mimicks the intensity spectrum (figure B16). The dip is nearly 0.1% in polarisation deep, or roughly 50% of the continuum. The original data from which the smoothed curves were derived show the same curve but with error bars about twice the size of those shown here. The position angle curve showed a little more variation from night to night. The smoothed data shows an increase in the position angle by about 10° on the blue wing of the band, and then a dramatic downward swing of some 25° on the red wing. The position angle appears to cross through the continuum value at approximately the band centre. On one night (3rd May) a simple decrease (of around 15°) was seen across the band. The polarisation is positive (position angles near 180°) but there is also a fairly large amount of information in the other Stokes parameter.

The linear polarisation curves from 1979 January/February are rather different. Little structure corresponding to the band shape is seen in either of the methane bands. Correcting for a polarised Sky background produces little difference in the curves, and no further structure emerges. The behaviour of the position angles from night to night is most curious. On February 9/10, the position angle was $\sim 110^{\circ}$ around the 6190 Å band and very similar (possibly a few degrees less) around the 7250 Å band. Two nights later, on a different telescope, the position angle had increased by 35° at 6190 Å and by 55° at 7250 Å. The next night the position angle at the

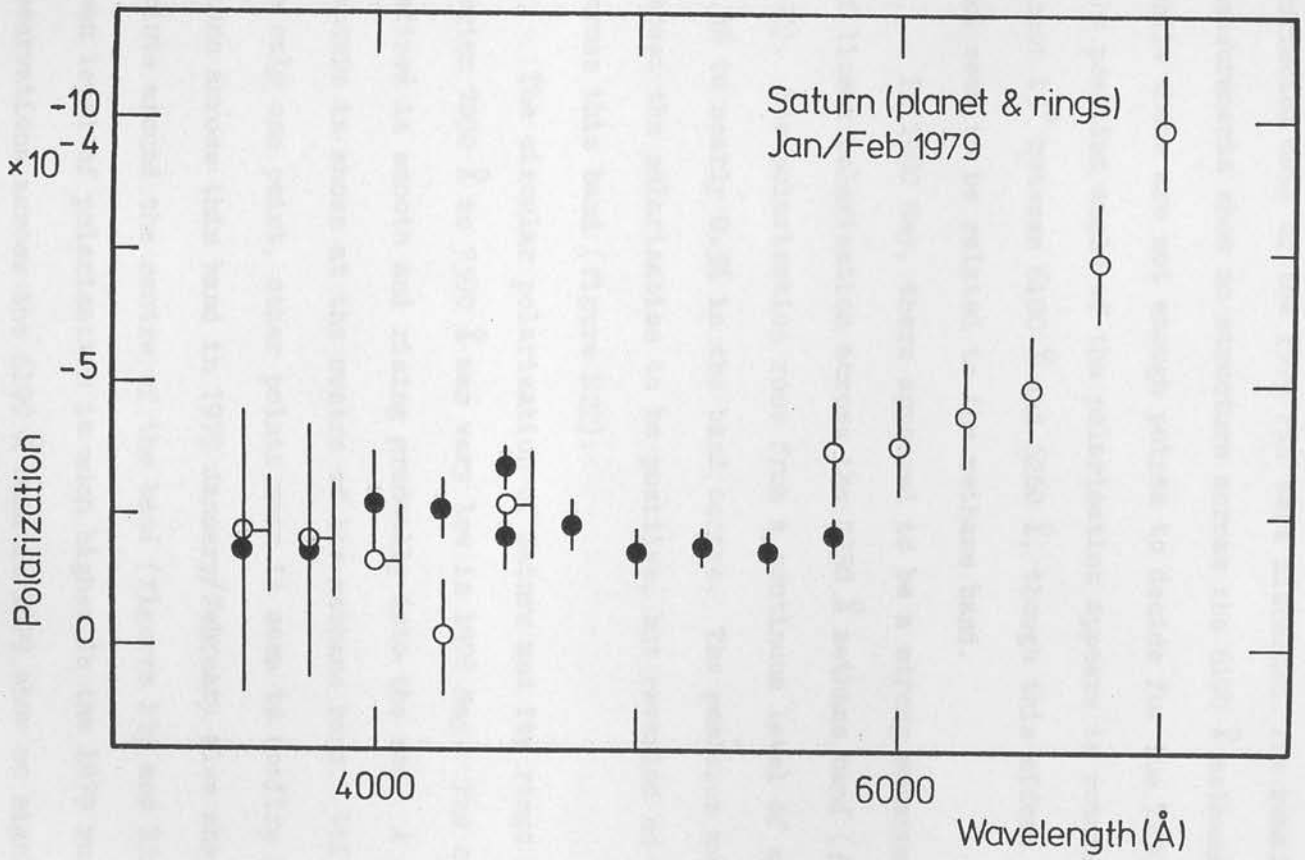

Figure B27: The wavelength dependence of the circular polarisation of Saturn in 1979. Symbols distinguish measurements taken at different phase angles.

7250 Å band had dropped back by 15° to 135°. When corrections for Sky background were applied for the night February 11/12 - the full moon - the position angles only changed by 3 to 4 degrees.

For reasons discussed in Section 6(b), all but the Sky-corrected data of the 1979 run were discarded. The remaining measurements show no structure across the 6190 Å methane band, while there are not enough points to decide for the 7250 Å. The position angle of the polarisation appears to rotate by about 15° between 6100 Å and 6260 Å, though this effect does not seem to be related to the methane band.

In 1980 May, there appeared to be a strong enhancement of linear polarisation across the 7250 Å methane band (figure B21). The polarisation rose from a continuum level of about 0.3% to nearly 0.5% in the band centre. The position angles showed the polarisation to be positive, but revealed no structure across this band (figure B22).

The circular polarisation of Saturn and its rings in the region 7000 Å to 7500 Å was very low in 1978 May. The curve as defined is smooth and rising gradually into the red. A possible feature is shown at the centre of the methane band. While this is only one point, other points near it seem to confirm it. Scans across this band in 1979 January/February also show discordant points around the centre of the band (figures B25 and B26). The mean level of polarisation is much higher in the 1979 runs. Observations across the 6190 Å band in 1979 show no significant structure (figure B24). In 1980, no feature is seen in the 7250 Å band (figure B22).

The 'continuum' circular polarisation of Saturn, obtained in January/February 1979, shows a roughly wavelength independant value of - 0.02% from 3500 Å to 5800 Å. The polarisation then begins to rise rapidly, reaching - 0.05% by 6500 Å and - 0.10% by 7000 Å (figure B 27). The observations in the methane bands at 6190 Å and 7250 Å fit in well with the general curve displayed in figure B 27. The continuum level has reached about - 0.15% by 7250 Å.

In 1980 the mean level of circular polarisation in the red was again low ($\sim$ 0.01%) possibly beginning to rise at 7800 Å.

6(b) Discussion of the data presented

The instrumental effects discussed in Section 5(b) on Jupiter are also important here. The finite size of the planetary disc should be of less consequence for Saturn. However, the effective resolution this imposes on the observations should be borne in mind when studying graphs claiming to show very sharp features.

The circular polarisation of Saturn found in 1979 January/February was very large, and growing very rapidly into the red. The constancy of the degree of polarisation from 3500 Å to 5800 Å might suggest that this represented an instrumental polarisation. It will be seen in other parts of this thesis that our instrumental polarisation for circular is certainly below this, though we have no other instrumental polarisation measures of sufficient accuracy for this particular observing run to abolish the suggestion completly. The important feature

is the polarisation at longer wavelengths. Notice that measurements of circular polarisation taken throughout the run are reasonably consistant on the level of circular polarisation in the red (i.e. across the methane bands) and so we can rule out any effect of scattered moonlight. We have measures of the circular polarisation of Capella at 7860 angstroms obtained on this observing run. While the errors in the measurements are quite large, their level (at around - 0.04 $\pm$ 0.02%) is much lower than the polarisation found on Saturn. The linear polarisation of the planet is quite small and any linear-to-circular conversion could not produce such a high degree of circular polarisation. In summary, while we cannot completely rule out an instrumental origin for the rise in the degree of circular polarisation of the reflected light from Saturn in the red, the evidence that is available argues against such an explanation.

Both graphs of position angles from the 1979 January/ February run show large night-to-night variations. Two different telescopes were used to obtain this data, and it happens that the correction applied to the position angles between the telescopes was exactly 30°. This is determined by the different geometry of the bolt holes used to secure the instrument to the two telescopes. The sense of the correction was to separate the instrumental position angles which were around 80° to 90°. The data for observations around 6100 Å would be nearly consistent if the correction were NOT applied. At 7250 Å, too, the various nights would be in better agreement. This coincidence is disturbing. If one of the two waveplates used in the measurement were tilted, or in some other way defective, the degree of polarisation would also be affected. In fact these are consistent to better than 10%. No other observations taken on this run show

a preference for this position angle or any variability. Two possibilities remain. Firstly that the finite size of the planetary disc is somehow affecting the measurement. Secondly, that sky corrections were necessary for the nights February 9/10 and 12/13. A couple of field dependant effects arising in the modulator have been discussed previously (Section A2.3). Neither telescope used here was fast enough to cause light to spill over the edge of the modulator. If the dependence of polarisation across the disk is also taken into account, the field variation in the retardance of the modulator could produce an effect very similar to that observed. However, the effect shown is larger than could be caused by the modulator. Field effects in the waveplates are more likely to be patchy rather than some systematic bias. The most marked field effect is that caused by the chromatic Fabry optics, and discussed previously (Section A2.6). The exact effect caused would be dependant upon the precise location of the planet in the aperture and upon the original lining up of the photocathode with the exit slit of the spectrometer. This lining up is redetermined whenever the instrument is set up on a different telescope. The size of any effect caused by this mechanism would be difficult to determine and, in any case, might well be expected to affect the degree of polarisation measured. In conclusion, field effects in the instrument cannot be ruled out, but it is difficult to see how a deviation of the size observed could be produced.

No sky polarisation measurements were made near Saturn on the nights of February 9/10 and 12/13. Checks on the intensity of the sky background near other objects observed on these nights (e.g. Capella, Sirius) seemed to indicate that correction

was not necessary. However, the Moon was rather close to Saturn during the period in question. The position angle of the polarised sky background on 11/12 February was around 5°. This is about 65° from the direction of the arc joining the Moon and Saturn and roughly the angle to be expected (c.f. HANNEMANN and RASCHKLE, 1974). If we conclude that the variations in position angle are due to scattered moonlight, the data for the nights 9/10 and 12/13 February must be discarded for the present purpose. A sky component large enough to cause 30° shifts in position angle must swamp the small effects we are seeking. The above explanation would imply that the rough agreement of position angle between the two telescopes was purely coincidental. There are two remaining problems. The degree of polarisation remains roughly constant and the actual correction for February 11/12 is quite small. In fact the scatter of points for the degree of polarisation could well hide a variation of the size required. Could the sky polarisation measurement be an underestimate, affected by light from Saturn or by scattered light in the instrument? The measured polarisation was about 0.1%. Reflections in the instrument would tend to raise the level of polarisation. With the largest aperture in use, light passing through the edges of the aperture has not passed through the modulator. This would hence dilute the measured polarisation. However only about 3% of the light would not have passed through the modulator, and, at these wavelengths, would in any case be attenuated by the Fabry optics. Since the sky measure was taken sufficiently far from the planet to avoid light from Saturn, it seems the sky measurement was indeed valid, and that the date of February 11/12 stands.

In conclusion, the most plausible instrumental cause of the night-to-night variation of position angle was the failure

to subtract sky-background. If this is accepted, linear polarisation data of 9/10 and 12/13 February must be discarded. Circular polarisation measurements would be to all intents and purposes unaffected by a linearly polarised sky background. The possibility that the polarisation of the planet had actually changed is dealt with later.

7. The Spatial averaging of polarisation across the planetary disc

The degree of linear polarisation detected in the integrated discs of Jupiter and Saturn is relatively small compared with the large local polarisations seen at the poles and at the East and West limbs of the planet. The non-zero polarisation seen at zero phase angle is accounted for by the incomplete cancellation of the strong polarisation of the poles by that of the limbs. The stronger pole is the one inclined towards the observer. Now if the strength of the methane band decreases towards the limbs, then light at the centre of the band will come preferentially from the limbs. Since the light from the centre of the disc is relatively unpolarised, the detected linear polarisation will appear to rise within the band when we look at the whole planet. Before attributing the observed rise in polarisation across the 7250 Å methane band to the properties of the Jovian or Saturnian atmospheres, we must therefore show that spatial averaging over the planetary disc cannot account for the observed dependences of polarisation with wavelength.

The strengths of the methane bands of Jupiter as measured by either their equivalent widths or central depths show little variation with position on the planetary disc. TEIFEL' (1976) summarises mainly photographic observations to conclude:

(a) In the equatorial band of Jupiter, molecular absorption decreases in strength towards the limb by 10-20%.

(b) To the North and South of the equator, absorption in weak bands (e.g. methane at 7050 Å, ammonia at 6450 Å) decreases with latitude; in the medium (e.g. methane at 6190 Å) and strong (e.g. methane at 7250 Å) bands

absorption increases in the latitude range 40-60°, but not more than 5-7%, sharply decreasing close to the poles.

(c) Differences in absorption between the light and dark cloud bands of Jupiter, according to measurements by various authors, are contradictory in character, but they are most likely absent or occur at the level of the errors of measurement.

(d) Time variations of absorption in the central region of the disc of Jupiter are noted by the majority of investigators. However, in the absence of systematic observations and control, it is impossible to determine exactly how much of the variation is real and how much can be attributed to methodological error.

Recently, WEST (1979a) has presented new data on the absolute reflectivity of Jupiter in methane bands and in nearby continua, obtained with a CCD camera. These results do not appear to confirm the 10-20% decline in the methane band strengths near the limbs. In passing we note a recent interesting paper that to some extent answers Teifel's point (d) (COCHRAN & COCHRAN, 1980).

In the light of the above information, it does not seem likely that the proposed mechanism of spatial averaging will produce the observed effect. A simple calculation confirms this. We suppose the centre of the disc (out to 0.8 R) to be unpolarised and to have a methane band of constant strength, while the remaining area contributes the observed polarisation and has a methane band of central depth 20% less than that of the centre of the disc. Mean intensities for the two regions were then derived from the 7500 Å continuum scans of WEST (1979). Call the residual polarisation

of the outer part of the disc p_o and the observed polarisation of the integrated disc p. With this very simple model we find that $p = 0.21\ p_o$ in the continuum and $p = 0.24\ p_o$ in the centre of the band, i.e. an enhancement of ~15% is seen in the polarisation at the centre of the band. This situation corresponds to small phase angles. If a phase dependant component of polarisation is present, the centre of the disc will also be polarised, and any variation in polarisation seen across the band in the integrated disc will be even smaller. In summary, this mechanism will not enhance the polarisation across an absorption band by more than an amount roughly equal to the proportion by which the strength of that band decreases towards the limb.

In Saturn, the pattern of polarisation over the visible disc is again radial (HALL & RILEY, 1974), becoming tangential at wavelengths greater than ~0.9μ. (BUGAENKO & GALKIN, 1973; KEMP et al 1978). The distribution in the strength of the methane bands and the limb darkening are however somewhat different (TEIFEL', 1976). Equatorial scans of the methane bands may show a slight decline in strength towards the limb (TEIFEL, 1974, but see TEIFEL et al 1971). The meridian scans show more obvious variations. The least amount of absorption is observed in the light equatorial belt and it increases to a maximum at moderate latitudes before declining again at the poles. These variations are certainly no greater than 50% and although this implies that any variation in polarisation over a band cannot be any larger, the distribution of these variations must put even lower limits on any polarisation effects on Saturn.

8. Interpretation of the polarimetry

Having eliminated in previous sections any possible instrumental effect, including that of spatial averaging across the planetary disc, we conclude that a real enhancement of polarisation is occurring across the 7250 Å methane band in both Jupiter and Saturn. This increase is most probably caused by the relatively greater contribution of the proportion of light from low-order scattering than in the continuum. In the continuum, multiple scattering results in an almost completely depolarised flux from the planet as a whole, except for a small phase-dependant polarisation, and local effects. Within a strong molecular band we observe the upper layers of the atmosphere, and light scattered back to an observer on Earth will have undergone only a few scattering encounters. For aerosols of the size thought to constitute the clouds of the major planets, low order scattering will imply relatively large polarisations. Hence, within the band, the linear polarisation is not destroyed by multiple scattering and the overall polarisation rises. With this mechanism in mind we look in detail at the observations, firstly of Jupiter.

8.1 Jupiter

In January 1978, Jupiter was observed at phase angle $i \sim 6.^{\circ}5$. In 1971, MOROZHENKO (1973) found the linear polarisation of the whole disc at this phase angle to be small and negative - about $(-0.05 \pm 0.05)\%$. Further, the polarisation was seen to become more negative towards the red. These results are in accord with the 1978 January data. WOLSTENCROFT & SMITH (1979) do not notice this increasing continuum polarisation into the infrared and associate

all of the increase with the 7920 Å ammonia band. The large increase in polarisation as compared with the depth of this line would then imply significantly different scale heights for methane and ammonia in the Jovian atmosphere, with the ammonia lying appreciably higher than the methane. We avoid this conclusion by associating some of the polarisation with the continuum. Morozhenko also found the polarisation to be varying with phase roughly linearly at about 0.07% per degree of phase (at this phase angle). The presented data cover a phase interval of $0^{\circ}.7$, and the apparent noise in the height of the polarisation peak is attributed to this phase effect.

Although laboratory measurements of the methane band at 7250 Å show structure in the centre of the band - specifically a double minimum with intensity rising by perhaps 8-10% between them (GIVER, 1978) it is unlikely (though possible) that this is related to the qualitatively similar structure seen in polarisation. The effect in polarisation is quite large, being 10-20% of the amplitude, and the low resolution of these measurements might be expected to smooth out any such effects. A 'shoulder' was noticed in the linear polarisation spectrum in the region 6950 - 7125 Å. This could be associated with the weak methane absorption at 7000 Å. However, we note that the central depth of this band is only 10% of that of the 7250 Å band, while the suggested associated polarisation enhancement is around 20%. If the mechanism outlined above was operative, we would not expect a weak band to show a larger proportional increase in polarisation than a strong band. Of course, the errors on these polarisation measurements are quite large in comparison to the amplitudes we are considering. Similarly errors are quite large in the region $\sim$7700 Å and no definite conclusion as to the existence of

structure related to the ammonia band can be made.

The minimum in position angle seen around 8000 Å could also be associated with the ammonia band, but is more likely to be an instrumental artifact related to the onset of birefringence in HNP'B polaroid. Any dispersion curve shaped feature in position angle might also be explained as an instrumental effect, as described below for the May 1978 data on Saturn.

The slow increase seen in measurements of the circular polarisation of Jupiter longward of 7700 Å is likely to be of instrumental origin (but see discussion of 1979 January data on Saturn). The dispersion shape shown at 7250 Å in circular polarisation is curious. The displacements necessary to correct data from different nights seem rather large to be connected with the rotation of the planet. KEMP et al (1971) studied Jupiter continuously for a five hour period and found no dependance of the circular polarisation on the rotation of Jupiter on its axis. The feature across the band is significant at the 3σ level at least, though the sharp feature seen at 7370 Å is probably spurious. We note that it is only 10 Å across while the effective resolution of these measurements is around 75 Å. Comparing the features in linear and circular polarisation at 7250 Å, one is reminded of the classical absorption/dispersion curves. Briefly, if an absorption feature (such as a spectral line) occurs at a particular wavelength, a dispersion curve-shaped dependence of the refractive index on wavelength is also seen. The two quantities are coupled through the Kramers-Kronig relations which are derived from very general considerations (see e.g. LIPSON & LIPSON, 1969). Further, since dichroism is merely the effect of different absorptivities for orthogonal states of polarised light, any feature in dichroism will be accompanied

by a dispersion curve-shaped feature in birefringence. The observed interstellar circular polarisation is thought to arise through this mechanism (MARTIN, 1975). However, the linear polarisation seen across the methane band is due to scattering in an optically thick atmosphere and not dichroism. It is not clear therefore that the Kramers-Kronig relations are useful in this case.

When light is totally internally reflected within, for example, an aerosol, a phase difference is introduced between the orthogonally polarised components parallel to and perpendicular to the local normal. This phase difference is given by the Fresnel relations:

$$(\text{Phase})_{\perp} = \mp 2 \tan^{-1} \frac{\mu\beta}{\cos\hat{\imath}} \qquad (\text{Phase})_{\parallel} = \pi \mp 2 \tan^{-1} \frac{\beta}{\mu \cos\hat{\imath}}$$

where: $\hat{\imath}$ = angle of incident light (to the surface normal)

$\hat{r}$ = angle of refracted ray (to the surface normal)

μ = relative refractive indix

and $\cos\hat{r} = \pm i\beta$ where β is real and positive, noting that $\cos\hat{r}$ must be complex for the case of total internal reflection.

Clearly then, any feature in the refractive index will produce a feature in the birefringence, and hence possibly in the circular polarisation. Such a feature would be associated with an absorption centred at or around 7250 Å. The obvious choice would then be to attribute the observed structure in the circular polarisation to methane aerosols (either liquid or solid). At the (partial) pressures of methane in the Jovian atmosphere, such aerosols would only form at a temperature of around $\sim$ 60K (PRINN & LEWIS, 1973). At such temperatures the aerosols would be solid, as the triple point of methane is at around 90K.

However present models of the Jovian atmosphere show temperatures always in excess of ~150K (e.g. TEIFEL, 1976). To allow the methane to condense (to a liquid at these temperatures) would require higher methane partial pressures. In passing we note that since methane is not a polar molecule, the spectra of the solid and liquid forms will be similar to that of the gas (e.g. RAMAPRASAD et al, 1978). Since the existence of methane aerosols is problematical, we consider what other compounds which have absorption in this region might exist as aerosols. We note that this methane band is an overtone frequency of fundamentals which lie at wavelengths $>3\mu$. There are four of these, at wavenumbers 2914, 1526, 3020 and 1306 cm^{-1} respectively (HERTZBERG, 1945), and they arise from "bond-stretching" and "bond-bending" vibrations of the -C-H bonds. As such any other organic molecule with carbon-hydrogen bonds in similar "molecular surroundings" might also be expected to produce absorption lines at similar wavelengths to those of methane. More specifically, compounds containing the methyl (CH_3-) group, might, if present in sufficient quantity, form an overtone absorption at around 7250 Å. The spectrum of ethane for example (CH_3-CH_3) has a number of absorptions near those of methane. Clearly the choice of compound is more limited by the required abundances rather than by the necessity of having a methyl group. Indeed we note that water vapour shows broad strong absorption at these wavelengths (7230 Å, HERTZBERG, 1945) in the Earth's atmosphere - the 'a' band - and H_2O is plentiful in the lower clouds of Jupiter though, admittedly, in the form of ice crystals. One would then need to call on convective processes to bring these up to the region of the atmosphere being probed by polarimetry.

Examination of the structure in circular polarisation shows it changing sign very close to the centre of the methane band. The problem then in using any other molecule besides methane is in this close correspondence. Problems also arise in the required abundances of these other materials, except possibly water. A further point to note is the relative size of the features in linear and circular polarisation. We find $q \sim p^2$, suggesting that linear and circular features are linked. For the most elegant explanation of the circular polarisation, and one in which the above relation arises naturally, we must return to the Fresnel equations quoted previously. We note that these involved μ - the relative refractive index i.e. of the denser medium with respect to the more rarified one. Previously we had considered a feature in the refractive index of the aerosol, but it is clear that a change in the refractive index of the medium outside the aerosol would be equivalent. However, such a feature in the refractive index of the medium must occur, by association (through Kramers-Krönig) with the strong methane absorption. By illuminating the aerosols with linearly polarised light, circular polarisation is produced. It remains to be seen whether the methane absorption can produce a large enough change in the refractive index of the medium, given that the concentration of methane in the atmosphere is only around 0.3%. Clearly detailed modelling of this mechanism should await the confirmation of this structure in circular polarisation in spatially resolved studies of the planet.

The 1980 May data confirm the rise in polarisation within the 7250 Å methane band. Since these measurements were taken with a telescope of significantly different platescale, possible

instrumental effects dependant upon this factor cannot be dominant. In 1980, the enhancement in the linear polarisation was found to be greater than that found previously. Continuum polarisation is also larger at this phase angle ($9^{\circ}.5$). Again the measured continuum polarisation agrees roughly with that found by MOROZHENKO (1973), and indeed a feature of this size (0.2%) might well have been detected by him had he used more filters in this part of the spectrum. The polarisation is again negative with little information in the other Stokes parameter.

No structure was found in the 6190 Å band in either linear or circular polarisation. While this result for circular polarisation is not surprising, the absence of an effect in the linear perhaps is. This band has a residual intensity at its centre of around 0.80, compared with 0.45 for the 7250 Å line. The lack of any structure in the polarisation $\geqslant$ 0.04% would suggest then that the linear polarisation seen in the 7250 Å band arises at a high level in the atmosphere, i.e. at a level not significantly contributing to the 6190 Å line. Both lines however are formed chiefly within the upper ammonia cloud - TEIFEL (1976) finds the optical depth of the gas above this cloud to be 0.03 in the 6190 Å band and 0.07 in the 7250 Å band. The only published work on the interpretation of polarisation profiles such as these - namely FYMAT (1974) - serves merely to show how model dependant the quantitative enhancement in polarisation is. Consider Fymat's figure 7, where integrated (i.e. over the planetary disc) spectropolarimetry of a line in a totally Rayleigh scattering atmosphere is presented for a phase angle of $99^{\circ}.2$. The resultant polarisation seen at the centre of a line 70% deep is about five times greater than that seen at the centre of a

line 20% deep. It seems therefore that we cannot make deductions about the relative enhancements seen in different lines without detailed modelling. Such modelling is outside the scope of this Thesis, and in any case would only be worthwhile if data existed for a number of bands and small areas of the planetary disc.

No effect was seen across the 6450 Å ammonia band, though a slight slope in the linear polarisation dependance with wavelength is present. Neither do the circular polarisation measures reveal any structure. Since the aerosols of the clouds of Jupiter are thought to be of solid ammonia there was the possibility of finding a dispersion-shaped feature in circular polarisation associated with the band. However the band is not strong, and in any case the effect may well cancel when integrating across the planetary disc. In order to detect any effect, a portion of the disc only must be observed, and a stronger band further into the infrared (e.g. the 1.1μ band) must be used.

Recently BURIEZ et al (1979) have discussed information that can be derived from spectropolarimetry of the gaseous planets. By generalising the concepts of the equivalent width of a line to the other Stokes parameters, "curves of growth" for I, Q, U and V can be constructed, the most informative of which are those of I and Q. Since the "Q" lines are sounding a level in the atmosphere near to the cloud top, and since one may derive a (rotational) temperature from the slope of the curve of growth, one may hence locate more accurately the cloud top height (given a temperature model of the atmosphere). Using the derived rotational temperature one may then derive scale-height ratios for the gas-to-cloud particles (using strong and weak lines of a particular molecular species) and for gas-to-gas using lines

of the respective species. It should be noted that the above paper was written with the expectation of obtaining infrared measurements. By studying multiplets, curves of growth as described can be constructed. However in the visible we have only a few bands of vastly differing strength, and the theory developed by Buriez et al is not useful in the interpretation of the data of sections B5 and B6.

8.2 Saturn

We shall find that the qualitative interpretation of the Saturn data is rather similar to that of Jupiter. We have seen though that larger variations appear to be occurring in the polarisation of this planet.

The variation of linear polarisation with wavelength across the 7250 Å band is very clear in polarisation measurements obtained in 1978 May. Unfortunately, this variation is unlikely to be related to the properties of the Saturnian atmosphere. These results were obtained with an aperture that included the rings as well as the whole planet. Since the spectrum of the rings does not show the absorption band at 7250 Å, the contribution of light from the rings will become more important in the centre of the band. As the polarisation of the rings is also different, a variation will be observed in their combined linear polarisation. If we use figures for the polarisation of the rings from DOLLFUS (1979), we may derive the relative contributions of Saturn and its rings to the light of the combined system.

Dollfus gives the polarisation of the rings at this phase ($6^{\circ}.2$) as $(-0.15 \pm 0.1)\%$. These measurements were made with the

visual fringe polarimeter described by DOLLFUS (1956) and with a filter of effective wavelength 5600 Å. KEMP and MURPHY (1973) show that the polarisation of the ring is roughly the same at 7250 Å as at 5600 Å, at phase $5^{\circ}.5$. Dollfus found the polarisation to be $(-0.2 \pm 0.1)\%$, at $5^{\circ}.5$, whereas Kemp and Murphy find $(-0.3 \pm 0.1)\%$, at 5600 Å. Since these measurements are taken at the ansae of the rings, and the East and West limbs of Saturn are strongly negatively polarised, any scattered light from the planet will increase the measured polarisation of the rings. As Kemp and Murphy used quite large apertures, we use the figure of Dollfus, and adopt a polarisation of the rings at phase angle $6^{\circ}.2$ of $(-0.15 \pm 0.1)\%$ at 7250 Å. Note that in the calculation to follow, we are obliged to ignore the variation of polarisation across the rings or variation connected with the angle of tilt of the rings, as seen from Earth. The error we have assigned to the above value has been roughly doubled to allow for this effect.

Consider the observed polarisation at two wavelengths, one in the continuum, and one at the centre of the band.

Let

P^c, I^c = observed polarisation and intensity of Saturn + Rings in the continuum.

P_s^c, I_s^c = observed polarisation and intensity of Saturn alone in the continuum.

P_R^c, I_R^c = observed polarisation and intensity of the Rings alone in the continuum.

and

P^1, I^1

P_s^1, I_s^1 be the corresponding quantities within the line.

P_R^1, I_R^1

Then: $p_s^c \; I_s^c + p_R^c \; I_R^c = p^c \; I^c$

$$I_s^c + I_R^c = I^c$$

$$p_s^1 \; I_s^1 + p_R^1 \; I_R^1 = p^1 \; I^1$$

$$I_s^1 + I_R^1 = I^1$$

Now, set $p_R^1 = p_R^c = p_R$, and $I_R^1 = I_R^c$. Normalise intensities to $I^c = 1$, and let

$$p_s^R = a p_s^c$$

i.e. a = the factor by which the polarisation of Saturn is enhanced within the band.

Also from the observations we have that $p^1 = 0.13$, $p^c = 0.21$ (in percent) and $I^1 = 0.532$.

Hence to determine I_R, we see that it is necessary to solve the quadratic equation

$$P_R \; I_R^2 \; (a-1) + I_R \; (P^1 \; I^1 - P^c \; a - a P_R I^1 + P_R) + (P^c \; a - P^1) \; I^1 = 0$$

If we set a = 1, i.e. no enhancement of polarisation, we see that

$I_R = 0.20 \; (+ 0.06 - 0.04)$, that is to say that 20% of the light from the combined system comes from the rings.

If we set a = 2, i.e. 100% enhancement, we find

$I_R = 0.39 \; (+ 0.03 - 0.02)$

where in both cases the error is derived solely from the error on P_R.

From the work of POLLACK (1975) we may compare this value with an expected value, after some manipulation. Pollack gives:

$$\frac{\text{Flux from Rings}}{\text{Flux from Saturn + Rings}} = 0.584$$

for the V band, with the rings fully open as viewed from Earth (i.e. $B = 26^\circ$). The spectral reflectivity of the Rings increases by a factor ~1.1 between 5600 Å (the V band) to 7250 Å (POLLACK, 1975); while that of Saturn increases by a factor of around 1.4 (TEIFEL, 1974).

Adopt $\frac{\text{Flux (Rings)}}{\text{Flux (Saturn + Rings)}}$ = 0.524 for the continuum around 7250 Å (that is, the perceived continuum rather than the true continuum).

Now this factor is as yet only for the rings fully open.

It is clear that Flux from Rings $F_{B,i} = S(B,i)\ \pi\ (a_1 - a_2)^2 \sin B$

where a_1 and a_2 are the inner and outer radii of the rings

i = phase angle.

B = Saturnocentric latitude of the Earth with respect to the ring plane.

In fact S(B, i) is different for the two brightest rings which contribute nearly all of the flux. For the A ring, which contributes 36% of the total light, S(B, i) is constant. For the B ring, we note that, ignoring phase dependance,

$$S\ (B = 26^\circ) = 0.77 \quad \text{and} \quad S\ (B = 13^\circ) = 0.71$$

(POLLACK, 1975), where $B = 13^\circ$ in 1978 May. Taking into account the proportions in which the two rings contribute, we then see

$$F\ (B = 13^\circ)\ /F\ (B = 26^\circ) = 0.47$$

Ignoring the phase dependance above will introduce an error of less than 20% since we are not near opposition.

Therefore the expected proportion of the flux contributed by the Rings at 7250 Å and in 1978 May is calculated to be 0.246.

The error on this result is probably in the region of 50%. However we do see clearly that the derived proportion is consistent with no enhancement of polarisation across the band,

and is only marginally consistent with a large (100%) enhancement.

The variation of position angle across the methane band in 1978 May is most curious. The dilution effect of the rings discussed above would merely rotate the position angle in one direction with the maximum deviation being at the centre of the band. The deviation would also be small ($\sim 10^{\circ}$). Such an effect was indeed seen on one evening. The spatial averaging of polarisation as discussed in the previous section would give a similar effect, if all areas of the disc contributed equally. However in the case of Saturn, part of the disc is partially obscured by the rings. Consider the two diagrams below, where the length of the arrows are intended to be representative of the strength of the polarised intensity contributed from that part of the disc. Only the "U" components are shown, i.e. neither perpendicular nor parallel to the scattering plane. In diagram (1), as we move from E to W across the disc, the NE and SE components contribute equally and in opposite senses - and hence cancel. Likewise for the NW and SW components. In case (2), where the Northern components are stronger, a residual polarisation occurs, which changes sign at the centre of the disc. In terms of the position angle of the polarisation of the integrated disc, this would lead to a dispersion curve-shaped feature centred at the band centre, as seen. The stronger polarisation seen in the North of the disc might arise because of the tilt of the polar region towards the observer when $B \neq 0^{\circ}$, rather than the partial obscuration of the rings. This

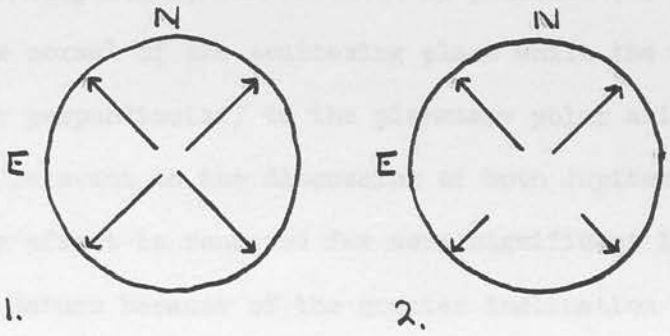

interpretation is not fully satisfactory, as the observed effect seems too large, did not occur every evening, and is at least as wide as the observed band. The structure in the position angle will not affect the calculation above which assumes no change in position angle, as at the centre of the band the position angle has returned to its continuum value.

The mean position angle of those measurements, relative to the normal of the scattering plane, was 164°, i.e. mainly perpendicular to the scattering plane (positive) but with a significant component not related to this plane. Given the geometry of the situation, it seems reasonable to resolve into two components, one of which is parallel (or perpendicular) to the normal of the scattering plane while the other is parallel (or perpendicular) to the planetary polar axis. The formulation is relevant to the discussion of both Jupiter and Saturn, but the effect is rendered far more significant in our measurements of Saturn because of the greater inclination of the pole of Saturn to the ecliptic. Any polarisation of the rings associated with the ring plane is probably small (JOHNSON et al, 1980). If we call the two components P_{SCATT} and P_{POLE}, then their ratio P_{SCATT}/P_{POLE} equalled roughly -0.6 in 1978 May (with P_{POLE} being negative). This ratio might be expected to vary with phase angle, with the angle between the scattering plane and the planetary axis, and with the aspect angle of the rings as seen from Earth.

The atmosphere of Saturn is rather different in detail to that of Jupiter, especially in the thickness of the cloud levels, lower temperature and (apparently) less vigorous atmospheric motions. As described in previous sections, the polarisation of the reflected light from the two planets is

also somewhat different. Physically the above (tentative) null result for enhancement of polarisation across the methane band would imply that even in the centre of the band we are looking at a level well into the ammonia clouds. In order to confirm this result, more observations of Saturn were made in 1979. During the period 1978-80 the aspect angle of Saturn's rings was decreasing (i.e. $B \rightarrow 0$). The observations of 1979 were taken when $B \sim 5^{\circ}$, and the contribution from the Rings was a good deal less than in 1978. If POLLACK (1975)'s figures are used we can estimate the importance of light from the Rings in 1979, and predict the polarisation variation expected. Specifically, since $S\ (B = 5^{\circ}) = 0.65$, we find $F\ (B = 5)/F\ (B = 26) = 0.17$ and

$$\frac{\text{Flux from Rings}}{\text{Flux from Planet + Rings}} = 0.09$$

The predicted drop in polarisation is only about 0.04%, and so any enhancement of polarisation should be more readily visible. Unfortunately, as previously described, much of the data for 1979 January/February had to be discarded. We note however that the magnitude of the polarisation within the band at 7250 Å was around 0.3% whereas it was 0.2% around the 6190 Å band. No significant structure was found over the 6190 Å band. The position angles of the measured polarisation average around 133° with respect to the normal to the scattering plane. The ratio P_{SCATT}/P_{POLE} described above equalled $\sim +0.75$ for these observations, where both components were negative. This value implies that the polarisation component connected with the planetary pole is still stronger than that linked to the scattering plane. A rapid variation of this ratio would give wild fluctuations in the position angle measured for the resultant polarisation. It

is possible therefore that the variations of position angles and polarisation that led us to reject most of the 1979 January/February linear polarisation measurements could have been caused by rapid changes in the linear polarisation of the planet associated with the phase angle = $2^{\circ}.7$ circular polarisation feature. Existing linear polarisation measurements in the literature are neither complete enough nor accurate enough to rule out this possibility. While further observations are needed to check on this, it seems more likely at the present time that a contribution from the Sky background produced the results tabulated.

The circular polarisation measurements across the 7250 Å band in 1978 (figure B23) and 1979 (figures B25 and B26) seem to show a sharp feature in the very centre of the band. The discussion of the circular polarisation across this band in Jupiter is also relevant here. The temperature of the Saturnian atmosphere, while lower than that of Jupiter, still is not thought to give partial pressures high enough and temperatures low enough to allow methane to condense (TEIFEL',1974). The tropopause is thought to be at around 90°K. The sharpness of the feature is puzzling. It may be that the circular polarisation only arises at a high level in the atmosphere, or that some geometrical effect is involved.

The 'continuum' measurements of circular polarisation for Saturn obtained at the 1979 opposition show a dramatic rise in circular polarisation into the red. When the circular polarisation measurements about the methane bands are also taken into account, we see that by 7250 Å the polarisation has reached -0.16%, a value more than twice the largest previously reported for this planet. These measurements were made at phase angles (-) $3^{\circ}.3$ to $1^{\circ}.9$, and hence cover the phase interval ($2^{\circ}.7 \pm 0^{\circ}.5$) within which

an enhancement has been reported in the circular polarisation of Saturn (SWEDLUND et al, 1972). Swedlund's measurements were of regions of the disc of the planet (or rings) and in wide spectral bandpasses. Our observations, on the other hand, are of the whole planet plus the rings and in 50 Å bandpasses (or less). Looking at the dependance of the circular polarisation with wavelength (figure B27), we see that the shape of our curve is roughly intermediate between those of Swedlund's obtained at phase angles $0^{\circ}.6$ and $6^{\circ}.3$, but that the magnitude of the polarisation we observe is significantly higher, especially around 5000 Å. The rise in the polarisation seen at wavelengths greater than 6000 Å is very marked. Measures obtained in and around the molecular bands of methane at 6190 and 7250 angstroms, while not appearing on figure B27 are completely consistent with the displayed 'continuum' values.

An examination of the Figure 2 of Swedlund et al (1972) and the associated table appears to show that the circular polarisation of the north polar region was small at the phase at which that of the south polar region was enhanced. While this may have been the result of shadowing by the rings, it does mean that if Swedlund had observed the whole planet, as we did, he would still have found an enhancement in the polarisation at phase angles near $2^{\circ}.7$, and one of similar magnitude to that observed from the South pole alone. Our observations were not made with the rings as open (as seen from Earth), and shadowing should be less important for these measurements. However it is interesting to note that the magnitude of the effect as detected by Swedlund (0.08% at 6700 Å) is also similar to that seen by us at these wavelengths (see figure B27). The continuum circular polarisation measurements of 1980 April/May taken at phase angle $5^{\circ}.7$ are also closely similar in magnitude to

Swedlund's 6°.3 points. The rise in polarisation seen in our data at 7800 Å is shown to be real. Note that all our listed polarisations are negative, implying that the South pole of the planet was still dominating the circular polarisation. The observed large circular polarisations are unlikely to be caused by our inclusion of the rings in the aperture. Swedlund et al found the circular polarisation of the rings to be small when compared to the planet (i.e. the poles), though he did not make measurements of them near phase angle 2°.7. Finally, although the observations here cover an interval in phase angle of 3°.3 to 1°.9, only small differences are seen during this time (e.g. between measurements at 5750 Å at phase angles 3°.3 and 2°.5, or in the red between 2°.5 and 1°.9). This might be taken as evidence that the presented polarisations are of instrumental origin. During this observing run, no measurements were made at phase angles sufficiently far from 2°.7 to yield a null result, though such measures were obtained on other runs. However, it is also perfectly reasonable to deduce that the circular polarisation peak must simply be somewhat broader than previously reported, and/or variable from opposition to opposition.

The rise in polarisation in the red is very rapid. Some idea of just how rapid can be seen from Appendix B1. The best fits to the observed wavelength dependance were either exponential, or a high order power low (i.e. $p = p_o + k\lambda^{x}$, where $x > 7$).

The circular polarisation of light reflected from the major planets is thought to arise from multiple scattering by (presumably ammonia) aerosols. On Jupiter, Rayleigh scattering (mainly by hydrogen molecules, due to their predominance) is thought to be important in the blue, but not in the red, a consequence of

the λ^{-4} wavelength dependance of this form of scattering (KAWATA & HANSEN, 1976). Saturn consistently exhibits the opposite sign of circular polarisation to Jupiter under identical scattering geometries. It has been suggested that this can be accounted for by presuming that Rayleigh scattering is much more important for Saturn (KAWATA & HANSEN, 1976; COFFEEN & HANSEN, 1974). However, linear polarisation measurements require that differing particle properties (particularly size) must also be invoked. At phase angles different from $2^{\circ}.7$, the magnitude of the circular polarisation observed (by Swedlund) is greater than that predicted by multiple scattering models (KAWATA, 1978). These models have a number of free parameters, but all seem to have the problem of producing enough circular polarisation (i.e. $>$ 0.02%) at small phase angles with the sort of cloud particles thought to exist in the Saturnian atmosphere. The models are integrated over a whole hemisphere, though, whereas Swedlund's observations refer to a more localised region about the pole. If the spatial distribution of circular polarisation predicted by WOLSTENCROFT (1976) on Jupiter is applicable to Saturn, we note that regions near the east and west limbs of the planet would only dilute the polarisation of the pole in the theoretical models. To obtain higher circular polarisations either within the circular polarisation peak or at long wavelengths outside it, KAWATA (1978) has suggested the inclusion of large (20μ) particles with a narrow size distribution, or preferentially orientated non-spherical particles into the models. The scattering of large spherical particles can be understood in terms of geometrical optics. As can be seen from figure 5 of HANSEN & TRAVIS (1974), large particles show sharp features in

intensity and linear polarisation such as the 'rainbows' and the backscattered (i.e. phase angle $\sim 0^{\circ}$) 'glory'. A narrow size distribution of such large particles would be necessary to maintain the sharpness of these features. To Kawata's suggestion we might also add that the relative refractive index of these large spherical particles be in the range $\sqrt{2} \lesssim n \lesssim 2$, for then light can be back-scattered after just one internal reflection, giving a strongly linearly polarised glory. Further, for higher values of the refractive index, the primary rainbow, which is also highly polarised, moves closer to phase angle 0°. (If ϕ = phase angle of primary rainbow, then : for n = 1.23, $\phi \simeq 43^{\circ}$; for n = 1.50, $\phi \simeq 23^{\circ}$; and for n = 1.60, $\phi \simeq 15^{\circ}$). Illumination of other aerosols by the strongly linearly polarised light would then give rise to the enhanced circular polarisation. Non-spherical particles are very likely present in the atmosphere of both Jupiter and Saturn. HOLMES et al (1980) have watched both ammonia and ice crystallise at low temperatures and pressures. They found that ammonia formed tetrahedral shaped crystals with rounded vertices, while ice formed into hexagonal patterns. Similar crystals of ammonia and 'snowflakes' of ice may constitute the clouds of Jupiter and Saturn. Large non-spherical crystals do not give the 'rainbows' and 'glory' seen with spherical aerosols as these features are dependant on the circular cross section and spherical shape respectively. In their place, shape-specific haloes appear. Like the rainbow, these occur at an angle of minimum deviation, given by,

$$2 \sin^{-1} (n \sin \psi/2) - \psi$$

where ψ is a dihedral angle formed by two faces, not necessarily contiguous, and is less than twice the angle of critical internal reflection (TRICKER, 1970). These haloes can be strongly polarised. If the crystals are partially aligned they might have a significantly stronger effect. How might such particles be aligned? No form of

magnetic alignment is feasible, the fields being too weak. "Streaming" of particles in a strong planetary wind, either associated with convection cells, or with the differential rotation of the planet could possibly provide the mechanism of alignment. Large plane hexagonal snowflakes would be easier to align than rounded tetrahedra.

An appealing explanation of the large circular polarisation of Saturn as opposed to Jupiter is the reflection of highly polarised light from the rings onto the planet. Since the rings only illuminate one hemisphere by reflection, the planet as a whole would exhibit a non-zero circular polarisation. However, Swedlund has made a North-South scan of Saturn with a 7" aperture at phase angle $2^{\circ}.6$ and found that the strongest circular polarisation was seen at the South pole, whereas south of Saturnicentric latitude -65°, there is no direct illumination by ring light. At the East and West limbs, where any effect of the rings might be expected to be greatest, the circular polarisation was small (at phase angles $\lesssim 0^{\circ}.5$, wavelength 6400 Å). The possibility of a large contribution from the East and West limbs at phase angles around $2^{\circ}.7$ is however not ruled out, though in observations of the whole disc they would presumably cancel.

In summary, it is necessary to explain the relatively high circular polarisation outside the polarisation peak, as well as the enhancement within it. Unfortunately no simple deduction can be made from the very rapid rise in circular polarisation with wavelength reported here at phase angles around $2^{\circ}.7$. It seems that illumination of the planet by the rings cannot account for both the effects, and indeed is unlikely to account for either. More modelling is necessary, using parameters for the atmosphere

derived from spacecraft-born experiments, in order to see if large spherical particles can match the observations. Ammonia crystals may well approximate to spheres in their scattering properties. The modelling of scattering by non-spherical particles is very difficult. One approach recently developed is to modify the Mie theory by "removing" features due specifically to the spherical shape of the particles. The technique is promising but remains to be fully developed and exploited (ACQUISTA, 1978).

There still remains the possibility that the wavelength dependance of circular polarisation presented is the result of some instrumental effect. It is clearly of the highest priority to confirm these measurements, and to extend them into the infrared.

The requirements of linear polarisation across the 7250 Å methane band in 1980 April/May show conclusively that there exists an enhancement in polarisation in Saturn as well as Jupiter. In the Spring of 1980, the rings contributed negligeable light to the measured flux from the planet ($B \simeq -1^{\circ}$), though of course they could still affect the measurement by reflecting polarised light onto the planet. The enhancement is of the order of 65% of the continuum polarisation and such a value for the rise in polarisation across the band is fully consistent with the measurements of 1978 May. It is coincidently similar to that found in Jupiter at about the same time, though the planets were at different phase angles. The fact that the enhancements are of similar order in the two planets points to the underlying similarity between their respective atmospheres. At the same phase, the relative sizes of the enhancements will provide information on the relative scale heights of gas-to-aerosols in the two planets. Since the clouds of Saturn are thought to be thicker and denser than those of Jupiter, we would

expect the enhancement to be less for this planet. The ratio P_{SCATT}/P_{POLE} described above equalled +3.64 for these measurements, both values being positive. This is confirmation of the low importance of light from the rings.

As mentioned previously, the "continuum" measurements of circular polarisation on Saturn were generally consistent with the data of SWEDLUND et al (1972) at phase angle $6^{\circ}.5$. It is curious that our whole planet measures are comparable to his values obtained from one pole only, especially as with the Earth in the ring-plane, both poles should contribute to the flux from the planet without shadowing by the rings. However, the Sun was not in the ring-plane at the time, and so the illumination geometry is still not identical for the two polar regions.

9. Conclusions

It has been shown that an enhancement of linear polarisation occurs across the 7250 Å methane band in both Jupiter and Saturn. While such an enhancement was predicted by FYMAT (1974), these are the first quantitative measurements reported. As yet effects across other bands have not been definitely found. It is likely that such effects will be present at some level, and indeed the relation between line strength and the enhancement in polarisation should be a useful constraint for modelling the vertical distribution of aerosols in the atmospheres of the Major planets. BURIEZ et al (1979) have shown some of the information which can be obtained from the polarisation equivalent widths: the complete polarisation line profile will provide a great deal more.

On Saturn, the wavelength dependance of circular polarisation within the feature at phase angle $2^{\circ}.7$ was secured. A dramatic increase in levels of polarisation into the red was observed. An effect may also exist in the linear polarisation spectrum at this phase angle. More observations are urgently needed.

The interpretation of the measurements across line profiles presented are complicated by a number of instrumental effects, mainly connected with measurement of the entire planetary disc. On Saturn, there is also the problem of separating out the component in the integrated light coming from the rings. Further complication results from the different atmospheric conditions existing above different parts of the planets, such as the poles of Jupiter (GEHRELS, 1969) or the equatorial band of Saturn (BUGA ENKO & GALKIN, 1973). In order to maximise the information obtained from the polarisation, and to relieve the modelling of at least one

stage of integration, it will be necessary to obtain spatially resolved measurements on the discs of both planets. Such measurements would require a high precision, 2-D multichannel spectropolarimeter to make them feasible. The new SIT-Vidicon spectropolarimeter approaching completion at the Royal Observatory is suitable for this project, and it is hoped to obtain the measurements outlined above in the near future.

The other major discovery reported here could easily be followed up with broad filters on a single channel instrument. The study of the linear and circular polarisation of Saturn at and around phase angle $2^{\circ}.7$ is of importance. More observations are vitally needed, especially in the near infrared. A logical extension of such a program would be to study Jupiter at phase angle $7^{\circ}.8$ where a similar feature in circular polarisation has been reported to occur (MICHALSKY & STOKES, 1974).

Finally, as has been made clear in previous sections, the basic polarisation measurements on which scattering models for the atmospheres of Jupiter and Saturn depend are still incomplete and of low accuracy. Even now the only reported circular polarisation measurements of Jupiter are in a broad red band centred about 6700 Å. The accuracy of the polarisation against phase angle curves for these planets could be improved relatively easily by a factor of at least 5. Such measurements are complementary to those obtainable from the spacecraft-born photopolarimeters, at least until a spectropolarimeter is carried to the vicinity of Jupiter. Earthbased observations can provide a wealth of spectral information unobtainable from the two-colour devices flown as yet. It is to be hoped that with the increased

incorporation of multichannel detectors into high precision spectropolarimeters in the next few years, some of this missing basic information will be secured.

Appendix B1 : The wavelength dependance of circular polarisation on Saturn in January/February 1979.

In January/February 1979 the 'continuum' circular polarisation of Saturn redward of 6000 Å was large and increased rapidly with wavelength (figure B 27). In order to gain some insight into just how fast the polarisation was growing with wavelength, some simple linear curve fitting was attempted. The data fitted included 6F9, the last two wavelengths of 29J8 and some averages obtained over the methane band at 7250 Å (table B 18). Linear least squares fits were obtained to two different forms of curve: a power law $q = b\lambda^x$ via $\log p = x \log \lambda + x \log b$; and an exponential fit, $q = k \exp(m\lambda)$, via $\log p = \log k + m\lambda$. Here, q is the absolute value of the circular polarisation in percent, λ is the wavelength in Ångstroms, and x, b, k and m are constants.

Initially all the data was fitted with these two curves. The resulting straight lines are seen in figure B 29 (power law) and figure B 30 (exponential). The constants were:

$$x = 7.25,\ b = 1.05 \times 10^{-4},\ m = 6.43 \times 10^{-4},\ k = 2.59 \times 10^{-6}$$

Following this a continuum level was subtracted before fitting. The average of the 6F9 data was used (-0.020%) and the last two wavelengths of 6F9 omitted from the fitting. The values for the constants derived were:

$$x = 9.67,\ b = 1.10 \times 10^{-4},\ m = 6.43 \times 10^{-4},\ k = 2.59 \times 10^{-6}$$

As can be seen in figures B 29 and B 30, the fits are now very good. As a final experiment, a continuum level of (-0.035%) was subtracted. This gave the best fits to the observed curve, but polarisation was increasing very rapidly by 7500 Å. The power

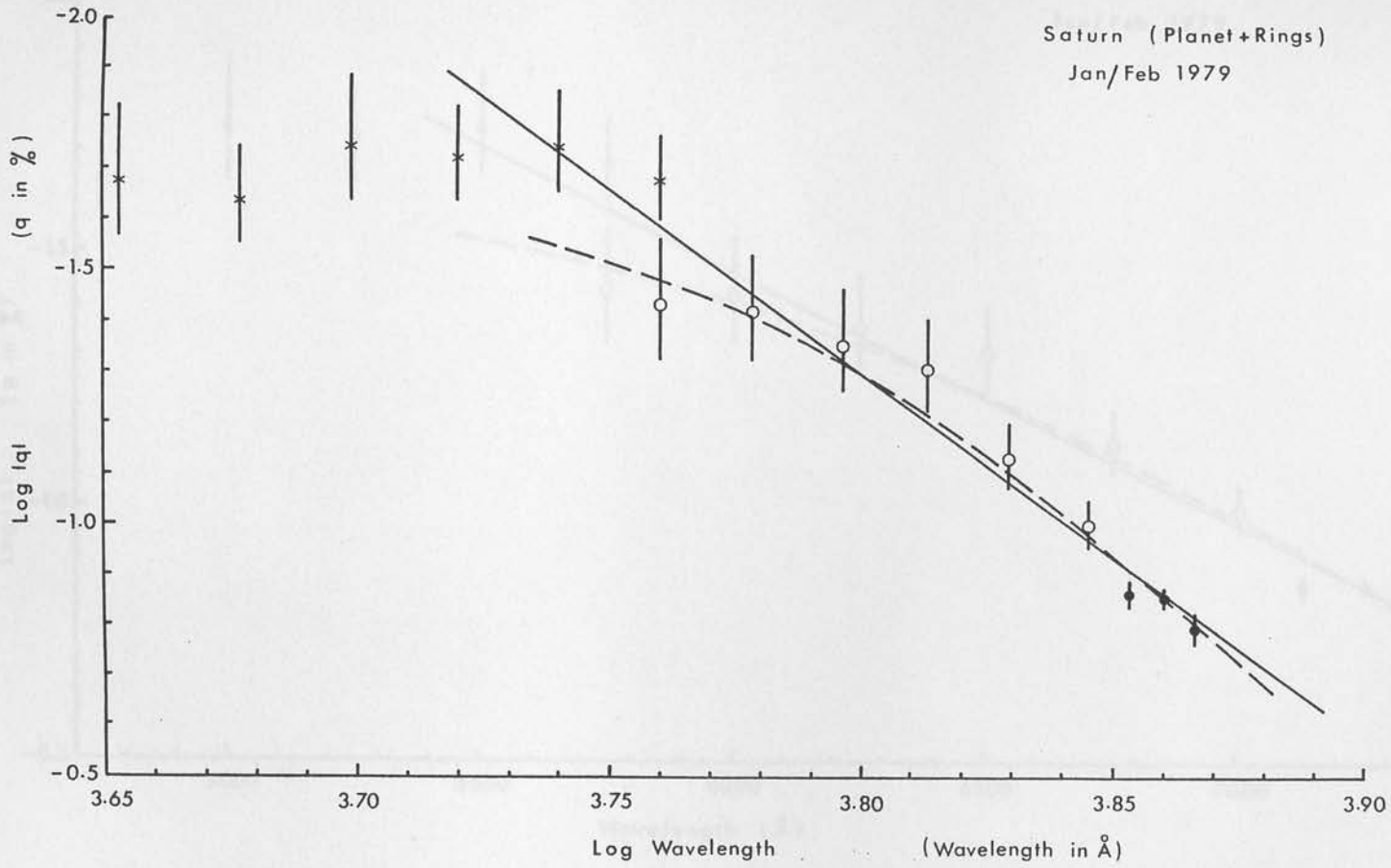

Figure B29 : An attempt to fit a power law relation to the continuum circular polarisation measurements of Saturn. Two possible fits are shown (see text).

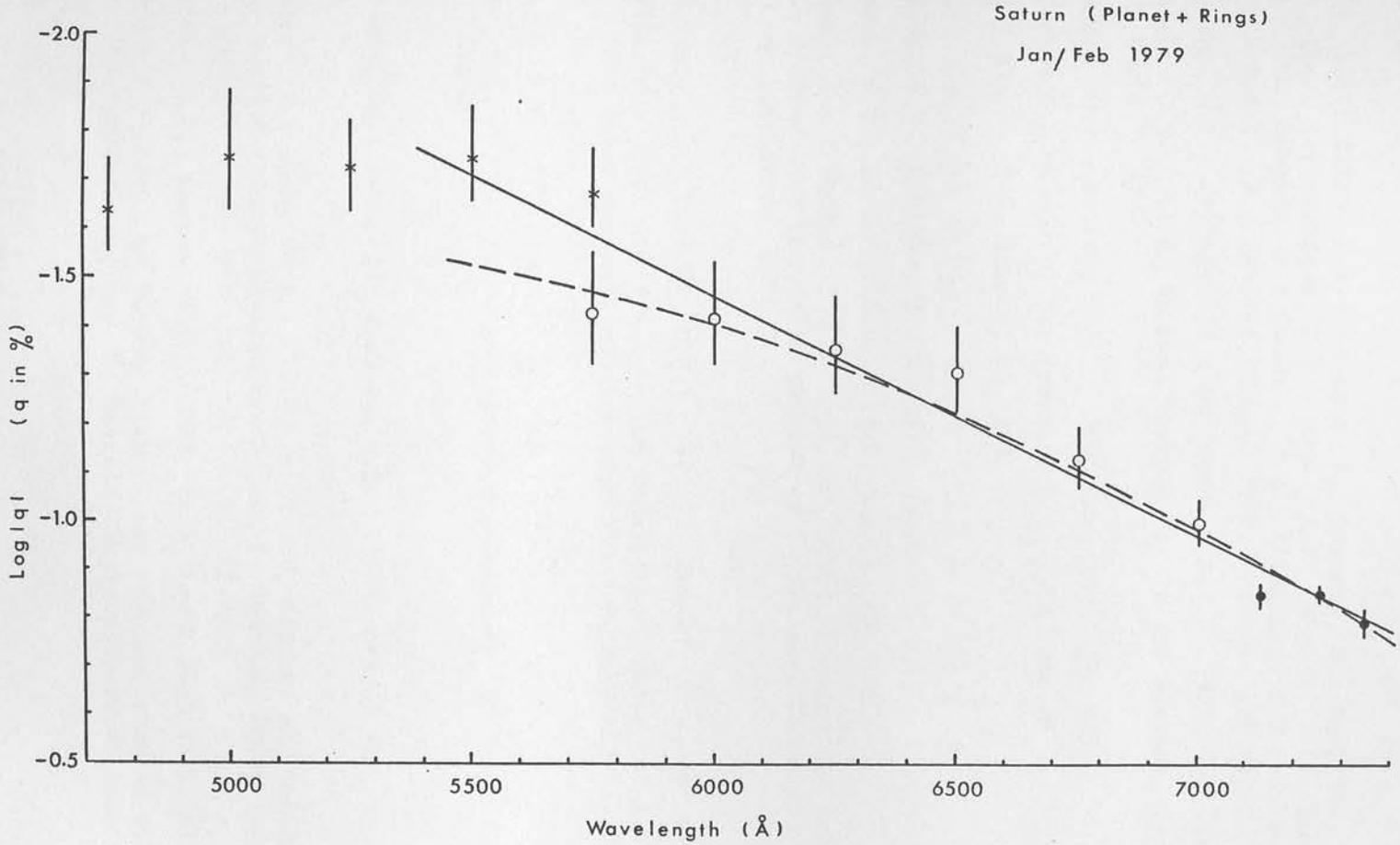

Figure B30 : An attempt to fit an exponential relation to the continuum circular polarisation measurements of Saturn. Two possible fits are shown (see text).

law constant x equalled 17.97!

In summary, the circular polarisation appears to be increasing with around the ninth power of the wavelength over this restricted range.

References

Acquista, C: 1978, App. Opt., 17, 3851

Axel, L: 1972, Ap. J, 173, 451

Baker, A.L.; Baker, L.R.; Beshore, E.; Blenman, C.; Castillo, N.D.; Chen, Y-P; Coffeen, D.L.; Doose, L.R.; Elston, J.P.; Fountain, J.W.; Gehrels, T.; Kendall, J.H.; Kenknight, C.E.; Norden, R.A.; Swindell, W.; Tomasko, M.G.: 1975, Science, 188, 468

Bugaenko, O.I.; Galkin, L.S.; Morozhenko, A.V.: 1971, Sov. Ast., 15, 290

Bugaenko, O.I.: 1972, Astron. Vestnik, 6, 19 (in Russian, quoted in Teifel', 1974

Bugaenko, O.I.; Galkin, L.S.: 1973, Sov. Ast., 16, 681

Buriez, J.C.; Fouquart, Y.; Fymat, A.L.: 1979, Ast. & Ap., 79, 287

Busse, F.H.: 1976, Icarus, 29, 255

Cochran, W.D.; Slavsky, D.B.: 1979, Icarus, 37, 84

Cochran, W.D.; Cochran, A.L.: 1980, Icarus, 42, 102

Coffeen, D.L.; Hansen, J.E.: 1974, in "Stars, Planets and Nebulae, studied with photopolarimetry" ed T. Gehrels, University of Arizona Press, p573

Danielson, R.E.; Tomasko, M.G.: 1969, J. Atmos. Sci., 26, 889

Dollfus, A.: 1961, in "Planets and Satellites", being Volume III of "The Solar System", ed G. Kuiper and B.M. Middlehurst, University of Chicago Press, p343

Dollfus, A.: 1979, Icarus, 37, 404

Doose, L.R.: 1973, PhD dissertation presented to the University of Arizona

Encrenaz, Th.; Owen, T.; Woodman, J.H.: 1974, Ast. & Ap., 37, 49

Forbes, F.F.; Fymat, A.L.: 1974, in "Stars, Planets and Nebulae, studied with photopolarimetry" ed. T. Gehrels, University of Arizona Press, p637

Fountain, J.W.; Larson, S.M.: 1973, Comm. Lunar Planetary Lab., 174

Fymat, A.L.: 1974, in "Stars, Planets and Nebulae, studied with photopolarimetry" ed. T. Gehrels, University of Arizona Press, p617

Galileo , G.: 1610, "Sidereus Nuncius"

Gauquelin, M.: 1969, "Cosmic Clocks", Peter Owen, London

Gehrels, T.: 1969, Icarus, 10, 410

Gehrels, T.: 1976, in "Jupiter" ed. T. Gehrels, University of Arizona Press, p531

Gehrels, T.; Herman, B.M.; Owen, T.: 1969, Ast. J., 74, 190

Giver, L.P.: 1978, J. Quant. Spect. Rad. Trans., 19, 31

Gribbin, J.R., Plaguemann, S.: 1974, "The Jupiter Effect", Macmillan, London

Hall, J.S.: 1968, Low. Obs. Bull., 7, 61

Hall, J.S.; Riley, L.A.: 1968, Low. Obs. Bull., 7, 83

Hall, J.S.; Riley, L.A.: 1974a, in "Stars, Planets and Nebulae, studied with photopolarimetry" ed. T. Gehrels, University of Arizona Press, p593

Hall, J.S.; Riley, L.A.: 1974b, Icarus, 23, 144

Hall, J.S.; Riley, L.A.: 1976, Icarus, 29, 231

Hanneman, D.; Raschke, E.: 1974, in "Stars, Planets and Nebulae, studied with photopolarimetry" ed. T. Gehrels, University of Arizona Press, p 510

Hansen, J.E.; Travis, L.D.: 1974, Sp. Sci. Rev., 16, 527

Hertzberg, G.: 1945, "Molecular Spectra and Molecular Structure", Vol III, Van Nostrand Reinhold, p526

Holmes, A.; Paxman, R.; Stahl, H.P.; Tomasko, M.: 1980, Bull. Am. Ast. Soc., 12, 705

Hord, C.W.; West, R.A.; Simmons, K.E.; Coffeen, D.L.; Sato, M.; Lane, A.L.; Bergstralh, J.T.: 1979, Science, 206, 956

Hunt, G.E.; Bergstrahl, J.T.: 1974, Nature, 249, 635

Huygens, C.: 1649, "Systema Saturnium"

Kawabata, K.; Hansen, J.E.: 1975, Bull. Am. Ast. Soc., 7, 382

Kawata, Y.: 1978, Icarus, 33, 217

Kawata, Y.; Hansen, J.E.: 1976, in "Jupiter" ed. T. Gehrels, University of Arizona Press, p516

Keay, C.S.L.; Low, F.J.; Rieke, G.H.; Minton, R.B.: 1973, Ap. J., 183, 1063

Kemp, J.C.; Swedlund, J.B.; Murphy, R.E.; Wolstencroft, R.D.: 1971a, Nature, 231, 169

Kemp, J.C.; Wolstencroft, R.D.; Swedlund, J.B.: 1971b, Nature, 232, 165

Kemp, J.C.; Murphy, R.E.: 1973, Ap. J., 186, 679

Kemp, J.C.; Rudy, R.J.; Lebofsky, M.J.; Rieke, G.H.: 1978, Icarus, 35, 263

Kuzmin, A.D.; Navmov, A.P.; Smirnova, T.V.: 1972, Astron. Vestnik, 6, 13 (in Russian, quoted in Teifel' 1974)

Lewis, J.S.: 1969a, Icarus, 10, 365

Lewis, J.S.: 1969b, Icarus, 10, 393

Lillie, C.F.; Hord, C.W.; Pang, K.; Coffeen, D.L.; Hansen, J.E.: 1977, Sp. Sci. Rev., 21, 159

Lipson, S.G.; Lipson, H.: 1969, "Optical Physics", Cambridge University Press

Low, F.J.; Davidson, A.W.: 1969, Bull, Am. Ast. Soc., 1, 200

Lutz, B.L.; Owen, T.: 1980, Ap. J., 235, 285

Lyot, B.: 1929, Ann. Obs. Paris (Meudon) VIII (In English, as NASA TTF-187)

Macy, W.: 1977, Icarus, 32, 328

Martin, P.G.: 1975, Ap. J., 201, 373

Michalsky, J.J.; Stokes, R.A.: 1974, Pub. Ast. Soc. Pac., 86, 1004

Morozhenko, A.V.: 1973, Sov. Ast., 17, 105

Morozhenko, A.V.; Yanovitskii, E.G.: 1973, Icarus, 18, 583

Owen, T.: 1969, Icarus, 10, 355

Owen, T.: 1976, Icarus, 29, 159

Podolak, M.; Danielson, R.E.: 1977, Icarus, 30, 479

Pollack, J.B.: 1975, Sp. Sci. Rev., 18, 3

Prinn, R.G.: 1974, Bull. Am. Ast. Soc., 6, 375

Prinn, R.G.; Lewis, J.S.: 1973, Ap.J., 179, 333

Prinn, R.G.; Owen, T.: 1976, in "Jupiter", ed. T. Gehrels, University of Arizona Press, p319

Ramaprasad, K.R., Caldwell, J.; McClure, D.S.: 1978, Icarus, 35, 400

Rasool, I.; Herman, D.; Kerrisk, D.; Brunk, W.: 1974, in IAU Symposium 65 "The exploration of the Planetary system", p 549

Ridgeway, S.T.; Larson, H.P.; Fink, U.: 1976, in "Jupiter" ed T. Gehrels, University of Arizona Press, p 384

Scattergood, T.; Owen, T.: 1977, Icarus, 30, 780

Serkowski, K.: 1974, in "Stars, Planets and Nebulae, studied with photopolarimetry", ed T. Gehrels, University of Arizona Press, p141

Sill, G.T.: 1976, in "Jupiter", ed. T. Gehrels, University of Arizona Press, p 372

Smith, B.A. et al: 1979a, Science, 204, 945 et seq

Smith, B.A. et al: 1979b, Science, 206, 925 et seq

Stoll, C.; Tomasko, M.: 1980, Bull. Am. Ast. Soc., 11, 617

Strobel, D.F.: 1973, J. Atmos. Sci., 30, 1205

Swedlund, J.B.; Kemp, J.C.; Wolstencroft, R.D.: 1972, Ap. J., 178, 257

Teifel', V.G.: 1974, in IAU Symposium 65 "The exploration of the Planetary System", p415

Teifel', V.G.: 1976, in "Jupiter", ed. T. Gehrels, University of Arizona Press, p441

Teifel', V.G.; Usol'tseva, L.A.; Kharitona, G.A.: 1971, Sov. Ast., 15, 296

Tomasko, M.G.: 1976, in "Jupiter", ed. T. Gehrels, University of Arizona Press, p486

Tomasko, M.G.; West, R.A.; Castillo, N.D.: 1978, Icarus, 33, 558

Tomasko, M.; McMillan, R.; Stoll, C.: 1980, Bull. Am. Ast. Soc., 11, 617

Tricker, R.A.R.: 1970, "Introduction to Meteorological Optics", American Elsevier, New York, p75

Weidenschilling, S.J.; Lewis, J.S.: 1973, Icarus, 20, 465

West, R.A.: 1979a, Icarus, 38, 12

West, R.A.: 1979b, Icarus, 38, 34

West, R.A.; Tomasko, M.: 1980, Icarus, 41, 278

Westphal, J.A.: 1971, unpulbished, reported in Teifel', 1974

Westphal, J.A.; Mathews, K.; Terrile, R.J.: 1974, Ap. J., 188, L111

Woodman, J.H.; Trafton, L.; Owen, T.: 1977, Icarus, 32, 314

Wolstencroft, R.D.: 1976, Icarus, 29, 235

Wolstencroft, R.D.; Smith R.J.: 1979, Icarus, 38, 155

Table B1 : Observing Log for Jupiter, 1978

Date	Name	RS (Å)	UT	P (°)	i (°)
22/23	22J1	37	05.40	- 1.38	6.3
	22J2	37	06.30		
24/25	24J1	24	03.00	- 1.43	6.7
	24J2	24	04.15		
	24J3	24	05.35		
	24J4	24	06.25		
	24J5	24	06.40		
	24J6	24	07.40		
	24J7	24	07.55		
25/26	25J1	23	04.20	- 1.46	6.8
	25J2	23	06.55		
26/27	26J1	37	03.15	- 1.48	7.0
	26J2	37	05.05		
	26J3	37	07.10		
	26J4	37	09.00		

Notes:

(a) Date refers to 1978 January.

(b) RS = Resolution as defined by the width of the exit slit.

(c) UT = Effective time of observation.

(d) All position angles are corrected to the scattering plane.

P = position axis of the scattering plane = $\theta_E - \theta$

where θ_E = position angle on equatorial system

θ = position angles in Table B2 .

(e) i = Phase angle at 0^h.

(f) All observations were made with aperture 1 (80" diameter), and with Order Sorter 3 (transmitting beyond 6600 Å).

(g) On 1978 January 24th, D_E = + 2°.21, the equatorial diameter of Jupiter was 45".6 and the polar diameter was 42".6. D_E is the latitude of the Earth as seen from Jupiter. P, i, and D_E are tabulated in the Astronomical Ephemeris.

(h) All measurements were taken at the Cassegrain focus of the 40" reflector of the Lunar and Planetary Laboratory at Mount Lemmon, Arizona.

Table B2 : Measurements of the linear polarisation of Jupiter (1978)

Name	λ (Å)	p (%)	σ(p) %	θ(°)	$\sigma(\theta)$ (°)
22J1	7000	0.041	0.018	91	13
	7125	0.046	0.016	47	17
	7250	0.131	0.021	87.2	4.8
	7375	0.047	0.021	71	16
	7500	0.072	0.018	84.2	7.3
22J2	7170	0.017	0.012	77	23
	7270	0.105	0.017	91.0	6.5
24J1	6770	0.006	0.009	16	46
	6960	0.013	0.010	108	22
24J2	7260	0.123	0.015	91.5	3.3
	7280	0.098	0.014	94.3	4.5
	7300	0.118	0.015	82.0	3.4
	7320	0.086	0.012	89.1	3.8
	7340	0.066	0.012	95.5	5.0
24J3	7790	0.133	0.022	78.5	5.4
	7825	0.113	0.028	84.2	5.7
	7860	0.109	0.030	82.9	8.0
	7895	0.174	0.035	80.2	4.8
	7930	0.163	0.036	99.3	6.1
	7965	0.123	0.035	94.7	8.8
	8000	0.184	0.041	75.5	6.0
	8035	0.200	0.040	85.1	8.1

Name	λ (Å)	P (%)	σ(p) %	θ(°)	$\sigma(\theta)$ (°)
24J4	7070	0.055	0.011	91.8	5.3
	7150	0.076	0.012	83.4	4.3
24J5	7195	0.098	0.012	80.4	3.6
	7465	0.060	0.011	98.3	5.2
24J6	7410	0.020	0.018	119	25
	7720	0.052	0.037	75	19
24J7	8105	0.020	0.14	150	180
25J1	7050	0.050	0.009	87.7	5.4
	7120	0.065	0.009	81.5	4.7
	7190	0.098	0.011	85.1	3.2
	7260	0.150	0.013	88.0	2.8
	7330	0.105	0.012	91.4	3.0
	7400	0.069	0.010	90.5	4.3
	7470	0.067	0.011	85.9	4.8
25J2	7155	0.062	0.011	81.4	4.8
	7225	0.128	0.015	85.9	3.3
	7295	0.141	0.014	98.7	3.0
	7365	0.078	0.012	72.2	4.7
26J1	7190	0.084	0.012	76.6	4.1
	7260	0.146	0.015	81.1	3.2
	7330	0.144	0.012	83.7	3.3

Name	λ (Å)	p (%)	σ(p) %	θ(°)	$\sigma(\theta)$ (°)
26J2	7720	0.078	0.017	72.1	6.8
	7825	0.102	0.023	81.4	5.9
	7930	0.195	0.032	88.5	4.8
	8035	0.177	0.039	73.6	6.5
	8140	0.157	0.061	69.6	11
26J3	7755	0.122	0.018	77.0	4.0
	7860	0.175	0.021	85.1	4.7
	7965	0.137	0.033	91.9	7.5
	8070	0.127	0.051	74.0	9.3
	8175	0.100	0.085	25	23
26J4	7790	0.147	0.016	96.8	3.0
	7895	0.161	0.022	86.3	4.6
	8000	0.159	0.026	86.7	5.0
	8105	0.160	0.040	53.4	6.6

Table B3 Measurements of the circular polarisation of Jupiter (1978)

Name	λ (Å)	q (%)	σ(q) (%)
22J1	7000	- 0.001	0.007
	7125	- 0.015	0.007
	7250	- 0.014	0.009
	7375	+ 0.008	0.008
	7500	- 0.018	0.007
22J2	7170	- 0.001	0.006
	7270	+ 0.005	0.009
25J1	7050	- 0.009	0.003
	7120	- 0.015	0.003
	7190	- 0.020	0.003
	7260	- 0.010	0.004
	7330	- 0.008	0.004
	7400	- 0.011	0.003
	7470	- 0.018	0.003
25J2	7155	- 0.006	0.003
	7225	- 0.003	0.004
	7295	+ 0.011	0.005
	7365	- 0.009	0.004
26J2	7720	- 0.015	0.006
	7825	- 0.005	0.009
	7930	+ 0.001	0.012

Name	λ (Å)	q (%)	σ (q) (%)
	8035	+ 0.020	0.015
	8140	+ 0.040	0.023
26J3	7755	- 0.011	0.006
	7860	+ 0.001	0.011
	7965	+ 0.015	0.015
	8070	- 0.001	0.022
	8175	+ 0.232	0.078
26J4	7790	- 0.006	0.006
	7895	- 0.008	0.009
	8000	- 0.016	0.011
	8105	- 0.079	0.018

Table B4 : Observing Log for Jupiter, 1980 April

Name	Time (UT)	Tele-scope	N(λ)	L or C	Wavelength Range (Å)	Optics (Å)	RS (f)	AP	Moon (°)	Phase	OS	HT (v)	MV	P (°)	Comments
22 AP 4	7.30	24"	5	LC	5950-6350	5825	11	3	8	9.55	4	1450	358	111.36	Cloud
22 AP 7	9.50	24"	5	LC	6000-6400	5825	11	3	8	9.55	4	1450	361	111.36	Cloud
24 AP 3	8.00	24"	6	LC	6400-6525	5825	11	3	10	9.71	4	1450	377	111.30	
24 AP 9	11.00	24"	7	L	7150-7450	5825	11	3	10	9.72	1	1450	427	111.30	0° pos. only

Table B5 : Linear polarisation measurements of Jupiter across methane and ammonia bands. April/May 1980

λ	Name	p (%)	σ	θ_r (°)	σ
λ 64 50	Ammonia band				
5382	24AP3 + 7	0.188	0.007	91.5	1.1
6407	24AP3	0.184	0.010	85.5	1.6
6432	"	0.204	0.011	86.5	1.5
6457	"	0.197	0.010	86.1	1.5
6482	"	0.207	0.010	87.9	1.4
6507	"	0.232	0.011	85.1	1.3
λ 72 50	Methane band				
7132	24AP9	0.305	0.012	93.7	1.1
7182	"	0.381	0.012	89.1	0.9
7232	"	0.476	0.013	91.4	0.8
7282	"	0.521	0.014	92.1	0.8
7332	"	0.403	0.013	92.0	0.9
7382	"	0.334	0.013	92.2	1.1
7432	"	0.316	0.013	91.0	1.1

Table B6 : Circular polarisation measurements of Jupiter across methane and ammonia bands. April/May 1980.

	Name	q (%)	o
6190 Methane band			
5932	22 AP 4	0.003	0.008
5982	22 AP 7	0.002	0.008
6032	22 AP 4	0.002	0.009
6082	22 AP 7	-0.004	0.009
6132	22 AP 4	0.006	0.009
6182	22 AP 7	-0.001	0.009
6232	22 AP 4	0.003	0.009
6282	22 AP 7	-0.011	0.009
6332	22 AP 4	0.004	0.009
6382	22 AP 7	0.005	0.009
6450 Ammonia band			
6382	24 AP 3	0.006	0.008
6407	24 AP 3	-0.007	0.008
6432	24 AP 3	-0 000	0.009
6457	24 AP 3	-0.000	0.009
6482	24 AP 3	-0.000	0.008
6507	24 AP 3	-0.010	0.009

Table B7 : Observing Log for Saturn 1978 (May)

Name	Time (UT)	Tele Scope	N (λ)	L or C	Range of Wavelengths	Optics	RS	AP	Moon (days)	Phase (°)	OS	HT (v)	MV (10^{-2}v)	P (°)	Comments
3M2	05.20	40"	8	L	7100 - 7450	5825	53	1	26	6.2	3	1550	400	19.67	
4M1	03.30	40"	8	L	7100 - 7380	5825	53	1	27	6.2	3	1550	400	19.65	Some Cirrus
4M2	05.00	40"	4	L	7120 - 7360	5825	53	1	27	6.2	3	1550	400	19.65	
10M3	04.20	61"	10	LC	7100 - 7550	5825	32	1	4	6.3	1	1550	400	19.53	Some Cloud
25M1	03.30	60"	4	LC	7130 - 7430	5825	36	4	19	6.2	1	1550	405	19.30	
25M2	05.00	60"	4	LC	7160 - 7400	5825	16	3	19	6.2	1	1500	400	19.30	
26M1	03.20	60"	10	LC	6940 - 7390	5825	18	1	20	6.2	1	1450	400	19.28	

Table B8: Abbreviations used in the Observing Logs

Name	A serial number. The day and month come first, e.g. 5F1 was obtained on the night of 5th/6th February.
Time (UT)	Mean time of observation (UT).
Telescope	Diameter of telescope used. Identifications are 40" University of Arizona Mt. Lemmon 60" NASA/University of Arizona Mt. Lemmon 61" University of Arizona Catalina 24" University of Hawaii (AF) Mauna Kea Platescales are 10, 8.5, 10 and 22.3 arcsec mm^{-1} respectively.
N (λ)	Number of wavelengths studied in this measurement.
L or C	Was linear polarisation (L), circular polarisation (C), or both (LC) measured?
Range	Range of wavelengths studied.
Optics	Set of quarterwave plates used.
RS	Resolution defined by the exit slit.
AP	Aperture used. 1 = 8 mm 3 = 2 mm 5 = ½ mm 2 = 4 mm 4 = 1 mm

Moon — Age of Moon, in days from New Moon.

Phase — Sun - planet - Earth angle.

OS — Order Sorter used. The wavelength beyond which these are transparent is given.

1	= 4100 Å	3	= 6600 Å	5	= Empty
2	= 5200 Å	4	= 3500 Å	6	= Empty

HT — High Tension Voltage applied to tube.

MV — Modulator excitation voltage used.

P — Position Angle of the scattering plane.
If θ_E is the position angle of a measurement in the equatorial system, and θ the position angle with respect to the scattering plane, $P = \theta_E - \theta$.

Table B9 : Linear polarisation measures of Saturn

Raw Data (May 1978)

λ(Å)	Name	p (%)	σ	θ (°)	σ(θ)
6930	26M1	0.238	0.021	167.5	3.2
	3M2	0.214	0.028	162.8	3.0
7090	4M1	0.242	0.023	166.9	2.4
	10M3	0.226	0.021	165.5	2.7
7105	26M1	0.219	0.024	159.8	3.1
7110	4M2	0.194	0.020	164.5	5.6
7120	25M1	0.290	0.025	177.5	2.5
7130	4M1	0.208	0.035	166.7	3.5
7140	3M2	0.240	0.029	161.8	3.1
	10M3	0.261	0.021	170.1	2.3
7145	26M1	0.244	0.025	166.2	3.3
7150	25M2	0.430	0.034	161.7	2.7
7170	4M1	0.191	0.035	173.0	4.0
7185	26M1	0.233	0.025	163.9	4.0
7190	3M2	0.300	0 036	157.0	3.1
7190	4M2	0.220	0.029	161.3	6.2
	10M3	0.190	0,027	171.1	4.0
7210	4M1	0.183	0.033	178.2	4.7
7220	25M1	0.276	0.045	179.9	5.1
	26M1	0.147	0.032	163.4	6.2
7230	25M2	0.255	0.043	169.1	6.1
7240	3M2	0.213	0.036	149.9	4.5
	10M3	0.105	0.029	12.0	7.9
7250	4M1	0.127	0.037	163.1	6.9
	26M1	0.120	0.035	155.0	8.4
7270	4M2	0.165	0.043	143.3	7.2
7275	26M1	0.166	0.031	155.5	5.0
	3M2	0.286	0.035	141.8	3.3

7290	4M1	0.133	0.049	156.2	8.1
	10M3	0.105	0.027	151.1	10.0
7300	26M1	0.162	0.032	149.9	5.5
7310	25M2	0.258	0.036	159.0	4.6
7320	25M1	0.318	0.036	6.2	3.3
7330	4M1	0.170	0.035	155.7	5.0
7340	3M2	0.196	0.034	154.7	4.2
7340	10M3	0.213	0.022	157.2	3.2
7345	26M1	0.175	0.025	160.6	4.2
7350	4M2	0.186	0.038	163.3	5.0
7370	4M1	0.167	0.030	170.2	4.0
7380	26M1	0.183	0.024	165.3	4.1
7390	3M2	0.282	0.035	158.7	3.5
7390	10M3	0.187	0.025	163.4	3.2
	25M2	0.188	0.032	156.7	5.6
7420	25M1	0.289	0.034	4.4	3.3
7440	3M2	0.221	0.033	159.4	3.7
	10M3	0.186	0.024	164.5	3.3
7490	10M3	0.178	0.023	161.2	3.5
7540[a]	10M3	0.126	0.027	164.2	6.5

(a) measurement possibly affected by dawn sky background

Table B10 : Linear polarisation measures of Saturn. Weighted running mean of 4 points (May 1978).

$\bar{\lambda}$ (Å)	P_m	σ_{pm}	θ_m	$\sigma_{\theta m}$
7059	0.222	0.010	165.2	1.4
7109	0.217	0.011	165.0	1.4
7121	0.222	0.012	166.3	1.6
7131	0.228	0.012	168.0	1.6
7146	0.238	0.013	169.0	1.5
7160	0.240	0.013	168.7	1.6
7173	0.219	0.012	167.7	1.8
7189	0.207	0.013	170.1	2.0
7201	0.199	0.013	168.5	2.1
7215	0.169	0.013	172.3	2.4
7230	0.135	0.015	171.5	2.9
7245	0.128	0.015	162.8	3.2
7259	0.134	0.015	160.0	3.0
7271	0.133	0.014	154.5	2.9
7284	0.143	0.015	151.6	2.9
7299	0.145	0.015	154.0	2.7
7315	0.166	0.013	155.3	2.3
7329	0.186	0.014	156.7	2.1
7341	0.191	0.014	158.8	2.1
7351	0.189	0.014	162.1	2.0
7361	0.177	0.014	165.1	2.1
7373	0.181	0.014	165.5	2.0
7395	0.182	0.013	165.5	1.8
7425	0.183	0.012	163.5	1.7
7465	0.171	0.012	163.2	1.9

Data used ; 4M1 , 4M2 , 10M3 , 26M1

Table B11 : Circular polarisation measures across the Methane bands of Saturn. Raw data. (May 1978).

λ(Å)	Name	q (%)	σ
6930	26M1	0.002	0.010
7090	10M3	- 0.002	0.012
7105	26M1	- 0.000	0.011
7120	25M1	- 0.032	0.022
7140	10M3	0.003	0.014
7145	26M1	0.009	0.011
7150	25M2	0.065	0.021
7185	26M1	0.020	0.012
7190	10M3	0.014	0.014
7220	25M1	0.009	0.032
7220	26M1	0.026	0.013
7230	25M2	0.079	0.029
7240	10M3	0.070	0.019
7250	26M1	0.007	0.015
7275	26M1	0.014	0.017
7290	10M3	0.008	0.023
7300	26M1	0.028	0.015
7310	25M2	- 0.024	0.022
7320	25M1	0.005	0.026
7340	10M3	0.038	0.014

λ (Å)	Name	q (%)	ς
7345	26M1	0.024	0.014
7380	26M1	0.029	0.013
7390	25M2	0.026	0.018
	10M3	0.017	0.013
7420	25M1	0.033	0.024
7440	10M3	0.071	0.014
7490	10M3	0.060	0.014
7540	10M3	affected by guiding errors	

Table B12 : Observing Log for Saturn : 1979 January/February

Name	Time (UT)	Tele Scope	N (λ)	L or C	Range of Wavelengths	Optics (Å)	RS (Å)	AP	Moon (days)	Phase (°)	OS	HT (v)	MV	P (°)	Comments
29J8	09.20	60"	6	C	4500 - 5750	5825	26	1	2	- 3.3	4	1300	285	19.60	
30J2	09.15	60"	5	C	3500 - 4500	3800	53	1	3	- 3.2	5	1300	215	19.47	
5F1	09.45	60"	5	C	3500 - 4500	3800	53	-	9	- 2.6	5	1300	200	18.41	AP = 1?
6F7	08.15	60"	1	C	4500	5825	31	1	10	- 2.5	5	1300	240	18.20	
6F9	09.20	60"	6	C	5750 - 7000	5825	21	1	10	- 2.5	4	1300	360	18.20	
9F12	09.30	60"	5	LC	6000 - 6300	5825	26	1	13	- 2.2	4	1300	345	17.39	
9F13	10.25	60"	4	LC	6050 - 6300	5825	26	1	13	- 2.2	4	1300	345	17.39	
9F15	11.50	60"	6	LC	7200 - 7300	5825	26	1	13	- 2.2	4	1300	405	17.39	
11F7	07.10	40"	4	C	6100 - 6160	5825	21	1	15	- 2.0	5	1300	335	16.79	
11F8	07.40	40"	4	L	6100 - 6160	5825	21	1	15	- 2.0	5	1300	335	16.79	
11F10	09.10	40"	5	LC	6180 - 6260	5825	21	1	15	- 2.0	5	1300	335	16.79	
11F12	11.05	40"	5	LC	7100 - 7360	5825	21	1	15	- 2.0	5	1300	410	16.79	
12F11	10.00	40"	5	LC	7240 - 7280	5825	21	1	16	- 1.9	5	1300	405	16.33	

Table B13 : Linear polarisation measures of Saturn Raw Data (February 1979).

λ(Å)	Name	p (%)	$\sigma(p)$	θ (°)	$\sigma(\theta)$
6000	9F12	0.173	0.022	118.0	3.9
6050	9F13	0.146	0.022	124.2	4.5
6090	9F12	0.143	0.023	116.3	4.3
6100	11F8	0.155	0.021	148.3	3.8
6120	11F8	0.169	0.021	153.3	3.6
6135	9F13	0.167	0.024	126.2	4.9
6140	11F8	0.169	0.020	146.2	3.4
6160	11F8	0.174	0.021	153.2	3.5
6180	9F12	0.188	0.025	117.2	3.8
	11F10	0.162	0.020	157.0	3.5
6200	11F10	0.217	0.021	159.6	2.7
6220	11F10	0.170	0.021	161.7	3.5
6225	9F13	0.152	0.021	117.4	4.5
6240	11F10	0.142	0.020	156.5	3.9
6260	9F12	0.171	0.023	115.9	4.1
6260	11F10	0.198	0.021	165.1	2.9
6300	9F12	0.185	0.023	119.6	3.5
	9F13	0.191	0.024	116.9	3.7

Table B14 : Linear polarisation measures of Saturn

Raw Data (February 1979).

λ (Å)	Name	p (%)	$\sigma(p)$	θ (°)	$\sigma(\theta)$
7100	11F12	0.316	0.022	140.9	2.0
7130	11F12	0.256	0.022	139.4	2.4
7160	11F12	0.353	0.023	140.6	1.9
7200	9F15	0.328	0.025	94.3	2.1
7220	12F11	0.341	0.024	127.9	1.9
7220	9F15	0.282	0.025	96.5	2.4
7226	12F11	0.287	0.024	125.7	2.3
7232	12F11	0.336	0.023	123.2	2.0
7240	9F15	0.277	0.023	90.6	2.5
7250	12F11	0.394	0.023	125.0	1.7
7260	12F11	0.317	0.023	120.6	2.1
	9F15	0.355	0.025	88.9	2.0
7280	9F15	0.421	0.024	88.9	1.7
7300	9F15	0.299	0.024	95.0	2.3
7330	11F12	0.355	0.024	140.6	1.9
7360	11F12	0.354	0.024	138.6	1.9

Table B15 : Linear polarisation measurements of Saturn. Sky-corrected data for 11/12th February 1979.

λ(Å)	Name	p (%)	$\sigma(p)$	θ (°)	$\sigma(\theta)$
6100	11F8	0.155	0.022	124.6	3.7
6120		0.168	0.020	129.6	3.6
6140		0.171	0.020	122.6	3.4
6160		0.173	0.021	129.6	3.6
6180	11F10	0.154	0.020	131.6	3.6
6200		0.210	0.020	135.5	2.8
6220		0.161	0.020	137.1	3.7
6240		0.136	0.021	131.2	4.1
6260		0.188	0.021	141.3	3.1
7100	11F12	0.297	0.022	138.6	2.1
7130		0.236	0.022	136.1	2.6
7160		0.323	0.024	137.5	2.1
7330		0.315	0.023	136.6	2.1
7360		0.318	0.023	134.5	2.1

Table B16 : Circular polarisation measurements of Saturn, across the methane bands. Raw data. (February 1979).

λ(Å)	Name	q (%)	σ(q)
6000	9F12	- 0.030	0.022
6050	9F13	- 0.032	0.020
6090	9F12	- 0.009	0.025
6100	11F 7	- 0.036	0.020
6120	11F 7	- 0.051	0.020
6135	9F13	- 0.088	0.024
6140	11F 7	- 0.054	0.020
6160	11F 7	- 0.050	0.019
6180	9F12	- 0.039	0.024
	11F10	- 0.047	0.016
6200	11F10	- 0.062	0.016
6220	11F10	- 0.053	0.016
6225	9F13	- 0.080	0.020
6240	11F10	- 0.063	0.015
6260	9F12	- 0.017	0.021
6260	11F10	- 0.054	0.015
6300	9F12	- 0.058	0.023
	9F13	- 0.048	0.023

Table B17 : Circular polarisation measurements of Saturn across the methane bands. Raw data (February 1979).

λ(Å)	Name	q (%)	σ(q)
7100	11F12	- 0.134	0.016
7130	11F12	- 0.136	0.015
7160	11F12	- 0.154	0.016
7200	9F15	- 0.100	0.015
7220	12F11	- 0.129	0.017
7220	9F15	- 0.119	0.015
7226	12F11	- 0.166	0.017
7232	12F11	- 0.112	0.017
7240	9F15	- 0.180	0.015
7250	12F11	- 0.143	0.017
7260	12F11	- 0.161	0.017
	9F15	- 0.134	0.015
7280	9F15	- 0.146	0.015
7300	9F15	- 0.159	0.015
7330	11F12	- 0.153	0.017
7360	11F12	- 0.170	0.018

Table B18 : **Continuum** circular polarisation of Saturn

Raw data (January/February 1979)

λ(Å)	Name	q (%)	σ(q)
3500	30J2	- 0.018	0.027
3750		- 0.018	0.024
4000		- 0.027	0.010
4250		- 0.026	0.006
4500		- 0.034	0.004
3500	5F1	- 0.022	0.012
3750		- 0.020	0.011
4000		- 0.016	0.011
4250		- 0.002	0.011
4500		- 0.027	0.010
4500	6F7	- 0.026	0.010
4500	29J8	- 0.021	0.006
4750		- 0.023	0.005
5000		- 0.018	0.005
5250		- 0.019	0.004
5500		- 0.018	0.004
5750		- 0.021	0.004
5750	6F9	- 0.037	0.010
6000		- 0.038	0.009
6250		- 0.044	0.010
6500		- 0.049	0.010

	Name	q	$\sigma(q)$
6750		- 0.074	0.011
7000		- 0.100	0.011

Table B19 : Observing Log for Saturn : 1980 May

Name	Time (UT)	Tele Scope	N (λ)	L or C	Range of Wavelengths	Optics (Å)	RS (Å)	AP	Moon	Phase (°)	OS	HT (v)	MV	P (°)	Comments
13MY6	09.40	24"	7	C	7140 - 7440	5825	26	3	29	5.49	1	1450	426	114.38	
14MY5	09.30	24"	7	L	7140 - 7440	5825	53	3	1	5.53	1	1450	428	114.32	
15MY6	09.10	24"	7	L	7115 - 7415	5825	53	3	2	5.58	1	1450	426	114.27	
16MY5	09.25	24"	5	L	7215 - 7415	5825	53	3	3	5.63	1	1450	425	114.22	
17MY5	08.50	24"	10	C	6000 - 7800	5825	106	3	4	5.66	1	1450	403	114.17	
18MY2	09.40	24"	7	L	7250 - 7500	5825	53	3	5	5.71	1	1450	424	114.13	

Table B20: Linear polarisation measurements of Saturn across the 7250 Å methane band. April / May 1980.

λ(Å)	Name	p (%)	σ	θ_r (°)	σ
6897	18 MY 2	0.427	0.016	175.6	1.1
6947	18 MY 2	0.419	0.015	175.3	1.0
7097	15 MY 6	0.367	0.014	174.9	1.0
7122	14 MY 5	0.333	0.013	171.2	1.2
7147	15 MY 6	0.370	0.013	174.6	1.1
7172	14 MY 5	0.383	0.013	174.5	1.0
7197	16 MY 5	0.427	0.014	175.8	0.9
7212	18 MY 2	0.465	0.016	176.4	1.0
7222	14 MY 5	0.402	0.014	173.9	1.0
7247	16 MY 5	0.486	0.014	174.1	0.8
7272	14 MY 5	0.401	0.014	174.8	1.0
7297	16 MY 5	0.408	0.014	173.8	1.0
7322	14 MY 5	0.309	0.014	172.5	1.4
7347	16 MY 5	0.376	0.014	174.7	1.1
7372	14 MY 5	0.317	0.014	172.3	1.3
7397	16 MY 5	0.323	0.014	172.3	1.2
7422	14 MY 5	0.269	0.014	175.6	1.5
7482	18 MY 2	0.316	0.016	174.2	1.5

Table B21 : Circular polarisation measurements of Saturn across the 7250 methane band. April/May, 1980

λ(Å)	Name	q (%)	σ
7122	13 MY 6	- 0.015	0.015
7172	13 MY 6	- 0.010	0.015
7222	13 MY 6	- 0.014	0.015
7272	13 MY 6	- 0.018	0.015
7322	13 MY 6	- 0.020	0.015
7372	13 MY 6	- 0.002	0.015
7422	13 MY 6	- 0.027	0.014

Table B22 : Continuum circular polarisation measurements of Saturn. April/May 1980.

	Name	q	(%)	o
5982	17 MY 5	-0.017		0.008
6182	17 MY 5	-0.004		0.009
6382	17 MY 5	-0.020		0.009
6582	17 MY 5	-0.015		0.009
6782	17 MY 5	-0.004		0.009
6982	17 MY 5	-0.012		0.009
7182	17 MY 5	-0.008		0.008
7382	17 MY 5	-0.012		0.009
7582	17 MY 5	-0.019		0.009
7787	17 MY 5	-0.033		0.009

Chapter C

Spectropolarimetry of Reddened Stars

Spectropolarimetry of reddened stars

1. Introduction

The existence of absorbing material in the interstellar medium can be inferred from naked eye observations of the Milky Way on any clear night. However, for a long time, the observed 'dark lanes' and bifurcations of the Milky Way were misinterpreted as being 'holes' in the star clouds. This was the interpretation, for example, of Herschel when in 1780 he mapped these dark areas. If the holes in the Milky Way are interpreted as dark clouds, then one way in which to quantitatively study them is by star counts, and as early as 1847, STRUVE had deduced the existence of an absorbing sheet in the galactic plane by this means. Struve found the medium to give rise to an absorption of about 1 magnitude per kiloparsec, a value later confirmed by KAPTEYN (1909.a,b) and JONES (1914).

At about the same time as ideas of an absorbing medium were being considered, the concept of a pervasive gas in interstellar space also arose. The first direct evidence was the observation by HARTMANN (1904) of a stationary line of Calcium in the spectrum of a spectroscopic binary. At the time it was considered that this line was more likely to be of circumstellar rather than interstellar origin (YOUNG, 1922). The discovery by PLASKETT and PEARCE (1930, 1933) that the strengths of these stationary lines (by that time known in a number of stars) increased with the distance of the star from the Sun gave convincing evidence that the gas giving rise to such lines in fact existed in interstellar space. The conclusive measurements for the existence of the dust were made by TRUMPLER (1930a, b), who presumed that the linear dimensions of open clusters

of similar appearance were the same. He then compared the distance scale derived from the apparent sizes of the clusters with that from the apparent brightness of cluster stars of particular spectral types. The derived mean value for the interstellar absorption was found to be 0.8 magnitude per kiloparsec. This value was confirmed by BOTTLINGER and SCHNELLET (1930) who considered the dispersion of Cepheids perpendicular to the Galactic plane, and by VAN DE KAMP (1932) who looked at the concentration of extragalactic nebulae towards the poles of our Galaxy. Using the new photomultiplier tubes, HALL (1937) and STEBBINS, et al (1939) investigated the wavelength dependence of the interstellar extinction and found it to vary roughly linearly with inverse wavelength. The complex line profiles obtained by ADAMS (1948) following earlier work by BEALS (1936) and MERRILL et al (1937) showed that components of the interstellar gas have quite different radial velocities and hence probably exist in a number of distinct clouds.

Early attempts to model the interstellar grains supposed them to be metallic in nature (GREENSTEIN, 1938). SCHALEN (1936) explained the extinction curves with 0.01 micron metallic particles which used up about 1% of the mass of the whole interstellar medium. LINBLAD (1935) investigated the possibility of grain growth by condensation from the interstellar gas and this was taken further by OORT and VAN DER HULST (1946). Dielectric grains consisting mainly of water and ammonia ice and having sizes of the order of the wavelength of light were proposed by VAN DER HULST (1946, 1949). The (linear) polarisation of light by the interstellar medium was discovered by HALL (1949) and HILTNER (1949) while looking for instrinsic polarisation effects in early type stars predicted by Chandrasekhar. Linear polarisation implies the existence of

aligned non-spherical dust grains in the interstellar medium. The grains are aligned by the galactic magnetic field and DAVIS and GREENSTEIN (1951) suggested a mechanism (paramagnetic relaxation) by which this might be achieved. Because of the difficulty of explaining the rather high values of interstellar polarisation with dielectric grains, CAYREL and SCHATZMAN (1954) (and subsequently HOYLE and WICKRAMASINGHE (1962)) proposed the existence of graphite flakes, which are very efficient polarisers. PLATT (1956) has suggested that the absorption arises in large molecules (10 Å) with unfilled electronic shells. (WICKRAMASINGHE, 1967; SPITZER, 1968; GREENBERG, 1968; MUNCH, 1968).

This chapter continues as follows. Section 2 discusses the state of our current knowledge about the composition and form of the solid grains present in the interstellar medium. Section 3 explains the aims of the present study, while Section 4 presents new observations of three reddened stars: ζ Ophiuchi, 55 Cygni and χ Aurigae. In Section 5 these new observations are examined to determine which of the observed features are real and which obviously instrumental, while the interpretation of the real features is dealt with in Section 6. Section 7 draws together the conclusions of the chapter and suggests what further work might profitably be undertaken.

2. The extinction and polarisation of starlight by interstellar grains

The many fields of research collectively referred to as the the study of the interstellar medium constitute without doubt one of the major divisions of Astronomy. Its results are vitally relevant to some of the most fundamental questions that Science can ask, including for example those of the future history of the Universe and the origin of Life. Of the very large number of papers published every year in this field, possibly 10 to 15% are directly relevant to the present work. It is these papers that this section seeks to review. The subsections below concentrate on the available evidence on the nature of the grains which cause the observed extinction and polarisation. An attempt is also made to summarise the conclusions about the grains that have been deduced from this evidence. The section is intended to be the selective introduction to the literature necessary as background for the rest of this chapter. Recent reviews are given by MERRILL (1979), SAVAGE and MATHIS (1979) and WHITTET (1981). Savage and Mathis also give references to a number of other reviews on closely allied subjects.

2.1 The extinction curve

Light passing through a particulate medium will either be absorbed or scattered by it. Both processes will remove light from the beam, and so we are concerned here with their sum - the extinction. The dependence of the extinction of the interstellar medium on wavelength is described in three sections corresponding to the visual, ultraviolet and infrared regions of the spectrum.

2.1.1 Visual extinction

As previously mentioned, the wavelength dependence of extinction in the visual region roughly follows a λ^{-1} law (STEBBINS et al, 1939; WHITFORD, 1958). The dependence is normally shown as a plot of $E(\lambda - V)/E(B - V)$ against wavelength, where $E(B - V)$ is the difference between the observed colour $(B - V)$ and the instrinsic colour $(B - V)_o$ of the background star before reddening, and $E(\lambda - V)$ is a similar quantity for the wavelength in question. Clearly the curve takes the values zero at V and 1 at B. The amount of extinction (in magnitudes) at a particular wavelength, A_λ, is given by:

$$\frac{A(\lambda)}{E(B - V)} = \frac{E(\lambda - V)}{E(B - V)} + R \qquad (2.1.1.1)$$

where R is termed the ratio of total to selective absorption, since when λ refers to the V band:

$$R = A_V/E(B - V) \qquad (2.1.1.2)$$

A large number of studies have sought to determine whether the form of the extinction curve depended on the direction of observation (e.g. NANDY, 1964; NANDY, 1967; JOHNSON, 1977; PENSTON et al, 1975). Because of the normalisation chosen the shape of the curve itself appears to be only slightly variable (see, for example, JOHNSON, 1968) and attention was concentrated on the normalisation constant, R. Knowledge of the correct value of this parameter to use was important because it related the observeable quantity, $E(B - V)$, to the unknown A_V, (through 2.1.1.2 above) and hence led to the determination of the distance to the star under consideration. Claims were made for large variations in the appropriate value of R for particular regions (the 'average' or 'canonical' value being close to 3) (VAN BREDA and WHITTET, 1977). The method used to find these values of R involved obtaining infrared

measurements of the reddened star or stars and of comparison stars to as long a wavelength as possible. The comparison stars were chosen to be of the same spectral type as the program stars and were assumed to be unreddened. The extinction was then derived by straight division of the two spectra. As the extinction falls to zero at infinite wavelength, the value of E (λ - V)/E (B - V) extrapolated from lower wavelengths with the help of the best fitting theoretical curve will give the value of R directly. (There are also other methods, see JOHNSON, 1968). This method is however seriously affected by the presence of infrared emission by circumstellar dust, and by nebulosity (SCHMIDT-KALER, 1967). The present picture is one of real, but somewhat smaller, variations of R with direction than previously thought (AANNESTAD and PURCELL, 1973; WHITTET, 1977).

The most obvious feature in the visual extinction curve is the apparently sharp change of slope in the region of 2.25 - 2.30 μ^{-1} (WHITFORD, 1958; NANDY, 1964; UNDERHILL and WALKER, 1966; HARRIS, 1969). The exact location of this 'knee' in the extinction curve has been a matter of debate and may in fact be variable. Other features are apparent. Besides the very sharp lines attributed to the interstellar gas (MUNCH, 1968) a large number of diffuse bands also appear. Discovered by MERILL (1934), these vary in width from 1 Å (e.g. λ 5797 Å) to nearly 30 Å for the strongest band at 4430 Å (WU, 1973). Various parts of the spectrum have been searched for these bands. HERBIG (1975) covered the range 4400 - 6850 Å and 3000 - 4400 Å (HERBIG, 1967). SANNER et al (1978) extended the range by searching between 6500 Å and 8900 Å, while SAVAGE (1975) covered 2200 Å to 3600 Å and SNOW et al (1977) looked between 1114 Å and 1450 Å. Except for the possible features

at 3970 Å (HERBIG, 1971) and 1416 Å (SNOW et al, 1977), the diffuse band of shortest wavelength is at 4430 Å. High resolution and correlation studies of these bands include those of: WU (1973) (λλ 5780, 5797); SAVAGE (1976) (λ5780); DANKS and LAMBERT (1976) (λλ 5780, 5797); WELTER and SAVAGE (1977) (λλ 6379, 6614); DANKS and LAMBERT (1975) (λ 4430); and MARTIN and ANGEL (1975) (λ 4430). A compilation of a number of previous catalogues reduced statistically to a common system was given by SNOW et al (1977), and further correlation studies have been made by SCHMIDT (1978) on the 5780 Å band and SCHMIDT-KALER (1980) on the 6284 Å band, amongst others. The following conclusions were reached by these studies.

(i) Some of the diffuse bands appear to have symmetric profiles (e.g. λ 4430, λ 6379) while others are definitely asymmetric (λ 5780, λ 5797, λ 6614).

(ii) There is a good correlation between the strengths of the diffuse bands and the reddening, E (B - V), but such correlations are not as good as the intercorrelation of the various bands one with another. HERBIG (1975) attributed part of the scatter in the plot of diffuse band strength against colour excess E (B - V) as being due to the fact that the aforementioned 'knee' in the extinction curve near 4400 Å fell within the "B" band. He suggested that plots using infrared colours might show a better correlation. This was found not to be the case (SNEDEN et al, 1978). High accuracy studies show a definite intrinsic scatter in the dependence which is not attributable to instrumental error (SCHMIDT-KALER, 1980). Although the intercorrelation of the various diffuse bands is good there are examples of

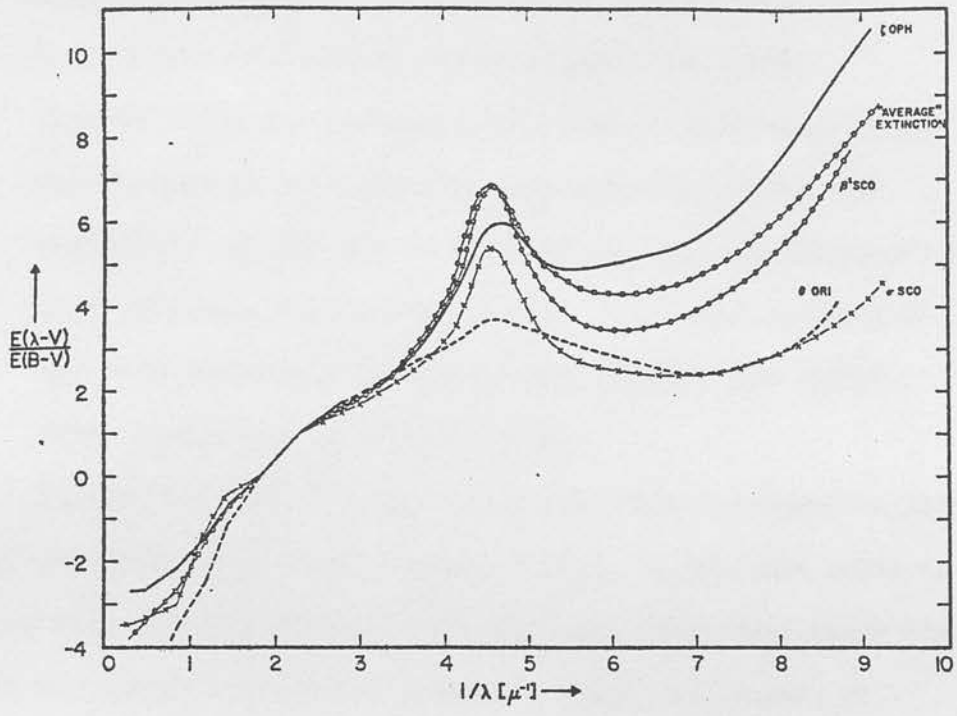

Figure C1: The Interstellar extinction curves which generally define the envelope of all such curves so far obtained. From BLESS & SAVAGE, 1972.

discordant ratios (WU et al, 1977). The correlations with the 2175 Å feature and far ultraviolet extinction are similarly imperfect (see on) and not better than the correlation with the HI column density (WU, 1972).

(iii) Diffuse bands are systematically weaker (with respect to the reddening) in stars with circumstellar shells, in reflection nebulae and in dark clouds, and are stronger in high velocity, low density clouds. This last conclusion has been challenged by recent work (WHITTET and BLADES, 1980; BLADES and SOMERVILLE, 1977).

Besides the 4400 Å 'knee' there are other broadband variations seen in the extinction curve. HERBIG (1975), in the same paper in which he discusses the diffuse features, also shows that there are broader but weaker absorptions present. These have widths 30 - 100 Å. There is also Very Broadband Structure (VBS) present, on scalelengths of 1000 Å and more (WHITEOAK, 1967; WALKER, 1967; HAYES et al, 1973; REX, 1974; REX, 1976; SCHILD, 1977; VAN BREDA and WHITTET, 1981). The main feature in the VBS is an apparent 'emission' or 'window' centred around 1.8 μ^{-1}, the depth of which correlates loosely with reddening. The difficulties associated in the measurement of the features probably account for most, if not all, of the scatter.

2.1.2 Ultraviolet extinction

The extension of the extinction curve into the ultraviolet (3600 Å to 1100 Å) produced a number of surprising discoveries. Figure C1 shows the derived exinction curve in the range 1 to 10 μ^{-1}. The most apparent feature is the 'hump' at 4.6 μ^{-1} (2175 Å) of width 1 μ^{-1} depending on definition. It was originally discovered by STECHER (1965) and well studied by BLESS and SAVAGE (1972).

Albedo measurements of the diffuse galactic light (LILLIE and WITT, 1976) show this to be a pure absorption feature. The other noteable feature is the rapid rise in extinction in the far ultraviolet.

The 2175 Å feature is found to be well correlated with E (B - V), (NANDY et al, 1975), but not so well correlated with the 4430 Å diffuse band (DORSCHNER et al, 1977; DANKS, 1980; SCHMIDT, 1978; WU, 1972). The strength of the far ultraviolet extinction is not particularly well correlated with the 2175 Å absorption (NANDY, 1978; BLESS and SAVAGE, 1972), nor with the diffuse band at 4430 Å (WU et al, 1977). In the Large Magellanic cloud, the 2175 Å feature seems to be a little weaker, and the far ultraviolet extinction somewhat stronger in some locations with respect to the mean curve for our own Galaxy (NANDY et al, 1980). Differences in the ultraviolet extinction relation with the direction of observation within the Galaxy also seem to occur (KOORNNEEF, 1978). There are several well-documented cases of anomolous 2175 Å band strengths with respect to reddening. In particular both θ^1 and μ Orionis show a weak feature (SAVAGE, 1975) while four stars in the Cass-Tau association show an unusually strong absorption (MORALES et al, 1980). In one star the 2175 Å equivalent width is about three times stronger than would be expected from its reddening. Several Wolf-Rayet stars show enhanced 2175 Å absorption: HD 193793 (KORNEEF and SITKO, 1979); HD192163 (WILLIS and WILSON, 1975) and HD156385 (WHITTET et al, 1979). WHITTET et al (1979) have shown that one of these Wolf-Rayet stars (HD192641) has diffuse band strengths consistent with the reddening. MILLAR (1979) has studied the correlation of the strength of the 2175 Å band with carbon depletion (i.e. in the gas) in the line of sight, and finds that the band declines in strength as carbon depletion increases.

2.1.3 Infrared extinction

Many infrared features seen in emission and absorption in the spectra of various astronomical courses are attributable to the material in the interstellar medium. The best known is seen at a wavelength of 9.7μ. In the BN object, it is a broad, assymetric band, extending to 13μon the long wavelength side. It appears in lines of sight containing diffuse clouds (WOOLF, 1973), molecular clouds (PERSSON et al, 1976), and oxygen-rich circumstellar shells (MERRILL and STEIN, 1976). In the latter it sometimes occurs in emission at calculated grain temperatures of up to 1000°C (MILLAR and DULEY, 1980). It does not appear in the spectra of carbon-rich stars with circumstellar shells, or planetary nebulae (which are also assumed to be carbon-rich). A further feature is seen at ~3.1μ. This is again broad and assymetric. In BN, the long wavelength wing stretches to 3.6μ. However this is not seen in the diffuse medium, but only in the dense clouds. It does not appear in circumstellar shells or in the spectra of reflection nebulae.

Other features that will be mentioned later include a weaker band at 18μ, often found in association with the 9.7 band, and a band at 11.2μwhich is only seen in the circumstellar shells of carbon-rich stars. The spectra of planetary nebulae (e.g. NGC 7027) often show a number of emission features including structure at 3.3, 3.4, 6.2, 7.7, 8.7 and 11.3μ(MERRILL, 1977).

2.2 Linear and circular polarisation

The dust grains present in the interstellar medium polarise the light passing through as well as attenuating it. The implication must be that the grains are non-spherical and aligned. Surveys of the polarisation of stars have been carried out by KRUSZEWSKI (1962); SERKOWSKI (1965); VISVANATHAN (1966); SERKOWSKI (1968); MATHEWSON

and FORD (1970); COYNE et al (1974); SERKOWSKI et al (1975); APPENZELLER (1968). The observations suggest an upper envelope for the ratio of polarisation to reddening given by

$$p_{\ell}/E\,(B-V) \lesssim 9 \quad (\% \text{ per magnitude}) \qquad (2.2.1)$$

SERKOWSKI et al (1975) have shown that the dependence of linear polarisation on wavelength is well represented by the analytic curve

$$\ln (p/p_{max}) = -k \ln^2 (\lambda/\lambda_{max}) \qquad (2.2.2)$$

where k was found to average 1.15, and λ_{max} is the wavelength at which the polarisation reaches a maximum value (p_{max}). λ_{max} varies from about 0.3μ to at least 0.8μ (for example, for VI Cyg No 12, λ_{max} = 0.33μ (WILKING et al, 1980), whereas for HD 147889, λ_{max} = 0.80μ (SERKOWSKI et al, 1975). It is noteworthy that the equation holds well for values of λ_{max} over this range, and when p_{max} is small or large. The wavelength coverage has been extended into the ultraviolet by GEHRELS (1974) who showed that the 2175 Å absorption feature was not polarised in Zeta Ophiuchi. Infrared observations were obtained by DYCK and JONES (1978) and WILKING et al (1980). The latter observations showed that if equation (2.2.2) were modified to

$$\ln (p/p_{max}) = -1.7\lambda_{max} \ln^2 (\lambda/\lambda_{max}) \qquad (2.2.3)$$

where λ_{max} is in microns, a better fit was obtained for polarisation measurements with large or small λ_{max}. Occasionally reports of structure in the polarisation curve have been presented (WOLSTENCROFT and NANDY, 1971; MAVKO et al, 1974). These have in general not been confirmed. SERKOWSKI et al (1975) have also pointed out that λ_{max} appears to be closely related to R, the ratio of total to selective absorption. When extinction curves are normalised to λ_{max} the

curves are in much better agreement (SERKOWSKI et al, 1975). By excluding stars showing evidence of circumstellar material, WHITTET and VAN BREDA (1978) tightened up this relationship and showed that λ_{max} is in fact a better predictor of R than the photometric methods normally used to determine this quantity. Recently surveys to find stars not strongly polarised have been carried out (TINBERGEN, 1979; TINBERGEN, 1981; KRAUTTER, 1980). In the infrared, the 9.7μ band has been shown to be polarised in the BN object (DYCK and BEICHMAN, 1974) and towards the Galactic centre (CAPPS and KNACKE, 1976; KNACKE and CAPPS, 1977).

While it had been realised that the rotation of position angle with wavelength implied a rotation of the angle of alignment of the grain axes along the line of sight (GEHRELS and SILVESTER, 1965), the smallness of the circular polarisation that consequently arose was responsible for the delay in its detection (SERKOWSKI, 1965; KEMP, 1972). It was found possible to derive the observed wavelength dependence of the circular polarisation from that of the linear polarisation, using the Kramers-Krönig relations (see for example LIPSON and LIPSON, 1969) (SHAPIRO, 1975; MARTIN, 1975). Several surveys for circular polarisation in reddened stars have been carried out (STOKES et al, 1974; MARTIN and CAMPBELL, 1976).

Various attempts have been made to see if polarisation changes occur across the diffuse bands. Early reports suggested that variations do occur (NANDY and SEDDON, 1970, 1973), but, more accurate studies show that the features are unpolarised (A'HEARN, 1972; MARTIN and ANGEL, 1974, 1975; FAHLMAN and WALKER, 1975).

2.3 The composition of interstellar grains

Using the Mie theory of scattering, theoretical extinction and polarisation curves can be produced for comparison with the observations. The input parameters to these calculations are the optical constants n and k of the grain material, their shape and size distribution and, if non-spherical, the degree and method of alignment of particle axes. (We use the notation $m = n - ik$ to denote the complex index of refraction.) Exact calculations are possible for spheres and infinite cylinders. If the polarisation curves are to be fitted then cylinders must be used, though the extinction produced by cylinders is similar (within 20%) to that of spheres with the same diameter. The same holds true for thin discs (GREENBERG, 1968). Calculations for infinite cylinders are a good approximation for grains with an axial ratio greater than about 2 (GREENBERG, 1968). Occasionally, other shapes have been used. SHAPIRO (1975), for example, used thin 'platelets' (oblate spheroids) of magnetite (Fe_3O_4) as the material occurs in this form in meteorites (JEDWAB, 1971). The imaginary part of the complex index of refraction, k, characterises the behaviour of a material at a particular wavelength as dielectric ($k \approx 0$) or metallic ($k > 0$). Materials with $k \gtrsim 0.1$ have an appreciable metallic character. As mentioned in section 1, the visual extinction observations can be fitted with rather general collections of dielectric or metallic particles. This is because scattering processes (i.e. those involving n rather than k) dominate in causing the observed extinction and polarisation. At present the visual polarisation and extinction are thought to be caused by aligned dielectric grains of radius $\sim 0.15\mu$. The derived radius is dependant on the refractive index (and hence specific material)

assumed. The scattering efficiency of a grain scales with the parameter (GREENBERG, 1968).

$$\rho = \frac{2\pi a}{\lambda}(n-1) \qquad (2.3.1)$$

where a is the radius of the grain, n its refractive index and λ the wavelength of interest. The above value for the radius was derived assuming n = 1.66, a value appropriate for terrestial silicates. If it is assumed that 'ices' of various sorts make up the scattering particles, with $n \simeq 1.33$, it is easy to see from (2.3.1) that the particles would need to be about 0.3μ in radius to fit the observations (McMILLAN, 1978). If metallic or graphite grains were used to fit the observations, they would be a lot smaller (0.05μ).

Evidence that the scattering grains are dielectric comes from several sources. Observations of the diffuse galactic light (LILLIE and WITT, 1976) and of reflection nebulae (MORGAN, 1980) suggest that the interstellar grains are non-isotropic scatterers in the visible. While both iron and graphite grains would scatter almost isotropically, dielectric particles could fit the observation (SPITZER, 1968). Observations of certain stars (eg ζ Ophiuchi) seem to show large depletions of certain elements with respect to cosmic abundance. The measurement imply large depletions not only of the light metals (Mg, Ca , Na) but also of O and N. Since O and N are cosmically abundant, it is necessary to postulate the existence of large amounts of H_2O and NH_3 ice in the medium. It would be natural to associate these ices with the interstellar grains. As will be discussed below, the circular polarisation observations also strongly indicate dielectric grains.

The visual observations of extinction and polarisation allow dielectric grains of almost any composition as long as the

refractive index of the material remains sensibly constant in the visual and near-infrared. This latter constraint arises from the observed validity of the Serkowski curve to describe the linear polarisation, according to certain authors (MARTIN, 1974; GREENBERG, 1979). When the 9.7μ infrared band was originally discovered it was remarked that terrestrial silicates exhibit a strong absorption here (WOOLF and NEY, 1969). However cosmic abundances rule out silicates forming the whole of the grains, and core-mantle models are more likely. The core could be silicaceous, of radius ~0.05μ and the mantle might be composed of 'dirty' ices (CH_4, NH_3, H_2O), of thickness ~ 0.12μ (GREENBERG, 1978). Oxygen-rich M-type supergiants often show the 9.7μ band which arises in the circumstellar shell. Such stars are thought to be producing silicate grains and ejecting them into the interstellar medium. The dirty ice mantle might then condense onto these silicate cores in one of the dense molecular clouds. Photodissociation and photoionization processes might cause more complex molecules to form in the mantle such as formaldelyde polymers (polyoxymethylene: ROCHE (1972); WICKRAMASINGHE (1974, 1975); COOKE and WICKRAMASINGHE (1977); WHITTET et al (1976)),'thiolins' (SAGAN and KHARE, 1979) or the intractable polymer of KNACKE (1977) that is found in the meteoritic carboneceous chondrites.

The latest studies of Oxygen depletion in the line of sight to ζ Ophiuchi (DE BOER, 1979) show that only about 25% of this element is missing rather than the 70% previously thought. The measurement allows (but does not require) a depletion of oxygen consistent with silicates alone. Several mixtures of uncoated particles have been proposed (GILRA, 1971; MATHIS et al, 1977). In order to be consistent with cosmic abundances, GILRA (1971) suggests that Silicon Carbide is an important constituent, while

MATHIS et al (1977) have silicon and graphite particles contributing roughly equally to the extinction in the visual.

Strong support for the visual polarisation being produced by grains consisting of at least some silicates comes from polarisation measurements across the 9.7μ band in the infrared. A clear increase in the polarisation is seen across the band, indicating that the feature arises in polarising grains (DYCK and BEICHMAN, 1974). Various workers have attempted to reproduce this band in the laboratory using samples of various sorts of silicates, (together with the 18μ band which is also attributed to silicates). Crystalline silicates, such as olivine, and pyroxine do not give good fits. These compounds show sharp absorption resonances occuring on top of the broad feature. The best fits are made with submicron particles of amorphous silicates (KRATSCHMER and HUFFMAN, 1979; DAY, 1979), but even here it is difficult to convincingly produce the 18μ feature at the correct wavelength and strength. MILLAR and DULEY (1978, 1980) have suggested that both the 9.7μ and 18μ bands arise in small metal oxide particles (MgO, CaO, SiO, FeO). The 9.7μ absorption is caused by SiO while the 18μ feature is attributed to MgO. Several authors have considered the ratio $\tau_{vis}/\tau_{9.7\mu}$ for amorphous silicates. Laboratory measurements suggest that the ratio should be of the order (1:1) (DAY et al, 1974). However, the observed ratio in the few objects for which such a comparison is possible (e.g. VI Cyg No 12) show the ratio may be as high as 20:1 (RIEKE, 1974). It is concluded that silicates are not a major contributor to the extinction in the visual. The band in astronomical sources may be weaker than is observed in the laboratory. Measurements of meteoritic silicates give a weaker 9.7μ feature (FRIEDEMANN et al, 1979), and porous or "fluffy" particles would also produce more visual extinction per unit

absorption at 9.7μ (BLANCO and BUSSOLETTI, 1980). Figure C2 shows such a fluffy particle collected from the interplanetary medium. Finally, if a component of the dust in the observed sources were showing the feature in emission, the apparent strength of the 9.7μ band would be reduced (GILLETT et al, 1975). If these attempts to reconcile the visual extinction and the 9.7μ feature are unsuccessful, models (such as that of MATHIS et al,(1977)) that use a substantial contribution from silicates in the visible may have to be reconsidered.

The infrared band at 3μ is usually interpreted as being due to water ice, which has an absorption at 3.07μ . LEGER et al (1979) have matched the short wavelength side of the profile with laboratory measurements of amorphous ice. The long wavelength 'tail' may be due to the C - H band stretching absorption at 3.4μ . However the ice band is only seen in dense clouds, and the problem then is: if core-mantle particles exist in the diffuse clouds, of what do they consist, if not of water ice? GREENBERG (1976) suggested that the H_2O was photolysed to form OH radicals which are unobserveable. Photolytic processes might also process the material of the mantle to form complex molecules (GREENBERG, 1979). All organic molecules containing C - H bands produce an absorption around 3.4μ , but this band has only been detected along a few lines of sight (e.g. Galactic centre, (WICKRAMASINGHE and ALLEN, 1980)). However the strength of the band is very dependant on the particular organic materials giving rise to it. Tholins (SAGAN and KHARE, 1979) show only a weak band, while the 'intractible polymer' (KNACKE, 1977) exhibits a strong feature. The lack of obvious absorption at 3.4μ is hence not a strong argument against the existence of complex organic molecules

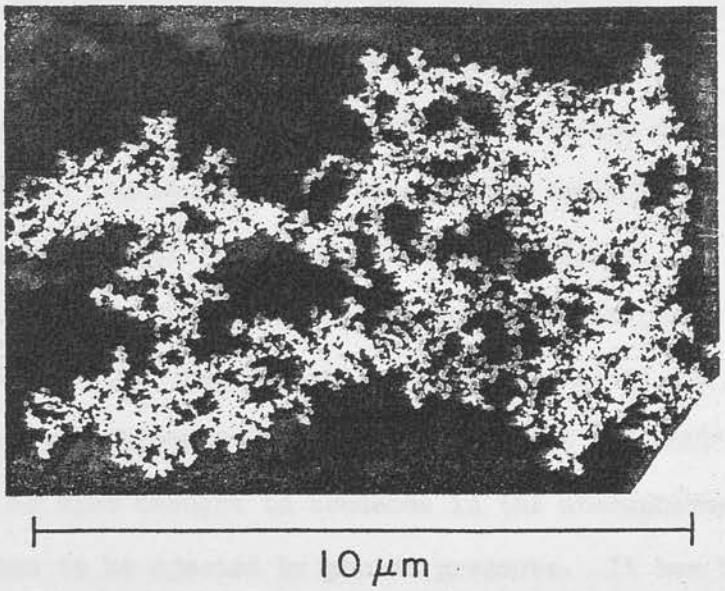

Figure C2: Example of a fluffy particle, collected at a height of 27 km over Mildwa, Australia, on March 16, 1971. From Millman, P.M. ("The Dusty Universe" ed.G.B. Field and A.G W. Cameron, Neale Watson, New York, p185).

making up or being part of mantles on the polarising grains.

It has been suggested that the 3μ & 9.7μ features arise in complex polysaccharides (HOYLE and WICKRAMASINGHE, 1977). Reasonable fits can be made to the observed profiles in BN (WICKRAMASINGHE and HOYLE, 1977). It is difficult to see however how the wide ratio in the strengths of these bands could be accommodated with this model (EGAN and HILGEMAN, 1978).

The circumstellar shells of carbon-rich stars do not show an absorption at 9.7μ but do exhibit a feature at 11.2μ. This is attributed to Silicon Carbide (SiC) (TREFFERS and COHEN, 1974). Graphite is also thought to condense in the atmospheres of these stars then to be ejected by photon pressure. It has been remarked (LEWIS and NEY, 1979) that in a number of objects, grains appear to condense at temperatures around 1000^{o}C (e.g. Novas, Wolf-Rayet stars). In some of these the 9.7μ silicate band is seen and the condensate is presumed to be silicaceous. In others it is not and the dust is thought to be graphite. It seems curious that the temperature of condensation is similar for the two types of grain. Lewis and Ney suggest that condensation is initiated about nuclei of Fe (in oxygen-rich stars) and Fe_3C (- Iron carbide cohenite, in carbon-rich stars). Both these substances would form condensation nuclei around 1000^{o}C. Other objects, such as the planetary nebular NGC 7027, show a number of infrared emission lines which are thought to be fluorescence from grains. These have been identified by comparison with laboratory spectra of a solid mixture of H_2O, CO, CH_3OH, CH_4, NH_3, C_2H_2, NO (ALLAMANDOLA and NORMAN, 1978; HAGEN et al, 1980). The lines are broad suggesting an origin in grains rather than in the gas. In particular, the 6.2μ and 11.3μ features are ice bands (ALLAMANDOLA and GREENBERG, 1979) rather than arising from the C = C double band in a polymerised

organic compound (KNACKE, 1977), or carbonate respectively. If the 11.3μ band had been carbonate, a stronger band at 7μ would have been seen (DORSCHNER et al, 1980). The band at 3.3μ is identified as being due to solid (rather than gaseous) methane (CH_4) (ALLAMANDOLA and GREENBERG, 1979). DULEY (1979) has suggested that some of the unidentified lines in the emission spectra of planetary nebulae in the visible are caused by fluorescence of zero-phonon lines arising at defect centres in small grains of MgO and CaO. The author supports the idea that the observed diffuse bands are also zero-phonon lines (see on), and so we are in effect seeing the diffuse interstellar bands in emission. In emission it is the sharpest bands that should be the most obvious.

The major features to explain in the ultraviolet are the 2175 Å 'lump' and the high very short wavelength extinction. A number of theories have been put forward for the 2175 Å absorption, but it is generally agreed that the symmetry of the feature implies that it arises in small grains ($a < 0.02\mu$). GILRA (1971) has argued that the absorption is due to collective processes in small near-spherical particles, rather than in transitions associated with multiple Carbon-Carbon bands in graphite (WICKRAMASINGHE, 1967). Such a resonance will occur at a wavelength close to $\varepsilon_1 = -2$, where ε_1 is the real part of the dielectric constant. The resultant band is rather dependant on both the shape and size of the particles and the very similar location of the peak wavelength ($\pm$ 40 Å, BLESS and SAVAGE (1972)) would imply that the graphite grains found along different lines of sight are of very similar shapes. Naturally by varying the number of graphite grains and the size distribution a good fit can be made to the observed profile (GILRA, 1971). Porosity ('fluffy' grains) can also widen the feature (BLANCO et al, 1980), while the near-sphericity of the grains implied by the

peak wavelength and the difficulty of aligning graphite grains presumeably explains the absence of polarisation in the band. GEHRELS (1974) has pointed out that other organic molecules containing the carbon-carbon double band might give rise to the 2175 Å feature. The absorption would be particularly strong in compounds containing - C = C - C = C - or - C = C - C $\equiv$ N. In particular HOYLE and WICKRAMASINGHE (1977) have suggested that the observed absorption is due to a sharp feature of bicyclic nitrogenated compounds ($C_8H_6N_2$, for example) on top of a broad feature formed by graphite in the manner discussed above. It is not clear how the considerable quantities of these compounds would be formed, though cosmic abundances would impose no constraints. A different suggestion is put forward by RUDKJØBING (1978) who attributed the band to an autoionization resonance in a photoionization continuum of O^-. The 2175 Å feature hence arises in the interstellar gas rather than the grains, and since it involves the destruction of O^-, an efficient mechanism must be invoked to regenerate the ion. As has been pointed out by KUMAR (1978) in connection with the diffuse bands a critical test of such a mechanism would be to observe the 2175 Å feature in the line of sight to a supernova. The pulse of electromagnetic radiation should upset the equilibrium and greatly weaken the feature. HUFFMAN and STAAP (1971) suggested that the 2175 Å band is caused by an absorption edge in silicates. However with this mechanism the position and shape of the band is very dependant on the size distribution. It also gives a 'flat-topped' and asymetric profile, neither of which is seen in practice. DULEY (1976) is of the opinion that the 2175 Å absorption arises from O^{2-} ions located at defect centres in very small grains of radiation-damaged metal oxides or silicates. MILLAR (1979) interprets the lack of correlation of carbon depletion with the strength of the band

as evidence for this interpretation. However, grains as small as these will not accrete (GREENBERG, 1968) and so a relation would not be expected even with the graphite or organic molecule interpretations.

The continuing increase in the extinction curve into the ultraviolet is attributed to large numbers of very small particles (0.005μ, if silicate, GREENBERG (1978)). Particles at these sizes are at the limit of validity of the Mie theory and bear more resemblance to the molecular aggregates of PLATT (1956). STEPHENS (1980) has shown that if these particles were amorphous silicates, the optical depth in the far ultraviolet is consistent with the strength of the 9.7μ infrared band. Possibly, the particles could be fragments of mantles from other grains which had 'exploded' perhaps by the exothermic reaction of free radicals (GREENBERG and YENCHA, 1973).

Serkowski's analytic representation of the wavelength dependence of linear polarisation has been very useful as a means of summarising linear polarisation measurements on reddened stars. It is usually written in a slightly different (but clearly equivalent) form to that shown as equation (2.2.2):

$$p(\lambda) = p_{max} \exp\left(-k \ln^2(\lambda_{max}/\lambda)\right) \qquad (2.3.2)$$

While this is a purely empirical curve, the parameters that characterise it (λ_{max} and k) can be interpreted in terms of the properties of the interstellar medium. The significance of a change in λ_{max} from its mean value (around 5500 Å) to a larger value (say, 6000 Å) can be seen directly from equation (2.3.1). An increase in λ_{max} by 10% implies either an increase in grain radius by 10% or a corresponding change in (n - 1), for example from 1.6 to 1.66. Observations show λ_{max} to vary by more than a factor of two, from 3300 Å (VI Cyg No 12) to 8000 Å (Walker 67, WILKING et al (1980)).

Increases in λ_{max} appear to be directly related to the observed depletion of heavy elements in the surrounding gas (CARRASCO et al, 1973). If the grains are accreting λ_{max} would increase as the grains became larger and would hence correlate with the depletion. Since R, the ratio of total to selective absorption is also correlated with grain size (MCMILLAN, 1978), the simple correlation between them is understandable (WHITTET and VAN BREDA, 1978). k is a measure of the 'sharpness' or halfwidth of the polarisation curve. As k increases, the halfwidth decreases. Because the wavelength interval over which visual and near infrared measurements can be obtained is relatively small, a change in k does not lead to a large difference in the observed wavelength dependence of polarisation. For ζ Ophiuchi, p_{max} = 1.5% and λ_{max} = 6000 Å. Changing the value of k from 1.15 to 1.25 would lead to the polarisation measured at 3000 Å decreasing from 0.86% to 0.82%, and the polarisation measured at 2.2μ decreasing from 0.22% to 0.18%. The width of the curve is dependant on a number of factors, the most important of these being the width of the size distribution of the grains, the degree of alignment of the grains and the grain shape and composition (GREENBERG, 1968). WILKING et al (1980) found a relation between k and λ_{max}, namely

$$k = 1.7 \lambda_{max} \qquad (2.3.2)$$

The authors interpret the relation in terms of prolate grains becoming more spherical as they accrete, or possibly in a narrowing of the size distribution as the mean grain size increases. Their discussion shows how few observational constrains there are on grain models. It is interesting to note that if changes in λ_{max} were due to changes in the real part of the refractive index, a relation similar to the above would be observed. With this

explanation one might need to think of low index ice grains 'fossilising' in interstellar clouds by replacement with heavy elements. Perhaps luckily, this mechanism probably would not give the observed range of k.

Equation (2.2.1) puts an observational lower limit on the polarising efficiency of a grain model which is dependant on both the properties of the grain material and on the degree of alignment of the grain axes in space (SERKOWSKI et al, 1975). Two sorts of alignment are commonly used in modelling: "picket fence" alignment, where static cylinders are all lined up with their axes parallel to each other; or "Davis-Greenstein" alignment where the cylinders spin very rapidly about a short axis and these short axes are aligned parallel to the local magnetic field (DAVIS and GREENSTEIN, 1951). While the former is assumed merely for computational convenience, the latter is generally accepted as describing the reality of the alignment process. DAVIS and GREENSTEIN (1951) presumed that the grains would rotate at a rate consistent with their temperature and the principle of equipartition of energy. Paramagnetic relaxation (for dielectric grains) would then align the spin axes with the local magnetic field. The theory has been extended to ferromagnetic particles by HENRY (1958). The problem is in generating the required amount of polarisation per unit reddening. With the strength of the magnetic fields found in the general medium, and the temperature of the grains estimated by energy balance considerations, the Davis-Greenstein mechanism does not give a good enough alignment to allow dielectric grains to produce the observed polarisation per unit reddening. Several solutions have been proposed involving either improving the alignment of the grains or increasing the polarisation produced. Graphite,

which acts as a dielectric or a metal depending on the plane of orientation, was suggested by CAYREL and SCHATZMAN (1954) to increase the amount of polarisation. Magnetic materials increase both the degree of alignment and the polarisation produced. Magnetite (Fe_3O_4) was proposed by SHAPIRO (1975) and shown to roughly fit extinction and both linear and circular polarisation observations within the constraint of cosmic abundance. It is possible to achieve considerably better alignment by incorporating magnetic impurities into dielectric particles (JONES and SPITZER, 1967; MATHIS, 1979) or using superparamagnetic ferrous oxide (FeO) (DULEY, 1978). Finally if the speed of rotation of the cylinders is increased, the aligning torque will be increased leading to improved alignment. A number of ways of achieving 'suprathermal' rotational velocities have been proposed (PURCELL, 1974; PURCELL, 1979; SPITZER and McGLYNN, 1979). The grains achieve near perfect alignment in this model. At the present time therefore it is not unreasonable to assume perfect or near-perfect Davis-Greenstein alignment when fitting models to the polarisation observations.

If the position angle of alignment of the grains varies along the line of sight due (presumeably) to variations in the galactic magnetic field, circular polarisation can be produced. The interstellar medium is acting as a waveplate, converting linear to circular polarisation. The wavelength dependence of the circular polarisation can be derived from the linear polarisation by the use of the Kramers-Krönig relations (see e.g. LIPSON and LIPSON, 1969). These relate the real and complex parts of the refractive index and hence also connect the birefringence and dichroism of the medium (MARTIN, 1975). The observations of circular polarisation

show a change in sign at a wavelength, λ_c, close to λ_{max} for the linear polarisation. MARTIN (1972) has shown that for a dielectric grain material, λ_c should be equal to λ_{max}. The observations suggest that in general this is very nearly the case, the ratio $\lambda_c / \lambda_{max}$ equalling 1.00 ± 0.03 (MARTIN and ANGEL, 1976). This is regarded as strong support for the dielectric nature of the grains. SHAPIRO (1975), however, by using magnetic grains to successfully model the linear and circular polarisation curves, has shown that certain metallic materials can reproduce this ratio. MARTIN (1975) has calculated polarisation curves with magnetite using a size distribution to fit the linear polarisation measurements, and rules out this particular material because it produces too much structure in the linear polarisation and gives a ratio $\lambda_c / \lambda_{max} = 0.87$. Observations of circular polarisation also give information on the galactic magnetic field MARTIN and CAMPBELL, 1976).

If the properties of the grains vary along the line of sight (i.e. k or λ_{max} change), as well as the angle of alignment of the grain axes, the position angle of polarisation will show a wavelength dependance. If only grain size (λ_{max}) varies, the wavelength variation will be monotonic (section 6). This property has been used to select stars which might exhibit circular polarisation (STOKES et al, 1975; McMILLAN, 1977). Measurements of position angle also give further information of the variation of grain parameters along the line of sight (SERKOWSKI, 1962; MARTIN, 1974; NEE and JOKIPII, 1979; NEE, 1980).

The origin of the diffuse interstellar lines is still very much an open question. The discussion of the last few pages has shown the necessity for several different grain populations in the

interstellar medium. Small (0.02μ) grains of graphite are needed to produce the 2175 Å absorption, very small grains (0.005μ) are required to give the large far ultraviolet extinction, and large grains (0.15μ) are needed to explain the visible extinction and polarisation. Which of these, if any, is the carrier of the diffuse bands? The features are generally thought to be formed on or by the grains because of their width, though some molecular transitions can produce broad bands. The lack of any variation in the continuum polarisation across the bands rules out their association with the polarising grains. If the polarising grains do not produce all the visual extinction, the grains responsible for the remainder could be the source of the diffuse bands. However even this is unlikely, because the constancy of the central wavelength and of the profiles from star to star as well as the symmetry of the profiles argues for an origin in very small grains (HERBIG, 1975; VAN DE HULST, 1957; GREENBERG and HONG, 1974). More recently PURCELL and SHAPIRO (1977) have shown that the profile would not be symmetric even in very small grains, though the band from an assembly of grains might well appear symmetric. The assymetries found in some bands could be caused by the contribution of components from clouds with differing radial velocities (SAVAGE, 1976; DANKS and LAMBERT, 1976; WELTER and SAVAGE, 1977). Since the larger grains are the only ones that can accrete (see for example GREENBERG, 1978) the diffuse bands cannot arise in grain mantles, but must arise in the grains themselves. Of course, the mantle material could be dispersed by various mechanisms and exist as independant small particles - debris - in the medium (GREENBERG and YENCHA, 1973)

Although the particles producing the 2175 Å feature are required to be of a specific material (probably graphite), the very small particles

could be a mixture of materials. This would explain the relatively poor correlation of the far ultraviolet extinction with the diffuse band at 4430 Å.

A number of differnt ideas have been put forward as to the source of the diffuse bands including both organic and inorganic materials. A high molecular weight compound, magnesium tetrabenzphorphyrin ($MgC_{46}H_{30}N_6$) was suggested (JOHNSON, 1972, 1977) but is not now thought to be a candidate (DONN and KHANNA, 1980). Other more general organic molecules have been suggested (DULEY and McCULLOUGH, 1977). Greenberg's 'yellow polymer' found in laboratory photolysis experiments (GREENBERG, 1981) can produce the 4430 Å band, and possibly the 5780 Å and 5797 Å bands too. This too has high molecular weight ($\sim$500). These complex molecules would have to be formed in the mantles of large grains and then expelled from the surface such that the material existing as small grains would totally dominate any material remaining on the grain. The necessity for photoprocessing would explain why the diffuse bands do not appear in dense clouds where the ultraviolet flux is less important, and further mantles could grow, and in circumstellar shells, where the dust is relatively young.

Solid-state transistions in small metal oxide grains (MgO, CaO) have been suggested by DULEY (1977). The transitions would be zero-phonon lines and sidebands which are sharper than transitions which involve multiple phonon production. Duley explains the bands at 5362 Å, 5705 Å, 6425.7 Å and 6699.4 Å as zero-phonon lines, and those at 5535 Å, 6177 Å, 6196 Å and 6314 Å as phonon sidebands. The oxide particles would be $\sim$50 Å in diameter. The transitions are associated with defect centres caused by radiation damage. Duley has also suggested that transition metal ions in oxide grains might cause some of the diffuse bands (DULEY, 1979). Transitions

that would be parity-forbidden in ordered crystals become allowed in disordered crystals. The high temperature of the grains in circumstellar clouds are supposed to 'anneal' the grains, removing these crystal defects and weakening the diffuse bands. In molecular clouds, the defect centres could be 'poisoned' by the growth of mantles (MILLAR and DULEY, 1979).

A number of problems have to be overcome if the diffuse bands are to be formed by molecular transitions in the interstellar gas. However, such a source does explain the lack of variations in the profile shape and in the central wavelength in different stars. Rudkjóbing has suggested that the diffuse bands at 4430 Å, 4760 Å, 4890 Å and 6180 Å might be produced be preionization of H^-, and the diffuse bands 5780 Å and 5797 Å might be produced by preionization of O^- (RUDKJØBING, 1969; INGEMANN-HILBERG and RUDKJØBING, 1970). Such processes give bandwidths of roughly the correct size, but involve the destruction of the ions involved. FANO (1961) has shown that preionization processes give assymetric profiles. WELTER and SAVAGE (1977) and SAVAGE (1976) show that the line profiles observed do not have the broad wings shown in Fano's theoretical profiles. Other forms of transition have been described which produce diffuse features without destroying the molecule (SMITH et al, 1977; DOUGLAS, 1977). Since the diffuse bands appear strongly in the diffuse clouds, a molecular origin for the bands can only involve relatively simple molecules. These nondissociative transitions can indeed occur in small chain or 'quasiplanar' molecules (above references, and WEBSTER, 1980; MITCHELL and HUNTRESS, 1979).

The Very Broad Structure (VBS) has been noticed by a number of authors, but little systematic study has been made of it.

HAYES et al (1974) interpreted the VBS in terms of two very broad absorptions. BORG (1967) attributed the features to structure in the optical constants of graphite, but more recent laboratory measurements fail to confirm the presence of such features (TOSATTI and BASSANI, 1970). MANNING (1975) suggested magnetite (Fe_3O_4), and HUFFMAN (1977) has indeed found structure similar to the VBS in the optical constants of this oxide. VAN BREDA and WHITTET (1981) have shown that an identification with magnetite is consistent with the cosmic abundance of iron.

It is worthwhile to summarise the picture for the visible part of the spectrum before proceeding to the new measurements. Elongated dust grains in physically distinct clouds are aligned at different angles along the line of sight and give rise to linear polarisation and reddening of light passing through them. The grains may be core-mantle particles with an outside radius of $\sim 0.15\mu$, the core being of silicate or metal oxide composition and the mantle of photolysed C:N:O:H compounds (Greenberg). Alternatively the particles may be bare but of more than one composition, including silicates and graphite (Mathis). The diffuse bands do not arise in these grains, but the VBS may do so.

3. Aims of the present study

The overall wavelength dependence of extinction in the range 4000-7000 Å follows an inverse wavelength law, with about 4½ magnitudes of absorption at 4000 Å, falling to 2.3 magnitudes at 7000 Å, when E(B-V)= 1.0. Superimposed on this λ^{-1} dependence there is structure of various scalelengths from 1-1000 Å, the nomenclature for which depends on which range of scale lengths is being considered. The fine structure in the extinction curve is identified with the diffuse bands, with scale lengths of 1 to 50 Å. These vary from the broad (30 Å) band at 4430 Å to the sharp (1 Å) band at 5797 Å. By broad band structure (BS) we shall mean structure of scale lengths 50 to 250 Å. Some features in the class have been listed by HERBIG (1975). Structure on scalelengths greater than this will be referred to as Very Broad Structure (VBS). These definitions differ slightly from those of REX (1974). The aim of the present study is to examine with high precision the wavelength dependence of linear polarisation in reddened stars, to detect structure in the polarisation of scalelengths 100-1000 Å and to examine how such structure relates to features in the extinction curve. At present the extinction curve and both circular and linear polarisation curves can be fitted with rather general mixtures of materials: the discovery of spectral features in the polarisation would introduce important constraints on the composition of the polarising grains, and the mechanism by which they are aligned. The relation of such features to structure in the extinction curve is also important, as of course is structure in the extinction curve in its own right. For various reasons it is easier to detect features in the polarisation curve than in the extinction curve. Extinction measurements are subject to a host of problems concerned with the

selection of the comparison unreddened star. Mismatching of spectral types and hence of the Balmer Jump and the hydrogen lines is one of them, while another is the possibility of circumstellar material. While circumstellar material may cause intrinsic polarisation, and the changing position angle of the galactic magnetic field may cause problems of interpretation, the detection of spectral features in the curves is relatively trouble-free. Further, once one has a reliable high precision spectropolarimeter, polarimetry is a lot easier and less subject to systematic errors than high precision photometry. The best extinction measurements available have errors of the order of 0.005 magnitudes. We may use the relation between a feature in the extinction and a feature in the polarisation proposed by MARTIN & ANGEL (1974) (see section 6.2),

$$\frac{\Delta p}{p} = f \frac{\Delta \tau}{\tau} \qquad (3.1)$$

where p and τ are the continuum polarisation and optical depth, Δp and $\Delta \tau$ are small changes in these quantities, and f is a constant with the value 1.4 ± 0.4. This relation is valid for an absorption feature carried on grains that give rise to both the extinction and the polarisation in the visible. It can hence be shown that a feature in the extinction of 0.005 magnitudes corresponds to $\Delta p/p \sim 0.2\%$, for E(B-V) = 1 mag at 5500 Å, or $\Delta p \sim 0.01\%$ on ζ Ophiuchi. The individual measurements on this star reported in the next section have errors of this order and are often below 0.010%.

The Very Broad Structure in the extinction curve was originally noticed by WHITEOAK (1966) and has scalelengths greater than 1000 Å. This study is not directed at such structure for the following reasons. Because of the high precision required, and the fact that we are only using a single channel detector, coverage over the complete

spectrum for any one star takes a great deal of observing time. Because of this, measurements have to be collected on a number of telescopes and combined. Because of small instrumental effects, this involves some normalisation of data, using multiplicative factors for the degree of polarisation, and zeropoint corrections for the position angles. The resulting cumulative effect of small errors makes deduction of small differences over large wavelength intervals unreliable.

As the spacing of data points was chosen as 50 Å, and the resolution of the instrument set to a similar value, the present observations are not very useful in detecting polarisation variations on scalelengths less than 100 Å. However, if the diffuse bands are 'carried' on the same dust grains as produce the polarisation, polarisation variations will occur and will be in accordance with the equation (3.1). Accurate measurements of the polarisation across diffuse bands have been carried out by MARTIN & ANGEL (1974, 1975), A'HEARN (1972) and FAHLMAN & WALKER (1975) and no detectable increase has been found. However, if the carrier of the diffuse bands is a chemical impurity rather than a property of small grains (as was suggested by DULEY & McCULLOUGH (1977)), it may well be present in the polarising grains in the line of sight to some stars. It is hence worthwhile to use the above equation (3.1) to calculate the effect of any polarisation increase across the strongest diffuse bands on the 50 Å resolution measurement containing the band.

The drop in magnitudes across a diffuse band is given by

$$\Delta M = -2.5 \log (1 - W/50) \qquad (3.2)$$

where W = equivalent width of the diffuse band. Writing (3.1) in magnitude terms we have

$$\frac{\Delta p}{p} = f. \frac{\Delta m}{A_\lambda} \qquad (3.3)$$

Where A_λ = continuum extinction at any wavelength, given by

$$A_\lambda = \frac{E(\lambda-V)}{E(B-V)} + R \quad E(B-V) \qquad (3.4)$$

E (λ-V) and E(B-V) being colour excesses and R a constant. We consider the cases of three stars (ζ Ophiuchi, 55 Cygni and χ Aurigae) and the diffuse bands (4430 Å, 5780 + 5797 Å and 6384 Å). In the above equations, f = 1.4 and p is given by the Serkowski curve with p_{max} and λ_{max} taken from SERKOWSKI et al. (1975). R = 3.1, $E(\lambda-V)/E(B-V)$ is taken from SAVAGE & MATHIS (1979) and E(B-V) is also taken from SERKOWSKI et al (1975). Values for the equivalent widths for the diffuse bands 5780, 5797 and 6284 Å were taken, along with the central depth for 4430 Å, from SNOW et al (1977). For ζ Ophiuchi, values for the 5797 Å and 6284 Å bands were not available. The equivalent width for 5797 Å band was hence derived from the relation with 5780 Å given in WU (1973) and that for 6284 Å estimated from the relation with E(B-V) also given in SNOW et al (1977). As HERBIG (1975) gives both the central depth and the equivalent widths of the 4430 Å band, it was possible to estimate the equivalent widths from the central depths by plotting Herbig's data, and reading off the value. The resulting predicted polarisation change measured in 50 Å bands including the diffuse bands is given in the table below (Δp in per cent).

$\frac{\Delta p}{\text{Star/band}}$	λ4430	λ5780 + λ5797	λ6284
ζ Ophiuchi	0.02	0.02	0.01
55 Cygni	0.07	0.03	0.02
χ Aurigae	0.05	0.03	0.02

The maximum effect in each case is roughly equivalent to the error of the individual measurements on that star. Clearcut effects are hence unlikely to be detected at the diffuse bands.

In this study, we use the Serkowski curve to fit the data:

$$\ln(p/p_{max}) = -k \ln^2 (\lambda/\lambda_{max}) \quad . \tag{3.5}$$

Previously, k was taken to be a constant averaging 1.15 over all stars (SERKOWSKI, 1973, 1975). Later authors have allowed k as a free parameter in fitting observations of the interstellar polarisation (e.g. CODINA-LANDABERRY & MAGALHAES, 1976), and recently WILKING et al (1980) have suggested the assignment

$$k = 1.7 \lambda_{max} \tag{3.6}.$$

The procedure adopted below in looking for features is first to calculate a best-fitting Serkowski curve allowing k as a free parameter, and then to display the data as deviations from this curve. The fitting was done using a weighted least squares fit to the quadratic equation

$$(y - y_o) = -k(x - x_o)^2 \tag{3.6}$$

solving for the three unknowns. The Serkowski curve is, in this thesis, only accepted as a convenient analytical curve that approximately matches the observed dependence of polarisation on wavelength. A major property of this curve, namely

$$p(\lambda/\lambda_{max}) = p(\lambda_{max}/\lambda) \tag{3.7}$$

is not characteristic of curves derived from detailed scattering calculations, although admittedly it is a good approximation. If structure is detected in the polarisation which is invarient (after scaling) from star to star, it may well be the result of the less than perfect approximation of the Serkowski 'law' to the more complex scattering curves. The analytic form of equation (3.5) has been used to derive expressions for the case of a medium with changing grain alignment (MARTIN, 1974) and for the investigation of the interstellar circular polarisation (MARTIN, 1975). Since the

analytic form of equation (3.5) has caused some problems, it should be pointed out that since the Serkowski curve is only an analytical approximation, we are at liberty to select another analytic expression which represents the data over the required band pass and has a more tractable form. As an example, consider the curve

$$p/p_{max} = 2^{K}\left\{\frac{\lambda}{\lambda_{max}} + \frac{\lambda_{max}}{\lambda}\right\}^{-K} \qquad (3.8)$$

The accompanying figure (Fig.C17) gives a comparison of this curve with the Serkowski curve where k = 1.15. When K = 2.5, the above representation (henceforward referred to as the Reciprocal curve) lies within ±1% of the Serkowski curve in the wavelength interval 0.22μ to 1.40μ. If k=2.6, the Reciprocal curve fits the Serkowski curve to within ±2% in the interval 0.18μ to 1.76μ. In both cases the Reciprocal curve is higher than the Serkowski curve in the 2-5μ region, and it is perhaps noteworthy that the observations also fall above the Serkowski curve in this region (e.g. MATHIS, 1979).

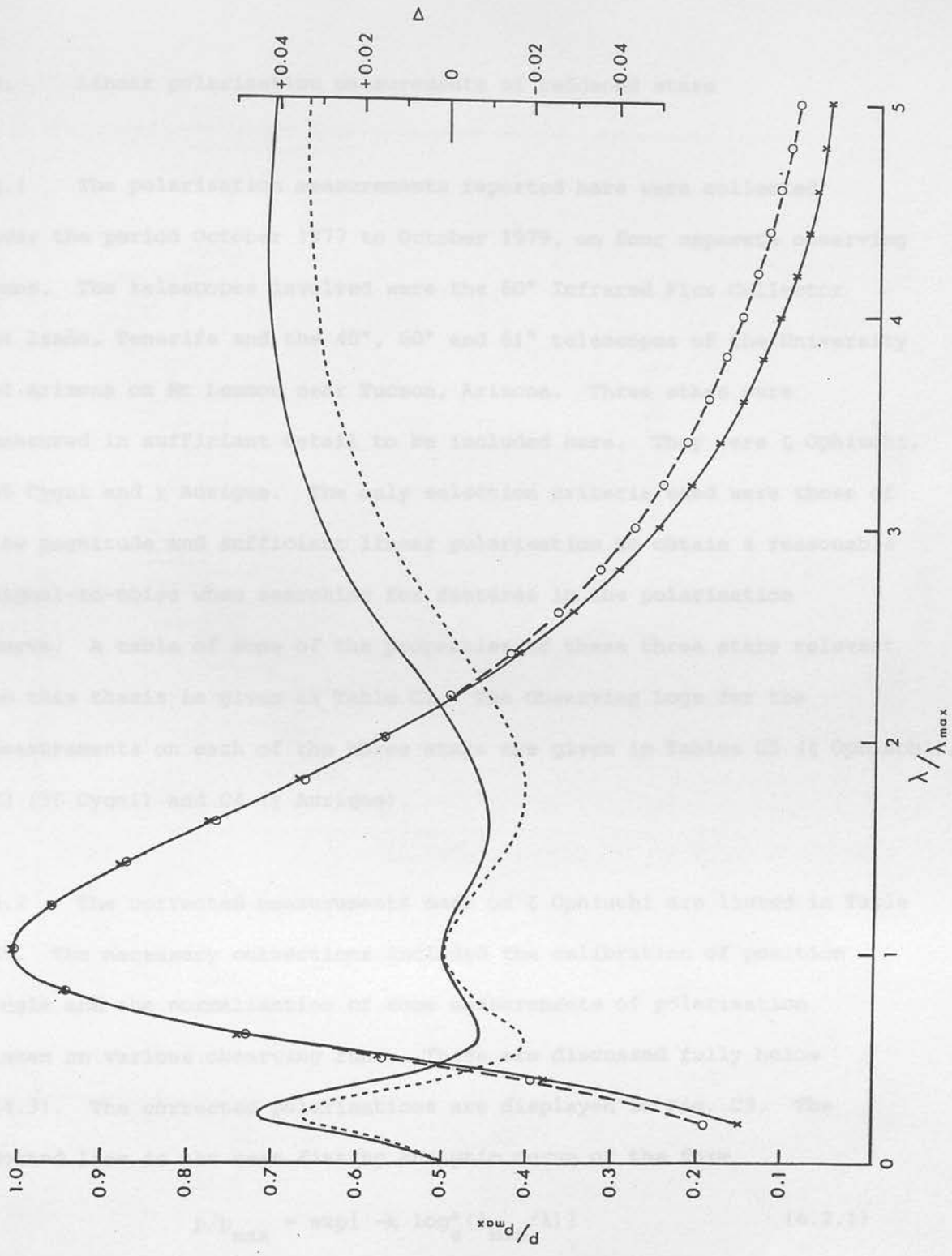

Figure C17: A comparison of the Serkowski analytic approximation to the wavelength dependence of interstellar polarisation and the Reciprocal approximation. The crosses connected by a solid line illustrate the Serkowski curve (with k = 1.15) while the open circles and dashed line follow a Reciprocal curve (K = 2.5). Observations show that polarisations are larger than predicted by the Serkowki law in the infrared. The solid line without crosses shows the difference between the above curves, in the sense Reciprocal minus Serkowski (righthand scale). The dotted line without points shows the difference between the Reciprocal and Serkowski curves when K = 2.6 (and k = 1.15).

4. Linear polarisation measurements of reddened stars

4.1 The polarisation measurements reported here were collected over the period October 1977 to October 1979, on four separate observing runs. The telescopes involved were the 60" Infrared Flux Collector at Izaña, Tenerife and the 40", 60" and 61" telescopes of the University of Arizona on Mt Lemmon near Tucson, Arizona. Three stars were measured in sufficient detail to be included here. They were ζ Ophiuchi, 55 Cygni and χ Aurigae. The only selection criteria used were those of low magnitude and sufficient linear polarisation to obtain a reasonable signal-to-noise when searching for features in the polarisation curve. A table of some of the properties of these three stars relevant to this thesis is given as Table C1. The Observing Logs for the measurements on each of the three stars are given in Tables C2 (ζ Ophiuchi), C3 (55 Cygni) and C4 (χ Aurigae).

4.2 The corrected measurements made on ζ Ophiuchi are listed in Table C5. The necessary corrections included the calibration of position angle and the normalisation of some measurements of polarisation taken on various observing runs. These are discussed fully below (4.3). The corrected polarisations are displayed in Fig. C3. The dotted line is the best fitting analytic curve of the form

$$p/p_{max} = \exp\{ -k \log_e^2(\lambda_{max}/\lambda) \} \qquad (4.2.1)$$

(SERKOWSKI, 1973). The curve was fitted by a weighted least squares procedure, from which all points at wavelengths less than 3300 Å were excluded. The parameters derived were:

$$p_{max} = 1.67\% \qquad \lambda_{max} = 6100 \text{ Å} \qquad k = 1.24$$

The full line is a freehand representation of the data after the

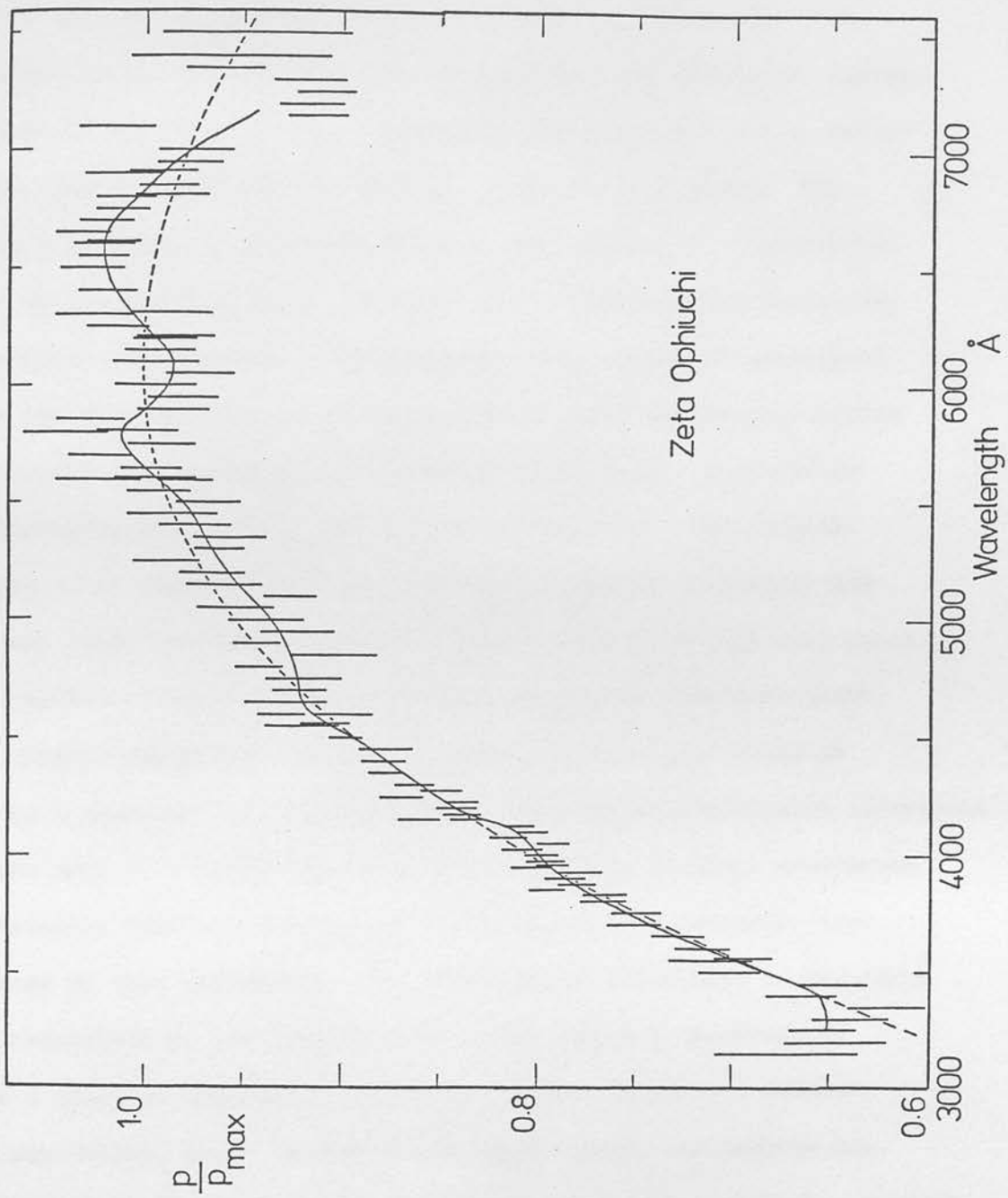

Figure C3: Wavelength dependence of the degree of linear polarisation for ζ Ophiuchi. The dashed line shown in the best-fitting Serkowski curve. The ordinate axis is normalised to the fitted value of p_{max}. The full line is a smoothed representation of the measurements.

smoothing procedure described below had been applied. Figures C4 and C5 show the dependence of position angle on wavelength. The position angles plotted have been corrected to the equatorial system. Figures C6 and C7 show the polarisation data again but now as deviations from the best-fitting analytic curve detailed above. The solid line shown on each of these last four graphs is a representation of the smoothed data. The smoothing procedure used is to take a weighted running mean of four points. The wavelength associated with the derived value is a simple mean of those of the four points concerned. The smoothed data are shown as Table C6. This choice of smoothing algorithm should perhaps be defended. The original points to be smoothed were very unevenly spaced in wavelength and in some cases had widely different errors associated with each point. Some method of weighting by the errors associated with each point was clearly essential. One way of smoothing this data would be to use a gaussian smoothing function. Here measurements would contribute to the mean at a particular wavelength according to their wavelength differences from that wavelength and weighted by a gaussian curve centred at that wavelength. The procedure is equivalent to degrading the resolution of the data to (say) 200 Å, using a spectrometer with a gaussian instrumental profile. Such a procedure, however, is complicated, would introduce wavelength errors and degrade the resolution in parts of the spectrum where it is not necessary. However, the instrumental profile of our spectrometer for measurements such as these is trapezoidal - nearly rectangular - and certainly far from a gaussian curve. The procedure adopted is equivalent to smoothing with a trapezoidal spectral profile. The effective resolution of the smoothed data varies with wavelength but this is clearly visible in the graph as a clustering of points. This procedure therefore

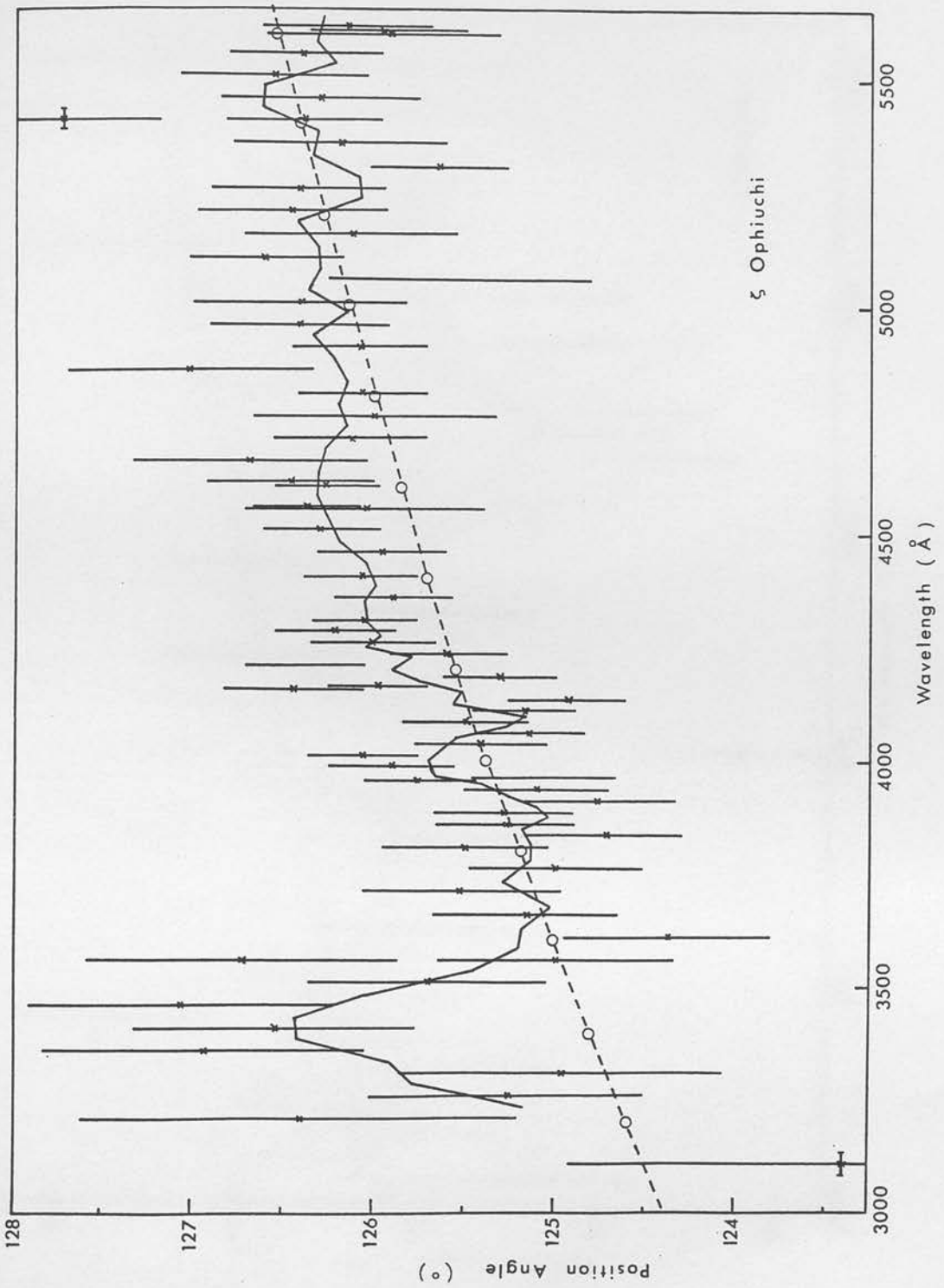

Figure C4· Wavelength dependence of the position angle of linear polarisation for ζ Ophiuchi. The full line represents a 4-point weighted running mean. The dashed line (and open circles) illustrate a rough model fit (see text). Position angles are in the equatorial system.

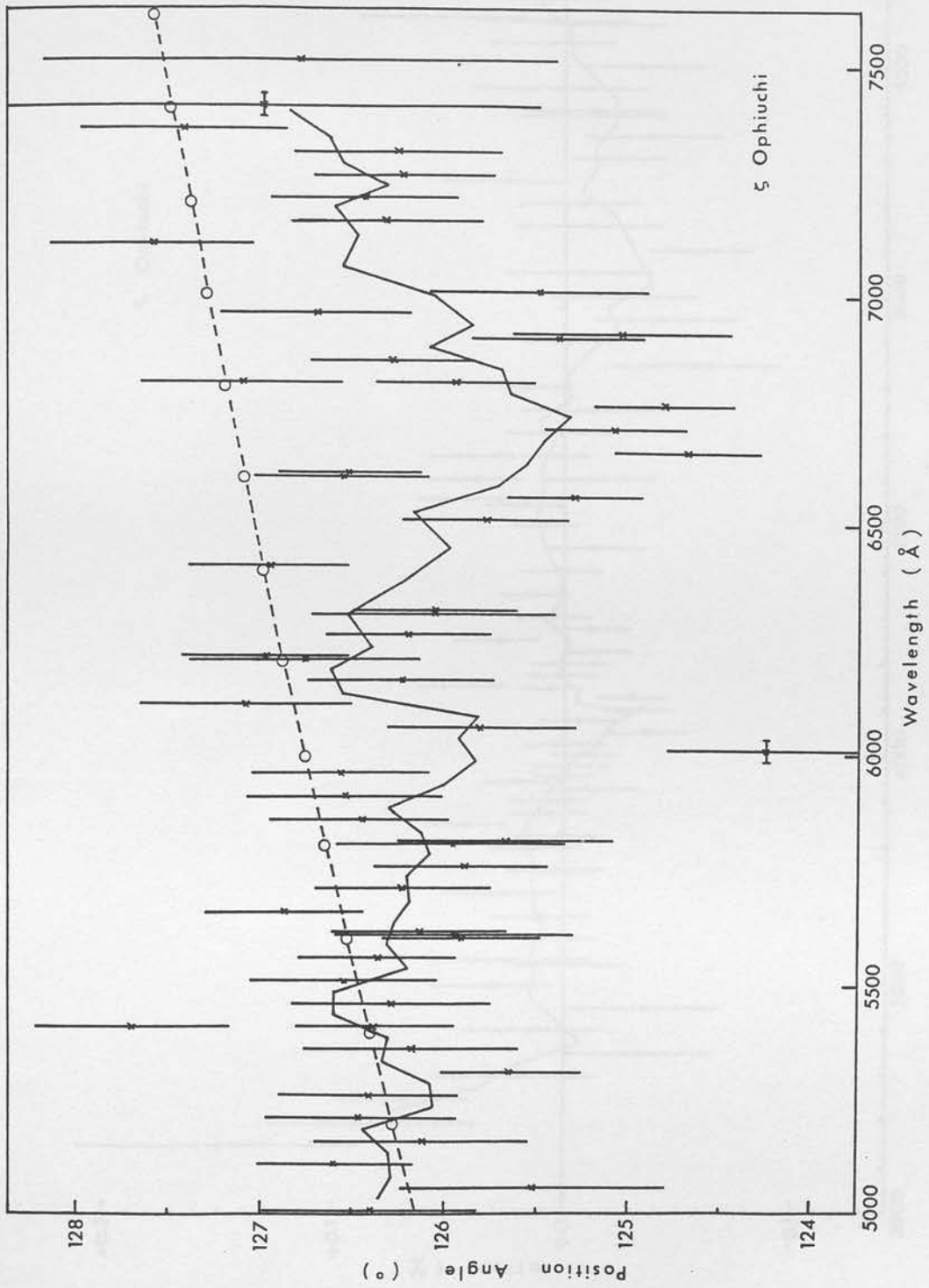

Figure C5: Wavelength dependence of the position angle of linear polarisation for ζ Ophiuchi. The full line represents a 4-point weighted running mean. The dashed line (and open circles) illustrate a rough model fit (see text). Position angles are in the equatorial system.

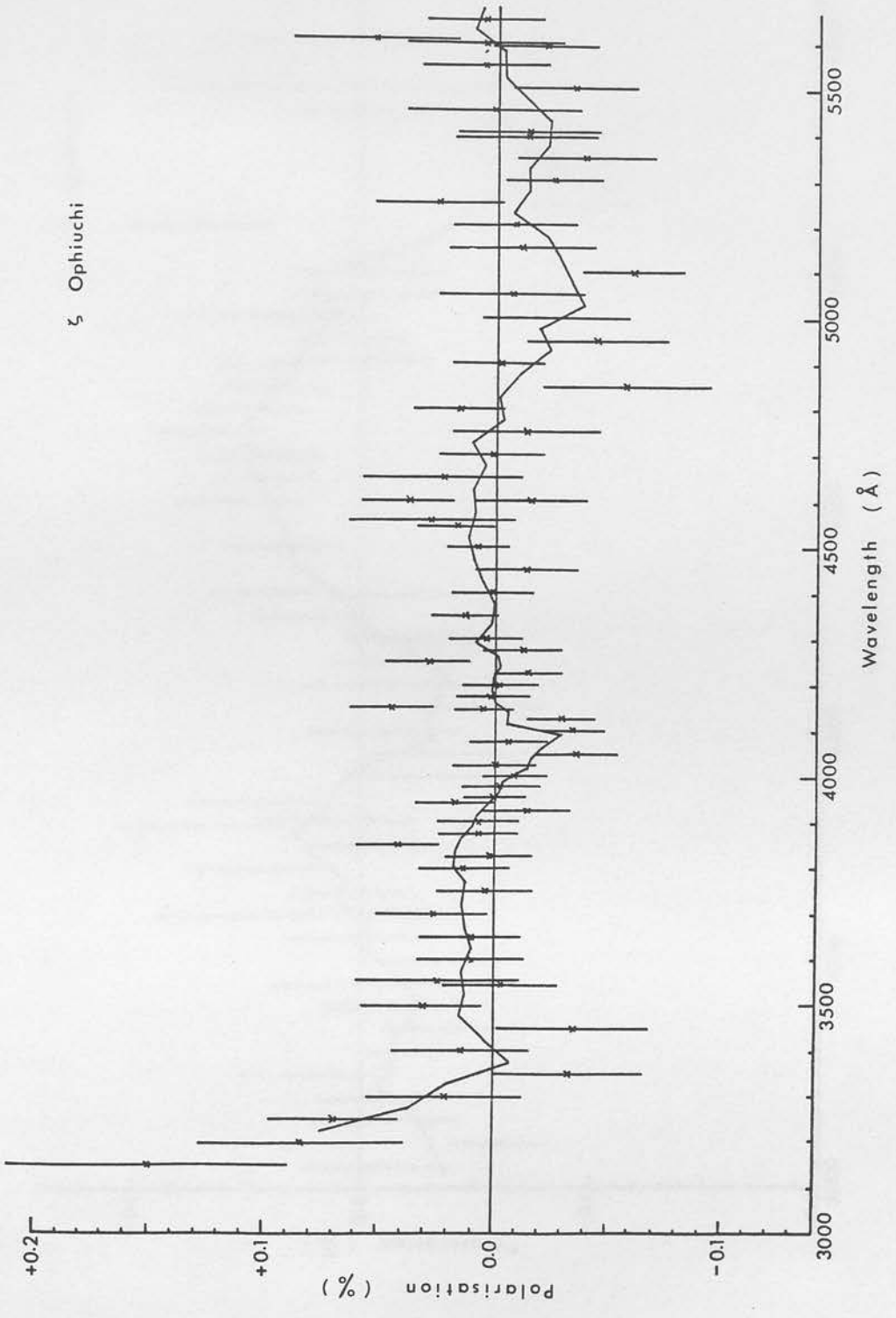

Figure C6· Wavelength dependence of the degree of linear polarisation for ζ Ophiuchi. The best-fitting Serkowski curve has been subtracted from the measurements shown. The full line represents a 4-point weighted running mean (see text).

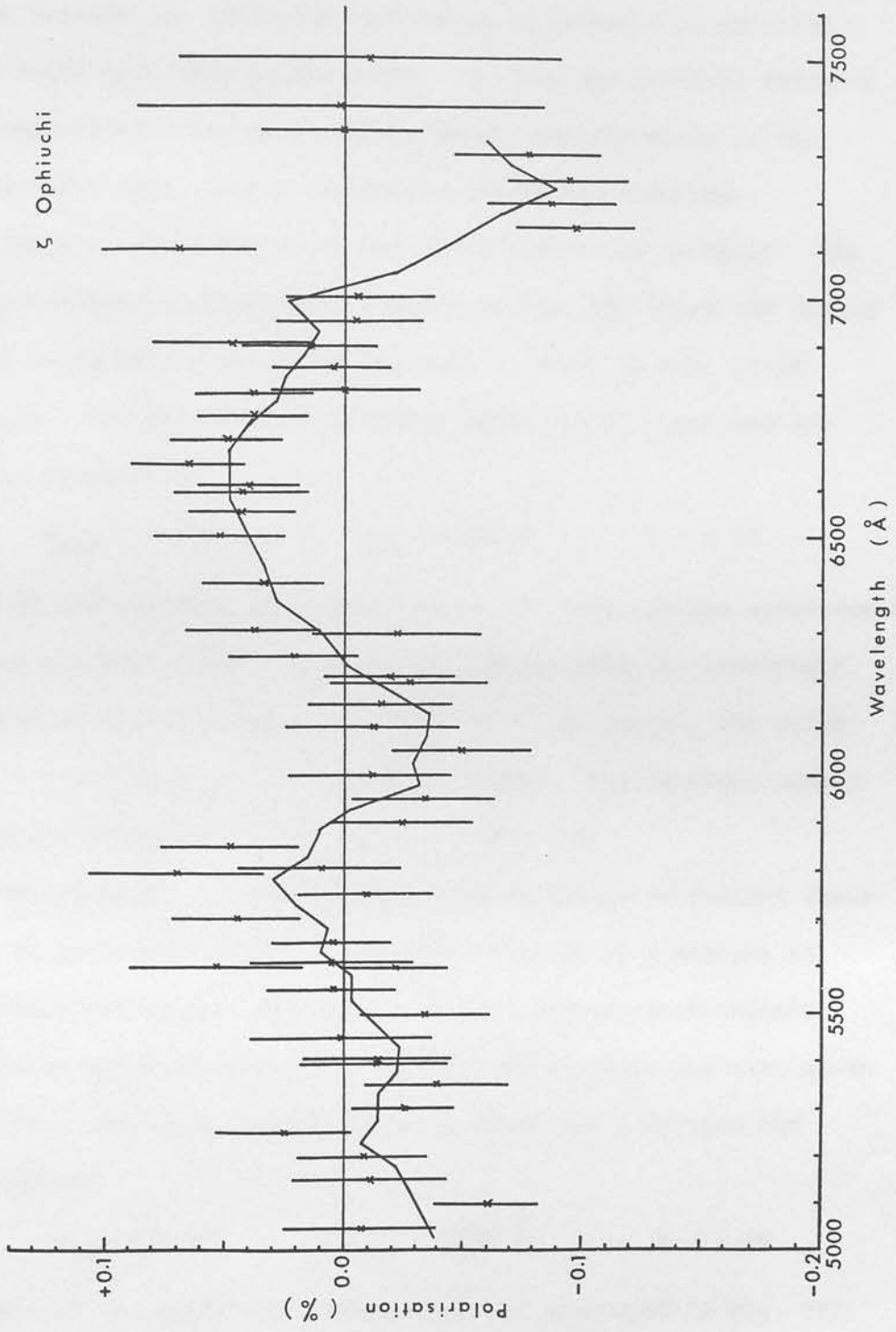

Figure C7: Wavelength dependence of the degree of linear polarisation for ζ Ophiuchi. The best-fitting Serkowski curve has been subtracted from the measurements shown. The full line represents a 4-point weighted running mean (see text).

does not degrade the effective resolution as severely in spectral regions where many data points exist. As such any possible features in the measurements are more clearly shown, and the error in the smoothed curve kept roughly comparable across the spectrum.

Table C7 shows the corrected measurements for 55 Cygni. The linear polarisation measurements appear in Fig. C8, where the dashed and full lines have comparative meanings to those in Fig. C3 of ζ Ophiuchi. The best-fitting analytic curve for 55 Cygni had the following parameters:

$$p_{max} = 3.00\% \qquad \lambda_{max} = 5410\ \text{Å} \qquad k = 1.36$$

Figures C9 and C10 show the deviations of the polarisation measurements from this analytic curve. Figures C11 and C12 show the wavelength dependence of position angles for this star. As before, the solid line is a representation of the smoothed data. The smoothed linear polarisation measurements are shown in Table C8.

Unfortunately, it was not possible to obtain sufficient observations to provide as good a wavelength coverage on χ Aurigae as on the other two stars. The corrected polarisation measurements are given in Table C9, while the smoothed data points are also given (Table C10). The best-fitting analytic curve for χ Aurigae had the parameters

$$p_{max} = 2.05\% \qquad \lambda_{max} = 6010\ \text{Å} \qquad k = 1.04$$

Deviations of the corrected measurements are displayed in Fig. C13. The wavelength dependence of the position angles is shown in Fig. C14.

4.3 When the spectropolarimeter is taken off one telescope and mounted onto another, certain calibrations are necessary. The most obvious of these is the necessity to recalibrate the zero of the

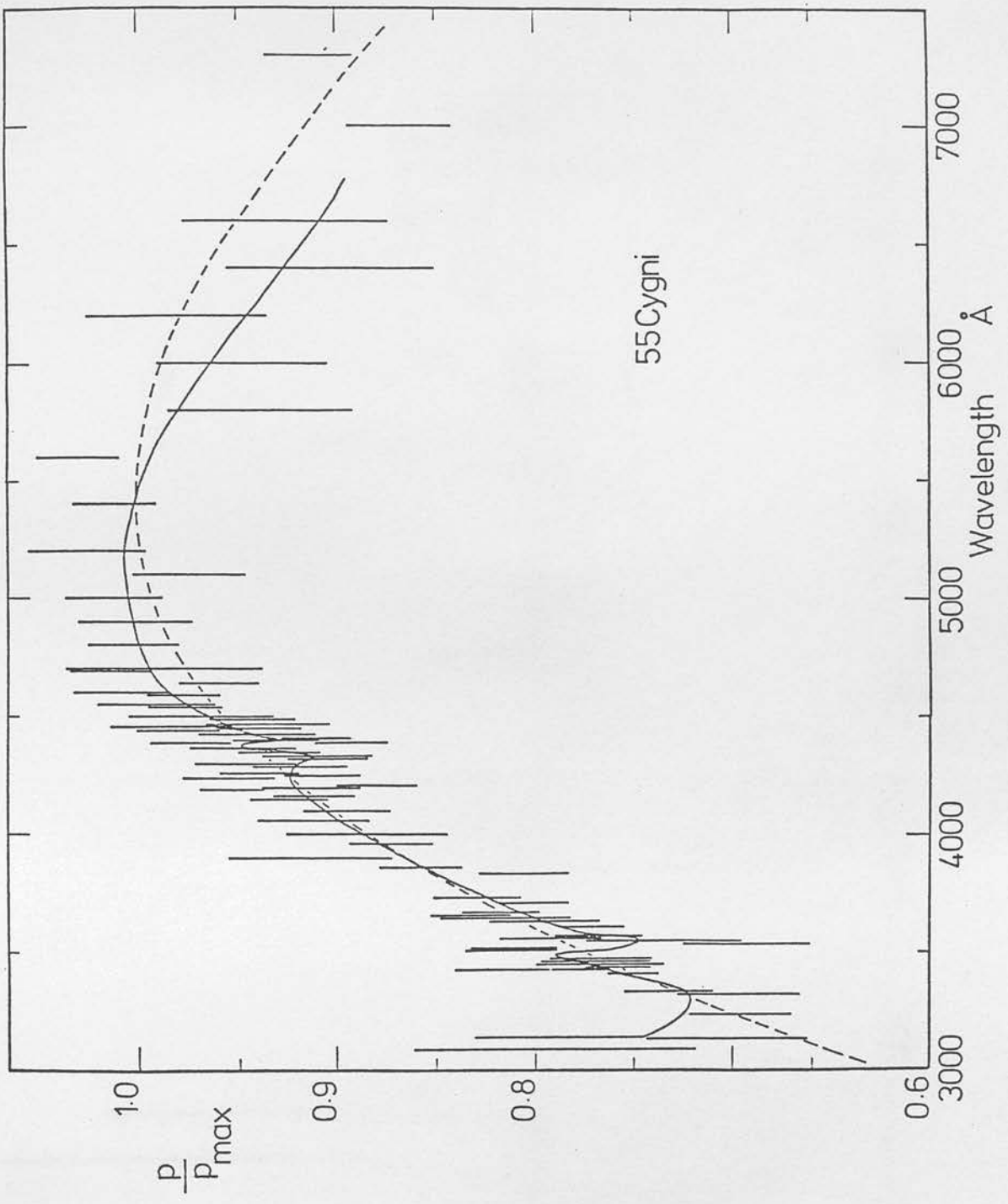

Figure C8: Wavelength dependence of the degree of linear polarisation for 55 Cygni. The dashed line shown is the best-fitting Serkowski curve. The ordinate axis is normalisdd to the fitted value of p_{max}. The full line is a smoothed representation of the measurements.

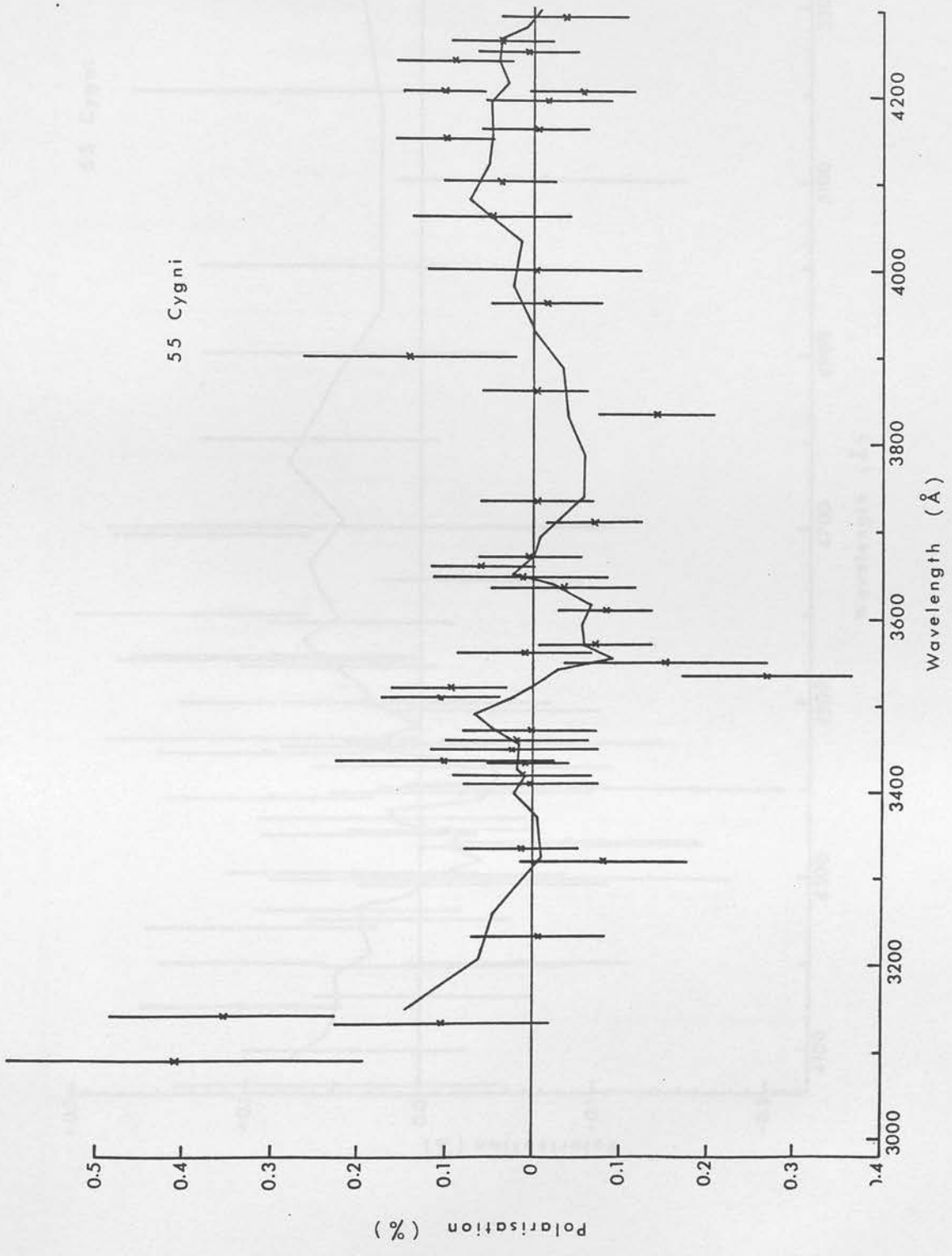

Figure C9: Wavelength dependence of the degree of linear polarisation for 55 Cygni. The best-fitting Serkowski curve has been subtracted from the measurements shown. The full line represents a 4-point weighted running mean (see text).

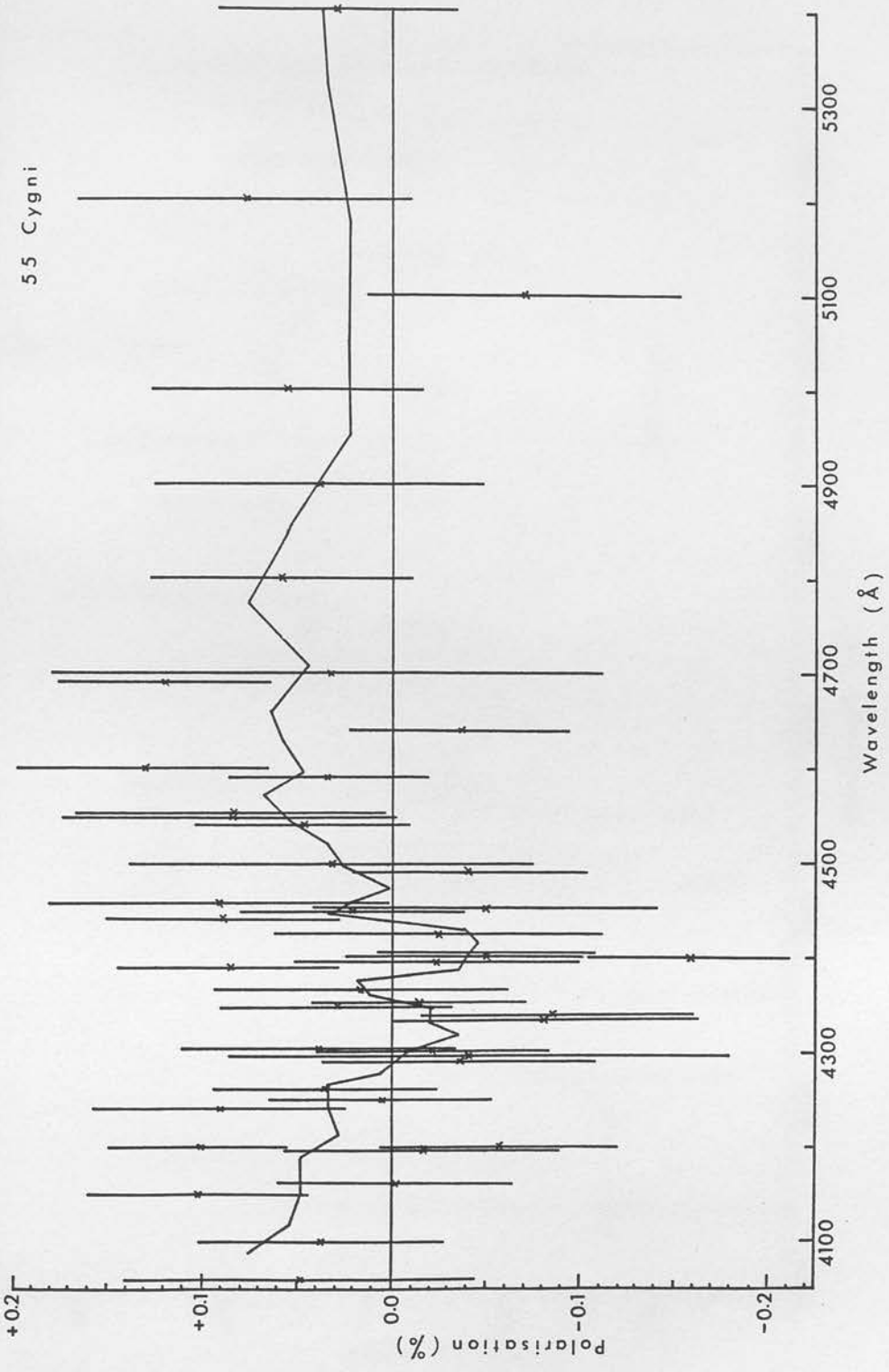

Figure C10: Wavelength dependence of the degree of linear polarisation for 55 Cygni. The best-fitting Serkowski curve has been subtracted from the measurements shown. The full line represents a 4-point weighted running mean (see text).

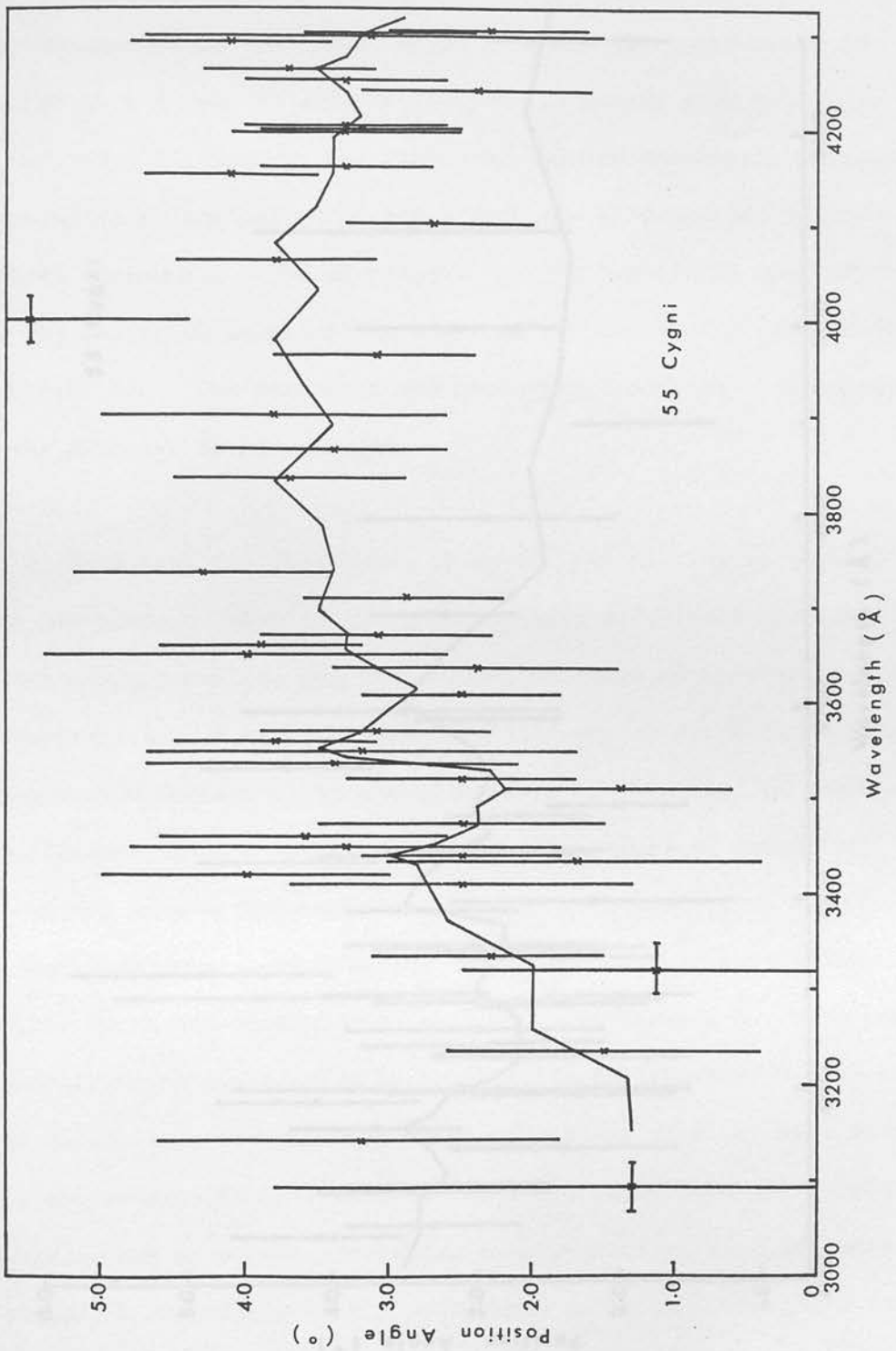

Figure C11: Wavelength dependence of the position angle of linear polarisation for 55 Cygni. The full line represents a 4-point weighted running mean (see text). Position angles are in the equatorial system.

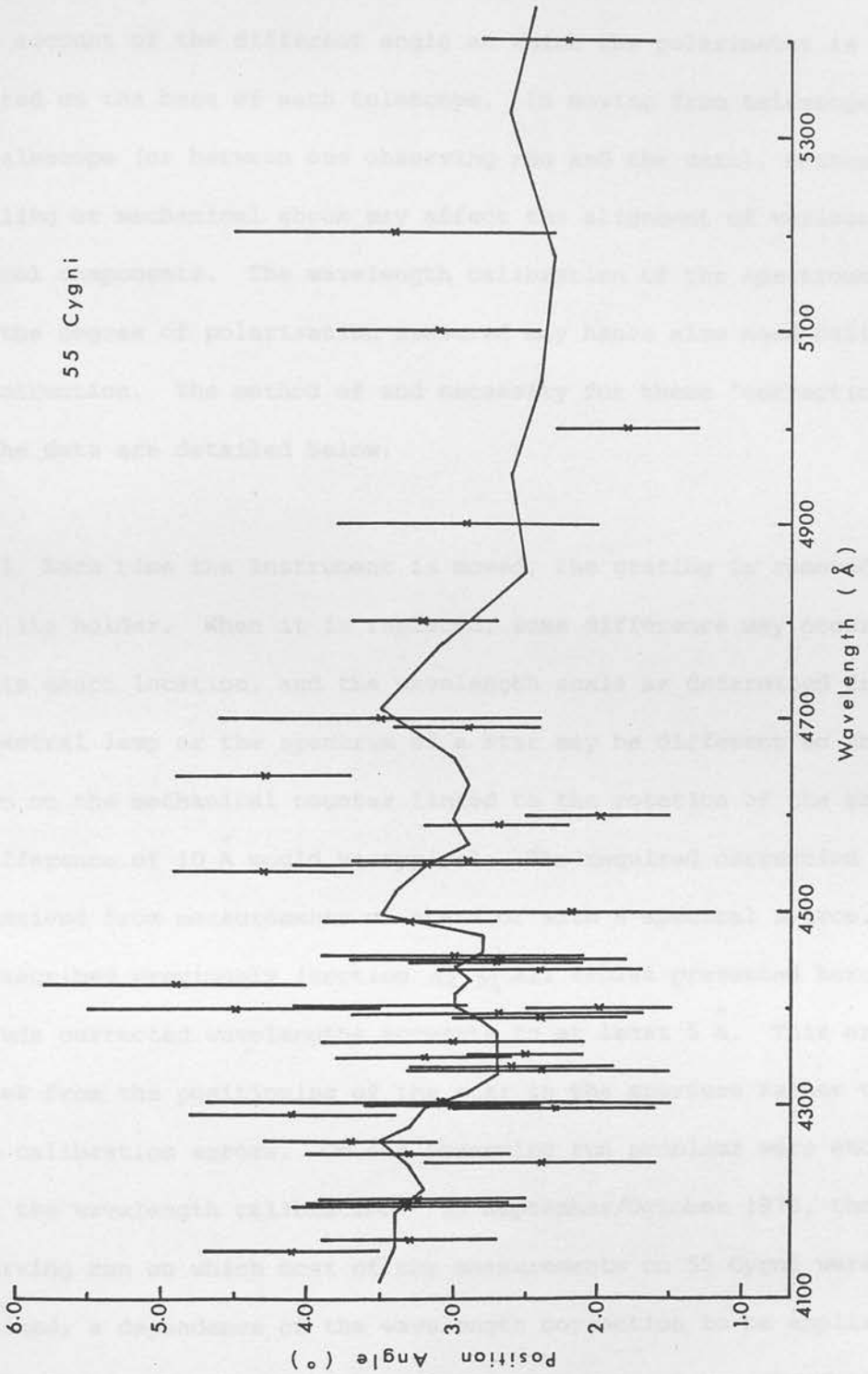

Figure C12: Wavelength dependence of the position angle of linear polarisation for 55 Cygni. The full line represents a 4-point weighted running mean (see text). Position angles are in the equatorial system.

position angle scale for each set of waveplates. This is done to take account of the different angle at which the polarimeter is mounted on the base of each telescope. In moving from telescope to telescope (or between one observing run and the next), mechanical handling or mechanical shock may affect the alignment of various optical components. The wavelength calibration of the spectrometer and the degree of polarisation measured may hence also need calibration or correction. The method of and necessity for these 'corrections' of the data are detailed below.

4.3.1. Each time the instrument is moved, the grating is removed from its holder. When it is replaced, some difference may occur in its exact location, and the wavelength scale as determined from a spectral lamp or the spectrum of a star may be different to that shown on the mechanical counter linked to the rotation of the grating. A difference of 10 Å would be typical. The required correction is derived from measurements on stars or with a spectral source, as described previously (section A2.5). All tables presented here include corrected wavelengths accurate to at least 5 Å. This error arises from the positioning of the star in the aperture rather than from calibration errors. On one observing run problems were encountered with the wavelength calibration. In September/October 1978, the observing run on which most of the measurements on 55 Cygni were obtained, a dependence of the wavelength correction to be applied on the wavelength at which the spectrometer was set was observed. Further, these corrections would vary from night to night (but by small amounts). After this run, these changes were attributed to the grating being tilted in its holder and moving slightly from night to night. Because of these changes in the wavelength correction,

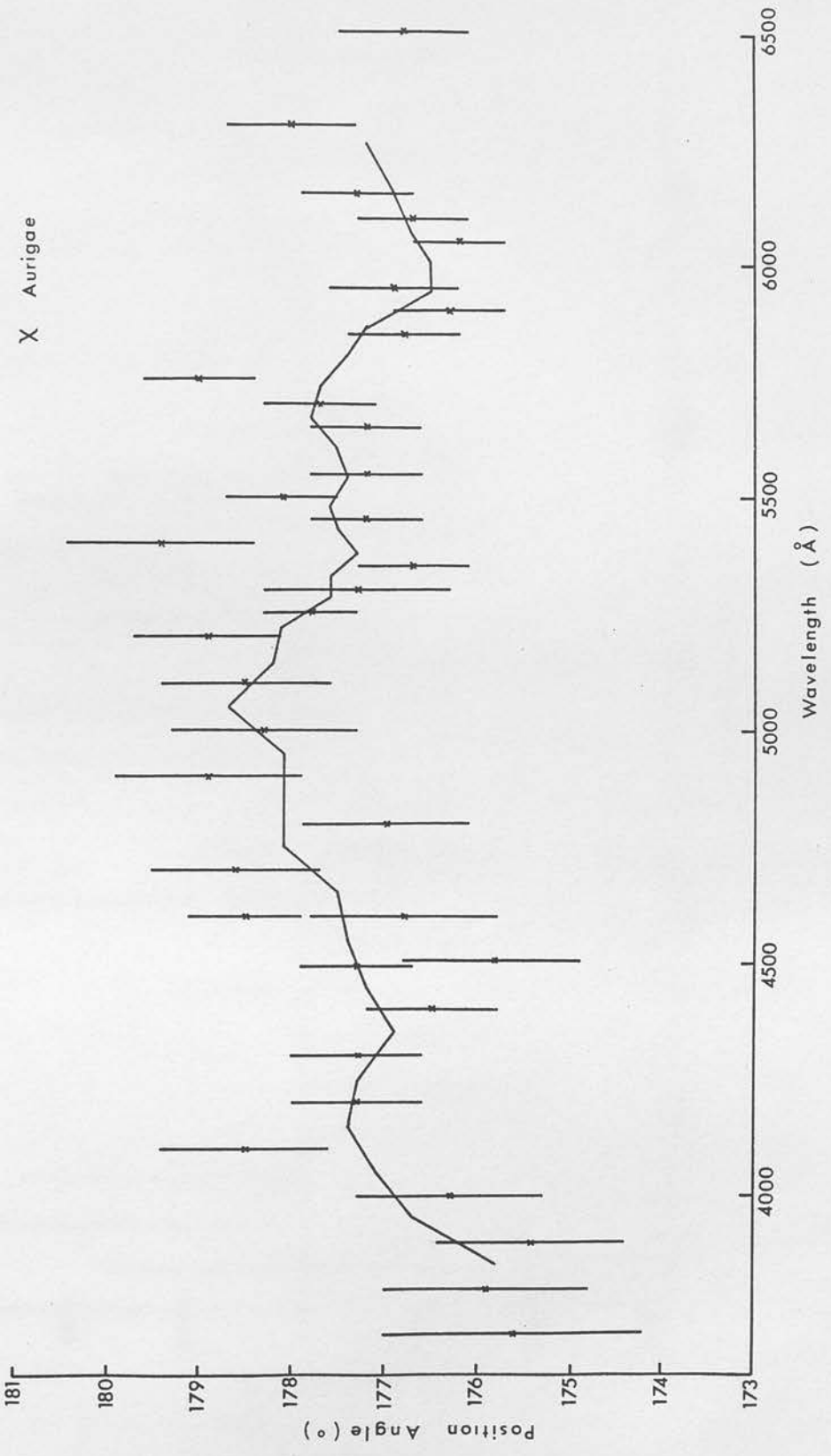

Figure C13: Wavelength dependence of the degree of linear polarisation for χ Aurigae. The best-fitting Serkowski curve has been subtracted from the measurements shown. The full line represents a 4-point weighted running mean (see text).

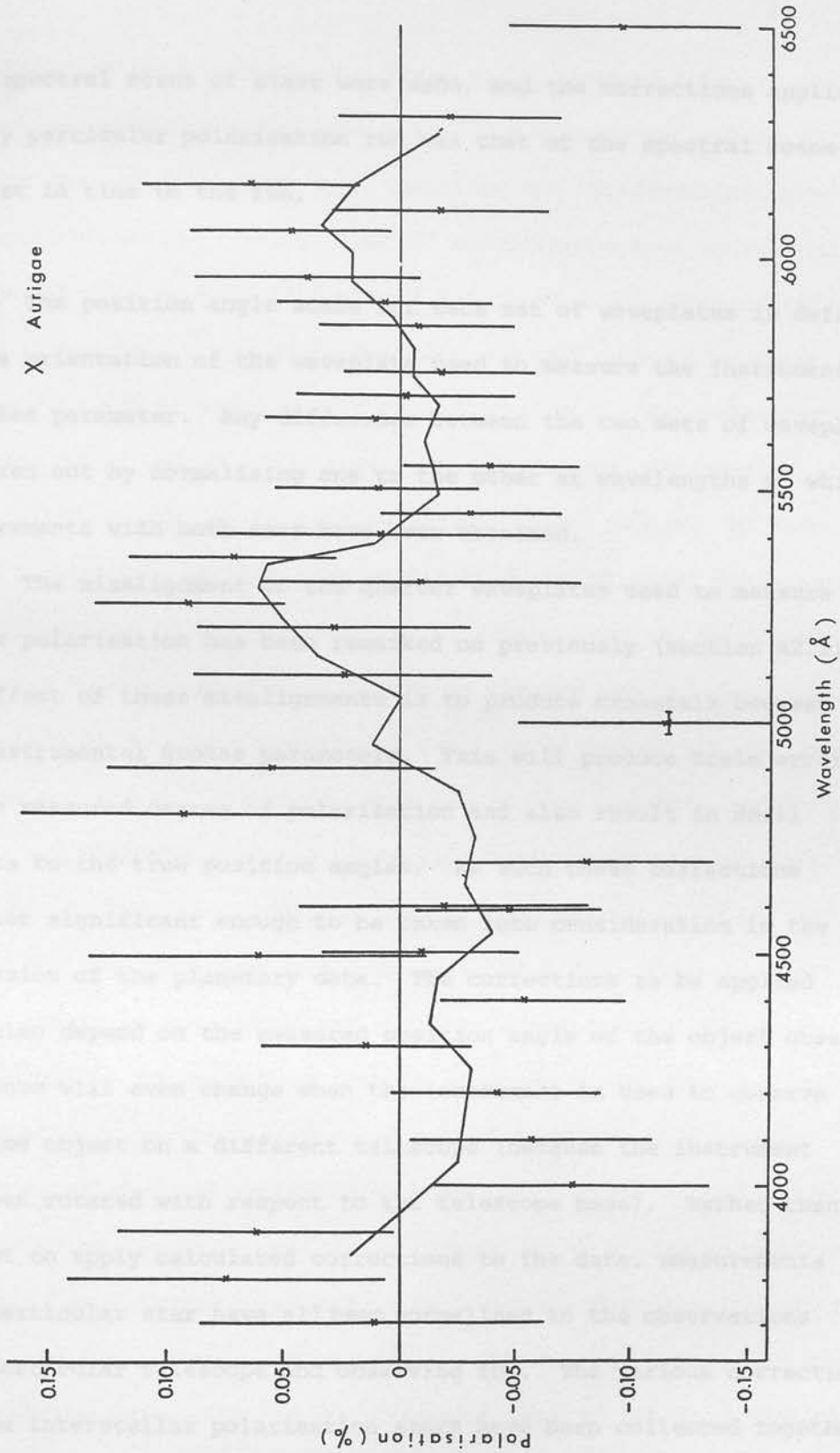

Figure C14: Wavelength dependence of the position angle of linear polarisation for χ Aurigae. The full line represents a 4-point weighted running mean (see text). Position angles are in the equatorial system.

many spectral scans of stars were made, and the corrections applied to any particular polarisation run was that of the spectral scans nearest in time to the run.

4.3.2 The position angle scale for each set of waveplates is defined by the orientation of the waveplate used to measure the instrumental Q Stokes parameter. Any difference between the two sets of waveplates is taken out by normalising one to the other at wavelengths at which measurements with both sets have been obtained.

The misalignment of the quarter waveplates used to measure linear polarisation has been remarked on previously (section A2.2). The effect of these misalignments is to produce crosstalk between the instrumental Stokes parameters. This will produce scale errors in the measured degree of polarisation and also result in small offsets to the true position angles. As such these corrections were not significant enough to be taken into consideration in the discussion of the planetary data. The corrections to be applied will also depend on the measured position angle of the object observed, and hence will even change when the instrument is used to observe the same object on a different telescope (because the instrument has been rotated with respect to the telescope base). Rather than attempt to apply calculated corrections to the data, measurements on a particular star have all been normalised to the observations on a particular telescope and observing run. The various corrections for the interstellar polarisation stars have been collected together in Table C11. To illustrate the procedure, and to justify it, we look more closely at the case of ζ Ophiuchi. Most of the polarisation measurements on this star were obtained on the 60" and 61" telescopes at Tucson in May 1978. Measurements were obtained with both sets of

waveplates on both telescopes. Since there appeared to be no need to correct measurements taken with the 3800 Å waveplates on both telescopes, the two sets of data taken with the other set of waveplates were corrected to these. Firstly, the 60" measurements were normalised to the 61" data by multiplying by a factor of 1.055 (about 0.08%). Then all the 5825 Å waveplate measurements were multiplied by a factor of 1.095 to bring them into accord with the data obtained with the other set of waveplates. The correction corresponded to about 0.13% at the 'normalisation point' around 4600 Å. To justify these corrections we take note of Fig. C15, which shows graphically the corrections to the degree of polarisation expected to be made necessary by the errors of alignment of the two sets of optics quoted in section A2.2. The instrumental position angles of the raw data for the 61" and 60" telescopes were ∿85-90° and ∿60-65°, respectively. We can see that the expected correction between the measurements taken on the two telescopes for the 5825 waveplates is ∿0.08% or 5-6%. For the 3800 waveplates, it is about 0.04%. This is small enough not to be noticed in the original normalisation procedure. Therefore, the normalisation factors found necessary are in complete accord with those calculated from the known errors of alignment of the waveplates. A quick check shows the 55 Cygni normalisation factors to be similarly justified, though in this case errors are larger. One discrepancy remains. When these corrections are applied, there should be no necessity to apply a further correction between measurements taken with the two different sets of optics. However, a residual effect of about 0.08% or 5% of the polarisation remains between the two sequences of data. As mentioned above, since the data taken with the ultraviolet waveplates did not seem to exhibit scale effects upon changing telescopes, all the 5825 waveplate data

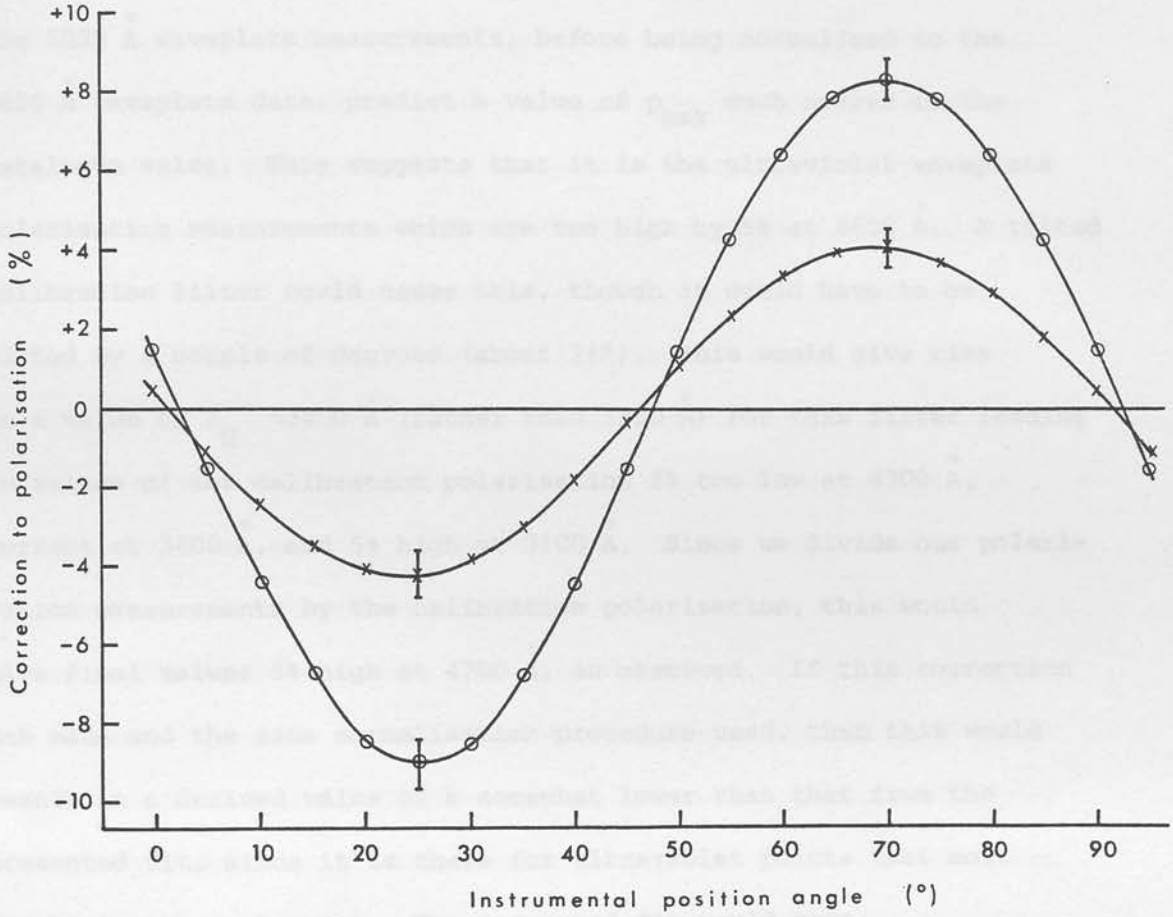

Figure C15: Predicted correction to the degree of linear polarisation made necessary by misaligned waveplates. The curve with crosses gives the correction necessary when using the 3800 Å set, while the curve with open circles gives that necessary for the 5825 Å set. A correction of -5% implies that the true polarisation is only 0.95 of the measured polarisation.

was corrected to it. This, however, seems to have led to the calculated value of p_{max} being too large by about 10% when compared with the catalogue figure (see Table C1). Fig. C3 also seems to show a discontinuity in slope at around 4600 Å. We notice that after correction, the 5825 Å waveplate measurements, before being normalised to the 3800 Å waveplate data, predict a value of p_{max} much nearer to the catalogue value. This suggests that it is the ultraviolet waveplate polarisation measurements which are too high by 5% at 4600 Å. A tilted calibration filter could cause this, though it would have to be tilted by a couple of degrees (about 2½°). This would give rise to a value of λ_Q ∿3400 Å (rather than 3800 Å) for this filter leading to values of the calibration polarisation 5% too low at 4700 Å, correct at 3600 Å, and 5% high at 3100 Å. Since we divide our polarisation measurements by the calibration polarisation, this would give final values 5% high at 4700 Å, as observed. If this correction was made and the same normalisation procedure used, then this would result in a derived value of k somewhat lower than that from the presented fit, since it is these for ultraviolet points that most constrain this parameter. The corrected fit would have

$$p_{max} \approx 1.55\% \qquad \lambda_{max} \approx 6100 \qquad k \approx 1.08$$

Examination of the 3800 Å waveplate calibration polarisations show them to be high already - around 90%. If the explanation above is correct, the true calibration values should be around 95%, higher than the theoretical maximum. It must therefore be rejected. The instrumental position angle of the raw data taken on the 61" telescope is around 90°, which implies that very nearly all the polarisation information is in the 'Q' instrumental Stokes parameter. If the corresponding waveplate were tilted in the opposite sense (i.e. in a different, orthogonal plane) it could produce a measured polarisation that was higher than the true value. However, if the calibration

is now completely flat and accurately quarter wave at 3800 Å, it is impossible to produce as large an effect as 5% of the polarisation by tilting the 'Q' waveplate. Of course, the combination of a slightly tilted calibration filter with a slightly tilted waveplate could give the described effects and this is also more likely. Intrinsic differences between the waveplates arising during their manufacture would also give effects similar to these described above, but at a lower level (½-1% of the polarisation). In summary, the residual difference between the measured degree of polarisation between the 3800 Å and 5825 Å waveplates may well be due to slight tilting of the elements of the 3800 Å set, possibly compounded by intrinsic differences between the waveplates of the set. The resultant difference in tilt angle between the calibrator and the waveplate used to measure the instrumental 'Q' Stokes parameter would in that case be in excess of 2°. A further consequence would be the slope of the degree of polarisation measures against wavelength for this set of waveplates would be untrustworthy. Examination of the measurements on 55 Cygni and on other data not presented here gave inconclusive and sometimes inconsistent results. If tilting of the waveplates is the culprit, this might be expected since tilt angles might be changed by mechanical shock if the retarders were at all loose in their holders. Because of these various speculations, and rather than make corrections based on theoretical estimates of supposed effects, the simpleminded normalisation procedure described above is retained. It must be borne in mind that the derived values of p_{max} and k will be affected by the above possible misalignments, and the fitted parameters quoted may not be reliable. Since our goal is the detection of structure in the polarisation curve with scale widths of 50-500 Å, this is not too important.

5. Examination of the new measurements presented

Looking at the measurements made on each star we see a number of features in the degree of polarisation and/or in its position angle. Some of these features occur in only one star, while others occur in more than one. In the detailed examination of the data that follows, we turn first to ζ Ophiuchi.

5.1 The degree of polarisation of the light from ζ Ophiuchi shows a marked upturn in the ultraviolet, as is shown in Figs C3 and C6. This is most obvious in the plot displaying deviations from the smooth Serkowski curve (Fig. C6). The degree of polarisation appears to start to depart from the analytic fit at a wavelength around 3400 Å with the difference becoming more obvious as we move to shorter wavelengths. At 3150 Å, the shortest wavelength for which a measurement was obtained, the deviation had reached 0.15%, or about 15% of the predicted polarisation at that wavelength. The next obvious feature is in the magnitude of the linear polarisation at (and around) 4100 Å. The measurements are above the analytic curve until about 3900 Å, where they cross the curve to form an apparently asymmetric depression 0.03 to 0.04% deep. The feature may be traced from 3800 Å to 4300 Å, a total width of 500 Å. The central part of the feature (at 3950 Å to 4150 Å) is rather convincing, being significant at the 3σ level or better. Fig. C16 shows this part of the wavelength dependence in more detail, with only the smoothed data points shown. After this feature the degree of polarisation remains higher than the best-fit analytic curve until the next crossover at 4650 Å.

The plot of position angle in the ultraviolet (Fig. C4) shows structure clearly related to that in the plots of the degree of

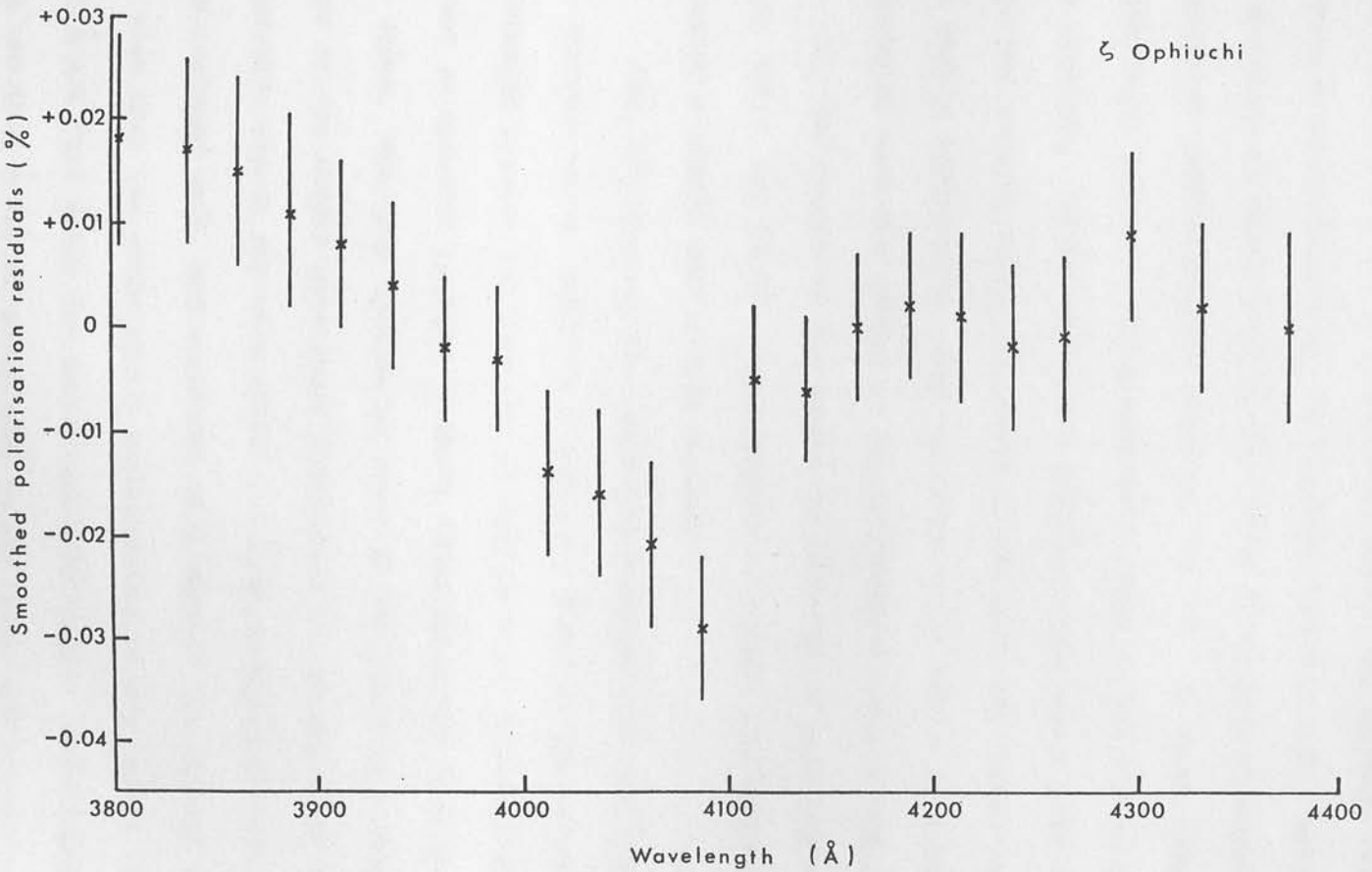

Figure C16: The 4100 Å feature in the linear polarisation of Ophiuchi. The points plotted are (4-point) weighted running means from which the best-fitting Serkowski curve has been subtracted.

polarisation. The main feature is of a gradual rotation in the position angle beginning at around 4500 Å and reaching a minimum at 3650 Å, by which time it has turned through an angle of 1°.2 compared with its value in the blue/green. In the same region the degree of polarisation has fallen from 1.5% to 1.15%. Around 4100 Å a deviation of about 0°.7 is seen which is clearly associated with the feature at this wavelength shown in Fig. C6. At about 3550 Å the curve turns back to a value similar to that in the visual part of the spectrum. Below 3400 Å the position angle again starts to turn from the average value, but since errors here are large, such changes are barely significant. Any structure below 3400 Å is presumably associated with the upturn in the ultraviolet seen in Figs C3 and C6. All the points in the region of 3300-3500 Å were taken on one night (1978, May 26/27), while points at longer wavelengths were obtained a little over a week earlier.

Fig. C3, showing the corrected polarisations and the best fit analytic curve, exhibits a distinct 'bump' at the crossover wavelength between the two sets of optics (i.e. 4600-4700 Å). This is not so apparent on Fig. C6 which shows deviation from the best fit curve. The bump appears to occur at the point of a change in slope in the smooth wavelength dependence of the degree of polarisation. A possible reason for this effect - tilted waveplates - has already been remarked upon, and would not only explain the feature at 4650 Å, but also that the polarisation measurements in the region 4700-5500 Å all fall below the smooth analytic curve. Measurements taken with the 5825 Å set of waveplates in the green and red parts of the spectrum seem to show oscillations in the magnitude of polarisation. A slight peak (1σ, 0.03%) appears at 5250 Å, a larger, noisier one (0.06%) at 5700-5800 Å, and the most obvious (0.08-0.09%) centred

on 6600 Å. It is not immediately clear whether there exists simply one depression of the polarisation at 6100 Å of amplitude about 0.08%, or multiple enhancements. However, the structure is certainly significant, expecially in the region 6000-7000 Å. The measurements of polarisation at wavelengths greater than 7000 Å are rather remarkable. The fall in polarisation is very steep, suggesting the possibility of further oscillations about some smooth curve at even longer wavelengths.

The position angles presented in Figs C4 and C5 are illuminating when compared with the graphs of the degree of polarisation. No obvious feature occurs at either 5250 Å or 5750 Å. The discontinuity in the smoothed curve at 6100 Å is caused by the wildly divergent point at 6010 Å. When account is taken of this, a slight increase in position angle is suggested (0°.4-0°.6), centred on 6150 Å. Such an increase does not coincide in wavelength with any feature in the degree of polarisation. However, if we suppose instead that a slight depression in position angle is present centred at 5750 Å and of magnitude 0°.3 or so, then the apparent increase at 6150 Å simply marks the return or partial return to a continuum level before a further depression associated with the 6600 Å polarisation feature. This further depression reaches about 1°.0 at maximum, returning to a continuum level by about 7100 Å. The measurements of position angle in the region (i.e. 6400-7100 Å) are rather noisy and might suggest fine structure. In particular a sharp rotation may occur at 6850 Å. Not well defined here it might repay further study. Finally we note that the position angle appears to show a gradual and monotonic increase throughout the visible spectrum. From 7500 Å, where $\theta \sim 126°.5$, it decreases smoothly to $\theta \sim 125°$ at 3600 Å. Below this the position angle turns back to its value in the blue/green (126°.3).

5.2 Wavelength coverage for 55 Cygni is mainly confined to the range 3100-4800 Å, and except for a few measurements, was obtained using the 3800 Å set of waveplates. Considering first the plots of degree of polarisation against wavelength, we note immediately that 55 Cygni also shows an upturn in polarisation in the ultra-violet. A smoothed curve drawn through the data points starts to deviate from the best-fit analytic curve at around 3300 Å (Fig. C9). In this respect the case of 55 Cygni is not significantly different to that of ζ Ophiuchi. At 3100 Å, the observed curve is ∿0.25% above the analytic curve which predicts a polarisation of 1.97% here. Hence the enhancement is 12-13% of the polarisation or again comparable to that seen in ζ Ophiuchi. A large number of linear polarisation measurements were made in the region of 3400-3700 Å, and possible structure appears centred on 3535 Å. The polarisation at this point changes from +0.1% to -0.2% (with respect to the analytic curve) in 10-15 Å. Such dramatic change is unlikely to be real considering the resolution of the individual measurement (50 Å). Setting aside the small scale sharp feature, it still appears that the degree of polarisation appears to be above the analytic curve before 3535 Å and below it afterwards, at least until 3660 Å. This is only marginally significant. Between 3300 Å and 3750 Å there are plotted 22 data points. According to gaussian statistics, 15 of these should lie within 1σ of the mean, 19 within 1.5σ and 21 within 2σ. By coincidence the actual numbers in this wavelength region are 15 within 1σ, 19 within 1.5σ and 21 within 2σ! (It is acceptable to use gaussian statistics here, since $\sigma(p) \ll p$.) An examination of the position angle in this wavelength region (Fig. C11) is similarly suggestive but again not significant. No feature is apparent at these wavelengths in ζ Ophiuchi in either position angle or degree of polarisation.

Returning to Figs C9 and C10, displaying the degree of polarisation, it is seen that no further structure is present until the vicinity of 4350 Å. Although the coverage is not as complete as in the case of ζ Ophiuchi, it is clear that there can be no structure around 4100 Å as found in the previous section. This holds for both the position angle and the degree of polarisation. The region 4300-4500 Å is particularly interesting because of the occurrence of the strongest diffuse band here (at 4430 Å) and also the famous 'knee' or change of slope in the interstellar extinction curve at ∿4350 Å (NANDY, 1964). The general appearance in the polarisation is of a broad depression in the interval 4150-4500 Å, declining by up to 0.10% from the mean level outside this interval. In the centre (4365 Å), an 'emission peak' is seen, of size ∿0.05%. Alternatively we may view it as two features centred respectively at 4320 Å and 4420 Å, leading to the strong temptation to identify the 4320 Å feature with the knee in the extinction curve and the 4420 Å one with the diffuse band. Neither however are 'well detected'. The structure at 4320 is only at the 1.5-2.0 σ level while that at 4420 Å is at the 2.0-2.5 σ level. No structure is seen in the position angles over these wavelengths, though of course such variation may not necessary occur even if variations in the magnitude occur. Since the 'knee' in the extinction curve is in fact a broad transition probably associated with the particular size distribution of the grains in the line of sight (see e.g. HAYES et al, 1973) it would be most strange to find small scale (i.e. 50 Å) structure associated with it. Since the 4320 Å feature is marginal, it is not considered further. The expected size of the polarisation change over the 4430 Å diffuse band was calculated earlier (section C3) with the assumption that the carrier of the diffuse band was the same as

that of the visual continuum extinction and the polarisation. The degree of polarisation was expected to change by 0.07%, consistent with that seen here. Note that (again) no structure is apparent in ζ Ophiuchi at these wavelengths, in either position angle or degree of polarisation.

The measurements of polarisation for wavelengths longer than 4900 Å are rather widely spaced and are of lower quality. Hence we have no information as to the possible occurrence of broad band oscillations in the degree of polarisation at wavelengths greater than λ_{max} as seen in ζ Ophiuchi. We note (Fig. C8) that the magnitude of polarisation is higher than that predicted by the fitted Serkowski curve in the region 4600-5100 Å. There is little evidence of the change of slope seen in ζ Ophiuchi at these wavelengths, where polarisations were below that predicted by the analytic curve. In section 4.3.2 it was argued that this change of slope was the probably result of slight tilting of the waveplates used in the ultraviolet part of the spectrum. As such the effect should also be present here. However, these measurements were obtained on a different observing run to those of ζ Ophiuchi, and the (instrumental) position angle of the data is also greatly different. Further, the derived wavelength of maximum polarisation - λ_{max} - lies quite near this interval, and is rather poorly defined. For the accurate determination of λ_{max}, good measurements are necessary at wavelengths greater than λ_{max}. In the case of 55 Cygni, such measurements are of poor quality. The differences between 55 Cygni and ζ Ophiuchi at the wavelength of the slope change in the degree of polarisation are hence not inconsistent with the existence of the instrumental effects proposed earlier.

The only structure in the position angles measured on 55 Cygni

occurs on very broad scalelengths. From a maximum value of 3°.7 at around 4000 Å, it rotates to 1°.2 at about 3200 Å in the ultra-violet and to 2°.8 or so at 5000 Å. The 'turning back' of the position angles at wavelengths less than 3400 Å, as seen in ζ Ophiuchi, is not seen here.

5.3 Wavelength coverage of χ Aurigae is restricted to the range 3700-6500 Å, and was covered exclusively with the 5825 Å set of waveplates. The only structure worthy of note is in the yellow and green where possible sinusoidal structure is seen with peaks at 5250 Å and 6050 Å. Both features are not statistically significant. The larger of the peaks (at 5250 Å) is only 1½-2 σ away from the analytic curve. However, it is interesting to compare these observations with measurements taken in a similar wavelength interval on ζ Ophiuchi. On that star possible enhancements in the degree of polarisation were seen at 5250 Å, 5750 Å and 6600 Å. The position angle measurements show no significant structure at either 5250 Å or 6050 Å. However, a broad-band change in the position angle similar to that seen in both 55 Cygni and ζ Ophiuchi is noticeable. From a maximum value of about 178°.2 at 5050 Å, it declines to 175°.8 at 3800 and 177°.0 at 6100 Å. χ Aurigae shows no structure at 4420 (as 55 Cygni does) or at 4100 Å (as ζ Ophiuchi does). It must be admitted though that errors are large and points relatively sparsely distributed about these wavelengths.

5.4 The structure found in interstellar polarisation curves for the three stars is summarised in Table C12. While the overall wavelength dependence of the degree of polarisation departs from the smooth analytic curve in similar ways for the three stars, there are no exact correspondences in wavelength between them such as would give

one confidence in the reality of the apparent structure or in its association with the interstellar medium. A similar statement may be made concerning the position angles. The one exception is the occurrence of an upturn in the polarisation in the ultraviolet and clearly seen in both 55 Cygni and ζ Ophiuchi. Before proceeding to the interpretation of the features seen, it is necessary to discuss which if any might be attributable to instrumental effects. Each of the features described in Table C12 has been tested to see if it could have arisen by mismatching data sets from different observing runs or telescopes. Though all survived, most could be rendered less significant by judicial choices of normalisation factors. The small very wide band variations of position angle in each of the three stars are particularly sensitive to small errors in these features. As mentioned above (section 4.3.2) slight tilting of the waveplates can cause a slow rotation of position angle over long wavelength spans (say 1000 Å). However, the maxima and minima found in these position angles do not correspond to 'normalisation points' either between data taken with different sets of waveplates or on different telescopes. The most convincing argument for the reality of these wavelength dependent position angle rotations is however an astronomical one. We shall therefore return to this question in section 6. The other instrumental effect to be discussed concerns the problem of scattered light entering the optical train after the analyser. This is considered immediately below.

Measurements of polarisation are difficult to make at wavelengths below 3300 Å, as the amount of light available is small so close to the atmospheric cutoff. Accordingly, when an apparent feature occurs in the polarisation at such wavelengths, it is necessary to consider very carefully the possible effects of unwanted light.

Such light might come from within the dome, or from the star itself at longer wavelengths. First of all we consider the effect of stray light in the dome reaching the photomultiplier. This is equivalent to a large Dark Count, i.e. if q = measured polarisation, p = true polarisation, I = photon counts collected from the star in a certain time, and S = photon counts contributed by stray light in the same time, then:

$$q = p \times (1 + S/I)^{-1}$$

where the 'certain time' is the time for which the counters were operative before the calculation of the polarisation measures above. Hence the polarisation is reduced and a decline in polarisation would be seen as the flux from the star weakened. However, all the polarisation measurements presented here have been calibrated by measurements made with an HNP'B polaroid calibrator and taken on the same star. The calibration measurement will therefore be more affected by the stray light since its transmission is only about 30% of that of the waveplate. If q^1 = measured calibrated polarisation, p = measured true polarisation, then:

$$q^1 = p^1 \frac{(1 + S/0.3I)}{(1 + S/I)} = kp^1$$

This will give an upturn in the ultraviolet on any polarised star.

S/I (in %)	k
1	1.023
2	1.046
5	1.111
6	1.132
7	1.153
10	1.212

It can be seen that the ultraviolet features in both 55 Cygni and ζ Ophiuchi could be reproduced with a stray light contribution of only 6-7% of the light from the star at 3200 Å. It is easy to see

that the observed upturns were not so caused. Since the measurements on both stars were taken with the same telescope (though admittedly on different occasions) any effect of stray light would be less for the brighter star, ζ Ophiuchi. The magnitude difference between them (V band) is $2^m.3$, and ζ Ophiuchi is also of earlier spectral type than 55 Cygni. Stray light should hence be at least a magnitude less important in the brighter star. Further, a stray light 'content' of 7% would alter (reduce) the calibration polarisations by almost a quarter. This is not seen.

Unwanted light from the star itself can affect the measurement in two ways. Either light multiply reflected within the polarimeter or flux from other than the desired wavelength may contribute to the detected intensity. Since the polarimeter turns polarisational information into intensity modulations, after the modulator multiple reflections can only have the 'diluting' effect described above. However, in stars that have a wavelength dependence of polarisation, incomplete elimination of light at other wavelengths in the spectrometer can also lead to polarisation effects. Light entering the spectrometer which is uncollimated or diffuse has little chance of reaching the exit slit. If it is of wavelength close to that for which the spectrometer is set, a little may succeed, but otherwise the comprehensive baffling will frustrate it. Light which enters the spectrometer focused and collimated, i.e. light from the stellar image focused on the entrance aperture, has a lot better chance. Such light can be scattered by dust on the mirrors or the grating or suspended in any of the light paths. Certain wavelengths of light may also reach the exit slit by the mechanism known as 'double diffraction', described in section A2.6. Of course, the amount scattered is still very small. A typical figure for this type of spectrometer would

be less than 10^{-4}, though it might be rather higher in this instrument as both the grating and mirrors were not in perfect condition. Now, spectral contamination at the 10^{-4} level would normally be unimportant, but with a small bandpass near the ultraviolet atmospheric cutoff, the flux level to be detected is very low compared with the flux integrated over the rest of the spectrum. Under these circumstances, scattered light from the rest of the spectrum may well make an important contribution to the flux at the wavelength of interest. As yet the consequences for the measurement of polarisation have not been touched on. Light of other wavelengths which reaches the exit slit is encoded according to the polarisation of the star at that wavelength. In a star such as ζ Ophiuchi, the ultraviolet wavelengths are a lot less polarised (up to 50%) than the average value across the rest of the spectrum. Hence light scattered to the exit slit will cause an increase in the measured polarisation at ultraviolet wavelengths.

To investigate the possible importance of this problem, a number of tests were carried out. The atmosphere will not transmit light of wavelengths less than 3000 Å, yet when α Lyrae was observed at Mt Lemmon, an easily measurable flux was seen at 2800 Å. When an ultraviolet filter was inserted, this flux declined by a factor of at least ten. The filter was a 3 mm thickness of UG11, and did not pass light of wavelengths greater than 4000 Å. Below 3000 Å the detected intensity seemed roughly independent of wavelength. Presuming that this is true, the following table shows the relative importance of scattered light at certain wavelengths in the ultraviolet, both with and without the UG11 filter.

In the table, $f_\lambda = \frac{\text{flux measured at 2850 Å}}{\text{flux measured at } \lambda} \times \frac{100}{1}$. Clearly, at 3150 Å, the scattered light is contributing about 10% of the

Wavelength Å	f_λ (without UG11) %	f_λ (with UG11) %
3000	67.0	57.5
3100	11.0	2.6
3200	2.9	0.6
3300	1.7	0.4
3400	1.4	0.3
3500	1.3	0.3

detected flux. A measurement of the polarisation of ζ Ophiuchi was made at 2800 Å, to investigate the state of polarisation of this scattered light. It appeared to be roughly twice as polarised as light at 3250 Å (errors were rather large). Hence this scattered light could (will) cause an increase in the measured polarisation of up to about 20% of the polarisation. This is of the same order as the observed enhancement of polarisation on both ζ Ophiuchi and 55 Cygni. As can be seen from the table above, the introduction of an ultraviolet filter reduces the effect of scattered light by at least a factor of 5 at 3100 Å. Several attempts were made to measure polarisation in the ultraviolet both with and without the UG11 filter. Incidentally, this filter was mounted in the Order Sorter wheel and will not affect the measurement of polarisation. For various reasons, only recently were these efforts successful. The measurements in the following table were obtained with an upgraded version of the described spectropolarimeter on the U.K. Infrared Telescope on Mauna Kea, Hawaii. A new grating was used in the spectrometer, so that the component of scattered light was less. However, it is clear that the measured polarisation is decreased when the filter is inserted. The measurements are strong evidence that the observed upturns in the tabulated polarisation of ζ Ophiuchi and 55 Cygni are of instrumental origin. The behaviour of the position angles in this region on the two stars, is worthy of mention. On

ζ Ophiuchi 20 August 1980

Wavelength Å	Without UG11 p	%	With UG11 p	%
3150	0.969	0.017	0.904	0.029
3300	1.023	0.015	1.016	0.026
3450	1.060	0.013	1.094	0.024

ζ Ophiuchi, the 'turning back' at 3600 Å could well be associated with the ultraviolet upturn, but then the further (tentative) structure at even shorter wavelengths is hard to account for. On 55 Cygni the position angle continues to rotate at these wavelength and no specific structure seems to be associated with the ultraviolet upturn. These position angles variations are difficult to explain, and may be connected with the particular wavelengths of light that make up the unwanted light reaching the photomultiplier.

In summary, it seems likely that the observed ultraviolet upturns seen in these observations are caused by unwanted light reaching the photomultiplier. While the instrumental effects may be hiding real structure at these wavelengths, further consideration of this 'feature' is not considered justified without further observations.

6. Interpretation of the polarimetry

Table C12 summarises the features found in either the degree or position angle of the linear polarisation detected in the light from the three stars under consideration. Each of these features will now be examined to see what physical mechanisms might be involved, and what new information these measurements provide on the nature of the interstellar medium.

6.1 The broadband dependence of position angle.

The detected rotations of position angle over large wavelength intervals are rather small in all three stars. Maximum rotations were $1°-1\frac{1}{2}°$ for ζ Ophiuchi, about $2°$ for 55 Cygni and around $2\frac{1}{2}°$ for χ Aurigae. As mentioned previously, the normalisation of results from different observing runs together makes it difficult to be fully confident about such small systematic variations on these long wavelength baselines. However, we note that no feature or discontinuity appears associated with the crossover wavelength between the two sets of optics. Not only should any normalisation errors be most apparent here, but also any effects caused by the waveplates could be detected (see section 5). While systematic position angle rotation with wavelength has been reported for χ Aurigae (MARTIN, 1974), neither ζ Ophiuchi nor 55 Cygni is supposed to exhibit such effects, even with a baseline extending into the infra-red (WILKING et al, 1980). Of course, there have been very few accurate studies of position angle over long wavelength baselines, and it is not unreasonable to suggest that such structure has simply been overlooked in ζ Ophiuchi and 55 Cygni. For example, we note that MARTIN (1974) deduced a monotonic position angle change with wavelength of roughly

$15° \mu^{-1}$ for χ Aurigae. Other measurements (SERKOWSKI et al. 1975), made simultaneously in a number of colours, suggest that the position angle of polarisation for this star reaches a maximum in the V band, and declines towards both the red and the blue. Until recently, even multichannel polarimeters (i.e. those using multichannel detectors) have been unsuitable for obtaining wide wavelength coverage of position angle measurements. Intensified systems, such as the SIT-Vidicon, have in general been restricted in their wavelength coverage, being limited in the blue to 0.4μ by the detector, and in the red to 0.7μ by the S20 photocathode of the intensifier. The modulating element in some multichannel polarimeter furthermore is a rotating super-achromatic waveplate. Such waveplates have an optic axis which rotates with wavelength and position angles measured with such devices require careful calibration.

The rotation of position angle in the ultraviolet found in ζ Ophiuchi and 55 Cygni is quite convincing. The critical factor in the case of ζ Ophiuchi is the correlation of position angle changes with structure in the degree of polarisation, both at 4100 Å and at wavelengths near 6600 Å. Such covariation of the degree and position angle of polarisation implies the presence of at least two components in the linear polarisation of the light we see from ζ Ophiuchi. While one of these components must be interstellar in origin, the other (or others) may be interstellar or intrinsic to the star. The variations seen in the degree of polarisation can then be assigned to the dominant interstellar component, or to the secondary component (interstellar or intrinsic) depending on the behaviour of the position angle.

Intrinsic polarisation is a well-known phenomenon in certain hot early-type stars. The linear polarisation arises from electron scattering in a disc of material situated about the equator of the

star. The characteristic feature in the wavelength dependence of polarisation arising by this mechanism is the sharp fall across the Balmer limit at 3650 Å, the polarisation being much smaller at wavelengths shorter than this wavelength (COYNE, 1976 ; KRUSZEWSKI, 1974). Such stars as these will normally show evidence of circumstellar matter through strong emission in the Balmer lines. While none of the stars studied here has noticeable emission in the hydrogen lines, evidence for circumstellar matter about ζ Ophiuchi has been presented (BARKER & BROWN, 1974 ; NIEMELA & MÉNDEZ, 1974). If the position angle of any intrinsic polarisation were at 45° to that of the interstellar polarisation, most of the effect would be seen in the position angle, while the degree of polarisation will still be well fitted by a Serkowski curve. Indeed, without loss of generality, we may resolve any intrinsic polarisation into components parallel to the interstellar polarisation and at 45° to it.

Do either ζ Ophiuchi or 55 Cygni show structure in either position angle or degree of polarisation associated with the Balmer Jump? We note a sharp change in position angle on ζ Ophiuchi at roughly these wavelengths, not associated with a feature in the degree of polarisation. The effect if due to intrinsic polarisation shows that a stronger intrinsic component implies a rotation of position angle away from the mean interstellar value. However, in the red, structure in the position angles is seen that with this interpretation would imply a decrease in the interstellar component or an increase in the intrinsic component. Since this is unlikely to be associated with an intrinsic component, the implication is that the interstellar component declines. However, this is inconsistent with the observed increase in the degree of polarisation. In 55 Cygni, sharp features may occur at wavelengths close to the

Balmer Jump. These are unlikely to be associated with the Balmer Jump. However, the position angle dependence is in some ways suggestive of an intrinsic source of polarisation, although the position angle rotations are smooth in their dependence on wavelength. With no real physical justification, an attempt was made to fit these position angle rotations with a component following a λ^{-4} wavelength dependence, i.e. a Rayleigh scattering law. Reasonable fits were easily obtained, though, of course, they could only explain the behaviour of the position angles in the ultraviolet. In ζ Ophiuchi, if this component was assumed to be completely orientated at 45° to the interstellar component, the effect on the degree of polarisation was only 0.002%. On 55 Cygni under the same conditions, the fitted component would have affected the degree of polarisation by 0.02%. Rayleigh scattering would imply an asymmetric distribution of small particles around the star, as any atoms would be ionised and their effect dominated by the resultant electron scattering. Such a model is problematical. Since the observations on χ Aurigae do not cover the critical wavelengths, nothing can be said on the possible presence of an intrinsic component in the observed polarisation of light from this star.

The assumption of just one component in the interstellar polarisation implies the acceptance of several assumptions about the particles in which that polarisation arises. Chief among these is that the characteristic direction of alignment for the grains (presumably due to the magnetic field) is sensibly constant along the line of sight to the star in question. If this assumption does not hold, variations in particle size, shape and composition along the line of sight also become important. On average, for stars at low galactic latitudes, the line of sight to a star 1 kiloparsec away will intersect 4 to 5 gas clouds, as evidenced by the multiple

components seen in high resolution observations of interstellar lines (HOBBS, 1974b). The correlation between the strength of interstellar lines and the reddening, E(B-V), (Bohlin et al.1978) suggests that at least some of these gas clouds could well be associated with a dust cloud. Since the direction of the magnetic field will vary along the line of sight (MATHEWSON, 1968 ; NEE, 1980) it seems likely that the characteristic direction of alignment of the dust grains in each of these clouds will be different. Under such conditions, circular polarisation will be produced.

Table C1 gives relevant properties of the stars considered in this section. The circular polarisation exhibited by linearly polarised reddened stars has been convincingly attributed to the interstellar particles (KEMP & WOLSTENCROFT, 1972 ; MARTIN, 1975). Since the interstellar medium is linearly dichroic as evidenced by the polarisation of starlight which has passed through it, it must also be (linearly) birefringent, as implied by the Kramer- König relations. Associated with this, some depolarisation will occur, i.e. the ratio of polarisation to reddening, p/E(B-V), will be lower. (This ratio will also depend on the efficiency of grain alignment, and the strength and orientation of the magnetic field.) We may hence deduce that more than one cloud must lie in the lines of sight to these stars, and that the position angles of grain alignment in each of these clouds must be different. In general then, it is reasonable to consider more than one component contributing to the interstellar linear polarisation. We now look at each of the stars in turn.

As can be seen from Table C1, both 55 Cygni and χ Aurigae exhibit detectable circular polarisation. Several approaches have been made to relate the circular polarisation produced to the medium through which the light has passed. SERKOWSKI (1962) considered

a model based on fluctuations (in the alignment direction) in a continuously polarising medium. Such an analysis is appropriate to distant stars ($r >> 1$ kpc) and the examination of clusters. MARTIN (1974) has dealt with the case of discrete clouds and develops in particular a 'two-slab' model. KEMP & WOLSTENCROFT (1972) used a model with a uniform change of the alignment direction of the grains along the line of sight. This model was considered because of the suggestion by MATHEWSON (1968) that the galactic magnetic field was helical in structure, at least out to 700 parsecs from the Sun. Such structure was evidenced by the distribution of position angles of interstellar linear polarisation over the sky (see e.g. MATHEWSON & FORD, 1970). It is to be noted that the existence of a 'twist' in the grain alignment along the line of sight is not sufficient to give a rotation of the position angle with wavelength. There must also be a variation in grain properties. MARTIN (1974) restricts his consideration to changes in λ_{max} along the line of sight, equivalent to a change in grain size. If we consider the 'two-slab' model we can see that such a variation would only give a monotonic rotation of position angle with wavelength. The 'turnover' is position angle seen in 55 Cygni and χ Aurigae could not arise. In his analysis, MARTIN (1974) started at the standard analytic Serkowski relation for the linear polarisation.

$$\ln(p/p_{max}) = k \ln^2(\lambda/\lambda_{max}) \qquad (6.1.1)$$

Consider two slabs, orientated such that the difference in the position angles of the grains in each slab is ϕ. Let r_λ be the ratio of polarisations produced by the two sheets, and θ_λ the observed position angle. MARTIN (1974) gives

$$\tan 2(\theta_\lambda - \theta_1) = r_\lambda \sin 2\phi \,/\, (1 + r_\lambda \cos 2\phi) \qquad (6.1.2)$$

where θ_1 is a constant. To see that this is monotonic, we differentiate the above expression.

$$\frac{d\theta_\lambda}{d\lambda} = \tfrac{1}{2} \cdot \frac{dr_\lambda}{d\lambda} \cdot (\sin 2\phi) \; / \; (1 + r_\lambda^2 + 2r_\lambda \cos 2\phi) \qquad (6.1.3)$$

Going back to the Serkowski curve and remembering that k is the same in both slabs:

$$\frac{dr_\lambda}{d\lambda} = \frac{2kr}{\lambda} \; \ln\left(\frac{\lambda_{2max}}{\lambda_{1max}}\right) \qquad (6.1.4)$$

where λ_{1max} and λ_{2max} are values of λ_{max} in the two slabs. From the above expressions we see that, provided $r \neq 0$, $\lambda_{1max} \neq \lambda_{2max}$, $\phi \neq 0$ and $\lambda \neq \infty$, then θ_λ does not reach a maximum. Hence the observed structure in the position angle of the linear polarisation of 55 Cygni and χ Aurigae is evidence of variation in both k and λ_{max} along the line of sight.

Table C1 gives the distances of each of the three stars, as calculated from their spectral types. These suggest that there will only be a couple of dust clouds in the line of sight to each of these stars. Direct evidence of the existence of separate clouds can be gathered from Fabry-Perot interferometry of the interstellar lines. Gas moving at different velocities with respect to the Sun will give rise to absorption lines displaced slightly in wavelength due to the Doppler effect. The supposition is that components of the gas moving at different velocities are physically separate and hence presumably at different distances. While the existence of interstellar gas clouds is not conclusive evidence of the same number of dust clouds, in general, the two are well correlated. Especially, the existence of CO is indicative of dust. Studies of ζ Ophiuchi show at least six components in high resolution spectra of interstellar

lines (HOBBS, 1974a). Their heliocentric velocities are -9.0, -12.6, -14.4, -17.5, -25.5 and -27.6 km/sec. The two strongest are the -12.6 km/sec and -14.4 km/sec components, which appear to represent clouds of significantly different composition. KI, CaII and possibly NaI are concentrated in the -14.4 km/sec component, while CH^+ is confined to the -12.6 km/sec component (MORTON, 1975). CO, which implies the presence of H_2 has also been detected in the -14.4 km/sec component (CRUTCHER, 1976). The molecular hydrogen is thought to be formed on grain surfaces. The two components at ∿-26km/sec contain NaI, but not CH^+ and probably not KI. The -9 km/sec component is thought to be associated with the Strömgren sphere at about 15 parsec from the star, while the main component (at -14.4 km/sec) arises from a cloud roughly equidistant between the Earth and ζ Ophiuchi. It is this major component that has been studied in detail (e.g. BLACK & DALGARNO, 1977 ; DE JONG, 1977 ; SMITH et al., 1978). The overall picture is of at least two dust clouds, associated with the -15 km/sec and the -26 km/sec component, respectively. In 55 Cygni, three velocity components are clearly visible (HOBBS, 1974), at -10.5 km/sec, -16.0 km/sec and -24.5 km/sec, while the radial velocity of the star itself is -7 km/sec. (The resolution of the interferometer was 1 km/sec when measuring the interstellar However, the accuracy of the stellar radial velocity is rather worse). All three of these components show up in NaI, CaII and KI lines (the KI line is at 7699 Å), and all are probably associated with dust. While we have not been able to find similar high resolution observations on χ Aurigae, its distance would also suggest that three or four clouds might on average be seen in that direction. It seems, therefore, that there is evidence for more than one dust cloud in the lines of sight to ζ Ophiuchi (interstellar line profiles),

55 Cygni (interstellar line profiles, circular polarisation) and χ Aurigae (circular polarisation and reported position angle changes). On the other hand, there is little evidence for circumstellar matter or intrinsic polarisation in the light of any of these stars. Accordingly we conclude that the position angle rotations are most likely the result of multiple dust clouds in the lines of sight to all three stars.

The small number of clouds along the lines of sight suggest that the most appropriate model to use for the polarisation would be the 'two-slab' model. As mentioned above, the analysis of MARTIN (1974) is only strictly applicable if only the position angle of grain alignment and the mean size of the dust grains in the two clouds change. In a full analysis, this might act as a first step in an iterative procedure which would finally give p_{max}, λ_{max} and k for each component. Because of the relative insensitivity of the curve of the degree of polarisation with wavelength, the position angle dependence would appear to be of premier importance in the process. However, the uncertainties in the measurements presented here make such an analysis inappropriate here. It may be worthwhile to use the simplified analysis of Martin to see what limits can be put on the model, and indicate whether further study would be appropriate. Circular polarisation measurements from the literature will be used, as tabulated in Table C1.

MARTIN (1974) gives the expression

$$q(\lambda_b/\lambda) = p^2_{max} \; B(\lambda_b/\lambda) \; D(\lambda_{max}/\lambda) \; G_\lambda \qquad (6.1.5)$$

where q = the observed circular polarisation

$D(\lambda_{max}/\lambda)$ = the dependence of linear polarisation on wavelength (the Serkowski curve)

$B(\lambda_b/\lambda)$ = the dependence of the birefringence of the interstellar

medium on wavelength (derived in MARTIN (1975). Also see MARTIN & ANGEL (1976)).

G is a 'geometrical factor' which is dependent on wavelength to roughly the same extent as r_λ defined above.

λ_b is the value of λ_{max} for the cloud nearest the observer.

We simplify by setting $\lambda_b = \lambda_{max}$, and take p_{max} and λ_{max} from SERKOWSKI et al. (1975).

For ζ Ophiuchi we have only an upper limit on the circular polarisation.

$$q(4400\ \mathring{A}) = 0.16 \pm 0.17 \quad \text{(units of } 10^{-4}\text{)}.$$

Also, $p_{max} = 1.43\%$, $\lambda_{max} = 0.59\mu$, $(\lambda_{max}/4400\ \mathring{A}) = 1.341$

$D(1.34) = 0.906$

$B(1.34) = 0.32$ (from MARTIN & ANGEL, 1976).

$\therefore \quad G = 0.27 \pm 0.29$

Now,

$$\lambda \frac{d\theta}{d\lambda} \approx 130\ G_\lambda\ \ln(\lambda_{max}/\lambda_b) \quad \text{(MARTIN \& ANGEL, 1976)(6.1.6)}$$

To see what sort of values λ_b and λ_{max} might take, we take $\frac{d\theta}{d\lambda}$ at 4400 Å from the measurements of position angle for ζ Ophiuchi presented here, and consider values of G of 0.27 and 0.56 (i.e. 1σ).

At 4400 Å, $\frac{d\theta}{d\lambda} = 8°\mu^{-1}$

$(\lambda_{max}/\lambda_b) = 1.106$ if G = 0.27

or 1.050 if G = 0.56.

If these are symmetric about the observed λ_{max}

G	λ_{max}	λ_b (Å)
0.27	6200	5600
0.56	6040	5760

Such values do not seem unreasonable. We note that the lower the

value of circular polarisation assumed for ζ Ophiuchi, the further apart λ_{max} and λ_b become. This is because a small value of circular polarisation implies that the angle between the grain alignment position angles in the two slabs (ϕ) will be small. In turn, if ϕ is small, λ_{max} and λ_b must be further separated to produce the observed position angle effect.

If we use the difference in the measured position angles between 3800 Å and 4400 Å, and assume that the two components are of equal strength at λ_{max}, we can derive $\phi \sim 46°$ from the equation for position angle θ quoted above. (If the ratio is less than one, ϕ is increased). One further quantity we can estimate is D - the depolarisation. Statistical studies show (SERKOWSKI et al., 1975) that the ratio $p_{vis}/E(B-V) < 0.195$, where p_{vis} is the observed degree of linear polarisation in the visible (and hence is close to p_{max}), expressed in magnitudes, and E(B-V) is the colour excess or reddening. Equality in the above relation indicates the case of maximum efficiency of polarisation by the grains. A number of mechanisms will cause the ratio $p_{vis}/E(B-V)$ to be less for any particular star. The alignment mechanism might not be as efficient, or have not acted for sufficient time. It may be stronger or weaker depending on the strength and orientation of the galactic magnetic field along the line of sight. Further, when light traverses more than one cloud some depolarisation will occur. It is this last factor we are interested in. Clearly, the depolarisation calculated to arise from the effect of two dust clouds must be less than the total depolarisation seen in the light from the star. More precisely, if

$$D_o = [p/E(B-V)] \; / \; 0.195 \quad (< 1) \qquad (6.1.7)$$

for any star, and D is the depolarisation arising in the two slab model, then we require $D > D_o$, where D_o is given for each of the

three stars in Table C1, and D is given by the expression:

$$D^2 = (1 + 2r_\lambda \cos 2\phi + r_\lambda^2) / (1 + r_\lambda)^2 \quad \text{(MARTIN, 1974)} \quad (6.1.8)$$

where r_λ and ϕ have been defined above. Since the value of r_λ is similar in the blue to its value at 5500 Å, we may deduce for ζ Ophiuchi, using the figures above:

$$D = 0.69$$

which is consistent with the value of D_o shown in the Table. To summarise, the published circular polarisation measurements of ζ Ophiuchi, taken together with the new observations on the rotation of position angle with wavelength, are consistent with a two cloud model where $\lambda_{max1} < 5760$ Å and $\lambda_{max2} > 6040$ Å. If the two components are of comparable size (which is unlikely, judging by interstellar line strengths), then the angle between the slabs, $\phi \approx 46°$. As the ratio of the strengths of the two components departs from unity, the derived value of ϕ is higher. A more homogenous set of accurate measures of position angles, and a more detailed analysis can give more information. For this star, it will also be necessary to detect and measure circular polarisation to higher accuracies in order to restrict the possible geometries. As an example, a calculated position angle dependence is shown as the dashed line on Figs C4 and C5. The model used assumed components of equal strength, $\lambda_{1max} = 5600$ Å, $\lambda_{2max} = 6200$ Å, $\phi = 46°$ and $k = -1.15$ for both components. Better fits can be obtained if the k's are allowed to be free parameters.

Although Martin's analysis is not applicable in the case of 55 Cygni, since the position angle reaches a maximum (at 3900 Å), we may derive some information from this approach. Using equation (6.1.5) in the same way as for ζ Ophiuchi and using the circular polarisation tabulated, we find

$$G = -0.87 \pm 0.15$$

where the error quoted comes just from the circular polarisation measure. This result is similar to, but not identical with, the value quoted by MARTIN & CAMPBELL (1976). As mentioned above it is necessary to allow the value of k in the Serkowski curve (equation 6.1.1) to vary along the line of sight to explain the position angle variations on 55 Cygni. The maximum in position angle may then correspond to the maximum in the polarisation of the minor component in a two cloud model. The peak is however displaced somewhat to shorter wavelengths by the major component, the peak of which corresponds to the observed maximum polarisation at 5400 Å. λ_{max} for the minor component probably lies at >4000 Å, its exact position depending on the relative strength of the two components and the angle between the two slabs. The analytic expressions for the location of this peak is complicated and not particularly useful. The best approach is probably one of numerical modelling of both the degree and position angle of polarisation. Since the linear polarisation peaks at 5400 Å, the major component must be considerably stronger than the minor one, while the location of the maximum in position angle implies that the minor component must have a narrower interstellar polarisation curve than the major one. This is equivalent to saying that k in the Serkowski curve is smaller (i.e. more negative) for the minor cloud. This last conclusion is opposite to what is normally observed. WILKING et al (1980) show that, statistically, k is smaller when λ_{max} is below average. There are at least four ways of narrowing the interstellar polarisation curve (summarised in the above paper):

a) increasing the real part of the refractive index, or decreasing the imaginary part;

b) presuming a more perfectly aligned distribution of grains;

c) presuming more spherical particles;

d) narrowing the size distribution.

For the particles thought to give rise to the interstellar polarisation, the imaginary part of the refractive index is already constrained by circular polarisation observations to be small (< 0.1). Further, it might be expected that more spherical particles would be harder to align, so that the effects of (b) and (c) above might cancel. We therefore suggest the existence of a cloud of smaller than average (0.05-0.1μ), high-index dielectric particles in the line of sight to 55 Cygni. To have a high index of refraction (say 1.6-1.7), such particles could not have thick mantles of 'dirty ice' or other low index material. At the present time it is questionable whether such mantles are a necessary feature of interstellar grain models (see e.g. WHITTET, 1981).

Using the two-slab model we may derive an upper limit to ϕ from D_o, tabulated in Table C1. If the components are of equal strength, we find $\phi < 55°$, while if one component is twice as strong as the other, the upper limit is $\phi < 60°$.

The behaviour of the position angle of χ Aurigae presents the same problems as did the position angle measurements of 55 Cygni. MARTIN (1974) reported a position angle rotation of -9° between 0.33μ and 0.94μ, equivalent to $15°\mu^{-1}$. This implies a difference of over 5° between U and R broad-band measurements, which is clearly inconsistent with the measurements of SERKOWSKI et al. (1975). The new measurements reported here peak at around 5000 Å, as do those of Serkowski et al., but seem to decrease into both the red and blue in contradiction to Serkowski's measures. In the case of χ Aurigae, the peak in position angle does not require us to postulate a secondary component with such small particles as that necessary in the case of 55 Cygni. However, it is still necessary

for the secondary component to have a 'sharp' (i.e. $k < -1.15$) polarisation dependence on wavelength. Since the position angle maximum is associated with the minor component, this component must again have a smaller average grain size than that of the major component. From the depolarisation D_o the two-slab model gives $\phi < 58°$ when both components are equal and $\phi < 64°$ when one is twice the size of the other. The similarity of the values of ϕ found for all three stars in this section might be a consequence of the fact that all lie well within the local spiral arm.

To summarise this section, we see that at least two interstellar components are required to explain the present observations of polarisation of ζ Ophiuchi, 55 Cygni and χ Aurigae. In the cases of 55 Cygni and χ Aurigae, where the position angle reaches a maximum, the minor component is required to have a smaller mean particle size and a 'sharper' (i.e. k smaller) distribution of polarisation with wavelength than the main component. Alternatively, the maximum in position angle can be explained by invoking an intrinsic component of polarisation in each star. There is no other evidence of this for these stars, and certain features of the polarisation also argue against it.

This study is not aimed at the very broad band dependence of the degree and position angle of linear polarisation on wavelength, and the measurements presented here incorporate too many 'instrumental corrections' and 'normalisation factors' to make detailed modelling worthwhile. However, some tantalising deductions have been (provisionally) made from these measurements. A full study might aim to separate out the polarisation characteristics of individual clouds along the line of sight. Candidate stars for study would show an above average value for the ratio p/E(B-V), would be relatively

nearby (r < 1 kpc) and would show interstellar line profiles with only a small number of components. It would be important to obtain as broad a wavelength base line as possible in order to have the best chance of separating out the several components. Any variability in position angle or degree of polarisation would be strong evidence of intrinsic polarisation. The best wavelength region to observe would be around 4000 Å.

6.2 Variations in the polarisation of ζ Ophiuchi at $\lambda \sim \lambda_{max}$. Together with the feature at 4100 Å which is discussed below, the most interesting structure seen in the degree of polarisation of ζ Ophiuchi is the oscillatory dependence seen in the red. As was previously discussed, the structure in the degree of polarisation is matched by changes in the position angle. Although coverage of 55 Cygni was unfortunately not complete enough to show if similar structure existed in that star, measurements of χ Aurigae do show suggestions of such oscillations. Throughout this chapter, the Serkowski curve has been used to fit the data and to decide where structure exists. This point was discussed in section 3, where a possible alternative 'summary' curve was suggested. Since the structure in the polarisation of ζ Ophiuchi has a scalelength of between 600 and 1500 Å, it is worth considering in passing whether such structure is merely an artifact of the analytic summary curve adopted. As an example, consider Fig. C18, which shows the structure expected in the data when plotted as deviations from the best-fitting Serkowski curve, if the Reciprocal curve (described in section 3) is in fact a better fit to the data. It is a feature of the wavelength dependence of the polarisation that there is an approximate symmetry about λ_{max}, i.e. if the polarisation is given by the form

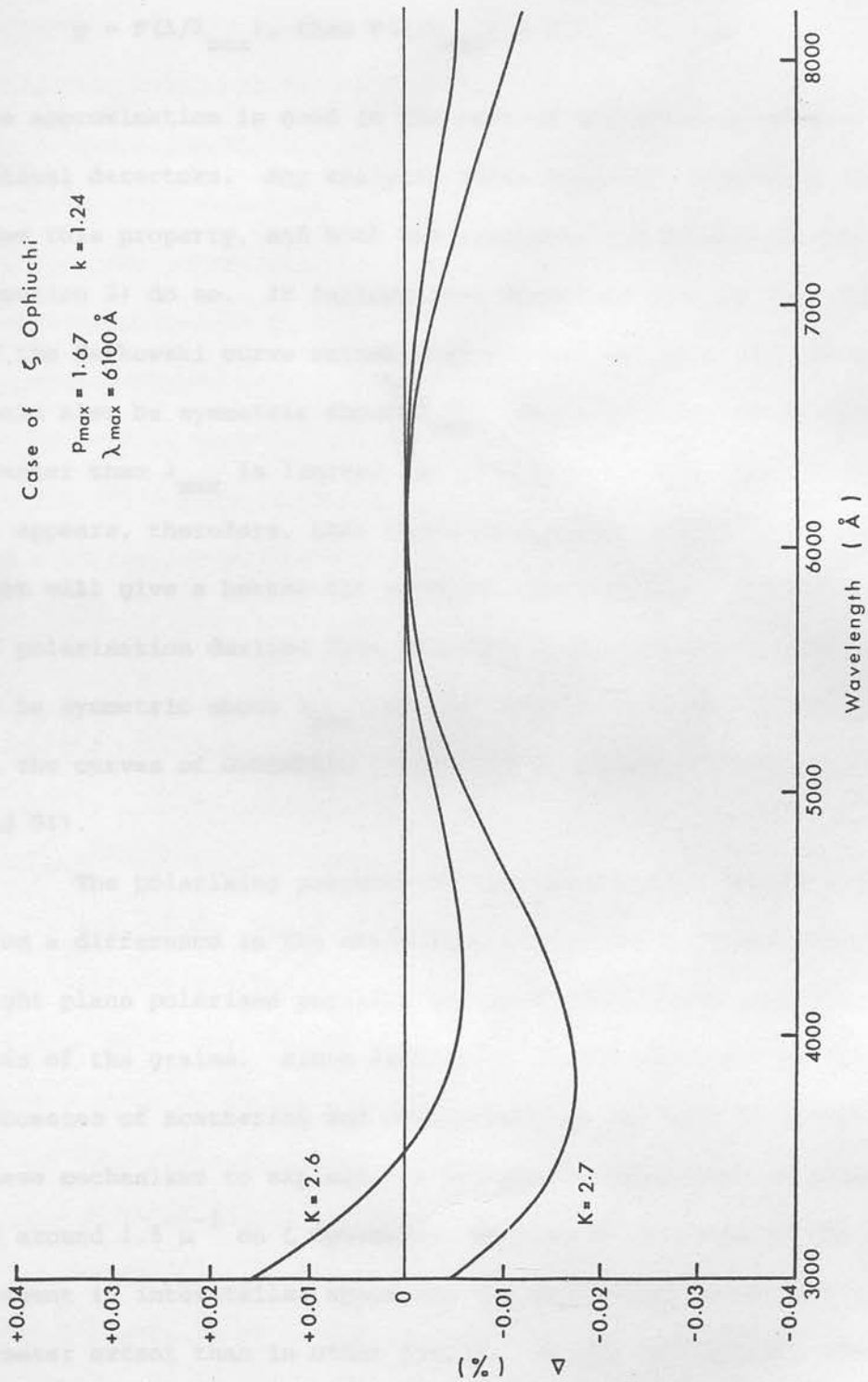

Figure C18: A comparison of the Serkowski and Reciprocal curves: the case of ζ Ophiuchi. Parameters for the best-fitting Serkowski curve to the data presented in this chapter are given. The solid lines show the difference Reciprocal minus Serkowski for two values of K in the Reciprocal curve expression. If the interstellar polarisation curve were better represented by a Reciprocal curve, the graphs of polarisation residuals (e.g. figures C6 and C9) would show structure following the solid curves shown here.

$p = F(\lambda/\lambda_{max})$, then $F(\lambda/\lambda_{max}) = F(\lambda_{max}/\lambda)$. (6.2.1)

The approximation is good in the part of the spectrum studied with optical detectors. Any analytic curve used must therefore also have this property, and both the Serkowski and Reciprocal curves (section 3) do so. It follows that structure arising from the use of the Serkowski curve rather than another analytic representation would also be symmetric about λ_{max}. While coverage of wavelengths greater than λ_{max} is limited, no structure of this kind is seen. It appears, therefore, that there is no other simple analytic curve that will give a better fit to these observations. Of course, curves of polarisation derived from detailed model fitting are not required to be symmetric about λ_{max}, as can clearly be seen, for example, in the curves of GREENBERG (1968) (e.g. his Figures 40, 82, 87 and 91).

The polarising property of the interstellar medium arises from a difference in the extinction efficiencies of the medium for light plane polarised parallel and perpendicular to some characteristic axis of the grains. Since extinction is the resultant of the two processes of scattering and absorption, we may look to either of these mechanisms to explain the wavelength dependence of polarisation at around 1.5 μ^{-1} on ζ Ophiuchi. Because of the size of the grains present in interstellar space the two mechanisms interreact to a greater extent than in other fields. In the 'continuum', the extinction by the grains is dominated by their scattering properties, with the complex part of the refractive index constrained to be < 0.1 by circular polarisation observations, at least in the general case. Any spectral absorption in the grains, it will be recalled, is bound to affect the real part of the refractive index through the Kramer-Krönig relations, and lead to a dispersion-curve shaped wavelength

dependence of this quantity. Calculations of absorption bands in dielectric cylinders by GREENBERG (1974) with the aim of predicting the polarisation variations expected if the diffuse bands arose in the grains, show dispersion-curve shaped features in both extinction and polarisation. Depending on the exact size of the particles the most noticeable feature of such absorptions can either be a dispersion-shaped curve, a clear absorption with a weak 'emission' wing or even a strong 'emission' with a weak absorption wing! MARTIN & ANGEL (1975) quantified earlier observations that the extinction and polarisation profiles had similar wavelength dependences, in the form

$$\frac{\Delta p}{p} = f \frac{\Delta \tau}{\tau} \qquad (6.2.2)$$

where p = continuum polarisation, τ = continuum optical depth, and Δp and $\Delta \tau$ are the polarisation and optical depth variations across the band. The value of f was model dependent but adequately represented by $f = 1.4 \pm 0.4$. While these calculations were done in connection with small scale (50-100 Å) structure about diffuse bands, the conclusions are also valid when considering larger scale variations. This is clearly shown by the work of HAYES et al. (1973) in their analysis of the Very Broad Structure (VBS) in the extinction curve. We shall return to these points below.

Broad band changes (rather than spectral absorption) in the optical constants of a candidate material for interstellar grains affect its derived polarisation and extinction wavelength dependence. The rapid decline of the refractive index of graphite and of magnetite in the infrared have been used by workers to model infrared polarisation measurements (e.g. DYCK & JONES, 1978).

It has been repeated often that the existence of the Serkowski 'Law' for interstellar polarisation implies that the optical constants of

the grain material are reasonably constant across the optical and near-infrared. In the main, it is the symmetry about λ_{max} that is being referred to. However, the baseline on which the Serkowski curve is usually fitted makes it rather insensitive to such changes, and, with judicial choices of mean size and size distribution, a great deal of structure can be reduced to unobservable levels.

The Mie theory of scattering for infinite cylinders has been extensively used to model the linear polarisation produced by the dust between the stars. GREENBERG (1968) has shown that the calculations for infinite cylinders are reasonably accurate for other elongated particles as long as their axial ratio is greater than two. When a particular size and refractive index are chosen, the calculated polarisation shows oscillations around λ_{max} not too dissimilar to those seen in ζ Ophiuchi. Typical curves for various indices of refraction are given in GREENBERG (1968) (his Figures 38, 39, 40 etc.). These oscillations in polarisation (and extinction) arise from interference between light hitting the edges of the particle (HANSEN & TRAVIS, 1974) and have a wavelength of $\sim 0.8x$, where $x = 2\pi a/\lambda$, and 'a' is the radius of the cylinder. According to the Mie theory cylinders scatter similarly to spheres with the same radius, and since cylinders clearly have more 'edges' than spheres of the same radius, these oscillations are stronger in calculations involving cylinders. If the features at 5750 and 6600 Å arise from this source, the characteristic wavelengths would be between 600 and 1600 Å. Structure of wavelength 600 Å could be caused by particles of $\sim 0.98\mu$, while that of wavelength 1600 Å would arise from particles of radius 0.25μ. If it is further required that the oscillations occur at low values of x (equivalent to supposing the particles in question produce some significant proportion of the observed continuum linear

polarisation) then it is possible to obtain structure of wavelength 1600 Å, but not less. The oscillations turn out to be at the 10-15% level, but would seem to be stronger towards shorter wavelengths. Similar low amplitude structure might also be expected if the grains were regular prisms, or other regular shapes. While possible, such shape-dependent effects are unlikely to be the explanation of the observed dependence of linear polarisation. GREENBERG (1968) makes it clear that even a small distribution of size will almost completely smooth out these oscillations, as might be expected of surface phenomena. To invoke this mechanism it would be necessary to postulate the existence of a number of large particles with a very small size distribution. The particles would also have to be very 'smooth' since surface texture will also tend to wipe out observable structure. As the grains are thought to grow by accretion from the interstellar gas or possibly by aggregation (WHITTET, 1981), such regularity seems very unlikely. It appears therefore that shape and surface effects will not prove to be of sufficient importance to give rise to the observed structure in the linear polarisation of the light from ζ Ophiuchi.

If absorption in the grains produces the structure in the polarisation and the grains are also those responsible for the extinction, we may use MARTIN & ANGEL's (1975) relation to predict the amplitude of the consequent extinction variations. The following table is calculated from equation (6.2.2) and presumes R = 3.1, f = 1.4, λ_{max} = 5500 Å, k (the 'sharpness' constant in the Serkowski curve) equals 1.15, and A_λ, the extinction in magnitudes at wavelength, λ, interpolated from Table 2 of SAVAGE & MATHIS (1979).

To use the table, note that the extinction change (in magnitudes) associated with a change in the polarisation of Δp (in units of 0.01%)

Wavelength Å	F_λ
3000	0.059
3500	0.044
4000	0.035
4500	0.030
5000	0.026
5500	0.022
6000	0.020
6500	0.018
7000	0.018
7500	0.016
8000	0.015

on a star with maximum polarisation p_{max} (in per cent) and reddening E(B-V) (in magnitudes) is:

$$\Delta m = \frac{\Delta p}{p_{max}} \times E(B-V) \times F_\lambda \qquad (6.2.3)$$

The error introduced into the resulting value of Δm is probably of the order of 50%. With the above table we see that the observed polarisation variation of 0.04 to 0.08 per cent at 6670 Å should appear as an 0.01 to 0.02 magnitude enhancement at the same wavelength in the extinction curve. Unfortunately spectrophotometric scans of sufficient accuracy to detect these small variations were not obtained, nor do such scans for ζ Ophiuchi appear in the literature. However, a very recent paper does give high precision extinction curves for some southern Milky Way stars, including two in the ρ Ophiuchi complex (VAN BREDA & WHITTET, 1981). Two extinction curves taken from these authors' Fig. 1 are reproduced here as Fig. C19. The extinction curves are plotted as residuals from a straight line drawn between the two points at which the extinction curves are normalised, namely 4560 Å and 7800 Å. The curve marked 'mean' is a mean of twenty long pathlength (d > 1 kpc) reddened stars. The lower curve is the extinction curve for HD 147889, a star in the ρ Ophiuchi complex. The mean curve shows the so-called VBS structure originally noticed by WHITEOAK (1966), but with considerable fine

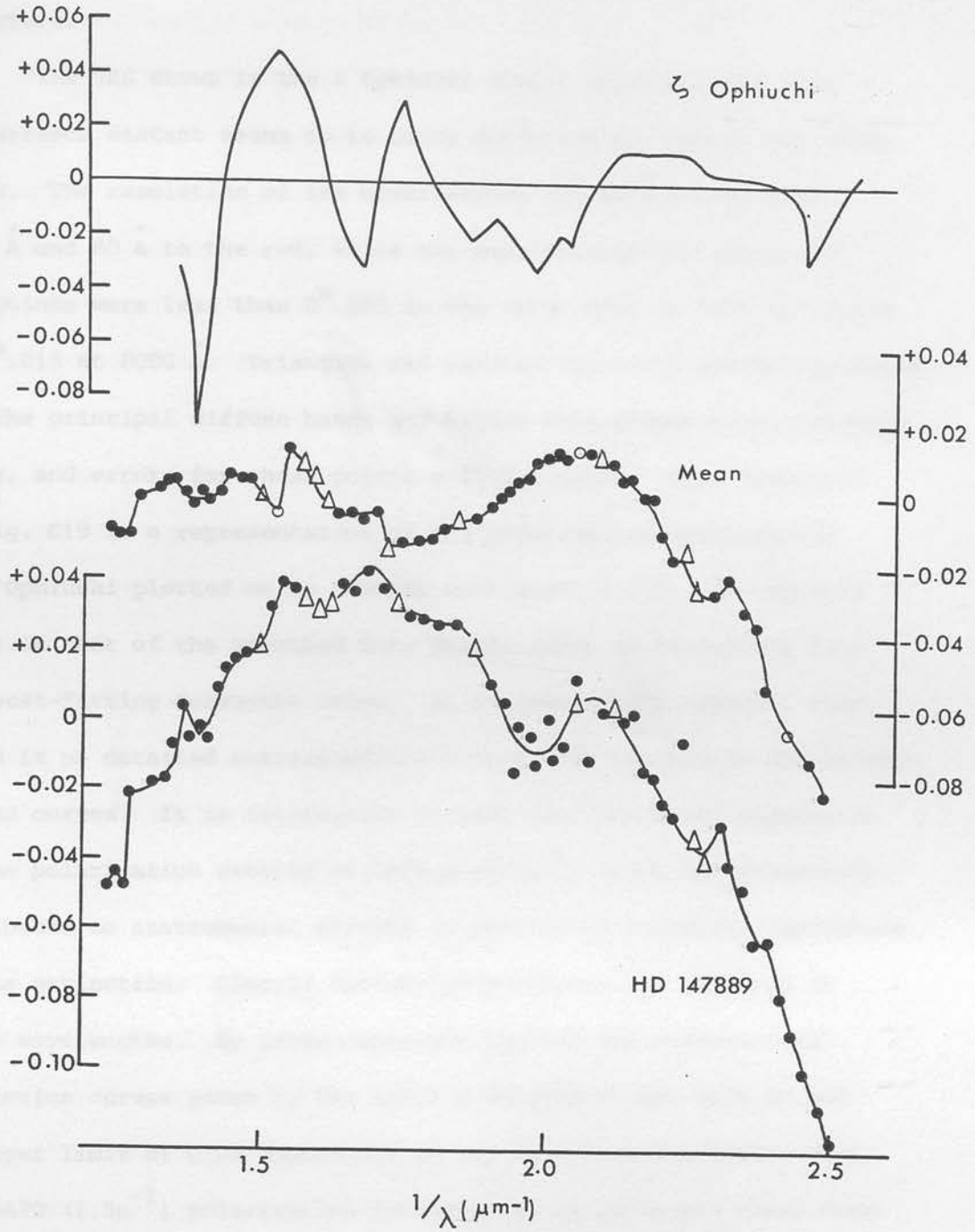

Figure C19: A comparison of the linear polarisation variations of ζ Ophiuchi with high quality extinction curves from VAN BREDA and WHITTET (1981). The top curve shows polarisation measurements of ζ Ophiuchi after subtraction of the best-fitting Serkowski curve. The ordinate scale is in percent. The centre and lower curves are extinction measurements after subtraction of a linear extinction, law normalised at 2.19 μ^{-1} and 1.28 μ^{-1}. The 'mean' curve is an average of 20 long path length ($d > 1$ kpc) reddened stars, while the lower curve is of the nearby HD 147889 which is in the ρ Ophiuchi complex. Both ordinate scales are in magnitudes. Triangles and circles represent points corrected for the principle diffuse bands and Balmer lines respectively.

structure.

The VBS shown in the ρ Ophiuchi stars, which are less than 200 parsecs distant seems to be quite different to that in the other stars. The resolution of the observations was 40 Å blueward of 5260 Å and 80 Å to the red, while the mean photometric errors of the points were less than $0^m.005$ in the range 4000 to 7150 Å, rising to $0^m.015$ at 8000 Å. Triangles and circles represent points corrected for the principal diffuse bands and Balmer line mismatching, respectively, and errors for these points will be larger. Also displayed in Fig. C19 is a representation of the polarisation measurements on ζ Ophiuchi plotted on an inverse wavelength scale. The plotted curve is that of the smoothed data points shown as deviations from the best-fitting Serkowski curve. It is immediately apparent that there is no detailed correspondence between the extinction and polarisation curves. It is interesting to note that the broad depression in the polarisation centred at 5000 Å ($2.0\mu^{-1}$) which was previously attributed to instrumental effects is matched by a similar depression in the extinction. Clearly further measurements are required at these wavelengths. By intercomparison between the differential extinction curves given by VAN BREDA & WHITTET we are able to put an upper limit of 0.02 magnitudes on any structure associated with the 6670 ($1.5\mu^{-1}$) polarisation feature. It is certainly clear from the paper referred to that real differences exist between scans of different stars (though these may be due to instrumental effects) and hence that the apparent absence of structure corresponding to the polarisation on these stars is not proof of the absence of structure at this level in the extinction curve of ζ Ophiuchi. If these variations in extinction between different stars are real, easily detectable polarisation variations may well be observable. Other references

for visual extinction were examined but none were found with measurements more accurate than for the extinction scans used. We conclude that the extinction curves presently available do not appear to show structure corresponding to the polarisation structure seen in ζ Ophiuchi. To this we add two caveats. Firstly, that the predicted variations in extinction would be at the limit of detectability, and secondly, that since ζ Ophiuchi may be a special case, this conclusion may be modified when very high precision scans of this star become available. If structure does not appear in the extinction curve the deduction might be that the grains carrying the visual extinction are not identical to those responsible for the linear polarisation. If more than one dust cloud is intersected by the line of sight and contributes to the polarisation, we must consider how this conclusion is modified. Any depolarisation caused by the changing grain alignment will not affect the validity of equation (6.2.3) since polarisation only appears as a ratio. The position angle rotation associated with the variation in the degree of polarisation implies that the feature appears much more strongly in some clouds along the line of sight than in others. Using the terminology of the two-slab model we may say that although the structure in polarisation is weaker (or possibly absent) in one of the clouds, both clouds must polarise the light passing through it. In ζ Ophiuchi the rotation in the position angle is in the same direction as the rotation in the ultraviolet. Since we expect a rise in polarisation across an absorption feature (but see section 6.3), it may be concluded that the polarisation feature is carried by, or is dominant in, the 'slab' that becomes more important in the ultraviolet.

If the polarisation structure is indeed not reproduced in the extinction curve then we may summarise the conclusions reached by

considerations of the new results as follows:

i) Extinction and polarisation arise from more than one grain population. The two (or more) populations polarise light that is passing through them with different efficiencies. One population might contribute to the extinction alone.

ii) Along the line of sight, the proportion of these populations changes. It is possible that they are in distinct, physically separate clouds.

iii) The polarisation structure arises in the grain population that is the more efficient polariser. This grain population, in the case of ζ Ophiuchi, must have either a smaller mean grain size or smaller refractive index (either by at least 10%) to explain the wavelength dependence of position angle.

These conclusions form a self-consistent explanation of the new polarisation measurements presented. Other explanations may of course be possible.

In the 'standard model' of the interstellar grains (insofar as such a thing exists), polarisation and extinction in the visible are caused by 0.1-0.2μ silicate particles, possibly with photolysed 'dirty ice' mantles. A second population of very small (0.02μ) grains of graphite (or amorphous carbon) is also postulated to explain the 2200 Å extinction feature. However, MATHIS et al. (1977) have fitted the extinction from 0.11 to 1.1μ with a mixture of bare graphite and silicate grains in which the graphite contributes something like 50% of the extinction in the visible. It is further proposed that the polarisation is only produced by the (larger) silicate grains (MATHIS, 1979), and that the graphite grains are not aligned. The modelling satisfies cosmic abundances and the

observed depletions of heavy elements in the medium but assumes that the silicate grains are perfectly aligned by the Davis-Greenstein mechanism. We may interpret the above conclusions in terms of this model by identifying the efficiently polarising dust component with the silicate grains, and the graphite grains as a non-polarising or weakly polarising component. The polarisation structure might then arise from impurities in the silicate grains and the difference in the polarising efficiencies (i.e. p/τ) of the two clouds in the two-slab model might then simply reflect a change in the proportions of the two sorts of grain. If the graphite grains are non-polarising, then the impurity giving rise to the polarisation variations may only occur in the silicate grains of one of the clouds. In either case, the corresponding structure in the extinction curve would be reduced in magnitude by at least a factor of two, and would hence become undetectable in presently existing extinction measurements. Clearly, any other model in which extinction and polarisation in the visible are caused by more than one sort of grain is also consistent with these observations.

It has been suggested that the Very Broad Structure (VBS) seen in the extinction curve (see HAYES et al., 1973 ; SCHILD, 1976) is caused by absorptions in magnetite (Fe_3O_4) grains or impurities (MANNING, 1975 ; VAN BREDA & WHITTET, 1981). Measurements of the refractive index of magnetite by HUFFMAN (1977) [or, more accessibly, HUFFMAN & STAPP, 1973] show structure in the visible comparable to the VBS, though an exact correspondence has not been found. However, magnetite grains, or grains including magnetite impurities, are expected to be well-aligned by the galactic magnetic field, and hence such structure should appear in the polarisation as well as in the extinction. We have seen, however, that there is no exact

correspondence between extinction and polarisation variations. It is noteworthy that the maximum value of the real part of the refractive index of magnetite occurs at very close to $1.5\mu^{-1}$ (6670 Å). In polarisation curves calculated from models using magnetite grains, this feature shows itself as a distinct 'bump' or enhancement in the polarisation at this wavelength (see, for example, CODINA-LANDABERRY & MAGALHAES, 1975). A feature is seen at such a wavelength in the linear polarisation of ζ Ophiuchi, though it appears to be rather 'sharper' than shown in the theoretical curves. VAN BREDA & WHITTET (1981) argue that the cosmic abundance of iron and the necessity for the grains giving rise to the circular polarisation to be a 'reasonable' dielectric imply that the magnetite if present, would exist either as small grains or as impurities in the larger grains carrying the polarisation. Accordingly, we tentative suggest that the structure in the polarisation curve may arise from magnetite impurities in certain (not necessarily all) silicate grains. The VBS would then be caused partially by the optical properties of magnetite impurities and partially by other sources. One possible source might be similar transitions to that which gives rise to the structure from magnetite but involving other transition metals, perhaps in a disordered lattice. The magnetite impurities would lead to good alignment of their host grains, in agreement with Mathis' model, and with constraints imposed by the observation of polarisation increases across the 9.7μ silicate band (MARTIN, 1975).

Summarising the previous sections, we see that shape and surface effects probably will not explain the observed polarisation variations in the red on ζ Ophiuchi. Since such effects would be rendered insignificant by averaging over any reasonable grain size distribution, broad absorption features must be invoked. It seems,

provisionally, that structure corresponding to the polarisation variations does not appear at the predicted level in the extinction curves. However, if more than about half of the visual extinction did not arise in the polarising grains the predicted features in the extinction would not be detectable. If the structure in the polarisation is caused by magnetite impurities in silicate grains, the efficient production of polarisation by such grains also becomes understandable. Of course, such an assignment is rather speculative at this time, and does leave open the question of the origin of the VBS. The apparent variability of the VBS from star to star in any case suggests multiple sources for these features.

The model used to interpret the polarisation observations is reasonably consistent with recent work on the fitting of grain models to the observed extinction and polarisation. Further work must focus on the two critical points in the above arguments. Firstly, the polarisation structure observed in ζ Ophiuchi must be confirmed in that star and the measurements extended to other reddened stars. If the structure were found to be significantly variable in shape and/or location from star-to-star this might be evidence of shape or grain size distribution effects, or, of course, in chemical composition of the grains. Secondly, the polarisation profiles obtained must be compared with high accuracy (<0.005 magnitude) extinction curves of the same star to determine if variations corresponding to the polarisation oscillations do occur, and if so, at what level. The prize to be won from such studies is no less than a new model of the interstellar dust.

6.3 The 4100 Å feature on ζ Ophiuchi

The 4100 Å feature found on ζ Ophiuchi is considerably 'sharper' than the polarisation variations discussed above. The polarisation curve is depressed by 0.03 to 0.04% at its lowest point, and a correlated rotation of position angle of 0°.7 is also found. This position angle rotation again implies that the feature only occurs in (or is markedly stronger in) just one of the two contributors to the polarisation found necessary by the broadband position angle wavelength dependence. The ratio of the position angle rotation found here to that found at the 6700 Å feature is roughly the same as the ratio of the corresponding features in the degree of polarisation. While this is as expected, the direction of the position angle rotation implies that the polarisation component that is of increased importance in the ultraviolet also becomes more important at the centre of this feature. Since the degree of polarisation declines across the feature, the implication is that the other component weakens. Hence this 4100 Å depression does not arise in the same component as the features discussed in the previous section (6.2).

An absorption feature carried by the polarising grains will give rise to changes in both the extinction and polarisation curves across it as discussed in section 6.2. The predicted change in the extinction curve corresponding to the 4100 Å feature is 0.005 to 0.010 magnitudes at the centre of the absorption band (i.e. a central depth of less than 1%), or even less if the polarising grains do not produce all of the extinction at these wavelengths. However, the sense of the polarisation variation implies an 'emission' by the grains. As previously discussed, the profile of a spectral absorption carried by small particles is greatly modified by scattering. Examination of Fig. 4 in GREENBERG & HONG (1974) shows that when

$2\pi a/\lambda \sim 2$ (where a = grain radius), the most obvious feature is the 'emission' wing, the absorption being barely visible. Normally grains of size $2\pi a/\lambda \sim 1.5$ are used to fit the interstellar polarisation curve. The fact that an emission feature appears is therefore giving information on the mean size of the grains carrying the feature. Indeed we have already seen that this feature arises in the dust cloud with the larger mean grain size (i.e. with the larger λ_{max}). The polarisation measurements obtained on 55 Cygni and χ Aurigae here do not appear to show structure at these wavelengths. This may be because of the larger errors in the measurements on these stars, but it is also possible that the absorption may only appear in certain lines of sight. It is worthwhile examining extinction curves of high precision to see if perhaps corresponding structure appears. Unfortunately this is a difficult part of the spectrum for which to obtain accurate extinction curves. In the early-type stars normally used to obtain extinction curves, spectral absorption may be present at 3970 Å (He), 4026 Å (HeI + II), 4101 Å (Hδ) and 4144 Å (HeI), and any mismatching of the reddened and unreddened stars can lead to 'features' here. While the available extinction curves do not show an effect at 4100 Å, those of VAN BREDA & WHITTET (1981), SCHILD (1977) and WALKER et al. (1968) all exhibit an increase in absorption in the region 4200-4300 Å. This increase seems to be quite narrow, but this is not well determined. It is possible that this is the absorption side of the feature observed in the polarisation in ζ Ophiuchi. We note that HAYES et al. (1973) suggest an absorption centred at 4170 Å.

Since this feature is constrained to arise in a different dust cloud to the cloud in which the structure at $\lambda \sim \lambda_{max}$ arises, we may not also seek to explain it using magnetite impurities in the polarising grains. The feature appears to arise in the cloud with

the larger grain size. If the grains are larger because of the existence of a thicker mantle, it is possible that this depression in the polarisation may be caused by an absorption in the mantle material. Mantle absorptions have been suggested as an explanation for the diffuse bands, but the lack of polarisational variations across these bands has thrown serious doubt on such a source. Transitions in complex organic molecules can give rise to broad absorptions in the visual part of the spectrum even in gaseous form. It may be that at 4100 Å in the polarisation spectrum of ζ Ophiuchi we are seeing a weak and broad diffuse band that does indeed arise in the polarising grains. We note that HERBIG (1975) has searched the region 3000-4400 Å and found no strong diffuse bands, though a weak band may appear at 3970 Å. If the 4100 Å is indeed a 'diffuse feature' (i.e. is formed in the same way as other diffuse features) it extends blueward the suggested energy cutoff of these features.

A decrease in the polarisation might arise if a component of the polarisation was intrinsic rather than interstellar, and if the star produced an emission feature at these wavelengths. If the intrinsic polarisation was by chance aligned at an angle roughly similar to that of one of the interstellar components of the polarisation, and was reasonably weak, it would not necessarily be detected in either the dependence of magnitude or position angle of polarisation over extended wavelength intervals. However, the origin of the emission would be problematic. If it is attributed to either Hydrogen or Helium emission, similar and probably stronger features would appear at other wavelengths. The emission would also have to appear in the spectrum of the star at about the 10% level at 4100 Å. Since no emission appears, we may rule out this possibility.

Finally we note that the spectrometer used to obtain these

measurements is calculated to have a Wood's Anomaly of ∿4100 Å (see section A2.6). This should appear as a weak 'band' in the spectrum and arises from the polarising properties of the grating. Such an intensity feature should not affect the measured polarisation in the present instrument.

To summarise: the 4100 Å feature appears to be an 'emission' feature in a different component of the polarisation to that giving rise to the features in polarisation in the red. This component is the one with the larger mean grain size. The feature may be related to the structure seen in the extinction curve in other stars and may be related to the well-known diffuse bands. Although the origin of the feature is unknown, it may arise in a mantle of complex molecules on the grains.

6.4 The 4420 Å feature on 55 Cygni.

It was suggested earlier that polarisation structure corresponding to the 4400 Å diffuse band might be present in the observations obtained of 55 Cygni. However, as previously mentioned (section 2) other authors find no evidence of polarisation variations across this band (A'HEARN, 1972 ; MARTIN & ANGEL, 1974). In particular A'Hearn (op. cit.) has measurements of 55 Cygni. His measurements of polarisation at 4410, 4430 and 4450 Å, respectively, are (2.64 ± 0.01)%, (2.68 ± 0.03)% and (2.76 ± 0.02)%. These errors are not reasonable as the Serkowski polarisation curve predicts that the degree of polarisation should only drop by 0.01% between 4410 and 4450 Å. Hence these continuum measurements should be identical within A'Hearn's errors. They are not, and it seems a more realistic error for these polarisation measurements would be 0.04 to 0.05%. Alternatively, real structure associated with the band could be occurring! In

any case, A'Hearn's measurements are now consistent with the feature reported here. The measurements of Martin & Angel (op. cit.) on HD 183143 and HD 21389 are more convincing and rule out any variation at more than 20% of the predicted level. While it is possible that the line of sight to 55 Cygni is different and that the 4430 Å band in this star may indeed show polarisation variations across it, the large scatter in our measurements makes such a conclusion premature. It may be that the observed polarisation features are real but unrelated to the diffuse band at 4430 Å. It should be noted that the apparent feature is a decrease in polarisation (corresponding to a grain 'emission') and is not associated with a position angle rotation. This latter point implies that it must arise in all or most of the clouds in the line of sight. We commend this part of the spectrum (4100 to 4500 Å) to our fellow observers for more detailed polarimetric study.

7. Conclusions and future work.

There are three main results of section 6. Firstly, structure in the polarisation of ζ Ophiuchi has been detected with scale lengths of 400 Å to 1400 Å and at wavelengths greater than or equal to λ_{max}. No exact correspondence was found with published high quality extinction curves of various stars. The structure was tentatively suggested as being due to magnetite impurities in large grains, while the VBS would then arise partially from the same source but also partially from other sources. In particular oxidation state changes of other transition metals in a disordered lattice might contribute. Structure due to magnetite is expected to be more clearly delineated in polarisation measurements than extinction measurements because of the enhanced alignment of grains carrying such impurities. Secondly, a broad (100 Å to 200 Å) feature has been found in the polarisation of ζ Ophiuchi at a wavelength of 4100 Å. The feature appears to arise in larger than average grains and may be associated with an extinction feature seen at slightly longer wavelengths in other stars. The absorption may be a true solid state transition of the sort originally postulated to cause the diffuse bands or may arise in the complex organic molecules that have been suggested to form the mantles on the grains that cause visual extinction and polarisation. Finally, the broad-band variations in position angle observed in ζ Ophiuchi, 55 Cygni and χ Aurigae have been interpreted as implying multiple dust clouds in the lines of sight to each of these stars. The various clouds differ in their mean grain sizes and their grain size distributions (as evidenced by variations in the fitted parameters k and λ_{max} in the Serkowski curve), and also have differences in chemical composition as shown by the appearance of features in the polarisation produced by some clouds, but not others.

Spectral features detected in the polarisation are certain to provide new and important constraints on the chemical composition of the polarising grains. I should also like to point out that differences in alignment of grains in the various clouds along the line of sight at least nominally allow the possibility of studying the properties of the individual clouds. Hence for simple lines of sight it might be possible to use polarimetry to study the dust clouds in the interstellar medium and to combine this information with the results of the study of the interstellar gas in order to obtain a better picture of the structure and distribution of matter in the voids between the stars. For example, interstellar shock fronts are often used to account for gas clouds of differing chemical composition detected by sharp lines in the light of various stars. Such shock fronts will also have important effects on grains in the vicinity. The grains may be completely or partially destroyed, may be concentrated in space and may be better aligned by the locally enhanced magnetic field in the vicinity of such shocks.

Clearly, the first priority for further observation is to confirm these measurements with a different polarimeter. Presuming that these features are indeed confirmed, further study will then be required on other stars to see how the detected structure varies in different parts of the sky and in lines of sight with differing mean grain sizes. In this way one may attempt to separate out the effects of scattering and absorption. It is of importance to compare the derived polarisation spectra with extinction scans of the same stars in order to see what proportion of the visual extinction is attributable to the polarising grains. Finally, accurate study of the wideband position angle dependence together with the polarisation in relatively simple lines of sight should allow physical

modelling (at some level) of individual dust clouds in the medium and reveal their correlation with the observed interstellar gas clouds. Most of the above observations would require high precision but only relatively modest resolutions (10 - 100 Å). Multichannel polarimeters are necessary to allow the measurements to be obtained efficiently.

The contribution of polarimetry to the study of the interstellar medium has been important in the past. It seems that this tool can contribute a great deal more information in the years to come.

Literature cited

Two useful texts are denoted by abbreviations:

PSN: "Planets, Stars and Nubulae, studied with photopolarimetry", ed. T. Gehrels, Univ. of Arizona Press, Tucson, 1974.

NIM: "Nebulae and Interstellar Matter", ed. B.M. Middlehurst and L.H. Aller, being Volume 7 of "Stars and Stellar Systems". University of Chicago Press, Chicago, 1968.

Aannestad, P.A.; Purcell, Em: 1973, Ann. Rev. Ast. and Ap., 11, 309.

Adams, W.S.: 1948, Ap. J., 109, 354.

A'Hearn, W.F.: 1972, Ast. J., 77, 302.

Allamandola, L.J.; Norman, C.A.: 1978, Ast. and Ap., 63, L23.

Allamandola, L.J.; Greenberg, J.M.: 1979, Ast. and Ap., 77, 66.

Appenzeller, I.: 1968, Ap. J., 151, 907.

Barker, P.K.; Brown, T.: 1974, Ap. J., 192, L11.

Beals, C.S.: 1936, M.N.R.A.S., 96, 661.

Black, J.H.; Dalgarno, A.: 1977, Ap.J. Supp., 34, 405.

Blades, J.C.; Somerville, W.B.: 1977, M.N.R.A.S., 181, 769.

Blanco, A.; Bussoletti, E.: 1980, Ap. and Sp. Sci., 67, 105.

Blanco, A.; Borgehesi, A.; Bussoletti, E.; Fonti, S.: 1980, Ap. and Sp. Sci., 68, 505.

Bless, R.C.; Savage, B.D.: 1972, Ap. J., 142, 1683.

Borg, K.: 1967, Nature, 215, 145.

Bottlinger, K.F.; Schnellet, H.: 1930, Z. für Ap., 1, Heft 5, 339.

Carrasco, L.; Strom, S.E.; Strom, K.M.: 1973, Ap. J., 182, 95.

Capps, R.W.; Knacke, R.F.: 1976, Ap. J., 210, 76.

Cayrel, R; Schatzman, E.: 1954, Ann. d'Ap., 17, 555.

Codina-Landaberry, S; Magalhaes, A.M.: 1976, Ast. and Ap., 49, 407.

Cooke, A; Wickranasinghe, N.C.: 1977, Ap. Sp. Sci., 50, 43.

Coyne, G.V.: 1976, I.A.U. Symp. 70, p.233.

Coyne, G.V.; Gehrels, T.; Serkowski, K.: 1974, Ast.J., 79, 581.

Crutcher, R.M.: 1976, Ap. J., 206, L171.

Danks, A.C.: 1980, Pub. Ast. Soc. Pac., 92, 52.

Danks, A.C.; Lambert, D.L.: 1975, Ast. and Ap., 41, 555.

Danks, A.C.; Lambert, D.L.: 1976, M.N.R.A.S., 194, 571.

Davis, L.; Greenstein, J.L.: 1951, Ap. J., 114, 206.

Day, K.L.: 1979, Ap. J., 234, 158.

Day, K.L.; Steyer, T.R.; Huffman, D.R.: 1974, Ap. J., 191, 415.

De Boer, K.S.: 1979, Ap. J., 229, 132.

De Jong, T.: 1977, in "Les spectres des molecule simple au laboratoire et en astrophysique". (21st Liège Symposium), Univ. of Liège, p.117.

Donn, B.; Khanna, R.K.: 1980, Ap. Sp. Sci., 68, 19.

Dorschner, J.; Friedman, C.; Gürtler, J.: 1977, Ast. and Ap., 58, 201.

Dorschner, J.; Friedman, C.; Gürtler, J.; Duley, W.W.: 1980, Ap. Sp. Sci., 68, 159.

Douglas, A.E.: 1977, Nature, 269, 130.

Duley, W.W.: 1976, Ap. Sp. Sci., 45, 253.

Duley, W.W.: 1977, Ap. Sp. Sci., 47, 185.

Duley, W.W.: 1978, Ap. J., 219, L129.

Duley, W.W.: 1979a, Ap. Sp. Sci., 61, 243.

Duley, W.W.: 1979b, Ap. J., 227, 824.

Duley, W.W.; McCullough, J.D.: 1977, Ap. J., 211, L145.

Dyck, H.M.; Beichman, C.A.: 1974, Ap. J., 194, 57.

Dyck, H.M.; Jones, T.T.: 1978, Ast. J., 83, 594.

Egan, W.E.; Hilgeman, T.: 1978, Nature, 273, 369.

Fahlman, G.G.; Walker, G.A.H.: 1975, Ap. J., 200, 22.

Fano, U.: 1961, Phys. Rev., 124, 1866.

Friedemann, C.; Gürtler, J.; Dorschner, J.: 1979, Ap. Sp. Sci., 60, 297.

Gehrels, T.: 1974, Ast. J., 79, 590.

Gehrels, T.; Silvester, A.B.: 1965, Ast. J., 70, 579.

Gillett, F.C.; Forrest, W.J.; Merrill, K.M.; Capp, R.W.;
Soifer, B.T.: 1975, Ap. J., 200, 609.

Gilra, D.P.: 1971a, Nature, 220, 237.

Gilra, D.P.: 1971b, O.A.O. results.

Greenberg, J.M.: 1968, in N.I.M., p.221.

Greenberg, J.M.: 1974, Ap. J., 189, L81.

Greenberg, J.M.: 1976, Ap. Sp. Sci., 39, 9.

Greenberg, J.M.: 1978, in "Infrared Astronomy", ed. G. Setti and
G. Fazio. D. Reidel. p.51.

Greenberg, J.M.: 1979, Moon and Planets, 20, 15.

Greenberg, J.M.: 1981, Lectures given at the Royal Observatory, Edinburgh.

Greenberg, J.M.; Hong, S.S.: 1974, in P.S.N., p.916.

Greenberg, J.M.; Yencha, A.J.: 1973, I.A.U. Symp. 52, 369.

Greenstein, J.L.: 1938, Harvard Obs. Circ. No. 422.

Hagen, W.; Allamandola, L.J.; Greenberg, J.M.: 1980, Ast. and Ap., 86, L1.

Hall, J.S.: 1937, Ap. J., 85, 145.

Hall, J.S.: 1949, Science, 109, 166.

Harris, J.W.: 1969, Nature, 223, 1046.

Hartman, J.: 1904, Ap. J., 19, 268.

Hayes, D.S.; Mavko, G.E.; Radick, R.R.; Rex, K.H.; Greenberg, J.M.:
1973, I.A.U. Symp. 52, p.83.

Henry, J.: 1958, Ap. J., 128, 497.

Herbig, G.H.: 1967, I.A.U. Symp. 31, p.85.

Herbig, G.H.: 1971, Bull. Amer. Ast. Soc., 3, 57.

Herbig, G.H.: 1975, Ap. J., 196, 129.

Hiltner, W.A.: 1949, Science, 109, 165.

Hobbs, L.M.: 1974a, Ap. J., 191, 381.

Hobbs, L.M.: 1974b, Ap. J., 193, 395.

Hoffleit, D.: 1964, "Bright Star Catalogue", Yale University Observatory, New Haven.

Hoyle, F.; Wickramasinghe, N.C.: 1962, M.N.R.A.S., 124, 417.

Hoyle, F.; Wickramasinghe, N.C.: 1977a, Nature, 268, 610.

Hoyle, F.; Wickramasinghe, N.C.: 1977b, Nature, 270, 323.

Huffman, D.R.: 1977, Adv. Phys., 26, 129.

Huffman, D.R.; Stapp, J.L.: 1971, Nature Phys. Sci., 229, 45.

Ingemann-Hilberg, C.; Rudkjøbing, M.: 1970, Ap. Sp. Sci., 6, 101.

Jedwab, J.: 1971, Icarus, 15, 319.

Johnson, F.M.: 1972, Mem. Soc. Roy. Sci. Liège, 6th Ser., 3, 391.

Johnson, F.M.: 1977, Bull. Am. Ast. Soc., 3, 429.

Johnson, H.L.: 1968, in N.I.M., p.167.

Johnson, H.L.: 1977, Rev. Mex. Ast. Ap., 2, 175.

Jones, H.S.: 1914, M.N.R.A.S., 75, 4.

Jones, V.J.; Spitzer, L.: 1967, Ap. J., 147, 943.

Kapteyn, J.C.: 1909a, Ap. J., 29, 46.

Kapteyn, J.C.: 1909b, Ap. J., 29, 268.

Kemp, J.C.: 1972, Ap. J., 175, L35.

Kemp, J.C.; Wolstencroft, R.D.: 1972, Ap. J., 176, L115.

Knacke, R.F.: 1977, Nature, 269, 132.

Knacke, R.F.; Capps, R.W.: 1977, Ap. J., 216, 271.

Koorneef, J.: 1978, Ast. and Ap., 68, 139.

Koorneef, J.; Sitko, M.: 1979, Ap. J., 234, 129.

Krätschmer, W.; Huffman, D.R.: 1979, Ap. Sp. Sci., 61, 195.

Krautter, J.: 1980, Ast. and Ap. Supp. Ser., 39, 167.

Kruszewski, A.: 1962, Pub. Ast. Soc. Pac., 74, 519.

Kruszewski, A.: 1974, in P.S.N., p.845.

Kumar, C.K.: 1978, Pub. Ast. Soc. Pac., 90, 552.

Léger, A.; Klein, J.; de Cheveigne, S.; Guinet, C.; Defourneau, D.: Belin, M.: 1979, Ast. & Ap., 79,256

Lewis, J.S.; Ney, E.P.: 1979, Ap. J., 234, 154.

Lillie, C.F.; Witt, A.N.: 1976, Ap. J., 208, 64.

Lindblad, B.: 1935, Nature, 135, 133.

Lipson, S.G.; Lipson, H.: 1969, "Optical Physics", Cambridge Univ. Press.

McMillan, R.S.: 1977, Ap. J., 216, L41.

McMillan, R.S.: 1978, Ap. J., 225, 880.

Martin, P.G.: 1972, M.N.R.A.S., 159, 179.

Martin, P.G.: 1974, Ap. J., 187, 461.

Martin, P.G.: 1975, Ap. J., 201, 373.

Martin, P.G.; Angel, J.R.P.: 1975, Ap. J., 195, 379.

Martin, P.G.; Angel, J.R.P.: 1976, Ap. J., 207, 126.

Martin, P.G.; Campbell, B.: 1976, Ap. J., 208, 727.

Mathewson, D.S.: 1968, Ap. J., 153, L47.

Mathewson, D.S.; Ford, V.L.: 1970, Mem. R.A.S., 74, 139.

Mathis, J.S.: 1979, Ap. J., 232, 747.

Mathis, J.S.: Rumpl, W.; Nordsieck, K.H.: 1977, Ap. J., 217, 425.

Mavko, G.E.; Hayes, G.E.; Greenberg, J.M.; Hiltner, W.A.: 1974, Ap. J., 187, L117.

Merrill, K.M.: 1934, Pub. Ast. Soc. Pac., 46, 206.

Merrill, K.M.: 1977, I.A.U. Coll. 42, p 446.

Merrill, K.M.; Stein, W.A.: 1976, Pub. Ast. Soc. Pac., 88, 294.

Merrill, P.W.; Sandford, R.F.; Wilson, O.C.; Burwell, C.G.: 1937, Ap. J., 86, 274.

Millar, T.J.: 1979, M.N.R.A.S., 189, 507.

Millar, T.J.; Duley, W.W.: 1978, M.N.R.A.S., 183, 177.

Millar, T.J.; Duley, W.W.: 1979, M.N.R.A.S., 187, 379.

Millar, T.J.; Duley, W.W.: 1980, M.N.R.A.S., 191, 641.

Mitchell, G.F.; Huntress, W.T.: 1979, Nature, 278, 722.

Morales, C.; Llorente, F.; Andrés, D.E.; Ruiz del Arbol, J.A.: 1980, Ast. and Ap., 85, 302.

Morgan, D.H.: 1980, M.N.R.A.S., 190, 825.

Morton, D.C.: 1975, Ap. J., 197, 85.

Münch, G.: 1968, in N.I.M., p.365.

Nandy, K.: 1964, Pub. ROE, 3, 142.

Nandy, K.: 1967, Pub. ROE, 6, 25.

Nandy, K.; Seddon, H.: 1970, Nature, 227, 264.

Nandy, K.; Seddon, H.: 1973, I.A.U. Symp., 52, p.79.

Nandy, K.; Thompson, G.I.; Jamar, C.; Monfils, A.; Wilson, R.: 1975, Ast. and Ap., 44, 195.

Nandy, K.; Thompson, G.I.; Carnochan, D.J.; Wilson, R.: 1978, M.N.R.A.S., 184, 733.

Nandy, K.; Morgan, D.H.; Willis, A.J.; Wilson, R.; Gondhalekas, P.M.; Houziaux, L.: N980, Nature, 283, 725.

Nee, S.F.: 1980, Ap. J., 237, 471.

Nee, S.F.; Jokipii, J.R.: 1979, Ap. J., 234, 140.

Niemela, V.S.; Méndez, R.H.: 1974, Ap. J., 187, L23.

Oort, J.H.; van der Hulst, H.C.: 1946, B.A.N., no.376.

Penston, M.V.; Hunter, J.K.; O'Neill, A.: 1975, M.N.R.A.S., 171, 219.

Persson, S.; Frogel, J.A.; Aaronson, M.: 1976, Ap. J., 208, 753.

Plaskett, J.S.; Pearce, J.A.: 1930, M.N.R.A.S., 90, 243.

Plaskett, J.S.; Pearce, J.A.: 1933, Pub. Dom. Ap. Obs. (Victoria B.C.), 5, 167.

Platt, J.R.: 1956, Ap. J., 123, 486.

Purcell, E.M.: 1975, in "The Dusty Universe", ed. G.B. Field, A.G.W. Cameron, Neal Wait, New York, p.155.

Purcell, E.M.: 1979, Ap. J., 231, 404.

Purcell, E.M.; Shapiro, P.R.: 1977, Ap. J., 214, 92.

Rex, K.H.: 1974, Thesis presented to Rensselaer Polytechnic Institute, New York.

Rex, K.H.: 1976, Newslett. Astron. Soc. N.Y., 1, 39.

Rieke, G.H.: 1974, Ap. J., 193, L81.

Roche, R.S.: 1972, Nature, 235, 217.

Rudkjøbing, M.: 1969, Ap. Sp. Sic., 5, 68.

Rudkjøbing, M.: 1978, Ast. and Ap., 63, 189.

Sagan, C.; Khare, B.N.: 1979, Nature, 277, 102.

Sanner, F.; Snell, R.; Vanden Bout, P.: 1978, Ap. J., 226, 460.

Savage, B.D.: 1975, Ap. J., 199, 92.

Savage, B.D.: 1976, Ap. J., 205, 122.

Savage, B.D.; Mathis, J.S.: 1979, Ann. Rev. Ast. Ap., 17, 73.

Schalén, C.: 1936, Medd. Upsala Ast. Obs., 64.

Schild, R.E.: 1977, Ast. J., 82, 337.

Schmidt, E.G.: 1978, Ap. J., 223, 458.

Schmidt-Kaler, Th.: 1965, Landalt-Börnstein, Vol. 1 of Ast. and Ap., Group VI, p.301, ed. H.H. Voigt, Springer-Verlag, Berlin.

Schmidt-Kaler, Th.: 1967, I.A.U. Symp. 31, p.161.

Schmidt-Kaler, Th.; Tüg, H.; Buchholz, M.; Schlosser, W.: 1980, Ast. and Ap., Supp. Ser. 39, 305.

Serkowski, K.: 1962, Adv. Ast. Ap., 1, 289.

Serkowski, K.: 1965a, Acta Astr., 15, 79.

Serkowski, K.: 1965b, Ap. J., 141, 1340.

Serkowski, K.: 1968, Ap. J., 154, 115.

Serkowski, K.: 1973, I.A.U. Symp. 52, p.145.

Serkowski, K.; Mathewson, D.S.; Ford, V.L.: 1975, Ap. J., 196, 261.

Shapiro, P.R.: 1975, Ap. J., 201, 151.

Smith, W.H.; Snow, T.P.; York, D.G.: 1977, Ap. J., 218, 124.

Sneden, C.; Gehrz, R.D.; Hackwell, J.A.; York, D.G.; Snow, T.P.: 1978, Ap. J., 223, 168.

Snow, T.P.; York, D.G.; Resnick, M.: 1977, Pub. Ast. Soc. Pac., 89, 758.

Snow, T.P.; York, D.G.; Welty, D.E.: 1977, Ast. J., 82, 113.

Spitzer, L.: 1968, "Diffuse matter in space", Wiley, New York.

Spitzer, L.; McGlynn, T.A.: 1979, Ap. J., 231, 417.

Stebbins, J.; Huffer, C.M.; Whitford, A.E.: 1939, Ap. J., 90, 209.

Stecker, T.P.: 1965, Ap. J., 142, 1683.

Stokes, R.A.; Swedlund, J.B.; Avery, R.W.; Michalsky, J.J.: 1974, Ast. J., 79, 678.

Struve, F.G.W.: 1847, "Etudes d'astronomie stellaire", Académie Impériale des Sciences, St. Petersburg.

Tinbergen, J.: 1979, Ast. and Ap. Supp. Ser., 35, 325.

Tinbergen, J.: 1981, preprint.

Trumpler, R.J.: 1930a, Lick Obs. Bull, 14, 154.

Trumpler, R.J.: 1930b, Pub. Ast. Soc. Pac., 42, 214.

Underhill, A.B.; Walker, G.A.H.: 1966, M.N.R.A.S., 131, 475.

Van Breda, I.G.; Whittet, D.C.B.: 1977, Ap. Sp. Sci., 48, 397.

Van Breda, I.G.; Whittet, D.C.B.: 1981, M.N.R.A.S., 195, 79.

Van de Kamp, P.: 1932, Ast. J., 42, 97.

Van der Hulst, H.C.: 1946, Rech. Ast. Obs. Utrecht, XI, Part 1.

Van der Hulst, H.C.: 1947, Rech. Ast. Obs. Utrecht, XI, Part 2.

Van der Hulst, H.C.: 1957, "Light scattering by small particles", Wiley, New York.

Visvanathan, N.: 1966, Ap. J., 148, 655.

Walker, G.S.H.: 1967, Ast. J., 72, 37.

Webster, A.: 1980, M.N.R.A.S., 192, 7P.

Welter, G.L.; Savage, B.D.: 1977, Ap. J., 215, 788.

Whiteoak, J.B.: 1966, Ap. J., 144, 305.

Whitford, A.E.: 1958, Ast. J., 63, 201.

Whittet, D.C.B.: 1977, M.N.R.A.S., 180, 29.

Whittet, D.C.B.: 1981, Q.J.R.A.S., 22, 3.

Whittet, D.C.B.; Dayawansa, I.J.; Dickinson, P.M.; Marsden, J.A.; Thomas, B.: 1976, M.N.R.A.S., 175, 197.

Whittet, D.C.B.; Blades, J.C.: 1980, M.N.R.A.S., 190, 41P.

Whittet, D.C.B.; van Breda, I.G.: 1978, Ast. and Ap., 66, 57.

Whittet, D.C.B.; Somerville, W.B.; McNally, D.; Blades, J.C.: 1979, M.N.R.A.S., 189, 519.

Wickramasinghe, D.T.; Allen, D.A.: 1980, Nature, 287, 518.

Wickramasinghe, N.C.: 1967, "Interstellar grains", Chapman & Hall, London.

Wickramasinghe, N.C.: 1974, Nature, 252, 468.

Wickramasinghe, N.C.: 1975, M.N.R.A.S., 170, 11P.

Wickramasinghe, N.C.; Hoyle, F.: 1977, Nature, 269, 674.

Wilking, B.A.; Lebofsky, M.J.; Martin, P.G.; Rieke, G.H.; Kemp, J.C.: 1980, Ap. J. 235, 905.

Willis, A.J.; Wilson, R.: 1975, Ast. and Ap., 44, 205.

Willis, A.J.; Wilson, R.: 1977, Ast. and Ap., 59, 133.

Wolstencroft, R.D.; Nandy, K.: 1971, Ap. Sp. Sci., 12, 158.

Woolf, N.J.: 1973, I.A.U.Symp. 52, p.485.

Woolf, N.J.; Ney, E.P.: 1969, Ap. J., 155, L181.

Wu, C-C.: 1972, Ap. J., 178, 681.

Wu, C-C.: 1973, I.A.U.Symp. 52, p.91.

Wu, C-C.; York, D.G.; Snow, T.P.; van Duinan, R.J.: 1977, reported in Smith, Snow & York, 1977 (q.v.).

Young, R.K.: 1922, Pub. Dom. Ap. Obs. (Victoria B.C.), 1, 219.

Addenda:

Bohlin, R.C.; Savage, B.D.; Drake, J.F.: 1978, Ap. J.,224, 132.

Hansen, J.E.; Travis, L.D.: 1974, Sp. Sci. Rev., 16, 527

Manning, P.G.: 1975, Nature, 225, 40.

Stephens, J.R.: 1980, Ap. J., 237, 450.

Treffers, R.; Cohen, M.: 1974, Ap. J., 188, 545.

Tosatti, E.; Bassani, F.: 1970, Nuovo Cim., 65B, 161.

Table C1 : Properties of the reddened stars

Property	ζ Ophiuchi	55 Cygni	χ Aurigae	Note
HR	6175	7977	1843	1
HD	149757	198478	36371	
ℓ	6°	86°	176°	2
b	+24°	+1°	-1°	2
V	2.56	4.83	4.89	1
E(B-V)	0.33	0.53	0.45	2
A_{vis}	1.13	1.63	1.46	3
Spectral type	09.5V	B3Ia	B5Iab	1
M_{vis}	-4.5	-6.8	-6.3	3
d (pc)	155	1000	880	3
R_c (4430)	3.41	7.67	6.27	4
W(5780)	0.29	0.38	0.39	4
W(5797)	(0.13)	0.17	0.21	4
W(6284)	(0.21)	0.25	0.29	4
p_{max} (%)	1.43	2.75	2.17	2
λ_{max} (μ)	0.59	0.53	0.56	2
k	1.17	0.88	-	5
$q(\times 10^{-4})$ (at λ)	+0.16 ± 0.17 (at ∿4400 Å)	+1.32 ± 0.22 (at ∿4400 Å)	-0.67 ± 0.17 (at ∿3900 Å)	6
$p_{vis}/E(B-V)$	0.094	0.113	0.105	
D_o	0.483	0.578	0.537	7

Notes to Table C1

1. Values taken from the "Bright Star Catalogue" (HOFFLEIT, 1964).

2. Values from SERKOWSKI, MATHEWSON & FORD (1975).

3. A_{vis} calculated from $A_{vis} = RE(B-V)$ and $R = 5.8\ \lambda_{max}$ (SAVAGE & MATHIS, 1979). The spectral type gives M_{vis} (SCHMIDT-KALER, 1965) and hence the distance to the star, d, can be calculated.

4. From SNOW, YORK & WELTY (1977). R_c (4430) is the central depth of the 4430 Å diffuse band, in per cent. W(5780), W(5797) and W(6284) are the equivalent widths of the 5780 Å, 5797 Å and 6284 Å diffuse bands, respectively. Values in brackets are estimates (see text).

5. From WILKING et al. (1980). The values of p_{max} and λ_{max} quoted in this reference are slightly different from those quoted here.

6. Circular polarisation in the blue. The figure for ζ Ophiuchi and 55 Cygni is taken from STOKES et al. (1974); it was obtained with a filter passing wavelengths (HPBW) 3800 Å to 4750 Å. The value for χ Aurigae is taken from MARTIN (1974). The filter passed wavelengths 3300 Å to 4700 Å.

7. $D_o = \{p_{vis}/E(B-V)\}/0.195$. D_o is a measure of the polarising efficiency of the dust grains in the line of sight.

Table C2 : Observing Log for Zeta Ophiuchi

Name	Time (UT)	Tele-scope	N (λ)	Range of wavelengths	Optics	RS	AP	Moon	OS	HT	MV	Comments
4MY5	08.40	40"	5	5000-5800	5825	53	3	27	1	1550	300	
6MY1	12.45	40"	10	4550-5450	5825	53	3	29	5	1550	270	Bad Guiding. 7 lost
7MY1	08.50	61"	10	4550-5450	5825	53	3:	1	5	1550	270	} Aperture may not have been
7MY2	10.00	61"	10	5400-6300	5825	53	3:	1	5	1550	325	} accurately central
9MY3	09.40	61"	10	4150-4600	3800	53	2	3	5	1550	240	Some cirrus
15MY5	08.10	60"	7	4600-5600	5825	53	2	9	5	1550:	290	Some wavelength used HT = 1450
15MY6	09.10	60"	8	5550-6250	5825	53	2	9	4	1550	325	
16MY1	10.05	60"	10	3500-3950	3800	52:	2	10	5	1550	205	Exit slit thread damaged here
16MY2	11.20	60"	1	3250	3800	52	2	10	5	1550	180	
17MY2	07.30	60"	10	6200-7100	5825	52	2	11	1	1550	275	
17MY3	09.15	60"	5	3950-4150	3800	52	2	11	5	1550	220:	MV unclear on record
17MY5	11.00	60"	5	7150-7350	5825	52	2	11	1	1550	420	Bad guiding
24MY2	07.10	60"	5	6500-6900	5825	52	2	18	1	1550	380	Cloud. 4 lost
25MY8	10.30	60"	9	6550-6950	5825	52	2	19	1	1550	380	
26MY4	08.05	60"	10	3825-4275	3800	52	2	20	5	1430	220	Note HT
26MY6	10.20	60"	7	3150-3550	3800	52	2	20	5	1550	180	
26MY7	11.30	60"	2	7400-7500	5825	52	2	20	1	1550	420	

Table C3 : Observing Log for 55 Cygni

Name	Time (UT)	Tele scope	N (λ)	Range of wavelengths	Optics	RS	AP	Moon	OS	HT	MV	Comments
0/14	-	60"T	5	3800-4600	3800	53	2	2	4	1300	-	
0/14	-	60"T	5	4800-5600	5825	53	2	2	4	1300	-	
0/15	-	60"T	9	3600-4700	3800	53	2	3	4	1300	-	
0/15	-	60"T	2	4900-5100	5825	53	2	3	4	1300	-	
0/17	-	60"T	7	5800-7000	5825	53	2	4	4	1300	-	
0/19	-	60"T	6	4200-4450	3800	53	2	7	4	1200-1300	-	
0/19	-	60"T	4	4550-8500	5825	53	2	7	4	1300	-	
25SP1	04.19	61"	10	4250-4700	5825	52	3	23	5	1400	240	Δλ = + 10 cloud
28SP1	04.28	60"	4	3150-3450	3800	52	3	26	5	1400	190	Δλ = + 15
28SP2	06.52	60"	5	3450-3850	3800	52	3	26	5	1400	205	Δλ = + 15
29SP3	03.45	60"	7	3460-3760	3800	52	3	27	5	1400	200	Δλ = + 50
29SP4	06.13	60"	5	3910-4310	3800	52	3	27	5	1400	215	Δλ = + 48
20C1	04.16	60"	2	3165-3215	3800	52	3	1	5	1400	180	Δλ = + 73 cloud
20C2	05.45	60"	3	3520-3720	3800	52	3	1	5	1400	200	Δλ = + 72
50C1	03.26	60"	6	3400-3750	3800	52	3	3	5	1400	200	Δλ = + 80 cirrus
90C2	03.22	40"	5	4360-4480	3800	52	3	8	5	1400	235	Δλ = + 25
7JN1	09.30	40"	8	4100-4450	3800	52	3	2	5	1550	230	

Table C4: Observing log for χ Aurigae

Name	Time (UT)	Tele-scope	N(λ)	Range of wavelengths	Optics	RS	Ap	Moon	OS	HT	MV	Comments
78/2FB1	4.40	60"	10	4550-5450	5825	53	-	25	-	-	-	
78/2FB2	7.30	60"	10	3750-4650	5825	53	-	25	-	-	-	Some calibration pols extrapolated
78/3FB1	4.30	60"	10	5300-6200	5825	53	-	26	-	-	-	Dark count high
79/12FB8	8.00	40"	6	5500-6500	5825	212	3	5	5	1300	330	

Some information unavailable from 1978 run.

Table C5 : Linear polarisation measurements of 5 Ophiuchi

Wavelength (Å)	Name	p (%)	σ	θ (°)	σ_θ
3160	26MY6	1.120	0.061	123.4	1.5
3210	26MY6	1.078	0.044	126.4	1.2
3260	16MY2	1.089	0.028	125.25	0.76
3310	26MY6	1.065	0.034	124.96	0.90
3360	26MY6	1.035	0.033	126.93	0.89
3410	26MY6	1.106	0.030	126.54	0.77
3460	26MY6	1.080	0.033	127.06	0.85
3510	16MY1	1.168	0.026	125.69	0.65
3560	16MY1	1.157	0.025	124.98	0.65
	26MY6	1.184	0.036	126.72	0.85
3610	16MY1	1.191	0.023	124.37	0.57
3660	16MY1	1.213	0.022	125.15	0.51
3710	16MY1	1.250	0.024	125.51	0.55
3760	16MY1	1.248	0.021	124.99	0.48
3810	16MY1	1.276	0.020	125.49	0.46
3835	26MY4	1.275	0.019	124.71	0.43
3860	16MY1	1.325	0.018	125.26	0.38
3885	26MY4	1.299	0.017	125.27	0.38
3910	16MY1	1.309	0.018	124.75	0.42
3935	26MY4	1.297	0.019	125.09	0.40

Wavelength (Å)	Name	p (%)	σ	θ (°)	σ_θ
3960	16MY1	1.338	0.018	125.06	0.40
	17MY3	1.320	0.014	125.75	0.30
3985	26MY4	1.326	0.017	125.89	0.35
4010	17MY3	1.329	0.014	126.05	0.30
4035	26MY4	1.346	0.018	125.40	0.36
4060	17MY3	1.319	0.014	125.13	0.30
4085	26MY4	1.357	0.017	125.49	0.34
4110	17MY3	1.338	0.014	125.16	0.28
4135	26MY4	1.351	0.015	124.92	0.32
4160	17MY3	1.393	0.013	125.97	0.27
4160	9MY3	1.433	0.018	126.44	0.38
4185	26MY4	1.397	0.016	125.30	0.31
4210	9MY3	1.402	0.017	126.38	0.33
4235	26MY4	1.397	0.015	125.59	0.32
4260	9MY3	1.448	0.018	126.00	0.34
4285	26MY4	1.414	0.017	126.20	0.33
4310	9MY3	1.438	0.016	126.04	0.29
4360	9MY3	1.461	0.015	125.89	0.32
4410	9MY3	1.463	0.018	126.07	0.31
4460	9MY3	1.461	0.022	125.95	0.36

Wavelength (Å)	Name	p (%)	σ	θ (°)	σ_θ
4510	9MY3	1.496	0.014	126.28	0.32
4560	9MY3	1.517	0.017	126.37	0.29
	7MY1	1.528	0.036	126.04	0.66
4610	9MY3	1.550	0.020	126.25	0.28
	15MY5	1.497	0.025	126.45	0.46
4660	7MY1	1.546	0.035	126.68	0.64
4710	15MY5	1.536	0.023	126.12	0.42
4760	7MY1	1.531	0.032	125.99	0.67
4810	15MY5	1.570	0.020	126.06	0.36
4860	7MY1	1.506	0.037	127.01	0.68
4910	15MY5	1.571	0.020	126.07	0.37
4960	7MY1	1.537	0.031	126.41	0.49
5010	4MY5	1.563	0.032	126.40	0.58
5060	7MY1	1.589	0.032	125.52	0.72
5110	15MY5	1.544	0.022	126.59	0.42
5160	7MY1	1.599	0.032	126.12	0.58
5210	4MY5	1.609	0.027	126.45	0.52
5260	7MY1	1.648	0.028	126.41	0.48
5310	15MY5	1.603	0.021	125.64	0.38
5360	7MY1	1.595	0.030	126.18	0.59

Wavelength (Å)	Name	p (%)	σ	θ (°)	σ_θ
5410	4MY5	1.625	0.031	127.71	0.54
	7MY2	1.624	0.031	126.38	0.43
5460	7MY1	1.644	0.038	126.29	0.54
5510	7MY2	1.613	0.027	126.55	0.51
5560	15MY6	1.655	0.027	126.37	0.42
5610	15MY5	1.633	0.023	125.91	0.43
	4MY5	1.707	0.036	125.95	0.64
	7MY2	1.659	0.034	126.14	0.47
5660	15MY6	1.662	0.025	126.87	0.43
5710	7MY2	1.704	0.027	126.24	0.47
5760	15MY6	1.653	0.028	125.91	0.47
5810	4MY5	1.734	0.036	125.96	0.62
	7MY2	1.674	0.034	125.67	0.59
5860	15MY6	1.713	0.029	126.46	0.48
5910	7MY2	1.643	0.030	126.55	0.53
5960	15MY6	1.635	0.030	126.57	0.48
6010	7MY2	1.657	0.034	124.26	0.53
6060	15MY6	1.620	0.029	125.81	0.51
6110	7MY2	1.657	0.036	127.09	0.57
6160	15MY6	1.654	0.030	126.24	0.50

Wavelength (Å)	Name	p (%)	σ	θ (°)	σ_θ
6210	7MY2	1.641	0.033	126.77	0.62
	17MY2	1.649	0.027	126.98	0.45
6260	15MY6	1.689	0.027	126.21	0.45
6310	7MY2	1.645	0.035	126.07	0,66
	17MY2	1.705	0.028	126.07	0.45
6410	17MY2	1.698	0.025	126.96	0.43
6510	17MY2	1.713	0.027	125.78	0.45
6560	25MY8	1.702	0.022	125.30	0.37
6610	17MY2	1.699	0.028	126.57	0.47
	25MY8	1.696	0.021	126.53	0.38
6660	25MY8	1.719	0.023	124.68	0.40
6710	25MY8	1.700	0.023	125.08	0.39
6760	25MY8	1.686	0.023	124.81	0.38
6810	25MY8	1.683	0.025	125.95	0.43
	17MY2	1.644	0.031	127.11	0.54
6860	25MY8	1.647	0.025	126.29	0.44
6910	25MY8	1.652	0.028	125.39	0.47
	17MY2	1.685	0.033	125.04	0.47
6960	25MY8	1.629	0.028	126.71	0.51
7010	17MY2	1.624	0.032	125.50	0.59

Wavelength (Å)	Name	p (%)	σ	θ (°)	σ_θ
7110	17MY2	1.691	0.032	127.60	0.55
7160	17MY5	1.521	0.025	126.33	0.51
7210	17MY5	1.526	0.027	126.45	0.51
7260	17MY5	1.515	0.025	126.24	0.49
7310	17MY5	1.527	0.030	126.27	0.56
7360	17MY5	1.599	0.033	127.43	0.56
7410	26MY7	1.595	0.085	127.0	1.5
7510	26MY7	1.572	0.080	126.8	1.4

Table C6: Smoothed linear polarisation measurements on ζ Ophiuchi.

The values below are of a weighted running mean over four points. The mean was weighted according to the errors of each of the four points. The associated wavelength is a simple average.

Wavelength (Å)	p_M (%)	σ_{PM}	θ_M (°)	$\sigma_{\theta M}$
3235	1.083	0.018	125.17	0.49
3285	1.068	0.017	125.78	0.45
3335	1.077	0.015	125.92	0.41
3385	1.073	0.016	126.41	0.42
3435	1.107	0.015	126.42	0.39
3485	1.141	0.013	126.03	0.33
3535	1.162	0.012	125.46	0.31
3585	1.185	0.011	125.20	0.28
3625	1.202	0.011	125.19	0.27
3675	1.226	0.011	125.02	0.26
3735	1.248	0.011	125.28	0.25
3779	1.264	0.010	125.13	0.24
3816	1.284	0.010	125.12	0.22
3848	1.295	0.009	125.18	0.20
3873	1.303	0.009	125.03	0.20
3898	1.308	0.009	125.11	0.20
3923	1.314	0.008	125.27	0.17
3948	1.319	0.008	125.40	0.16
3964	1.323	0.007	125.66	0.15
3998	1.330	0.007	125.69	0.15

Wavelength (Å)	p_M (%)	σ_{PM}	θ_M (°)	$\sigma_{\theta M}$
4023	1.328	0.008	125.62	0.16
4048	1.335	0.008	125.53	0.16
4073	1.338	0.008	125.27	0.16
4098	1.339	0.007	125.16	0.15
4123	1.371	0.007	125.56	0.14
4148	1.378	0.007	125.52	0.14
4173	1.392	0.007	125.77	0.14
4198	1.402	0.007	125.90	0.14
4223	1.409	0.008	125.79	0.16
4248	1.413	0.008	126.04	0.16
4273	1.422	0.008	125.96	0.16
4304	1.441	0.008	126.03	0.16
4341	1.444	0.008	126.05	0.16
4385	1.455	0.009	125.99	0.16
4435	1.474	0.008	126.05	0.16
4485	1.491	0.008	126.18	0.16
4535	1.506	0.008	126.25	0.14
4585	1.515	0.008	126.32	0.15
4635	1.527	0.010	126.30	0.16
4685	1.533	0.011	126.27	0.19

Wavelength (Å)	p_M (%)	σ_{PM}	θ_M (°)	$\sigma_{\theta M}$
4735	1.550	0.013	126.15	0.24
4785	1.546	0.013	126.19	0.24
4835	1.558	0.012	126.16	0.23
4885	1.558	0.012	126.23	0.22
4935	1.554	0.014	126.34	0.25
4985	1.566	0.013	126.15	0.25
5035	1.555	0.014	126.36	0.26
5085	1.567	0.014	126.29	0.27
5135	1.579	0.014	126.31	0.26
5185	1.592	0.013	126.43	0.24
5235	1.613	0.013	126.07	0.24
5285	1.612	0.013	126.08	0.24
5335	1.617	0.012	126.33	0.21
5385	1.614	0.013	126.31	0.21
5435	1.618	0.014	126.61	0.23
5485	1.632	0.013	126.60	0.22
5535	1.646	0.012	126.20	0.20
5585	1.649	0.011	126.32	0.19
5635	1.665	0.011	126.28	0.19
5685	1.665	0.011	126.20	0.19

Wavelength (Å)	p_M (%)	σ_{PM}	θ_M (°)	$\sigma_{\theta M}$
5735	1.681	0.013	126.22	0.22
5785	1.693	0.014	126.09	0.23
5835	1.680	0.014	126.14	0.24
5885	1.677	0.014	126.31	0.24
5935	1.663	0.015	126.01	0.25
5985	1.637	0.015	126.84	0.26
6035	1.640	0.016	125.93	0.26
6085	1.645	0.016	125.82	0.26
6135	1.643	0.014	126.57	0.23
6185	1.660	0.013	126.63	0.23
6235	1.667	0.012	126.40	0.20
6298	1.676	0.012	126.54	0.20
6373	1.694	0.012	126.25	0.21
6448	1.697	0.012	125.98	0.20
6523	1.701	0.011	126.18	0.19
6585	1.705	0.011	125.72	0.18
6635	1.703	0.010	125.57	0.18
6685	1.700	0.010	125.47	0.18
6735	1.691	0.011	125.33	0.19
6785	1.675	0.011	125.66	0.19

Wavelength (Å)	p_M (%)	σ_{PM}	θ_M (°)	$\sigma_{\theta M}$
6835	1.668	0.011	125.69	0.19
6885	1.657	0.011	126.09	0.20
6935	1.647	0.013	125.86	0.23
6998	1.654	0.013	126.07	0.24
7060	1.605	0.014	126.57	0.27
7123	1.577	0.014	126.49	0.27
7185	1.550	0.013	126.61	0.26
7235	1.522	0.013	126.32	0.26
7285	1.536	0.014	126.57	0.26
7335	1.542	0.016	126.63	0.30
7398	1.563	0.021	126.86	0.37

Table C7 : Linear polarisation measurements of 55 Cygni

Wavelength (Å)	Name	p (%)	σ	θ (°)	σ_θ
3092	20C1	2.37	0.21	1.3	2.5
3135	28SP1	2.11	0.12	178.0	1.8
3142	20C1	2.36	0.13	3.2	1.4
3235	28SP1	2.086	0.077	1.5	1.1
3320	50C1	2.087	0.094	1.2	1.3
3335	28SP1	2.194	0.066	2.3	0.8
3410	29SP3	2.247	0.076	2.5	1.2
3420	50C1	2.264	0.079	4.0	1.0
3435	28SP1	2.274	0.050	2.5	0.7
	28SP2	2.37	0.12	1.7	1.3
3448	20C2	2.297	0.096	3.3	1.5
3460	29SP3	2.304	0.082	3.6	1.0
3470	50C1	2.298	0.078	2.5	1.0
3510	29SP3	2.431	0.069	1.4	0.8
3520	50C1	2.429	0.066	2.5	0.8
3535	28SP2	2.077	0.097	3.4	1.3
3548	20C2	2.203	0.116	3.2	1.5
3560	29SP3	2.373	0.077	3.8	0.7
3570	50C1	2.300	0.066	3.1	0.8
3610	29SP3	2.316	0.053	2.5	0.7

Wavelength (Å)	Name	p (%)	σ	θ (°)	σ_θ
3635	28SP2	2.383	0.083	2.4	1.0
3648	20C2	2.441	0.098	4.0	1.3
3660	29SP3	2.494	0.059	3.9	0.7
3670	50C1	2.448	0.059	3.1	0.8
3710	29SP3	2.402	0.055	2.9	0.7
3735	28SP2	2.484	0.065	4.3	0.9
3835	28SP2	2.412	0.067	3.7	0.8
3862	29SP4	2.568	0.061	3.4	0.8
3900	0/15	2.734	0.062	3.8	1.2
3962	29SP4	2.614	0.122	3.1	0.7
4000	0/14	2.649	0.121	5.5	1.1
4062	29SP4	2.731	0.092	3.8	0.7
4100	7JN1	2.739	0.065	2.7	0.7
4150	7JN1	2.829	0.058	4.1	0.6
4162	29SP4	2.730	0.062	3.3	0.6
4200	0/14	2.734	0.073	3.3	0.8
	0/19	2.852	0.047	3.3	0.7
	7JN1	2.693	0.063	3.2	0.7
4240	25SP1	2.857	0.067	2.4	0.8
4250	7JN1	2.778	0.059	3.3	0.7

Wavelength (Å)	Name	p (%)	σ	θ (°)	σ_θ
4262	29SP4	2.812	0.059	3.7	0.6
4290	25SP1	2.753	0.072	4.1	0.7
4300	0/15	2.752	0.140	3.1	1.6
	0/19	2.831	0.072	3.0	0.6
	7JN1	2.771	0.062	2.3	0.7
4335	90C2	2.726	0.082	2.4	0.9
4340	25SP1	2.723	0.074	2.6	0.7
4350	7JN1	2.841	0.062	3.2	0.6
	0/19	2.797	0.057	2.5	0.4
4365	90C2	2.834	0.077	3.0	0.9
4390	25SP1	2.913	0.058	2.4	0.6
4395	90C2	2.805	0.076	2.7	1.0
4400	7JN1	2.792	0.063	3.5	0.6
	0/19	2.673	0.054	4.5	1.0
	0/14	2.781	0.058	2.0	0.5
4425	90C2	2.815	0.086	4.9	0.9
4440	25SP1	2.934	0.061	2.4	0.7
4450	7JN1	2.870	0.060	2.7	0.6
	0/19	2.799	0.091	2.7	1.0
4455	90C2	2.941	0.090	3.0	0.9

Wavelength (Å)	Name	p (%)	σ	θ (°)	σ_θ
4490	25SP1	2.821	0.062	3.3	0.6
4500	0/15	2.897	0.107	2.2	1.0
4540	25SP1	2.925	0.056	4.3	0.6
4550 {	0/19	2.966	0.088	2.9	0.8
	0/19	2.966	0.082	3.2	0.9
4590	25SP1	2.926	0.053	2.7	0.5
4600	0/14	3.026	0.066	2.0	0.5
4640	25SP1	2.870	0.058	4.3	0.6
4690	25SP1	3.038	0.056	2.9	0.5
4700	0/15	2.954	0.145	3.5	1.1
4800	0/14	3.001	0.069	3.2	0.5
4900	0/15	2.999	0.087	2.9	0.9
5000	0/14	3.031	0.072	1.8	0.5
5100	0/15	2.917	0.083	3.1	0.7
5200	0/14	3.071	0.088	3.4	1.1
5400	0/14	3.030	0.063	2.2	0.6
5600	0/14	3.087	0.061	2.5	0.6
5800	0/17	2.809	0.139	3.0	1.6
6000	0/17	2.836	0.127	2.8	1.7
6200	0/17	2.935	0.137	4.7	1.1
6400	0/17	2.701	0.155	3.8	1.5
6600	0/17	2.770	0.153	4.1	1.8
7000	0/19	2.598	0.077	3.2	1.1
7300	0/19	2.735	0.066	2.6	0.6

Table C8 : Smoothed linear polarisation measurements of 55 Cygni

The following table has been smoothed in an (exactly) similar way to Table C6 :

Wavelength (Å)	P_M (%)	σ_{P_M}	θ_M (°)	σ_{θ_M}
3151	2.162	0.056	1.3	0.8
3208	2.130	0.049	1.3	0.7
3258	2.159	0.042	2.0	0.5
3325	2.163	0.038	2.0	0.5
3371	2.206	0.038	2.6	0.5
3400	2.257	0.031	2.7	0.4
3428	2.278	0.033	2.8	0.4
3441	2.288	0.034	3.0	0.4
3453	2.294	0.033	2.7	0.4
3472	2.343	0.040	2.4	0.5
3490	2.376	0.036	2.4	0.5
3509	2.347	0.038	2.2	0.5
3528	2.342	0.040	2.3	0.5
3541	2.319	0.042	3.3	0.5
3553	2.268	0.042	3.5	0.5
3572	2.313	0.035	3.2	0.4
3594	2.333	0.033	3.0	0.4
3616	2.339	0.035	2.8	0.4
3638	2.399	0.033	3.1	0.4
3653	2.452	0.035	3.3	0.4

Wavelength (Å)	P_M (%)	σ_{PM}	θ_M (°)	$\sigma_{\theta M}$
3672	2.445	0.031	3.3	0.4
3694	2.454	0.030	3.5	0.4
3738	2.434	0.030	3.4	0.4
3786	2.465	0.031	3.5	0.4
3833	2.513	0.035	3.8	0.4
3890	2.554	0.035	3.4	0.4
3931	2.611	0.039	3.6	0.4
3981	2.661	0.044	3.8	0.4
4031	2.681	0.038	3.5	0.4
4078	2.766	0.037	3.8	0.4
4119	2.765	0.033	3.5	0.3
4153	2.776	0.024	3.4	0.3
4188	2.792	0.024	3.4	0.3
4213	2.784	0.027	3.2	0.3
4239	2.800	0.026	3.3	0.3
4261	2.810	0.038	3.5	0.3
4276	2.790	0.032	3.3	0.3
4297	2.782	0.030	3.2	0.3
4316	2.763	0.031	2.9	0.3
4331	2.786	0.027	2.7	0.3

Wavelength (Å)	P_M (%)	σ_{PM}	θ_M (°)	$\sigma_{\theta M}$
4348	2.791	0.031	2.7	0.3
4361	2.829	0.029	2.7	0.3
4375	2.828	0.029	2.7	0.3
4388	2.782	0.025	2.8	0.3
4403	2.779	0.026	3.0	0.3
4415	2.781	0.026	3.0	0.3
4429	2.784	0.024	2.9	0.3
4443	2.862	0.033	3.0	0.3
4459	2.858	0.031	2.8	0.3
4474	2.838	0.034	2.8	0.3
4496	2.890	0.036	3.5	0.4
4520	2.906	0.033	3.4	0.3
4545	2.934	0.031	3.2	0.3
4570	2.955	0.029	2.9	0.3
4595	2.941	0.029	3.0	0.3
4630	2.961	0.029	2.9	0.3
4658	2.975	0.033	3.0	0.3
4708	2.967	0.034	3.5	0.3
4773	3.014	0.038	3.1	0.3
4850	3.007	0.041	2.5	0.3

Wavelength (Å)	p_M (%)	PM	M	(°) M
4950	2.991	0.038	2.6	0.3
5050	3.005	0.041	2.4	0.3
5175	3.015	0.037	2.3	0.3
5325	3.035	0.035	2.6	0.3
5500	3.043	0.038	2.5	0.4
5700	3.017	0.040	2.4	0.4
5900	3.000	0.048	3.0	0.5
6100	2.828	0.069	3.8	0.7
6300	2.820	0.071	4.0	0.7
6550	2.695	0.057	3.9	0.6
6825	2.687	0.046	2.9	0.5

Table C9 : Linear polarisation measurements of χ Aurigae

Wavelength (Å)	Name	p (%)	σ	θ (°)	σ_θ
3706	78/2FB2	1.621	0.074	175.6	1.4
3806	78/2FB2	1.727	0.068	175.9	1.1
3906	78/2FB2	1.754	0.059	175.4	1.0
4006	78/2FB2	1.655	0.059	176.3	1.0
4106	78/2FB2	1.708	0.052	178.5	0.9
4206	78/2FB2	1.756	0.045	177.3	0.7
4306	78/2FB2	1.843	0.045	177.3	0.7
4406	78/2FB2	1.800	0.040	176.5	0.7
4506	78/2FB2	1.874	0.042	177.3	0.6
	78/2FB1	1.944	0.072	175.8	1.0
4606	78/2FB2	1.860	0.040	178.5	0.6
	78/2FB1	1.888	0.062	176.8	1.0
4706	78/2FB1	1.849	0.056	178.6	0.9
4806	78/2FB1	2.042	0.069	177.0	0.9
4906	78/2FB1	2.022	0.070	178.9	1.0
5006	78/2FB1	1.868	0.066	178.3	1.0
5106	78/2FB1	2.021	0.064	178.5	0.9
5206	78/2FB1	2.038	0.058	178.9	0.8
5256	78/3FB1	2.106	0.040	177.8	0.5
5306	78/2FB1	2.011	0.069	177.3	1.0

Wavelength (Å)	Name	p	(%)		(°)
5356	78/3FB1	2.097	0.044	176.7	0.6
5406	78/2FB1	2.037	0.070	179.4	1.0
5456	78/3FB1	2.003	0.039	177.2	0.6
5500	79/12FB8	2.047	0.044	178.1	0.6
5556	78/3FB1	2.001	0.038	177.2	0.6
5656	78/3FB1	2.056	0.047	177.2	0.6
5700	79/12FB8	2.045	0.047	177.7	0.6
5756	78/3FB1	2.032	0.041	179.0	0.6
5856	78/3FB1	2.045	0.042	176.8	0.6
5900	79/12FB8	2.060	0.046	176.3	0.6
5956	78/3FB1	2.093	0.048	176.9	0.7
6056	78/3FB1	2.100	0.043	176.2	0.5
6100	79/12FB8	2.036	0.047	176.7	0.6
6156	78/3FB1	2.116	0.047	177.3	0.6
6300	79/12FB8	2.028	0.048	178.0	0.7
6500	79/12FB8	1.944	0.050	176.8	0.7

Table C10: Smoothed linear polarisation measurements of χ Aurigae.

The following table has been smoothed in a similar way to Table C6.

Wavelength (Å)	p_M (%)	σ_{PM}	θ_M (°)	$\sigma_{\theta M}$
3856	1.694	0.032	175.8	0.6
3956	1.710	0.029	176.7	0.5
4056	1.723	0.026	177.1	0.4
4156	1.754	0.025	177.4	0.4
4256	1.783	0.022	177.3	0.4
4356	1.830	0.020	176.9	0.3
4456	1.855	0.019	177.2	0.3
4556	1.856	0.020	177.4	0.3
4656	1.891	0.021	177.5	0.3
4756	1.907	0.025	178.1	0.4
4856	1.932	0.032	178.1	0.5
4956	1.987	0.034	178.1	0.5
5056	1.990	0.032	178.7	0.5
5144	2.038	0.027	178.2	0.4
5219	2.062	0.027	178.1	0.4
5281	2.079	0.025	177.6	0.3
5331	2.081	0.025	177.6	0.3
5381	2.039	0.025	177.3	0.3
5430	2.044	0.023	177.5	0.3
5480	2.017	0.022	177.6	0.3

Wavelength (Å)	p_M (%)	PM	M (°)	M
5542	2.023	0.021	177.4	0.3
5603	2.033	0.022	177.5	0.3
5667	2.030	0.021	177.8	0.3
5742	2.044	0.022	177.7	0.3
5803	2.045	0.022	177.4	0.3
5867	2.055	0.022	177.2	0.3
5942	2.074	0.022	176.5	0.3
6003	2.073	0.023	176.5	0.3
6067	2.087	0.023	176.7	0.3
6153	2.072	0.023	176.9	0.3
6264	2.034	0.024	177.2	0.3

Table C11 : Normalisation factors applied to the observations

Position angles were all corrected to the data on one observing run and one telescope. The applied corrections are shown here. Before tabulation, they were then converted to the equatorial system.

ε Ophiuchi

Correction applied to the wavelength scale was +10 Å

Observations	Polarisation Factor	Position angle rotation
4 MY5, 6 MY1	1.050	-9°.0
7 MY1, 7 MY2	1.095	-9°.0
16 MY1, 16 MY2, 17 MY3 26 MY4, 26 MY6	1.000	+26°.51
15 MY5, 15 MY6, 17 MY2 17 MY5, 24 MY2, 25 MY8 26 MY7	1.155	+26°.51
9 MY3	1.000	0°

55 Cygni

No correction to wavelength scale of Tenerife 60" data. Correction to September/October 1978 measurements as shown in the Observing Log (table C3). June 1978 measurements were corrected by +10 Å.

Observations		Polarisation Factor	Position angle rotation
O/14, O/19	(OP = 3800)	0.982	-89°.18
O/14 O/17, O/19	(OP = 5825)	1.049	-89°.18
O/15	(OP = 3800)	0.921	-89°.18
O/15	(OP = 5825)	0.984	-89°.18
25 SP1		1.116	-29°.6
28 SP1, 28 SP2, 28 SP3, 28 SP4		1.000	+2°.3
2 OC1, 2 OC2, 5 OC1		1.000	0
7 JN1		1.030	-27°.92

χ Aurigae

Wavelength correction to 1978 data was -44 Å, while 1979 measurements did not require correction.

Observations		Polarisation factor	Position Angle rotation
1978:	2 FB1, 2 FB2 3 FB1	1.000	0
1979:	12 FB8	0.896	+26°.28

Table C12

Feature \ Star	ζ Ophiuchi	55 Cygni	χ Aurigae
1. Ultraviolet upturn in degree of polarisation.	Starts at 3400 Å. Reaches 15% of polarisation at 3150 Å.	Starts at 3300 Å. Reaches 13% of polarisation at 3100 Å.	--
	Associated position angle rotation.	No associated position angle rotation.	--
2. Feature in position angle and degree of polarisation at 4100 Å.	Amplitude is 0.03-0.04% and position angle rotation 0°.7	No structure seen.	No structure seen (but errors large).
3. Feature in position angle and degree of polarisation at 4420 Å.	No structure seen.	Possible 0.08% feature in degree of polarisation. No position angle change.	No structure seen (but errors large).
4. Broadband position angle rotations.	Levels off at 4500 Å. Has rotated 1°.2 by 3400 Å. Small (0°.2) rotation in red.	Peaks at 4000 Å. Rotates 2°.5 into the ultraviolet, and a little less than 1° into the red (5500 Å).	Peaks at 5050 Å. Rotated 2°.5 by 3800 Å, and a little over a degree in the red (6500 Å).
5. Oscillatory structure in the degree of polarisation at $\lambda \geqslant \lambda_{max}$.	Polarisation peaks at (5250 Å), 5750 Å and 6600 Å. (Up to 0.08%).	--	Possible enhancements of polarisation at 5250 Å and 6050 Å.
	Associated position angle rotation. (Up to 1°.5)	--	No associated position angle rotation.